Endocranial Volume and Shape Variation in Early Anthropoid Evolution

by

Kari Leigh Allen

Department of Evolutionary Anthropology
Duke University

Date:_____

Approved:

_____
Richard F. Kay, Supervisor

_____
Blythe Williams

_____
Christine E. Wall

_____
Daniel Schmitt

_____
V. Louise Roth

Dissertation submitted in partial fulfillment of
the requirements for the degree of Doctor
of Philosophy in the Department of
Evolutionary Anthropology in the Graduate School
of Duke University

2014

ABSTRACT

Endocranial Volume and Shape Variation in Early Anthropoid Evolution

by

Kari Leigh Allen

Department of Evolutionary Anthropology
Duke University

Date:_____

Approved:

_____
Richard F. Kay, Supervisor

_____
Blythe Williams

_____
Christine E. Wall

_____
Daniel Schmitt

_____
V. Louise Roth

An abstract of a dissertation submitted in partial fulfillment of the requirements for the degree of Doctor of Philosophy in the Department of Evolutionary Anthropology in the Graduate School of Duke University

2014

Abstract

Fossil taxa are crucial to studies of brain evolution, as they allow us to identify evolutionary trends in relative brain size and brain shape that may not otherwise be identifiable in comparative studies using only extant taxa, owing to multiple events of parallel encephalization among primate clades. This thesis combines indirect and direct approaches to understanding primate evolution, by evaluating variation in the endocranial morphology of extant primates and their fossil representatives. I use a comparative approach to examine the relationships between interspecific adult endocranial volume and shape, and brain evolution and cranial form among extant primate clades and their fossil representatives. The associations are evaluated via phylogenetically informed statistics perfomed on volumetric measurements and three-dimensional geometric morphometric analyses of virtual endocasts constructed from micro-CT scans of primate crania. Fossil taxa included in these analyses are: 1) anthropoids *Parapithecus, Aegyptopithecus* (Early Oligocene, Egypt), *Homunculus* and *Tremacebus* (Early Miocene, Argentina), and 2) Eocene euprimates *Adapis* and *Leptadapis* (Eocene adapoids, France), and the *Rooneyia* (Eocene omomyoid, Texas).

The first part of this work (Chapter 2) explores variation in residual mass of brain components (taken from the literature) among primates, and evaluates the correlated evolution of encephalization and brain proportions with endocast shape, quantified via

three-dimensional geometric morphometric techniques. Analyses reveal a broad range of variation in endocast shape among primates. Endocast shape is influenced by a complex array of factors, including phylogeny, body size, encephalization, and brain proportions (residual mass of brain components). The analysis supports previous research, which concludes that anthropoids and tarsiers (Haplorhini) share the enlargement of several key brain regions including the neocortex and visual systems, and a reduction of the olfactory system. Anthropoids further differ from strepsirrhines in endocranial features associated with encephalization—a more flexed brain base, an inferiorly deflected olfactory fossa—and those associated with brain proportions—a small olfactory fossa, and a more caudally extended cerebrum that extends posteriorly past the cerebellar poles. Tarsiers are unique in having a mediolaterally broad and rostro-caudally short endocast with an attenuated anterior and middle cranial fossae. This morphology is likely related to the extreme orbital enlargement in this taxon, which limits anterior expansion of the endocranium. Finally, despite the correlation between residual endocranial volume and endocast shape among modern primates, early anthropoid fossils demonstrate a disconnect between these factors in sharing key features of endocast shape with extant anthropoids at a relatively small brain size.

The second part of this thesis (Chapter 3) explores the relationship between craniofacial organization—cranial base angle, facial size, facial hafting—and encephalization via the lens of the Spatial Constraints and Facial Packing Hypotheses.

These hypotheses predict that interspecific adult variation in encephalization correlates with endocranial shape such that a larger brain for a given body size will be more "globular" or spherical in shape. These hypotheses futher predict that basicranial angle covaries with encephalization and that the relative size of the endocranium and facial skeleton will have an antagonistic effect on basicranial angle and facial hafting. Results show that various measures of globularity have inconsistent and weak relationships to phylogeny, encephalization, and basicranial flexion, owing to a diversity of clade-specific scaling patterns between the maximum length, breadth, and width of the endocast. Among extant primates, there is weak but significant evidence to suggest that both facial size and encephalization influence variation in basicranial flexion. Considering the fossil specimens in isolation, their relative ranks in encephalization, basicranial flexion, and midline facial size and shape follow the pattern expected from the Spatial and Facial Packing Hypotheses outlined above; however, relative to modern species, the early fossil anthropoids have more flexed cranial bases and shorter facial skeletons at much smaller level of encephalization than seen in modern anthropoids.

Together, the extant data suggest a moderately conserved pattern of correlated evolution among endocranial size, endocranial shape, brain proportions, and craniofacial organization, which may explain differences in endocranial and facial shape between extant strepsirrhine and anthropoid primates; however, the fossil record for early anthropoid evolution demonstrates that a shift towards key anthropoid-like traits

of the endocranium, basicranium, and facial skeleton were initiated early in anthropoid evolution, with subsequent encephalization occurring within and among members of this clade. Thus, these anthropoid cranial traits evolved in tandem with changes in the relative size of brain components, rather than absolute or relative brain size alone. Basicranial flexion, facial length and orientation are influenced by both: 1) shifts in endocranial shape associated with changes in brain proportion—accounting for the initiation of the anthropoid-like craniofacial plan early in the evolution of the clade—and 2) encephalization, which influenced subsequent morphological divergence among extant anthropoid groups.

Dedication

To my mom, whose passion for learning is contagious.

Contents

Abstract iv

List of Tables xiii

List of Figures xv

Acknowledgements xix

1. Introduction 1

1.1 Primate Encephalization 2

1.1.1. Scaling Patterns (Strepsirrhine/Anthropoid Dichotomous "Trends") 6

1.1.2. Fossil Evidence for Anthropoid Brain Evolution 8

1.2 Theoretical Considerations 12

1.2.1 Cognitive Implications of Brain Size and Brain Proportions 12

1.2.2. Strepsirrhine/Anthropoid Cognitive Differences 14

1.2.3. "Developmental Constraints Hypothesis" 17

1.2.4. Coevolution of the Brain and Skull 20

1.2.5. Tarsier Brains and Their Implications for Haplorhine Brain Evolution 23

1.2.6. Importance of the Fossil Record of Brain Evolution 28

1.2.7. Geometric Morphometrics and Endocast Shape Variation 30

1.3. Outline of Thesis Purpose 33

2. Endocast Shape in Primate Evolution 35

2.1. Introduction 35

2.2. Materials and Methods 37

2.2.1. Micro-CT Scans of Extant Primates 37

2.2.2. Fossil Specimens 41

2.2.3. Data Collection 43

2.2.4. Analysis 49

2.3. Results 54

2.3.1. Analysis of Extant Primate Brain Proportions 54

2.3.2 Endocast Shape Analysis 65

2.3.2.1. Extant-Only Analysis 65

2.3.2.2. Correlated Evolution Between Stephan (1981) Brain Proportion Data and Endocast Shape 70

2.3.2.3. Endocranial Shape of Fossil Specimens 73

2.4. Discussion 79

2.4.1. Endocast Shape and Brain Proportions 79

2.4.2. Tarsier Endocranial Morphology and Its Implication for Haplorhine Brain Evolution 83

2.5. Conclusions 85

3. Co-evolution of Encephalization and Cranial Form in Primates 88

3.1. Introduction 88

3.1.1. The Effects of Encephalization on Cranial Base Angle and Facial Size 89

3.1.2. Brain Shape and Basicranial Form 92

3.1.3. Previous Studies 93

3.2. Materials and Methods 95

3.2.1. Data Collection 95

3.2.2. Variables Used In This Study 97
3.2.2.1. Midline Globularity 98
3.2.2.2. Three-Dimensional Globularity 101
3.2.2.3. Globularity Index 102
3.2.2.4. Facial Size and Shape 103
3.2.3. Analysis 103
3.3. Results 105
3.3.1. Neurocranial Globularity 105
3.3.2. Group Differences In Basicranial Angle and Facial Size 111
3.3.3. Exploratory Analysis of Midline Landmark Shape 114
3.3.4. Correlated Evolution Among Traits 124
3.4. Discussion 132
3.4.1. Interaction Between Endocranial Shape and Craniofacial Form 134
3.4.2. Implications of the Fossil Record 136
3.4.3. Additional Factors Affecting Globularity 137
3.4.3.1.Variability in Measurements of Endocranial Globularity 137
3.4.3.2. Adaptive Implications of Brain Sphericity 139
3.5. Conclusions 140
4. Conclusions and Future Directions 144
4.1. Order of Acquisition of Traits in Primate Brain Evolution 144
4.2. Implications of Tarsier Morphology for Brain Shape and Cranial Evolution in Haplorhini 147

4.3. Implications for Cognitive Interpretations from the Fossil Record 150

4.4. Avenues for Future Research..... 152

Appendix A: CT Scan Information..... 155

Appendix B: Primate Phylogeny 159

Appendix C: Residual Mass of Brain Parts 162

Appendix D: Species Mean Coordinates for Procrustes-Aligned Landmarks 164

References..... 184

Biography 201

List of Tables

Table 1: Summary of specimens used in this analysis, including the number of individuals (n) for each genus and the higher order taxonomic classifications for each genus. See text for explanation of specimen number collection prefixes. 39

Table 2: Names and definitions of landmarks collected on virtual renderings of the endocanial surface. Landmark abbreviations refer to the landmarks pictured in Figure 2. 46

Table 3: Summary of regression results for the mass of brain components on brain weight. n = number of species included in analysis, PGLS = phylogenetic analysis, OLS = ordinary least squares regression, lambda refers to values of Pagel's λ estimated from the data and incorporated into the PGLS variation-covariation matrix error term. * = significance at alpha 0.05 level. 57

Table 4: Results of Wilcoxon pairwise comparisons in residual mass of brain components. * = significant difference at alpha 0.05 level. 60

Table 5: Mean and standard deviations for anthropoid and strepsirrhine residual brain component masses with a comparison to tarsier values. SD = standard deviation. 61

Table 6: Principal Component (PC) scores for analysis of residual brain components. N = number of specimens in Stephan dataset. PC = Principal Component score. 63

Table 7. Eigenvectors for Principal Components (PC) analysis of residual mass of brain components. 64

Table 8: Genus mean Principal Component (PC) scores for extant-only endocast analysis. Details for species names and samples available in Appendix A. 67

Table 9: Phylogenetically informed (PGLS) and ordinary least squares (OLS) regression results for endocast Principal Components (PC endocast), brain Components (PC1 Stephan), and endocranial size, * denotes significance using Bonferroni significance criterion = 0.0083, for multiple comparisons. 72

Table 10: Principal Component (PC) scores for extant and fossil endocast analysis. 75

Table 11: Craniofacial landmarks and angular measurements collected from midsagittal tomographs of primate crania. # refers to the landmark labels in Figure 20. 99

Table 12: Species means for globularity and basicranial variables. See text for abbreviations..... 107

Table 13: Means and standard deviations (SD) for endocranial globularity measures by taxonomic group. n = number of species per taxonomic group..... 109

Table 14: Results for multiple sample comparison of endocranial globularity measures by taxonomic group. * denotes significance at the 0.05 level, ** denotes significance using Bonferroni correction criterion of p<0.003. 109

Table 15: Means and standard deviations (SD) for basicranial angles (BCA1 and BC2) and residual facial size (resFS) by taxonomic group. n = number of species per taxonomic group. 112

Table 16: Results for multiple sample comparison of basicranial angle (BCA1 and BCA2) and residual facial size (resFS) by taxonomic group. * denotes significance at the 0.05 level, ** denotes significance using Bonferroni correction criterion of p<0.003. 113

Table 17: Principal Component (scores for analysis of Procrustes-aligned midsagittal landmark configurations..... 115

Table 18: Principal Component (PC) scores, basicranial angle (BCA) and facial size for fossil specimens. 120

Table 19. Correlation (Spearman's ϱ) and partial correlation coefficients for species mean endocranial volume (ECV), residual endocranial volume (resECV), and braincase dimensions. All variables are log transformed prior to analysis. Top right portion of matrix presents correlation coefficients, bottom right represents partial correlation scores. Fill color gradient represents magnitude of the score: red = highest values, green = lowest values..... 124

Table 20: Results for phylogenetically informed generalized least squares (PGLS) regressions of extant primate endocranial and basicranial varibles. See text for abbreviations..... 128

Table 21: Correlation (Spearman's ϱ) and partial correlation matrix for midline globularity, residual endocranial volume (resECV), residual facial size (resFS), and basicranial angle (BCA1). Top right portion of matrix presents correlation coefficients, bottom right represents partial correlation scores. Fill color gradient represents magnitude of the score: red = highest values, green = lowest values..... 130

List of Figures

Figure 1: Bivariate plots of brain weight and cerebellum weight on body weight. Data from Stephan et al. (1981). The red line represents an ordinary least squares regression fit to the anthropoid data, and the blue line is fit to the strepsirrhine data. 7

Figure 2: Brain (left) and virtual endocast (right) of *Saimiri sciureus* with labeled anatomical features. Top row: lateral view. Bottom: inferior view. Rostral is to the right. 10

Figure 3: Midsagittal tomographs of a lemur (top), ape (middle), and human (bottom), illustrating the proposed relationship among increasing encephalization, sphericity of the endocranial shape, and increasing basicranial angle (highlighted in red). Modeled after Figure 1 in Ross and Ravosa (1993). 24

Figure 4: Reconstruction of the endocranial surface of *Saimiri sciureus*, demonstrating landmarks taken on virtual endocasts. Upper: lateral view, lower: inferior view. Abbreviations refer to landmark definitions in Table 2. Distance from the frontal-occipital pole = 49.49mm. 45

Figure 5: Cutaway illustration of the anterior cranial fossa of *Tarsius* (=*Carlito*) *syrichta* (DPC 045): a) dorsocaudal view of the ectocranial surface as reference for the point of view; b) oblique lateral view of the specimen illustrating the cutting planes (orange lines) applied to the surface, c) reconstructions of cranial surface with cutting planes applied, cranium is oriented in the same view as "a", the black box contains an enlarged view of the anterior cranial fossa. Note the rostral extension of the olfactory canal through the interorbital space and its termination, which contains multiple foramina. . 47

Figure 6: a) midsagittal micro-computed tomograph of *Tarsius syrichta* (DPC 045), with the olfactory fossa and nerve canal highlighted in yellow hatching; b) photographs of *Tarsius syrichta* brain in inferior (left) and lateral (right) views. Top row: unlabelled specimen, bottom row: the olfactory bulb is outlined in yellow. All images are oriented with the rostrum to the right. Brain images modified from specimen images in the Comparative Mammalian Brain Collections (brainmuseum.org), specimen #61-193. 50

Figure 7: Consensus tree used for phylogenetically-informed endocast shape analyses. Green = Catarrhini, Red = Platyrrhini, Orange = Tarsiidae, Blue = Strepsirrhini. See Appendix B for divergence dates and complete phylogeny in nexus format..... 53

Figure 8: Bivariate plots of the mass of various brain components on brain weight. All measures are log transformed prior to analysis. Data comes from masses reported (in grams) by Stephan *et al.* 1981. Red line = PGLS regression, black line = OLS regression. 55

Figure 9: Bivariate plots of the mass of various brain components on brain weight. All measures are log transformed prior to analysis. Data comes from masses reported (in grams) by Stephan *et al.* 1981. Red line = PGLS regression, black line = OLS regression. 56

Figure 10: Box and whisker plots for residual mass of brain components between haplorhine and strepsirrhine primates. Pairwise comparisons show significant differences between group mean rank for all analyses ($p < 0.05$), except residual mesencephalon ($p = 0.89$). 59

Figure 11: Principal Components Analysis of residual brain components in primates, data from Stephan *et al.* (1981). Red polygon = platyrrhine distribution, blue polygon = strepsirrhine distribution, green polygon = catarrhine distribution. 64

Figure 12: A sample of extant primate endocasts with associated wireframes. Left column: wireframes in lateral view, middle column: endocasts and associated landmarks in lateral view, right column: endocasts in inferior view. a) *Lemur catta*, b) *Alouatta seniculus*, c) *Saimiri sciureus*, d) *Homo sapiens*..... 66

Figure 13: Principal Components analysis of extant primate endocast shape. Left: bivariate score plot of individual specimen values for components 1 and 2. Wireframes depict morphology of the genus contained and labeled within the grey circle. Right: wireframes depicting shape variation along the first two Principal Components (PC). The consensus wireframe represents the morphology at the origin (0,0) of the biplot. ... 68

Figure 14: Biplots of Principal Component scores (Components 1, 2, 3) for extant endocast analysis. Points indicate individual specimen values. 69

Figure 15: Bivariate plots of endocast shape Principal Component scores and residual brain masses from Stephan dataset. Points represent species means, and PGLS regression is depicted as red line. 71

Figure 16: Virtual endocast reconstructions of fossil specimens used in this analysis. All specimens are depicted in lateral view and scaled to equal fronto-occipital pole length (rostal to the right). 74

Figure 17: Principal Component Analysis of extant and fossil endocast shape. Blue = strepsirrhines, red = platyrrhines, green = catarrhines, orange stars = tarsiers. Points indicate individual specimen values. 76

Figure 18: 3D plot of 95% confidence ellipsoids from Principal Components 1, 2, and 3, derived from endocast landmark configurations of extant and fossil primates. Blue = strepsirrhine confidence ellipsoid, red = haplorhine confidence ellipsoid, orange stars = tarsiers. Points indicate individual specimen values. 77

Figure 19: Variation in endocast shape associated with encephalization differences within primate clades. Each column represents a pair of related taxa, scaled to equal fronto-ccipital pole length. Species on the bottom row have greater residual endocranial volume than their relative depicted on the top row. Orange arrows point to the confluence of sinus, yellow arrows highlight the inferior deflection of the olfactory fossa and associated rounding of the frontal region in more encephalized species. 80

Figure 20: Landmarks taken on midsagittal tomographs of primate crania. Numbering refers to # column of Table 11. Red (1-5) = facial set, blue (6-13) = cranial base, yellow (7, 15, 15) = additional landmarks used to define midsagittal plane. 100

Figure 21: Box-and-whisker plots of endocranial globularity measures by taxonomic group. Among Hominoidea, green 'H' = *Homo sapiens*, among Lemuroidea, blue 'D' = *Daubentonia madagascarensis*. At right: taxon names are H = Haplorhini, S = Strepsirrhini. Points represent species mean values. 110

Figure 22: Bivariate plot of basicranial angles 1 (BCA1) and 2 (BCA2). PGLS regression line depicted in red: BCA1 = 0.55*BCA2 + 80.86. $R^2 = 0.68$, $p < 0.0001$. Green 'H' = *Homo sapiens*. Points represent species mean values. 112

Figure 23: Box-and-whisker plots of residual facial size measures by taxonomic group. Among Hominoidea, green 'H' = *Homo sapiens*, among Lemuroidea, blue 'D' = *Daubentonia madagascarensis*. At right: taxon names are H = Haplorhini, S = Strepsirrhini. Points represent species mean values. 114

Figure 24: Principal Components Analysis of Procrustes-aligned endocranial outline landmarks for extant-only dataset. Grids represent relative warp deformations of landmark configurations visualizing the maximal and minimal values for each axis. Rostral is to the right. Points represent values for individual specimens. 117

Figure 25: Principal Components Analysis of Procrustes-aligned facial + basicranial landmark set. Grids represent relative warp deformations of landmark configuration visualizing the maximal and minimal values for each axis. The endocranial outline is included in the visualizations for reference, but is not incorporated into the landmark analysis. Rostral is to the right. Points represent values for individual specimens. 119

Figure 26: Principal Components Analysis of a) midline endocranial outline and b) midline facial + basicranial landmarks. Green = extant catarrhine distribution, red = extant platyrrhine distribution, blue = extant strepsirrhine distribution. 121

Figure 27: Relative warps visualizations (left) and midsagittal tomographs of fossil specimens illustrating basicranial, facial (in red) and endocranial outline landmarks (in blue). From top to bottom: a) *Adapis*, b) *Parapithecus*, c) *Aegyptopithecus*, d) *Homunculus*—missing points interpolated from surrounding three-dimensional morphology. Specimens are scaled to equal skull length. 122

Figure 28. Bivariate plots of endocast maximal dimensions on endocranial volume (ECV). Points represent species means. Dotted green line represents regression fit to catarrhine-only distribution (slope = 0.33, $p < 0.001$ for each). 125

Figure 29: Bivariate plots of PGLS regression results for midline globularity and residual facial size (resFS) with residual endocranial volume (resECV). D = *Daubentonia*, H = *Homo*. Points represent species mean values. 130

Figure 30: Bivariate plot representing two-block partial least-squares (2B PLS) analysis of covariation among the midline endocranial and facial landmark configurations. 132

Figure 31: Endocast shape differences between extant strepsirrhines and anthropoids. a) *Lemur catta*, b) *Saimiri sciurus*..... 145

Figure 32. Fossil primate endocasts and associated skulls in lateral view. All specimens are scaled to equal length..... 146

Figure 33. A phylogeny of extant primate clades illustrating the proposed timing of shifts in encephalization (EQ) and endocast shape (indicated by orange stars) as evidenced by a combination of modern distributions and fossil evidence. 148

Acknowledgements

I'd like to thank my family, friends, and colleagues for their encouragement throughout this process. I am grateful to the entire Duke Evolutionary Anthropology community for providing a supportive and enriching environment, which fostered countless productive conversations about both life and research. The faculty, postdocs, staff, and students continually lead by example in their passion to teach, explore, and to live productively and happily both in and out of the lab.

I am particularly indebted to my committee members for their feedback and mentoring. Thank you, Dr. Christine E. Wall, for instilling in me an appreciation for simply basking in and exploring biological variation. You've done the impossible, by proving to me that math can be both creative and exciting. I'd like to thank Dr. Daniel Schmitt for always bringing a unique perspective to any research discussion. Your boundless enthusiasm for gathering and sharing knowledge is infectious. Dr. Louise Roth, your course on Macroevolution, taken in my first semester at Duke, continues to inspire me to think of the bigger picture. Dr. Richard F. Kay and Dr. Blythe Williams have been the best mentors a student could hope for. I only hope that I have absorbed some of your skill and enthusiasm for critical thinking, project planning, productivity, and of course, mentoring. Collaborating with you is like taking a master's class in project

design and writing. Thank you for always treating me as a colleague and welcoming me into your lab. You have been gracious hosts and an inspiration to work with.

I'd like to thank the many colleagues who have provided access to fossils and/or CT scan data. Thank you to Dr. Elwyn Simons and Dr. Gregg Gunnell of the Duke Lemur Center, Fossil Division, for access to the Fayum anthropoid material, Dr. Richard F. Kay for providing the Patagonian material, Renaud Lebrun for micro-CT scans of the Quercy Adapoid crania, and Dr. E. Christopher Kirk for providing me with a virtual reconstruction of the *Rooneyia* endocast. Without access to these fossil specimens, this project would not have been possible. I am also grateful to Dr. Matthew Tocheri and the Smithsonian Institute for Human Origins for sharing CT scans of extant catarrhines from the National Museum of Natural History collections, and to micro-CT technicians Morgan Hill and James Thostenson for scanning specimens for this project at the American Museum of Natural History Imaging Facility. I would also like to thank Dr. Doug Boyer for sharing micro-CT scans of *Daubentonia*, for providing a means for collecting and sharing scans—by spearheading efforts to develop a Duke micro-CT facility and file sharing site Morphosource.org, both of which have greatly expanded the available sample for this and other projects—and for countless conversations about CT techniques, file management, and data sharing efforts.

I would also like to thank those who have helped me acquire the essential skills to complete this work. I have learned a great deal about phylogenetic comparative

methods from Dr. Charles Nunn and the 2010 AnthroTree Workshop, as well as conversations with Dr. Evan MacLean and correspondences with Dr. Theodore Garland. I greatly appreciate James Thostenson for training me to collect and process my own micro-CT data at the Duke Shared Materials Instrument Facility. I was hesitant to add yet another complex skill to my ever-growing thesis "to do" list, but your experience, intuition, and patience made data acquisition a painless experience, and unlocked unlimited possibilities for future projects. I owe an extreme amount of gratitude to those who have helped me navigate the world of landmark-based morphometrics, including Marisa Macias, Dr. Siobhan Cooke, and Dr. Claire Terhune. I extend a special thanks to Marisa Macias and Nichelle Reed for being both fantastic friends and patient and encouraging math gurus.

Finally, I'd like to thank my family and friends for their encouragement. Thank you to my parents and siblings for being overly impressed by all my achievements, and to Chris, Jenn, and Twiggy Allen in particular for sharing their couch and company during my NY data collection trips (again). Thank you to my "academic siblings" Dr. Michael Malinzak, Dr. Jonathan Perry, Dr. Terry Mitchell, Lauren Gonzales, and Jackson Spradley for the many conversations we have had over the course of developing this project. I am especially thankful for the company of Tara Clarke-Fontana, Nichelle Reed, Marisa Macias, and Tyler Johnson, which kept me sane and pushed me to the finish line.

Funding for CT scan acquisition and museum travel related to this project was provided by grants from the Leakey Foundation (award #181951), the National Science Foundation (Doctoral Dissertation Improvement Grant, BCS-1232534), and the Duke University Graduate School (Dissertation Research Travel Award).

1. Introduction

This thesis takes a comparative approach to examine the relationships between brain evolution and cranial form among extant species of primates and the fossil representatives of early anthropoids. The project evaluates these associations via analyses of virtual endocasts constructed from micro-CT scans of primate crania. A total of 51 species of extant primates were examined, including 16 platyrrhine, 22 catarrhine, 1 tarsioid, and 12 strepsirrhine species. Fossil specimens under consideration include representatives of basal anthropoids (Early Oligocene *Parapithecus*), basal catarrhines (Early Oligocene *Aegyptopithecus*), and basal platyrrhines (Early Miocene *Homunculus* and *Tremacebus*), with Eocene euprimates considered as an outgroup comparison (Eocene adapoids *Adapis* and *Leptadapis*, and the omomyoid *Rooneyia*).

This project combines both a direct and indirect approach to studying primate brain evolution. In taking a comparative approach, relationships among aspects of endocast shape, brain proportions, and brain size can be explored across extant primates; however, as pointed out by Radinsky (1974:15):

> "While limited in the kind of data they provide--primarily brain size, shape, and details of external morphology--endocasts are important for understanding brain evolution, for they are the only direct evidence of that evolution. The other major source of data, comparisons between brains of living species, provides much

more information, but is at best indirect evidence, and must be interpreted with caution in inferring the actual course of brain evolution."

In this thesis, both fossil and extant primate endocasts are examined to identify evolutionary trends in relative brain size and brain shape in anthropoid evolution that may not otherwise be identifiable in comparative studies using only extant taxa, owing to the accumulating evidence for parallel encephalization among primate clades.

1.1 Primate Encephalization

It has long been recognized that extant primates tend to have larger brains relative to their body weight than most other mammals (Jerison 1955; Le Gros Clark 1959; Jerison 1973; Gould 1975). In their landmark studies on the scaling of brain components, Stephan and colleagues compared the volumes of various functional brain components among primates and a collection of extant species taken to represent the 'basal' mammalian condition (Stephan and Andy 1964; Stephan *et al.* 1981; Stephan *et al.* 1982; Baron *et al.* 1983). The out-group, collectively referred to as "insectivores" is now known to be a polyphyletic group consisting of members from the superorders Afrotheria (i.e. Order Afrosoricida: otter shrews, tenrecs, golden mole; Order Macroscelidae: elephant shrews) and Laurasiatheria (i.e. Order Eulipotyphla: hedgehogs, shrews, desmans, European mole), whose higher order divergence is thought to have been concurrent with the separation of the South American and African continents, approximately 103 mya (Stanhope *et al.* 1998; Murphy *et al.* 2001). These

small-bodied insectivorous species have been used by many researchers to represent the inferred basal mammalian niche (Jerison 1979; Allman 1982; Jerison 2007).

Data collected by Stephan and colleagues demonstrate that in comparison to the 'basal insectivores', the volume of the neocortex is enlarged, relative to body mass, and the olfactory bulb reduced in primates (Stephan and Andy 1964; Stephan and Andy 1969; Stephan *et al.* 1981; Frahm *et al.* 1982; Baron *et al.* 1983; Jolicoeur *et al.* 1984). These data have been interpreted as evidence for neuroanatomical adaptation towards increased cognitive complexity or intelligence in primates and a shift in sensory ecology towards an increased reliance on visual rather than olfactory cues in foraging and social interactions (Jerison 1973; Barton 1998; Kirk 2006).

Viewed phylogenetically among primates, the anthropoid clade represent a further "grade shift" in brain size, with larger brains at a given body weight than strepsirrhines and tarsiers (Jerison 1955; Le Gros Clark 1959; Jerison 1973; Radinsky 1974; Gould 1975; Smaers and Soligo 2013). As such, encephalization and brain proportions are often highlighted in discussions of differing adaptive niches between strepsirrhines and anthropoids. It is thought that the large brains of anthropoids relate to increased social complexity (Dunbar 1992; Dunbar 1998), increased use of cognitive abilities such as complex problem solving and spatial memory skills to "buffer" against food shortages (Allman *et al.* 1993; vanWoerden *et al.* 2010), and enhanced visual senses

associated with reduced olfactory reliance (Barton 1998; Kirk 2006), as compared to tarsiers and strepsirrhine primates (lemurs, lorises, galagos).

So far, this scenario relies on the indirect approach to evaluating primate brain evolution, relying on comparisons among living taxa—primates and those mammals thought to have departed little from the last common ancestors of primate and non-primate mammals. The reason for the largely neontological comparison is clean cut. Information on neural connectivity and other features of the internal structure of the brain are not observable in the fossil record. In fossils, we must rely entirely on the surface structure and the volume of the endocranial cavity and various distinguishable brain regions to make inferences about brain function and what that might mean for the behavioral repertoire in these animals (Jerison 1970; Radinsky 1970; Radinsky 1974; Radinsky 1977; Falk 1982; Gurche 1982).

Recent evidence has called into question a basic tenent of the neontology-based comparative approach. The fossil record now indicates parallel increases in relative brain size among a number of anthropoid clades. Stem representatives of catarrhines (*Aegyptopithecus)*, cercopithecoids (*Victoriapithecus*), and platyrrhines (*Chilecebus* and *Homunculus*) have relative endocranial volumes that are smaller than the extant representatives of these clades (Benefit and McCrossin 1997; Kay *et al.* 2006; Simons *et al.* 2007; Kay and Kirk 2008; Sears *et al.* 2008; Kay *et al.* 2012). Montgomery et al. (2010) utilize ancestral character state reconstructions to estimate the directionality and rates of

changes in brain and body size evolution in primates. The authors demonstrate that the use of parsimony-based reconstructions utilizing an extant-only dataset overestimates ancestral levels of encephalization, as compared to reconstructions that incorporate the fossil data. In other words, the fossil specimens have much smaller brains than would have been reconstructed from the distribution of relative brain sizes among extant species (Montgomery *et al.* 2010). In fact, the residual endocranial volumes reported for the Oligocene catarrhine *Aegyptopithecus* (Simons *et al.* 2007), Miocene cercopithecoid *Victoriapithecus* (Gonzales *et al.* 2010), Miocene platyrrhines *Chilecebus* (Sears *et al.* 2008) and *Homunculus* (Kay *et al.* 2012) place these specimens within the extant strepsirrhine range. As such, the modern levels of encephalization in anthropoid primates—with comparable mean residual endocranial volumes for both platyrrhine and catarrhine monkeys (Isler *et al.* 2008)—must have been achieved in parallel.

Having established the pervasive parallelism in overall brain size, it is as yet unclear whether the brain proportions that characterize anthropoid primates as distinct from strepsirrhines had likewise already occurred in the earliest representatives of these clades. This is a central question to this project: did shifts in brain proportions preceed significant additional encephalization within extant primate lineages? Alternatively, did the enlargement of the occipital and frontal lobes, and reduction of the olfactory complex occurred in parallel between platyrrhine and catarrhine clades? It is possible that the genetic and metabolic potential for regional volume increases in anthropoid

evolution preceded the utilization of these developmental constraint releases. In this case, shifts in brain proportion may have occurred in parallel between extant anthropoid lineages, perhaps owing to parallel selective pressures. Information from the fossil record concerning regional and global endocast shape and size provides an opportunity to test the different predictions of these two scenarios.

1.1.1. Scaling Patterns (Strepsirrhine/Anthropoid Dichotomous "Trends")

Anthropoid primates differ from strepsirrhine primates in the relative size of the total brain and in the proportions of brain components, including the olfactory bulbs, the cerebellum, and the neocortex, especially the visual centers and the frontal lobe. The dataset published by Stephan and Andy (1964), and presented here in Figure 1, reveals that the encephalization of anthropoid primates is primarily the result of greater neocortex volume, relative to body weight, with anthropoid and strepsirrhine regression lines sharing similar slopes but divergent intercepts in log space. A regression of log cerebellum vs. log body mass demonstrates clade-specific scaling patterns, with anthropoids demonstrating a relatively larger cerebellum at larger body sizes (Stephan and Andy 1964).

In addition to differences in relative brain size and the size of brain components, extant anthropoid and strepsirrhine brains differ in the shape of their endocasts, with many researchers inferring a relationship between these brain proportions and the shape

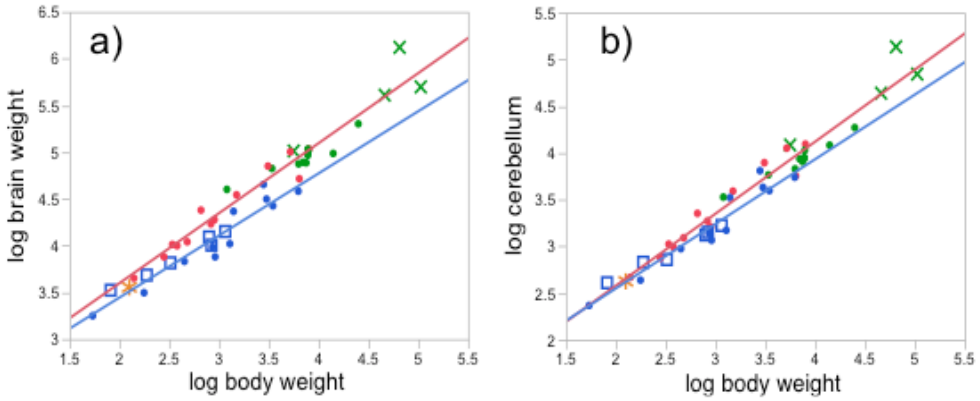

Figure 1: Bivariate plots of brain weight and cerebellum weight on body weight. Data from Stephan et al. (1981). The red line represents an ordinary least squares regression fit to the anthropoid data, and the blue line is fit to the strepsirrhine data.

of the endocranium (Simons 1959; Radinsky 1968; Radinsky 1970; Radinsky 1974; Simons 1993; Simons 1995; Simons 2001). For example, Radinsky (1974) asserts that anthropoids tend to have more inflated or rounded frontal lobes, reflecting their larger size, while the reduction of the olfactory bulb is reflected in the size and orientation of the olfactory fossa—with strepsirrhines having larger and more rostrally directed olfactory fossae and anthropoids demonstrating smaller and more inferiorly directed olfactory fossae. Quantification of these shapes has not yet been attempted, precluding any analysis of the allometric effects of total and local brain size on the surface shape of the endocranium. These and other proportional changes in the endocranium will be subject to quantitative examination herein.

1.1.2. Fossil Evidence for Anthropoid Brain Evolution

Unfortunately, brain tissue does not fossilize; however, the close developmental relationship between the brain and neurocranium results in a strong correlation between the volume and general shape of brain with that of the inner surface of the bony neurocranium (Smith 1928; Shellshear and Smith 1934; Weidenreich 1936; Weidenreich 1947; Edinger 1948; Jerison 1955). The endocast is not a cast of the brain itself, but includes the volume of intervening structures—including the intracranial blood supply, meningeal layers, and cerebrospinal fluid. Thus, the volume of the endocranial cavity is a slightly inflated estimate of brain volume. Holloway et al. (2004) report that the endocranial volume is approximately 10% larger than brain volume. Isler *et al.* (2008) report a tight isometric scaling relationship between endocranial volume and brain volume among primates, with a correction factor of 1.036. Although the size of the endocranium reflects brain size, the surface impression of the endocranial cavity does not provide an absolutely faithful representation of the brain's surface. While some sulci are often represented on the endocranial surface, the presence and absence of gyri on the brain are not captured with high fidelity on the endocast (Holloway *et al.* 2004). Thus, absence of primary, secondary, and tertiary gyri on the endocast is not evidence of absence in the living brain. Nevertheless, many homologous points can be reliably identified on mammalian endocasts, including the rhinal fissure separating the olfactory fossa from the frontal region of the cerebrum, the confluence of sinuses, transverse, and

petrous curves which denote the separation of the posterior cranial fossa (containing the cerebellum, medulla, pons) from the rest of the brain. Additionally, measures of overall dimensions of brain parts (frontal, occipital, temporal, and cerebellar poles) and basicranial features related to the transmission of blood supply and nerve complexes into and out of the neurocranium can be reliably identified on sufficiently complete specimens (see Figure 2). Thus, the overall size of the brain and the relative size and orientation of some major the brain parts (cerebellum, cerebrum, olfactory bulb) can be interpreted from studying natural or manmade endocasts (Edinger 1948; Radinsky 1968).

Early anthropoid endocasts have been described demonstrating a mixture of strepsirrhine and anthropoid-like qualities, suggesting that reorganization of the brain occurred early in anthropoid evolution. Radinsky (1974) describes the Oligocene anthropoid *Aegyptopithecus* as being "more advanced" than most modern strepsirrhines in having a rostrally located lunate sulcus—perhaps indicating a larger visual cortex, a qualitatively smaller olfactory bulb, and the presence of the central sulcus separating the primary somatic sensory and motor cortices (Radinsky 1974). Despite these similarities with modern anthropoids, *Aegyptopithecus* was described as "less advanced" than modern groups in having less surface complexity, a rostrally projecting olfactory fossa, and a seemingly less expanded frontal region with a dorsally receding rostral aspect to the anterior cranial (Radinsky 1974). Radinsky's descriptions have largely been

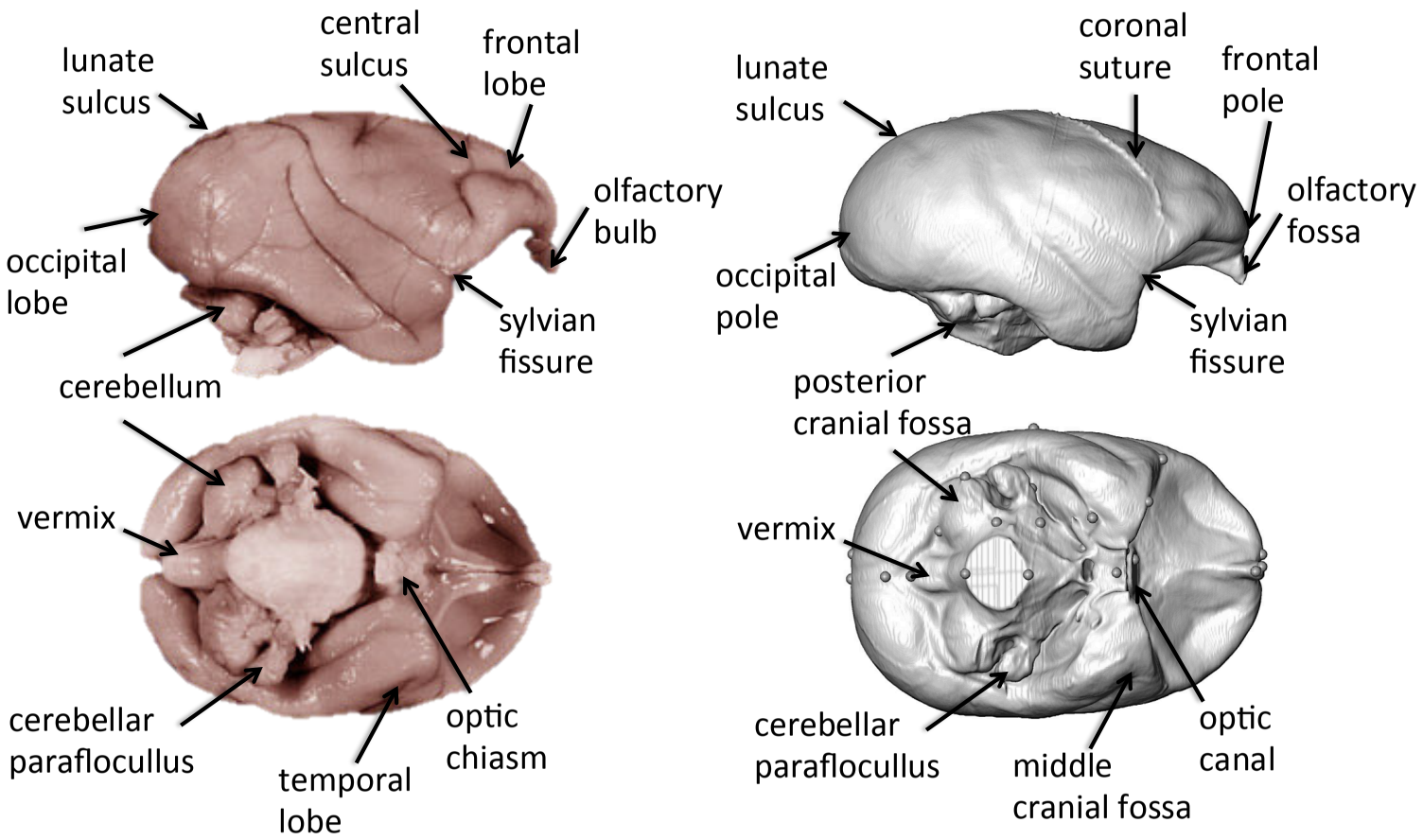

Figure 2: Brain (left) and virtual endocast (right) of *Saimiri sciureus* with labeled anatomical features. Top row: lateral view. Bottom: inferior view. Rostral is to the right.

validated by subsequent workers and the addition of new specimens, including a nearly complete female cranium, CGM40237 (Simons 1993; Simons *et al.* 2007). Based on reconstructions from partial endocasts, Radinsky (1974) concludes that *Aegyptopithecus* falls within the modern anthropoid range of encephalization (using foramen magnum dimensions as a body size proxy); however, subsequent reconstructions from more complete specimens have demonstrated that the brain of *Aegyptopithecus* is relatively smaller than in extant anthropoids (Simons *et al.* 2007).

Similarly, analyses of Oligocene basal anthropoids *Parapithecus grangeri, Apidium phiomense,* and *Apidium bowni*, also from the Fayum Depression of Egypt, highlight many of the same features. *Apidium* is represented by an isolated frontal (AMNH 14556) (Simons 1959), a fragmented skull representing only the dorsum of the neurocranium and a portion of the facial skeleton(DPC 9867), and a distorted partial cranium (DPC 5264) (Simons 1995). Radinsky (1974) notes that the endocranial surface of the frontal bone resembles that of many strepsirrhines in having a rostrally placed olfactory fossa and low and unexpanded frontal fossa. Based on the more complete specimens, Simons (1995) observed that the endocranial volume appeared to be considerably smaller than similarly sized platyrrhine monkeys. A well-preserved cranium of *Parapithecus* (DPC 18651) likewise has a low endocranial volume, a smooth endocranial surface, a moderately size and rostrally projecting olfactory fossa, and (as compared to strepsirrhines) an enlarged optic canal (Simons 2001; Bush *et al.* 2004). All told, the

morphology of the Fayum material has been interpreted as evidence for an increased visual acuity, visual sensory integration, and reduced olfactory capabilities in the earliest anthropoid representatives, despite levels of encephalization below that of modern representatives.

1.2 Theoretical Considerations

1.2.1 Cognitive Implications of Brain Size and Brain Proportions

Much debate exists in the literature concerning the relationship between absolute brain size, relative brain size, and 'intelligence'. Jerison (1973) and Holloway (1966) present two seemingly opposing views on the significance of brain volume. Jerison's work emphasizes the importance of brain volume, while Holloway argues that neural reorganization is a key element in differentiating cognitive abilities of various primates. Jerison's "principle of proper mass" proposes that the relative or proportionate size of neural tissue is somehow related to it's computational power and/or to the relative importance of the behavior it controls (Jerison 1973). It is reasoned that the size of the brain or brain region is indicative of the number of neurons it contains. Jerison's principle has gained support in some cases. Metadata analyses of cognitive performance have concluded that absolute brain size is correlated with general cognitive ability (Deaner *et al.* 2007) and that absolute and relative brain size are correlated with the prevalence of innovative behaviors (Reader and Laland 2002) among primate species. Furthermore, recent studies confirm that neuron density is independent of brain size in

primates, implying that neuron size remains stable across primate species (Herculano-Houzel *et al.* 2007; Gabi *et al.* 2010). As a result, absolute brain size differences among primate species do linearly reflect differences in the number of neurons they contain (Herculano-Houzel *et al.* 2007; Herculano-Houzel 2009; Gabi *et al.* 2010). Significantly, this scaling trend differs from that of rodents and other mammals (Haug 1987; Herculano-Houzel 2007), whose neuron size increases and neuron density decreases with body mass. For example, a macaque monkey has over four times as many neurons in its cerebral cortex than the similarly size brain of a large-bodied aquatic rodent, the capybara (Herculano-Houzel 2007; Herculano-Houzel *et al.* 2007). In part, this may explain why primates appear to possess greater cognitive skills than non-primate mammals of similar absolute brain size, while also providing a mechanism supporting the notion that increased brain size in primates reflects increased in intelligence. Nevertheless, Jerison's principle does not take into account the internal structure of the brain, including neural connectivity, or the presence and absence of specialized neural regions, factors that have been argued by many to be at least as important to cognitive function as brain volume (Holloway 1966; Healy and Rowe 2007).

Often discussed as an opposing view to Jerison's principal of proper mass, many researchers stress the importance of neural reorganization over sheer size of the organ(Holloway 1966; Holloway 1974; Holloway 1978; Holloway 1979; Holloway *et al.* 2004). Holloway *et al.* (2004) define brain reorganization as "differences in the

quantitative relationships between brain nuclei and fiber tracts among different primate species" (p.1), and note that difference in neural wiring can occur among individuals or species without significant concomitant changes in the volume of the whole brain or its components. Unfortunately, the microstructure of the brain does not fossilize, but reorganization involving localized volume changes may be preserved in the shape of the endocast (Holloway 1974; Holloway 1978; Preuss 2001). Many workers now argue that the contrast between brain size and neural reorganization is a false dichotomy, and that both aspects of brain evolution—size and structure—are likely to be vital in determining cognitive abilities (Gould 2001; Jerison 2001; Falk 2007).

1.2.2. Strepsirrhine/Anthropoid Cognitive Differences

If we accept the implications of Jerison's principal of proper mass—that is that the enlargement of specific brain regions in one clade over another reflects a functional and adaptive differences between taxa—then we may make several predictions concerning the differing cognitive and sensory abilities in strepsirrhines versus anthropoids. Compared with extant strepsirrhines, extant anthropoids have enlarged visual processing centers (occipital lobes, lateral geniculate region) of the brain and reduced olfactory bulbs (Stephan and Andy 1969; Radinsky 1974; Smaers and Soligo 2013), indicating a reduced reliance on olfactory cues, and greater reliance on visual cues for foraging and communication. Williams et al. (2010) summarize the evidence for the reduction of olfactory reliance in anthropoids as a two step process, beginning with a

reduction in the size of the olfactory bulb and associated receptor epithelium in stem haplorhines, and a subsequent reduction in olfactory function in catarrhines. This is generally supported by genetic evidence indicating that, among Catarrhini, nearly half of the olfactory receptor genes do not functionally code for receptor proteins, supporting a loss of olfactory function in this group (Gilad *et al.* 2004; Niimura and Nei 2007). Likewise, a corresponding increased reliance on visual capabilities in anthropoids is supported by measurements of high visual acuity (the ability to distinguish two nearby objects as distinct) (Kay and Kirk 2000; Williams *et al.* 2010), nearly ubiquitous diurnality (only one species of anthropoid, *Aotus*, is nocturnal), and potentially greater incidences of trichromacy among anthropoid species, as compared to strepsirrhines (Heesy and Ross 2004; Jacobs 2008; Williams *et al.* 2010).

An increase in the relative size of the cerebellum and cerebral hemispheres (especially the neocortex) in anthropoids also suggest that anthropoids possess greater capacities for executive decision-making, critical thinking, and complex learning, and speed and precision in motor control and motor learning as compared to strepsirrhines.

Unfortunately, little data exists concerning the cognitive complexity of strepsirrhines or tarsiers. Strepsirrhines and tarsiers are rarely the subject of cognitive performance tests used for anthropoid species, preventing direct comparison among these groups. Recent research has demonstrated that at least some strepsirrhine primates share several key cognitive traits with extant anthropoid species. Scheumann et al. (2007)

take a comparative approach to review evidence for predator recognition and avoidance strategies among strepsirrhine species. Anecdotal reports of behavioral responses to predator calls, during natural contexts and/or playback experiments, indicate that most of the included strepsirrhine species demonstrate evidence for semantic calls and sophisticated predator avoidance strategies (i.e. "mobbing"). The authors conclude that these strepsirrhines possess similar cognitive abilities vital to predator recognition as those previously reported for anthropoid primates (Scheumann *et al.* 2007). Tests of memory recall and number ordering shows that *Lemur catta* is able to learn serial lists of items and recall these lists with speed and accuracy rates on par with those reported for anthropoid monkeys (*Macaca*, *Cebus*), suggesting they may use similar cognitive mechanisms for mentally organizing these kinds of information (Merritt *et al.* 2007).

In spite of the above, some evidence does exist to support differences in neurocognitive abilities between anthropoid and strepsirrhine clades. In a comparison of four lemur species on a food competition task, Sandel et al. (2011) found that only one species (*Lemur catta*) utilized social cues to avoid feeding competition when faced with a human competitor. They conclude that the use of visual perception cues—the ability to reason that a competitor's gaze or posture indicates they are aware of the subject's actions—likely evolved independently in ring-tailed lemurs and anthropoids, as a result of convergent levels of social complexity. In contrast, the other strepsirrhines sampled diverged from anthropoids in their inability to utilize these social cues (Sandel *et al.*

2011). Limited experimental evidence likewise suggests that anthropoid primates outperform strepsirrhines on tests of sensorimotor control and inhibiting trained responses to stimuli (Gibson *et al.* 2001). Due to a dearth of comparative data, it is not as yet possible to directly examine the relationship between clade specific cognitive abilities and aspects of endocranial shape, however, these studies provide initial steps towards determining how differences in brain proportion and neural wiring may affect cognitive abilities among primates.

1.2.3. "Developmental Constraints Hypothesis"

In contrast to the traditional emphasis on the adaptive implications of varying mass of brain components, the "developmental constraints hypothesis" predicts that brain regions will evolve in concert. According to this hypothesis, changes in the size of one brain region will cause correlated changes in other regions such that "major brain structures grow or shrink together in evolution" (Finlay et al. 2001: 267). Finlay and Darlington (1995) propose that the developmental sequence of neurogenesis is a constraint, such that an increase in one region of the brain will result in corresponding growth in components that develop later in the life of the embryo. Their reasoning for this expectation is that delayed neurogenesis in one region will be correlated with elongated periods of precursor cell formation in that structure. More precursor cells mean a greater potential for neurogenesis in that region (Finlay and Darlington 1995). The "Developmental Constraint Hypothesis" is based on the observation that the order

of development of brain regions is fairly consistent across Mammalia, and that the size of most brain regions are highly predictable from overall brain size. Furthermore, among mammals, body size and phylogeny tend to have less effect on the size of brain components than the covariance between structures (Finlay *et al.* 2001). If this hypothesis is correct, it may mean that the enlargement of some brain regions was not selected for, and is therefore not a 'true' adaptation, that is, the enlargement of one region relative to body or brain size may be an unintentional—though not necessarily non-functional—consequence of selection for increased total brain size.

The Developmental Constraints Hypothesis has not gone unchallenged. In a multivariate cluster analysis of brain component mass, de Winter and Oxford (2001) find that the mass of brain components is tightly linked to body mass; however, lineage-specific scaling patterns have evolved independently among multiple mammalian groups, and parallel selective pressures explain similar patterns of regional expansion within clades. For example, atelids and hominoids show similar patterns of brain proportions, as evidenced by adjacent locations in the multivariate space generated from residual mass of brain regions, and the authors attribute this similarity to a convergent forelimb dominated locomotor repertoire (de Winter and Oxnard 2001). In a comprehensive analysis of scaling patterns among the masses of variation brain components, Barton and Harvey (2000) find compelling evidence for independent selection on functionally distinct brain components. Their analysis supports the

hypothesis that correlated evolution in the residual mass of functionally linked brain components does occur independent of other brain systems. The authors conclude that:

> " Although there may be some constraints on evolutionary change in individual neural systems, tending to result in coordinated evolution among the majority of brain structures, such constraints are evidently insufficiently tight to prevent the type of system-specific change documented here." (p. 1057-8).

A logical extension of the developmental constraints hypothesis is that increases in the size of brain components should accompany increases in overall brain size, with the proportions of brain components remaining stable. If Finlay and Darlington's (1995) hypothesis is correct, mosaic evolution in the size of brain components should not occur, or should only do so rarely in the face of very strong selective pressures. To the extent that endocast shape reflects brain proportions, we would expect that a fundamental shift in endocranial proportions would indicate a change in the developmental paradigm. The expectations of the developmental constraints hypothesis would be violated if grade-shifts in brain proportion precede, rather than accompany changes in overall brain size. This study examines the co-variation among residual mass of brain components and endocast shape, and includes information from the fossil record to determine the order of acquisition of endocast shape and volume changes in anthropoid evolution.

1.2.4. Coevolution of the Brain and Skull

Numerous studies concerning co-variation of cranial traits indicate that the mammalian skull demonstrates patterns of both independent and correlated evolution among the neurocranium, basicranium, and facial skeleton (Lieberman *et al.* 2000b; Lieberman *et al.* 2000c; Porto *et al.* 2009). The cranium is a highly modular organ, though patterns of integration among various functional and developmental modules have been noted in primates (Ackermann and Cheverud 2004; Porto *et al.* 2009). Highly integrated sets of landmarks, which are independent of other landmark sets are considered "modules", whereas "integration" refers to the tendency of landmark features to co-vary more tightly with one another than with landmarks outside the module. It is thought that traits which are developmentally or functionally linked to one another will have higher degrees of co-variation (Olson and Miller 1958). Within the cranium, Ackermann and Cheverud (2004) note that differing functional and spatial constraints, as well as discrete hormonal and developmental cascades influence the neurocranium and facial skeleton. Nevertheless, these two regions are joined at the cranial base, and co-variation between the neurocranium and face are frequently discussed, particularly in terms of their relationship to basicranial morphology (Enlow and McNamara 1973; Enlow and Azuma 1975; Ross and Ravosa 1993; Ross and Henneberg 1995; Ross 1995; Lieberman and McCarthy 1999; Lieberman *et al.* 2000a; Lieberman *et al.* 2000b; Lieberman *et al.* 2000c; McCarthy and Lieberman 2001; Bruner *et al.* 2004; Zollikofer *et al.* 2005; Bastir *et al.*

2008; Lieberman *et al.* 2008; Bastir *et al.* 2010). Noteably, Goswami (2006) does not find support for the hypothesis that basicranial structure is highly integrated with other cranial modules across Mammalia. He finds, that although the basicrania itself forms a strongly supported module, it has low levels of integration with the neurocranium and facial skeleton. These differing conclusions may be due to differing definitions of the basicranial module, as Goswami (2006) notes that Lieberman's (Lieberman *et al.* 2000c) "basicranium" includes landmarks from two separate modules—the basicranium and the zygomatico-pterygoid regions.

Variation in brain size, brain shape, and brain proportions (e.g. the frontal lobe, olfactory lobe, and cerebellum) have each been proposed as explanatory variables for differences in overall cranial form between strepsirrhine and anthropoid primates. In a geometric morphometric analysis of overall cranial shape, Fleagle et al. (2010) demonstrated that anthropoid primates primarily differ from strepsirrhines in the orientation of their bony eye sockets and the angle with which their braincase and facial skeleton are hafted to one another (basicranial angle) (Fleagle *et al.* 2010). Interestingly, variation in both of these traits have been linked to brain size in extant primates for either adaptive reasons, or as a result of evolutionary or spatial constraints on morphology (Ross and Ravosa 1993; Ross 1995; Lieberman *et al.* 2000b; Lieberman *et al.* 2000c; Bastir *et al.* 2010).

Several workers have proposed a link between encephalization and the midline morphology of the cranial base (Biegert 1963; Gould 1977; Ross and Ravosa 1993; Ross and Henneberg 1995; Lieberman *et al.* 2000c). The enlargement of the brain relative to the length of the basicranium (endocranial midline surfaces of the basioccipital, sphenoid, and ethmoid) may result in a concerted anterior, posterior, and dorsal expansion of the endocranial space, thus causing a reduction in the angle formed by the anterior and posterior cranial base, around the midline point of the pituitary fossa (Biegert 1963; Hofer 1969; Jerison 1982; Ross and Ravosa 1993; Lieberman and McCarthy 1999; Lieberman *et al.* 2000c; Bastir *et al.* 2010). Thus, there is a shortening of the distance between basion (anterior point of foramen magnum) and the posterior extent of the palatine process (Ross and Ravosa 1993). Among non-human primates, it has been demonstrated that the angle of the cranial base is correlated with encephalization in interspecific comparisons of adult representatives of anthropoid species (Ross and Ravosa 1993; Lieberman *et al.* 2000c). However, basicranial angle was not found to co-vary with relative brain size among strepsirrhine primates (Ross and Ravosa 1993), or within an ontogenetic series of human fetal specimens (Jeffrey and Spoor 2002). Thus, the proximate mechanism for basicranial flexion remains cloudy, but Lieberman et al. (2000) note that the relationship between brain size and cranial base flexion may be strongly related to constraints on endocranial shape during encephalization. Among primates, a reduction in olfactory bulb size and increase in orbital convergence may

cause a spatial packing problem in which the brain must expand rostrally over the orbits, and dorsally, such that the brain achieves a more spherical or globular shape (Lieberman *et al.* 2000c), see Figure 3. If true, this version of the Spatial Packing Hypothesis would predict a relationship among encephalization, the shape of the endocranial outline, and flexion of the cranial base. This study tests these predicted relationships using midline tomographs of extant and fossil primates.

1.2.5. Tarsier Brains and Their Implications for Haplorhine Brain Evolution

Historically, the phylogenetic relationship of tarsiers to anthropoids and strepsirrhines has proved controversial due to a mosaic of behavioral, ecological and morphological traits demonstrated by this group. On the basis of shared primitive traits, Gregory (1915) classified tarsiers together with strepsirrhines in the group Prosimii; however, analyses using cladistics approaches have generally favored the placement of tarsiers as a sister group to anthropoids (suborder Haplorhini), as suggested by Pocock (1918) on the basis of shared sensory and reproductive features. Most recent analyses of genetic and morphological evidence strongly support a close phylogenetic relationship between tarsiers and anthropoids (Zietkiewicz *et al.* 1999; Schmitz *et al.* 2001; Waddell *et al.* 2001; Yoder 2003; Perelman *et al.* 2011).

Although the majority of researchers now accept the cladistic affinities of anthropoids and tarsiers (i.e. Haplorhini), the diversity of taxa within Tarsioidea

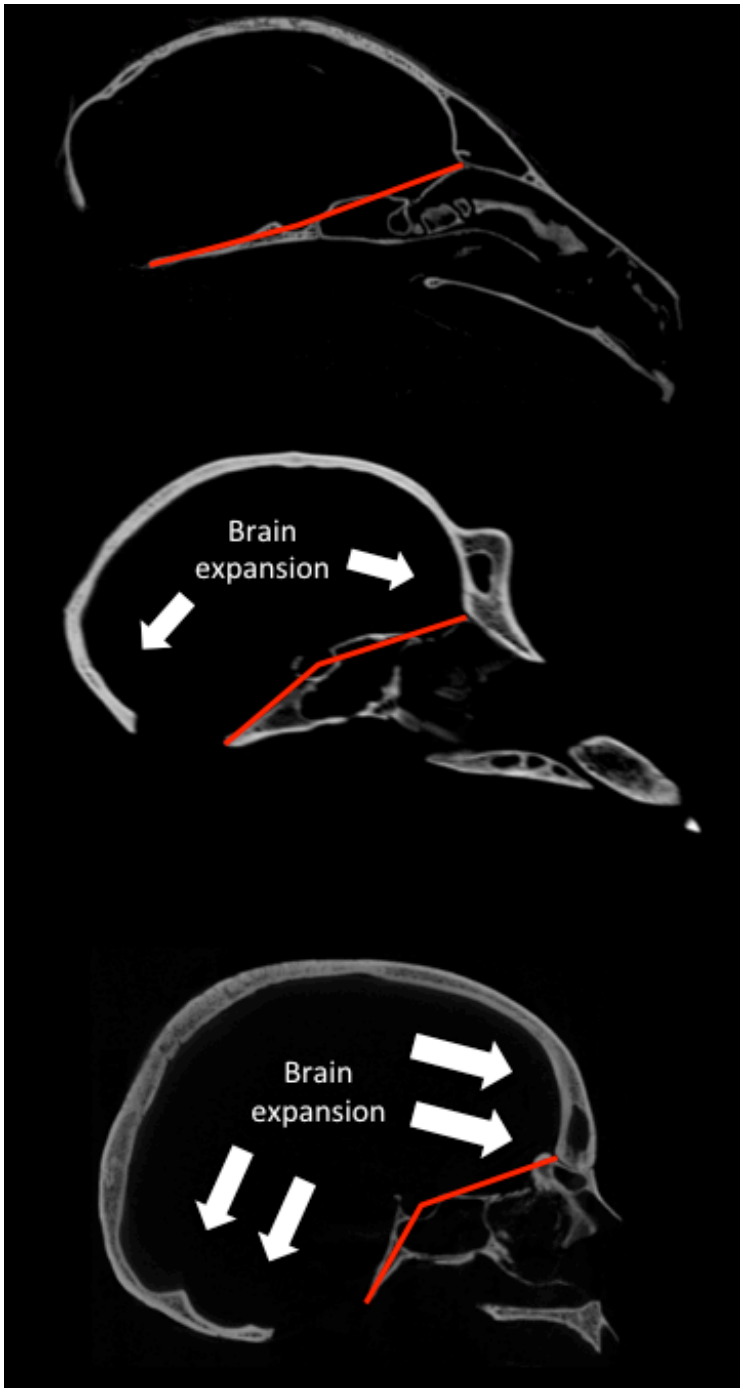

Figure 3: Midsagittal tomographs of a lemur (top), ape (middle), and human (bottom), illustrating the proposed relationship among increasing encephalization, sphericity of the endocranial shape, and increasing basicranial angle (highlighted in red). Modeled after Figure 1 in Ross and Ravosa (1993).

remains uncertain. Tarsiers have traditionally been lumped into a single genus—*Tarsius*—with species level distinctions diagnosed primarily on pellage, basicranial osteology, and geographic distribution (Hill 1955; Musser and Dagosto 1987). Recently, Groves and Shakelle (2010) propose that Tarsioidea contains at least three distinct genera distinguished by geographic distribution, morphological features and patterns of acoustic repertoire: *Tarsius* (Phillipine tarsier), *Cephalopachus* (Western tarsier), and *Carlito* (Eastern tarsier). The authors suggest that the taxonomic and behavioral diversity in this group has been underestimated due to a lack of study of the Western and Eastern tarsier groups (Groves and Shekelle 2010). Despite the variation described in acoustic style, which may act as a mate recognition complex in this group (Shakelle 2008), the authors describe only minor variation in cranial form among these proposed groups (Groves and Shekelle 2010). As such, the tarsioid specimens included in this thesis (*Tarsius* (= *Carlito*) *syrichta* and *T.* (= *Cephalopachus*) *bancanus*) are considered as a single group.

Despite being the closest living phylogenetic outgroup to anthropoids, tarsiers are often neglected in discussions of the adaptive implications and timing of encephalization and mosaicism in the relative mass of brain components among haplorhine primates by reference to their strepsirrhine-like levels of encephalization (Stephan and Andy 1964; Stephan and Andy 1969; Radinsky 1974; Stephan *et al.* 1981). Nevertheless, among those limited numbers of studies in which they have been

included, tarsiers have been demonstrated to possess key similarities in brain proportions and architecture with anthropoids. Although Stephan and colleagues (Stephan and Andy 1964; Stephan and Andy 1969; Stephan *et al.* 1988) conclude that tarsiers are strepsirrhine-like in their anatomy based solely on their level of encephalization, Joffe and Dunbar (1998) re-analyzed their dataset from a cladistic perspective and arrived at a very different conclusion. On the basis of the relative mass of brain parts, the authors conclude that tarsiers share key derived traits with anthropoids, thus supporting the monophyly of Haplorhini. When the mass of brain components is regressed on brain size, and the resulting residuals are regressed on a measure of encephalization (Jerison's (1953) encephalization quotient, EQ), Joffe and Dunbar (1998) show that tarsiers more closely resemble anthropoids than strepsirrhines in having some reduction of the olfactory bulb, an enlarged neocortex, reduced paleocortex, and particular elaboration of the visual centers of the brain—the primary visual cortex and lateral geniculate nucleus—for their absolute and relative brain size. Wong et al. (2010) draw a similar conclusion in their description of the architectural anatomy of the tarsier brain in comparison to the strepsirrhine *Otolemur* and platyrrhine *Aotus*.

The tarsier brain is described as having cellular differentiation of the layers of the lateral geniculate nucleus—a visual processing center of the brain—similar to that of extant anthropoids, rather than strepsirrhines, and a particularly large primary visual

cortex, with distinct differentiation of the cellular layers reminiscent of analogous systems in birds of prey (Wong *et al.* 2010). Additionally, the auditory system is elaborated in tarsiers (Wong *et al.* 2010), which is consistent with many aspects of its known behavior. Observations during feeding suggest that tarsiers use auditory cues to locate and visually orient to prey (Bishop 1964), and recent analyses of their auditory communication reveal that spectral tarsiers are able to produce and aurally process ultrasonic vocalizations—well above the range typically perceptible by primates—to communicate with conspecifics (Gursky-Doran 2012; Ramsier *et al.* 2012).

Tarsier endocranial morphology is likewise rarely considered in studies of correlated evolution between encephalization and cranial form. Radinksy (1975) depicts a lateral view of the tarsier endocast in his discussion of mammalian brain shape, but mentions the specimen only briefly in relation to the effects of the extreme orbital size on the orientation of the splanchnocranium. In their comparisons of strepsirrhine and anthropoid basicranial flexion and/or craniofacial hafting, Lieberman and colleagues either do not include tarsiers in their sample (McCarthy and Lieberman 2001), or fail to discuss the tarsiers specimens in relation to the strepsirrhine-anthropoid shape dichotomy (Lieberman *et al.* 2000c; Lieberman *et al.* 2008). In their analysis of facial kyphosis, cranial base angulation, and encephalization among primates, Ross and Ravosa (1993) do not discuss the tarsier morphology in great detail, but they do propose that the anthropoid-like cranial "*bauplan*"—in which enlargement of the brain for a

given basicranial length causes correlated changes in orbital and basicranial morphology—may have been in place at the base of the haplorhine clade. Their evidence for this is a significant correlation between encephalization and both basicranial angle and orbital orientation in haplorhines, but not extant strepsirrhines. As the only living sister taxon to anthropoid primates, tarsiers present both an often neglected opportunity to establish polarity and timing of the establishment of anthropoid traits and a puzzle given their unique morphological and ecological specialization.

1.2.6. Importance of the Fossil Record of Brain Evolution

Relatively complete primate fossil crania are now available from basal representatives of many primate clades. Basal anthropoids are particularly well represented in the Late Eocene to Early Oligocene deposits in the Fayum region of Egypt. Endocranial volumes of well-preserved crania of the stem anthropoid *Parapithecus* (=*Simonsius*) and stem catarrhine *Aegyptopithecus* have been measured (Simons 1995; Bush *et al.* 2004; Simons *et al.* 2007), although brain shape has been less rigorously analyzed.

Diagenetic alteration has impeded quantitative analyses of other basal anthropoids from this region (*Catopithecus* and *Proteopithecus*) (Simons and Rasmussen 1994; Simons and Rasmussen 1996; Simons 1997). Stem platyrrhines are represented in the fossil record by moderately to well-preserved Early Miocene crania of *Homunculus* (Kay *et al.* 2006; Kay *et al.* 2012), *Tremacebus* (Kay *et al.* 2004), and *Dolichocebus* (Kay *et al.*

2008) from Argentina, *Chilecebus* (Sears *et al.* 2008) from Chile (not available for use in this study), and a crushed Middle Miocene cranium of *Lagonimico* (Kay 1994) from Colombia. Previous descriptions of Oligocene and Miocene primate endocasts have been largely qualitative with respect to their shape and regional proportions (Simons 1993; Simons and Rasmussen 1994; Simons and Rasmussen 1996; Simons 1997; Simons 2001; Bush *et al.* 2004; Simons *et al.* 2007). For this study, the inclusion of fossil a fossil out-group—euprimates—is critical to the determination of trait polarity. Included in this sample is the late Oligocene omomyoid *Rooneyia* from Texas (Hofer and Wilson 1967) and the Eocene adapid *Adapis* from Europe (Lebrun 2008). These crania provide invaluable direct evidence for brain evolution in the primate order that has in many cases challenged the assumptions of brain evolution based on the study of extant-only character distributions. Furthermore, the use of the euprimate out-group provides a means of recognizing convergence, as opposed to symplesiomorphy among extant primate endocrania.

Fossil data provide an often-neglected temporal perspective to testing of adaptive patterns using comparative methods. Inclusion of fossil species in ancestral character state reconstructions improves the accuracy of these estimates by providing information for additional nodes (branching events) and decreasing the unrepresented distance between the root and tips of the tree (Finarelli 2006; Finarelli and Flynn 2007). This is particularly important in the study of brain evolution, as previous fossil analyses

have revealed multiple occurrences of parallel increases in relative brain size both within and among multiple mammalian orders, including Cetacea (Marino 1998; Marino 2002), Carnivora (Finarelli and Flynn 2007), and Primates (Kay *et al.* 2006; Simons *et al.* 2007; Kay and Kirk 2008; Sears *et al.* 2008; Williams *et al.* 2010; Kay *et al.* 2012). This thesis incorporates fossil data into analyses of endocranial shape and cranial form in order to determine the order of acquisition of traits that have previously been proposed to co-vary and/or co-evolve as a result of spatial and developmental constraints. Furthermore, the data produced by this study will facilitate the incorporation of fossil data into tests of hypotheses about the evolutionary trajectory of primate brain size, a feature that forms part of the core of traits that define the order.

1.2.7. Geometric Morphometrics and Endocast Shape Variation

The field of paleoneurology, once focusing on qualitative descriptions of brain shape and sulcal patterns, has recently benefited from the availability of computed tomography (CT) technology and landmark-based morphometric techniques. Previously, the internal shape of the braincase could only be accessed via natural endocasts (Hrdlicka 1925; Radinsky 1967), latex molds prepared from dry crania (Harris 1926; Le Gros Clark *et al.* 1936; Radinsky 1975), or planar radiographs. In the late 1980s, paleoanthropologists began experimenting with CT-based techniques for estimating endocranial volume in fossil specimens (Conroy *et al.* 1990; Tobias 2001). Technology has advanced such that conventional medical CT and micro-CT scanners are relatively

accessible for documenting the internal anatomy of the cranium, *in vivo* (medical scanners), using cadaveric or dry osteological and fossil specimens. Micro-computed tomography allows the researcher to distinguish matrix from biologically meaningful structures using high-resolution images of fossil specimens. Furthermore, computer-based techniques allow for the creation of "virtual endocasts", forgoing the need to extensively handle the physical specimen or prepare the endocranial cavity for casting.

Three-dimensional geometric morphometric (GM) techniques are useful for quantifying and visualizing shape variation among homologous structures. GM techniques confer an advantage over traditional two-dimensional linear measurements in that they preserve the relationship of all landmark points to one another throughout the analysis, therefore retaining important aspects of shape that may be lost when linear dimensions are considered in isolation (Bookstein 1997; Adams *et al.* 2004; Zelditch *et al.* 2012). Furthermore, the recent innovative use of "sliding semi-landmark" techniques allows for the quantitative description of outlines and surfaces bearing few discretely homologous landmarks, and therefore defying most other attempts at shape quantification. This technique has been particularly useful in quantitatively describing the curvature of ecto- and endo-cranial surfaces (Gunz *et al.* 2004; Neubauer *et al.* 2009; Neubauer *et al.* 2010).

GM analyses of endocasts, segmented from brain MRIs (Aldridge 2011) or from endocranial cavities of dry skulls (Bruner 2004; Neubauer *et al.* 2010; Bienvenu *et al.*

2011), have successfully quantified shape differences between apes and humans. Human "neurocranial globularity", or the degree of spherical geometry of the brain, has been found in these studies to be associated with dorsal and lateral expansion of the brain. This reflects the expansion of the neocortex and reorganization of the frontal and parietal lobes in human evolution (Aldridge 2011; Bienvenu *et al.* 2011). These studies quantify and visualize aspects of hominoid endocranial shape variation that were previously described qualitatively, and have examined the progression of these traits in the hominin fossil record (Zollikofer *et al.* 1998; Bruner 2004; Bastir *et al.* 2008).

A conspicuous gap I address herein is that the application of geometric morphometric techniques have not been applied to examine aspects of shape variation potentially related to the divergence of haplorhine and strepsirrhine primates. It is therefore unknown the degree to which the early anthropoid fossil specimens differ from extant primate representatives, or from Eocene adapoids and omomyoids. Quantification of these shape variables will allow us to test the extent to which they have changed over time, and to explore their relationship to aspects of cranial form. Analysis of endocranial shape may provide further insight into regional brain enlargement, brain reorganization, and developmental spatial constraints imposed on encephalization by identifying localized regions of change between and within clades. Furthermore, the quantification of global and regional shape change provides shape

variables that can be used in subsequent analyses of the association with endocranial volume, ecto- and endocranial form.

1.3. Outline of Thesis Purpose

The objectives of this study are as follows: 1) analyze endocranial shape in living and fossil primates, via geometric morphometric analyses of virtual endocasts, in order to identify global and regional shape differences that characterize living and fossil primates; 2) evaluate the relationship between brain size, brain shape and features of overall cranial form (orbital convergence, basicranial flexion) in fossil and living primates.

Chapter two addresses the first objective using a geometric morphometric approach. I explore variation in endocranial shape among extant primate species using three-dimensional landmark data, collected from virtual endocasts generated from micro-CT scans of extant and fossil primates. Landmark data is used to test the prediction that interspecific differences in endocranial shape co-varies with differences in absolute and/or relative brain size or the size of brain components. Endocranial shape and volume is assessed for fossil anthropoid specimens from the Early Oligocene of Egypt, and the Middle Miocene of Argentina, representing stem anthropoids (*Parapithecus*), stem platyrrhines (*Homunculus, Tremacebus*), and stem catarrhines (*Aegyptopithecus*) to determine whether these specimens conform to expectations of co-variation among traits over evolutionary time.

The third chapter focuses on the interaction between the brain size and cranial organization (objective 2). These analyses seek to test predictions made by the "Spatial Packing" and "Facial Packing Hypotheses" concerning the co-evolution of the brain and overall shape of the cranium. In particular, I examine the relationship between: i) endocranial globularity—the tendency of the brain to approximate a sphere—and encephalization, ii) the variation in the size and shape of the endocranium with that of the midline facial skeleton. iii) endocranial size and midline shape and aspects of cranial organization, including basicranial angle, palate angle, and facial hafting—the orientation of the anterior cranial base relative to the facial skeleton.

2. Endocast Shape in Primate Evolution

2.1. Introduction

Extant anthropoid primates differ from strepsirrhines and tarsiers in having larger brains for their body size (Stephan and Andy 1964; Stephan and Andy 1969; Stephan *et al.* 1981). Much emphasis has been placed on these differences; however, evidence suggests that haplorhine primates (anthropoids + tarsiers) have undergone a reorganization of the brain since their divergence from strepsirrhines, and differences in brain proportions, not just encephalization, more fully characterize the evolutionary divergence of these groups (Joffe and Dunbar 1998). In particular, haplorhine primates have enlarged telencephalon relative to brain and body size (the anterior-most embryonic subdivision of the brain, which develops into the mature cerebral cortex, hippocampus, basal ganglia, and olfactory bulb)—with a particular elaboration of the visual processing centers—visual cortex, tractus opticus, corpus geniculate lateralis—and a reduction of the olfactory bulb (Stephan and Andy 1964; Stephan and Andy 1969; Stephan *et al.* 1981; Smaers and Soligo 2013).

Overall increases in encephalization and changes in component proportions have anecdotally been linked to endocast shape differences between strepsirrhine and anthropoid primates (Radinsky 1974; Simons 2001), while tarsiers are rarely discussed in these comparisons. Although the fossil record for early anthropoid evolution demonstrates that early representatives of anthropoid subclades are small-brained, and

thus encephalization must have occurred in parallel between these groups (Simons 2001; Kay *et al.* 2006; Simons *et al.* 2007; Kay and Kirk 2008; Sears *et al.* 2008; Kay *et al.* 2012), qualitative descriptions of these endocasts emphasize a shift toward anthropoid-like traits at a small brain size (Simons 2001; Bush *et al.* 2004). No prior attempts have been made to quantitatively evaluate the variation in endocranial shape among strepsirrhine and haplorhine primates; therefore, it has yet to be determined whether Radinsky's (1974) qualitative descriptions of the shape dichotomy between "typical" prosimian (lemurs, lorises, and tarsiers) and anthropoid endocasts are quantitatively justified, and whether tarsiers more closely resemble the similarly encephalized strepsirrhines, or their more encephalized phylogenetic sister taxon, the anthropoids.

In the present analysis I use three-dimensional landmark-based techniques to examine endocranial volume and shape in extant and fossil primate species to determine whether brain size differences are predictably related to differences in brain shape and proportion within and between the strepsirrhine and haplorhine clades across an evolutionary time scale. I take both an indirect approach in comparing the variation in these features among extant primates, and then examine the direct evidence for primate brain evolution (fossil endocasts) to evaluate the order of acquisition of these traits.

2.2. Materials and Methods

2.2.1. Micro-CT Scans of Extant Primates

Data was collected on virtual endocasts created from medical and micro-CT scans of crania from extant and fossil primates. The extant sample includes 107 specimens representing 20 platyrrhine, 26 catarrhine, and 14 strepsirrhine genera (n = 1 to 5 specimens per genus). Scans were borrowed from a variety of sources, following requests from: research collections belonging to R.F. Kay and J. Rossi, the American Museum of Natural History (specimen prefix AMNH), the Smithsonian Institute of Human Origins (provided by M. Tocheri), the Digital Morphology Museum at Kyoto University (www.pri.kyoto-u.ac.jp/dmm/WebGallery/index.html), and the European Virtual Anthropology Network (EVAN) Archives (www.evan-society.org). Borrowed computed tomography scans of dry crania were conducted on a variety of machines housed at multiple institutions, including: the University of Texas at Austin Computed Tomography Laboratory (UTCT), Penn State University Center for Quantitative Imaging, Kyoto University Primate Research Institute, and the American Museum of Natural History Microscopy and Imaging Facility. Additional specimens from the Smithsonian National Museum of Natural History (specimen prefix USNM), Duke University Primate Center (DPC), and Duke University Biological Anthropology and Anatomy osteological collection (specimen prefixes BAA, Kay) were micro-CT scanned

at the Duke University Shared Materials Instrument Facility. Specimen numbers and museum sources are listed in Table 1.

Voxel dimensions for the scan collection range from 0.002mm to 0.5mm, depending on the scanning instruments and the size of the cranium. Scanning resolution will affect the bony detail captured by some scans relative to others as a result of the maximum scanning parameters allowable by the machine (maximum achievable resolution, maximum field of view). For example, on a given machine a smaller specimen may achieve higher resolution scan if the resolution is limited by the field of view of the detector. Conversely, a scanner whose resolution is independent of object size would produce a scan with a greater number of voxels within the endocranium of a large-bodied animal than a small-bodied animal. In this case, there would be a greater potential to capture surface detail in the larger-bodied animal. Thus, a cranial scan may have greater or lesser resolution relative to the body size of the animal, depending on the scanner type and adjustability of its parameters. To account for this possibility (to the extent that is possible), and to reduce file sizes for faster processing speeds, scans were down-sampled to a more homogenous resolution, independent of the body size of the animal.

The criterion for scan resampling was as follows: A scan was considered to be of sufficient quality to be included in the analysis if the endocranial cavity was captured in

Table 1: Summary of specimens used in this analysis, including the number of individuals (n) for each genus and the higher order taxonomic classifications for each genus. See text for explanation of specimen number collection prefixes.

Taxonomic Group 1	Taxonomic Group 2	Genus	n	Specimen #
Haplorhini	Platyrrhini	*Alouatta*	2	USNM 51825, USNM 281756
		Aotus	2	Kay 1492, USNM 503920
		Ateles	2	BAAna, Kay
		Brachyteles	1	AMNH 80405
		Cacajao	4	USNM 302626, USNM 319516, USNM 395027, USNM 406427
		Callicebus	3	USNM 269827, USNM 397933, USNM 406416
		Callimico	3	USNM 30332, USNM 241413, USNM 395455
		Callithrix	2	USNM 503885, USNM 503895
		Cebuella	1	USNM 337324
		Cebus	2	USNM 338960, USNM 518268
		Lagothrix	1	Kay
		Leontopithecus	1	USNM 337333
		Mico	1	USNM 239463
		Pithecia	1	Fleagle NP5
		Saguinus	3	Kay1492, USNM 518577, USNM 306845
		Saimiri	2	USNM 398699, USNM 518538
	Cercopithecoidea	*Cercocebus*	1	KUPRI 1030
		Cercopithecus	5	AMNH 52483, USNM 453574, USNM 453581, 481007, 481770
		Chlorocebus	1	USNM 381445
		Colobus	4	KUPRI 1043, KUPRI 1100, KUPRI 1103, KUPRI 1105
		Erythrocebus	1	USNM 270440
		Lophocebus	1	KUPRI 1725
		Macaca	1	KURPI 1701
		Mandrillus	1	KUPRI 1487
		Miopithecus	1	Kay
		Nasalis	1	USNM 198277
		Papio	4	KUPRI 1677, KUPRI 3390, KUPRI 44450, KUPRI 7147
		Piliocolobus	1	USNM 481795

		Presbytis	3	AMNH 113723, USNM 121668, USNM 121692
		Procolobus	3	USNM 477327, USNM 477331, USNM 481792
		Semnopithecus	2	USNM 122634, USNM 196986
		Simias	2	USNM 121654, USNM 121663
		Theropithecus	1	KUPRI 9030
		Trachypithecus	2	USNM 257685, USNM 277618
	Hominoidea	*Gorilla*	1	KUPRI 7219
		Homo	1	ULAC 012
		Hylobates	1	USNM 11989
		Pan	5	KUPRI 9783, USNM 176238, USNM 236971, USNM 297856, USNM 395820
	Tarsioidea	*Tarsius*	3	DPC 045, DPC 0127, USNM
Strepsirrhini	Lemuroidea	*Daubentonia*	1	AMNH 185643
		Eulemur	3	DPC 057, DPC 058, DPC 061
		Hapalemur	1	DPC 1311
		Indri	1	AMNH 100506
		Lemur	1	AMNH 100596
		Lepilemur	1	AMNH 170563
		Microcebus	1	DPC 098
		Mirza	2	DPC 0137 , DPC 1139
	Lorisoidea	*Varecia*	1	DPC 050
		Loris	1	AMNH 16593
		Nycticebus	2	BAA 0002, BAA 0161
		Galago	1	AMNH 187355

at least 300 coronal slices. Many of the microCT scans obtained for this study have voxel sizes such that the endocranial cavity was depicted by greater than 400 coronal slices; in these cases, the scans were resampled to 512 x 512 voxels in the medial-lateral (x) and superior-inferior (y) aspects, with a slice thickness (z) adjusted to fit 400 slices through the endocranium. A detailed list of the scanning sources, resolutions, and resampled voxel dimensions is presented in Appendix A.

2.2.2. Fossil Specimens

The fossil sample includes six species: the *incertae sedis* euprimates *Adapis* (Adapoidea, Late Eocene), *Rooneyia* (Omomyoidea?, Early Oligocene), early anthropoids *Parapithecus* (Parapithecidae, Early Oligocene) and *Aegyptopithecus* (Propliopithecidae, Early Oligocene), and Early Miocene stem platyrrhines *Homunculus* and *Tremacebus* from Patagonia, Argentina.

While the degree of matrix filling and post-mortem damage varied by specimen, the fossils sampled here are the most complete and minimally distorted specimens. The Eocene sample comes from the Eocene deposits of Quercy, France, and includes a well-preserved cranium of *Adapis parisiensis* (ACQ209) and a cranium of *Leptadapis magnus* (ACQ208), which has some damage to the dorsum of the neurocranial vault in the frontoparietal region (Lebrun 2008). Both specimens exhibit highly dense matrix filling of the endocranium, which was in some cases difficult to distinguish from the cranial material. Careful inspection of surrounding material allowed for interpolation of the ambiguous regions, and I would expect that these choices have only minimal effect on the resulting shape and volume of the endocast.

Parapithecus (= *Simonsius*, Gingerich (1978)) *grangeri* is represented in this sample by a well preserved adult cranium (DPC 18651), from the Early Oligocene deposits (Quarry I) of the Jebel Quatrani Formation, Egypt (Simons 2001). The specimen is relatively undistorted and complete but for the loss of the upper anterior dentition

(incisors, canines) and left zygomatic arch. The endocranial cavity is filled with a sandstone matrix, necessitating manual segmentation of the endocast. Previous estimates of endocranial volume (11.4cm^3) and olfactory fossa volume (75mm^3) were generated by Bush *et al.* (2004).

Aegyptopithecus zeuxis is represented by a complete subadult cranium (M^3 erupting) from the Early Oligocene Jebel Qatrani Formation, Egypt (Simons *et al.* 2007). The neurocranium of this specimen has some breakage and plastic distortion, including damage to the superior margin of the orbit, and the medial displacement of a portion of the right temporal, near pterion (Simons *et al.* 2007). The shape of the foramen magnum, in particular, reveals distortion of the basioccipital region, resulting in a mediolaterally-constricted foramen. In most cases, the affected regions can be manually interpolated based on surrounding morphology, and the resulting endocast displays only minor asymmetry due to plastic deformation.

Both Miocene platyrrhines *Homunculus patagonicus* (MPM-PV 3502, Early Miocene, Santa Cruz Formation, Santa Cruz Province, Argentina) and *Tremacebus harringtoni* (Rusconi collection, Early Miocene, Sarmiento Formation, Chubut Province, Argentina) specimens exhibit significant amounts of localized fragmentation. MPM-PV 3502 preserves the facial skeleton, neurocranium, and cranial base of the right side, while a significant portion of the left half of the neurocranium is missing (Kay *et al.* 2012). Nevertheless, the well-preserved structure of the remaining portion allows for the

reconstruction of the anterior endocast and right middle and posterior cranial fossae. Thus, the full morphology of the right side is well preserved. The Rusconi skull of *Tremacebus* is missing small pieces of the parietal and frontal region of the neurocranial vault, as well as a large component of the occipital region (Kay *et al.* 2004). While the parietal regions of the endocast can be interpolated based on the surrounding contour and principals of symmetry, the morphology of the occipital poles, vermix, and posterior cerebellum cannot be interpreted from the available material. As such, this skull will be evaluated more qualitatively, described in terms of its visible morphology as it compares to the more complete fossil anthropoid specimens.

2.2.3. Data Collection

The endocranial cavity was segmented from tomographs in the coronal plane, using a combination of grey scale thresholding and manual segmentation in the software *Avizo*, version 7.1 (FEI Visualization Sciences Group 2013). When a clear contrast between bone (high density) and adjacent air (low density) is apparent, it is possible to label a range of grey scale values as "air", using the wand tool, with a limit line to constrain the selection to the endocranial area and prevent the selection from "bleeding" through sutures or foramina (i.e. grey scale thresholding). The brush tool was used to manually add and remove volume from the outlined cross-section in cases where the grey scale histogram provided less contrast between the two materials. This manual segmentation method is more subjective, but necessary for specimens in which

matrix prevented a clean separation between the neurocranium and endocranial space using one simple threshold. This was particularly common with the fossil specimens, each of which required at least some degree of manual segmentation. The volume of the segmented material (endocranial volume, ECV) was measured in cm^3 using the "Material Statistics" module of *Avizo*. The resulting virtual object was rendered as a polygon mesh surface file (.ply file type), and landmarks were placed on the surface renderings in *Avizo* using the "Landmark Editor" module.

Landmarks were chosen to represent the overall shape of the endocast, including the maximum length and breadth of the object, the relative size and position of the olfactory fossa, the anterior projection of the temporal poles, the flexion of the endocast base, and the position of the posterior extent of the cerebral hemipheres (landmark: occipital pole) relative to that of the cerebellum (landmarks: posterior cerebellum and vermix point). A list of landmarks and landmark definitions is presented in Table 2. Landmark locations are depicted in Figure 4. Landmarks were placed on the right side only, for the following reasons: i) this study is primarily concerned with interspecific differences in overall shape and not patterns of intra-individual bilateral asymmetry, ii) the condition of the fossil specimens in some cases prevented the reliable identification of landmarks on both sides of the endocast, iii) including bilaterally symmetrical landmarks may give greater statistical weight to the lateral morphology, over the midline morphology, in subsequent statistical analyses.

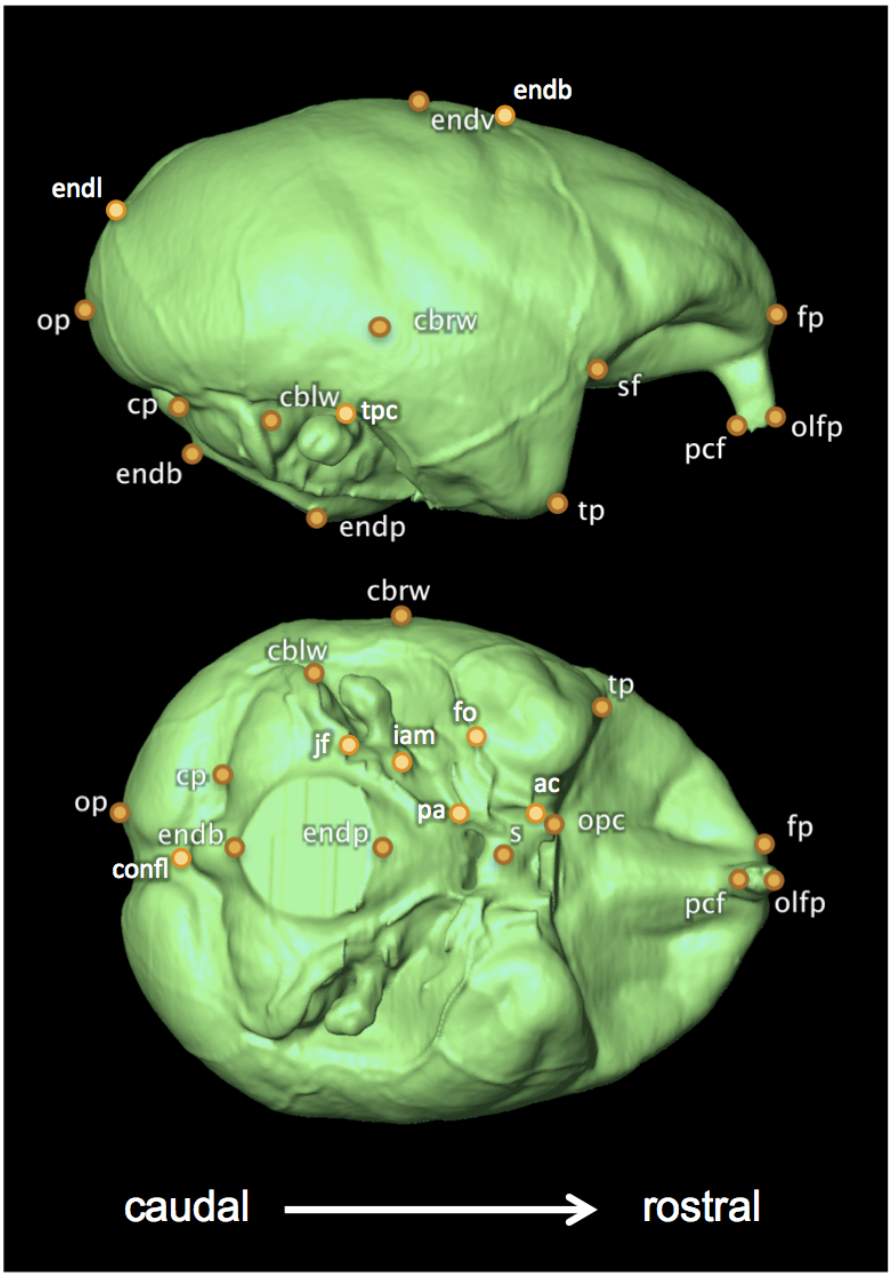

Figure 4: Reconstruction of the endocranial surface of *Saimiri sciureus*, demonstrating landmarks taken on virtual endocasts. Upper: lateral view, lower: inferior view. Abbreviations refer to landmark definitions in Table 2. Distance from the frontal-occipital pole = 49.49mm.

Table 2: Names and definitions of landmarks collected on virtual renderings of the endocanial surface. Landmark abbreviations refer to the landmarks pictured in Figure 2.

Abbrev.	Landmark	Definition
fp	frontal pole	rostral-most projection of the frontal lobe (anterior cranial fossa)
op	occipital pole	posterior-most projection of the occipital lobe
endv	endovertex	superior-most point on the endocast surface when oriented in the fronto-occipital plane
endb	endobregma	the endocranial surface marking for the point at which the coronal and sagittal sutures intersect
endl	endolambda	the endocranial surface marking for the point at which the sagittal and lambdoidal sutures intersect
confl	confluence of sinuses	the midpoint of the intersection between the endocranial surface markings for the intersection of the transverse and sagittal sinuses
endo	endopisthion	the most posterior point of the foramen magnum
endb	endobasion	the most anterior point of the foramen magnum
s	sella	the center of the convexity formed by the sella basin
pcf	posterior cribriform plate	the posterior lateral most point of the cribrifom plate
olfp	olfactory point	the anterior most point of the cribriform plate
opc	optic canal	the center point of the optic canal
ac	anterior clinoid process	the caudal most point on the anterior clinoid process
pa	petrous apex	the point at which the petrous curve ends anteriorly near the sellar basin
tpc	max curve of transverse and petrous curves	the maximum point of curvature between the curve formed by the transverse sinus, and that of the petrous pyramid
fo	foramen ovale	the centerpoint of the foramen ovale
iam	internal acoustic meatus	the centerpoint of the internal acoustic meatus
jf	jugular foramen	the centerpoint of the jugular foramen
cbrw	maximum cerebral breadth	the most lateral point of the cerebral hemisphere with reference to the midsagittal plane
cblw	maximum cerebellum breadth	the most lateral point of the cerebellar hemispheres
cp	posterior cerebellum	the most caudal point of the posterior cranial fossa, on the impression for the cerebellar hemisphere
tp	temporal point	the most anterior-inferior point on the temporal lobe (middle cranial fossa)
sf	sylvian fissure	the point at which the endocranial surface representation of the sylvian fissure terminates at the border with the greater wing of the sphenoid

The olfactory fossa of *Tarsius* presents an unusual condition in which the cribriform plate is situated rostral to the olfactory fossa, at the end of a sizeable canal, which extends anteriorly through the interorbital space. Figure 5 depicts this morphology from a posterior-superior view of the endocranial surface. To produce a

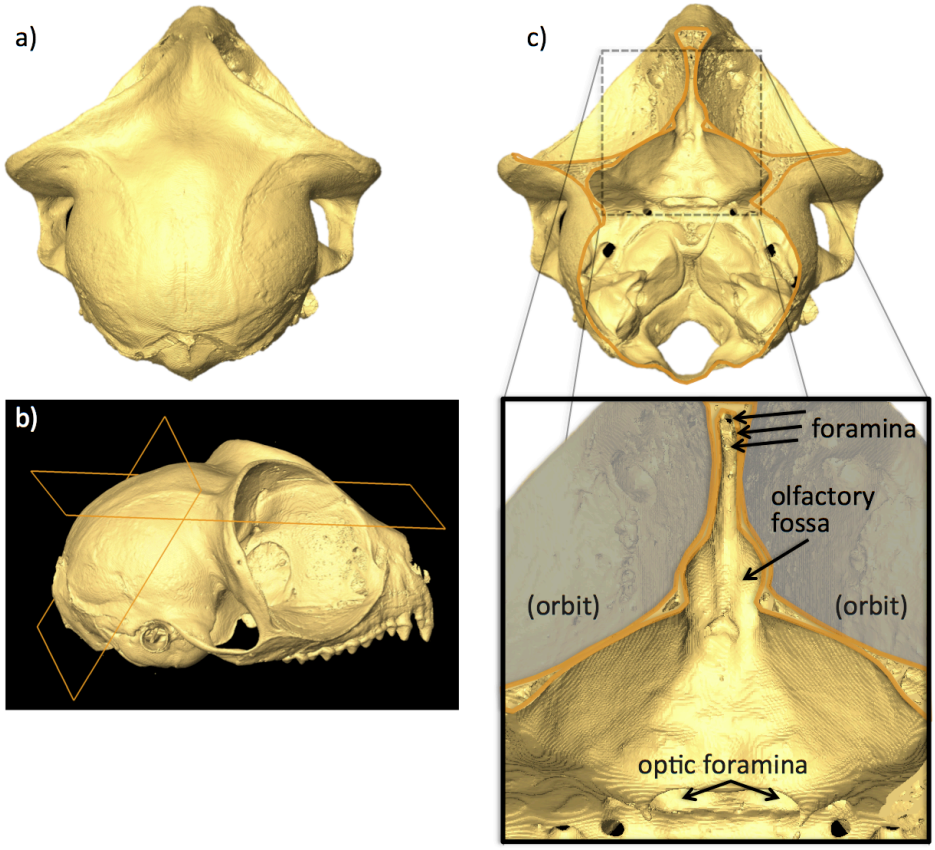

Figure 5: Cutaway illustration of the anterior cranial fossa of *Tarsius* (=*Carlito*) *syrichta* (DPC 045): a) dorsocaudal view of the ectocranial surface as reference for the point of view; b) oblique lateral view of the specimen illustrating the cutting planes (orange lines) applied to the surface, c) reconstructions of cranial surface with cutting planes applied, cranium is oriented in the same view as "a", the black box contains an enlarged view of the anterior cranial fossa. Note the rostral extension of the olfactory canal through the interorbital space and its termination, which contains multiple foramina.

strictly homologous endocast using the criterion applied to other primates in this sample, the canal would be included in the endocranial volume; however, this would produce quite a large addition to the volume of the olfactory fossa, which is not reflected in the moderate size of the olfactory bulb recorded by comparative anatomical data collected by Stephan *et al.* (1981). Furthermore, photographic depictions of the tarsier brain available from the University of Wisconsin Comparative Mammalian Brain Collections (http://www.brainmuseum.org, see Figure 6) do not depict a rostral elongation of the olfactory bulb. In his laterally oriented line drawings of tarsier endocranial surface and associated skull, Radinsky (1975) does not include this canal in his endocasts, thus I feel justified in following suit. This morphology presents difficulty, however, in placing landmarks. If one were to place a landmark on the anterior extent of the cribriform plate, it would give the impression of an enormous and rostrally projecting olfactory fossa. Instead, I placed this point on the anterior-superior margin of the canal. Though it may not be strictly anatomically homologous with the landmark placed on the other species (anterior extent of the cribriform plate), it more faithfully reflects the proportions of the brain in this species.

Information on body mass and the mass of brain parts was gathered from the literature. Species means for body mass and relative endocranial volume were taken from Isler *et al.* (2008). Isler *et al.* compiled ECV and body mass data from the published literature, museum databases, and collections of their own. I estimate relative

as the residual from a PGLS regression of log (base 10) ECV on log body mass (BM). Stephan and colleagues report the masses of various brain parts in a number of published studies (Stephan and Andy 1964; Stephan and Andy 1969; Stephan *et al.* 1981; Frahm *et al.* 1982; Stephan *et al.* 1982; Baron *et al.* 1983; Jolicoeur *et al.* 1984; Matano *et al.* 1985a; Matano *et al.* 1985b). From these sources, I compiled masses (in grams) of the following brain components for 45 primate species: whole brain, medulla, cerebellum, mesencephalon, diencephalon, telencephalon, olfactory bulb, septum, schizocortex, hippocampus, neocortex, visual cortex, and corpus geniculate lateralis. The Stephan dataset includes complete data (masses of all included brain components) for all but 7 of the 45 species, and of the 45 included species, 39 of these are also included in the endocast dataset generated herein.

2.2.4. Analysis

The relative volumes of brain components were measured as the vertical distance (residual) from the PGLS line of log transformed (base 10) component mass on log whole brain mass incorporating all species included in the Stephan dataset into the model. Regression equations, values for Pagel's lambda (λ), coefficient of determination (R^2), and significance (p-value) for all regressions are presented. To account for the non-independence of multiple tests using the same independent variable, the significance criterion for these regression equations was subject to Bonferroni correction (significance for each test $= \alpha/k$, where k is the number of comparisons (Sokal and Rohlf 2003).

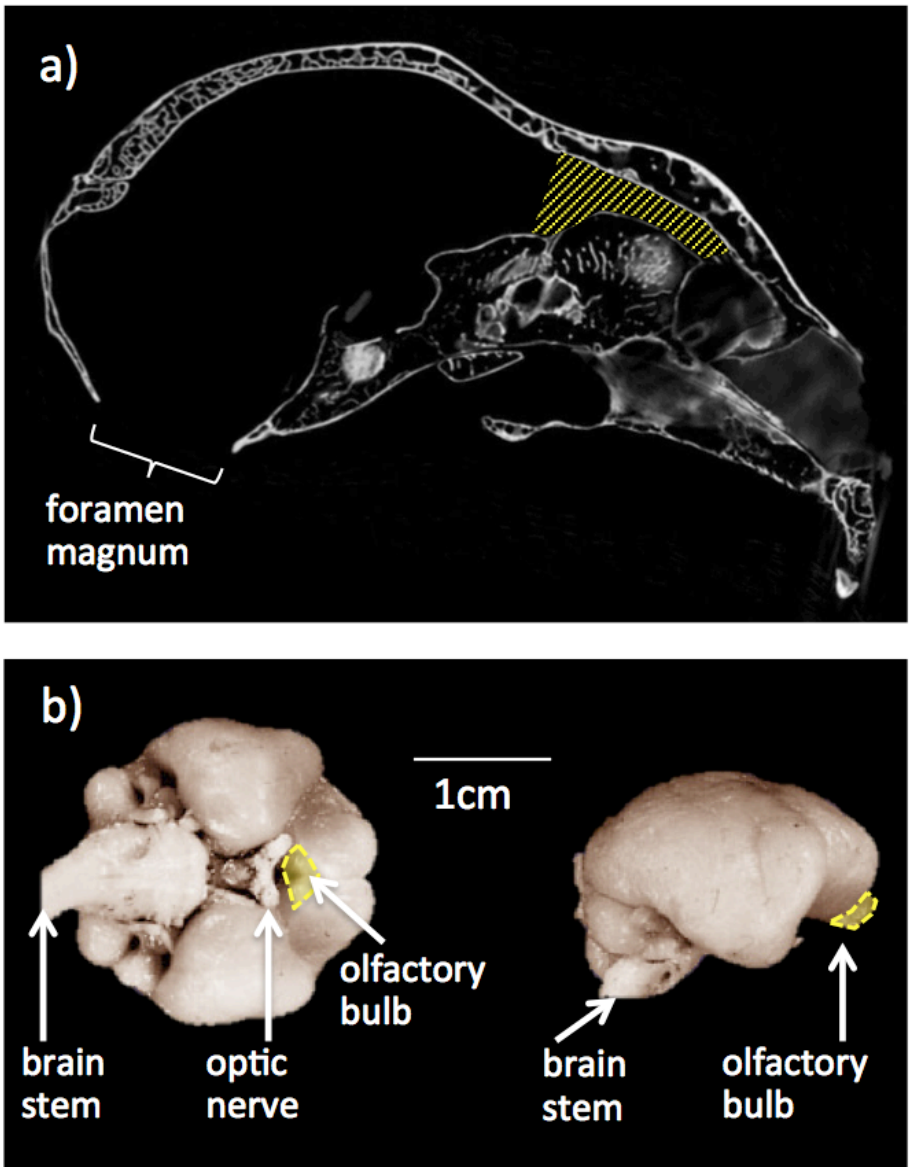

Figure 6: a) midsagittal micro-computed tomograph of *Tarsius syrichta* (DPC 045), with the olfactory fossa and nerve canal highlighted in yellow hatching; b) photographs of *Tarsius syrichta* brain in inferior (left) and lateral (right) views. Top row: unlabelled specimen, bottom row: the olfactory bulb is outlined in yellow. All images are oriented with the rostrum to the right. Brain images modified from specimen images in the Comparative Mammalian Brain Collections (brainmuseum.org), specimen #61-193.

The residual masses of brain components were then examined for differences among primate clades (Haplorhini vs. Strepsirrhini) using non-parametric pair-wise comparisons (Wilcoxon tests). Residual masses of all brain components were used as variables in a Principal Components Analysis (PCA) to evaluate patterns of brain proportions, as opposed to overall encephalization (residual brain mass) among extant primate species. Multiple sample comparisons (Wilcoxon rank sum tests) were used to test for differences in the residual mass of brain component between haplorhine and strepsirrhines, and the values for tarsiers will be discussed. Standardized scores (Z-scores) calculated for these tests represent the deviation of the group from the total sample mean in number of standard deviations. A significance criterion of $\alpha = 0.05$ was use for each test. The null hypothesis for this test is the two samples share the same distribution of rank sum scores, and $p < 0.05$ indicates that the two sample distributions are distinct (Sokal and Rohlf 2003).

Endocast shape was explored using geometric morphometric methods, with subsequent analysis of phylogenetic and allometric signal in the shape data. Landmarks were subjected to general Procrustes-aligned transformation, which rotates, translates, and resizes the objects to minimize the least squared distance among homologous landmark points (Bookstein 1997). A PCA of the Procrustes-aligned landmark data was performed in the software program *Morphologika* (O'Higgins and Jones 2006). The following landmarks were not visible on one or more fossil specimens: optic canal,

anterior clinoid process, foramen ovale, posterior vermix. As such, two separate PCAs were run: one analysis included all landmarks applied to an extant-only dataset, and the second analysis was repeated with the removal of these landmarks to allow for the inclusion of the fossil specimens. Endocast shape changes along Principal Component axes were visualized using a "wireframe" to connect nearby landmarks. The wireframe is constructed purely for visualization purposes and does not influence the statistical analysis. Wireframes representing the maximum and minimum extent of each PC axis were interpolated in *Morphologika* and are presented in the results.

The 'geiger' package for the statistical program *R* was used to test for the effects of phylogenetic signal in the raw data and residuals (Harmon *et al.* 2008). A fully resolved primate phylogeny with associated branch lengths was downloaded from a consensus tree built from 5,000 ultrameric trees generated by the 10K Trees site, version 3 (Arnold *et al.* 2010). See Appendix B for the phylogeny with divergence dates in both an image and in nexus format. Figure 7 depicts the phylogeny used for the endocast shape analysis. The 10K Trees Project utilizes a Markov Chain Monte Carlo (MCMC) approach to sample the trees in proportion to their posterior probability likelihood from a genetic dataset (including 11 mitochondrial, 6 autosomal genes) available from the GenBank database. Tests for correlated evolution between the landmark-based endocast shape variables (Principal Components) and absolute and residual ECV were performed using Phylogenetic Generalizes Least Squares regression (PGLS) methods in the 'caper'

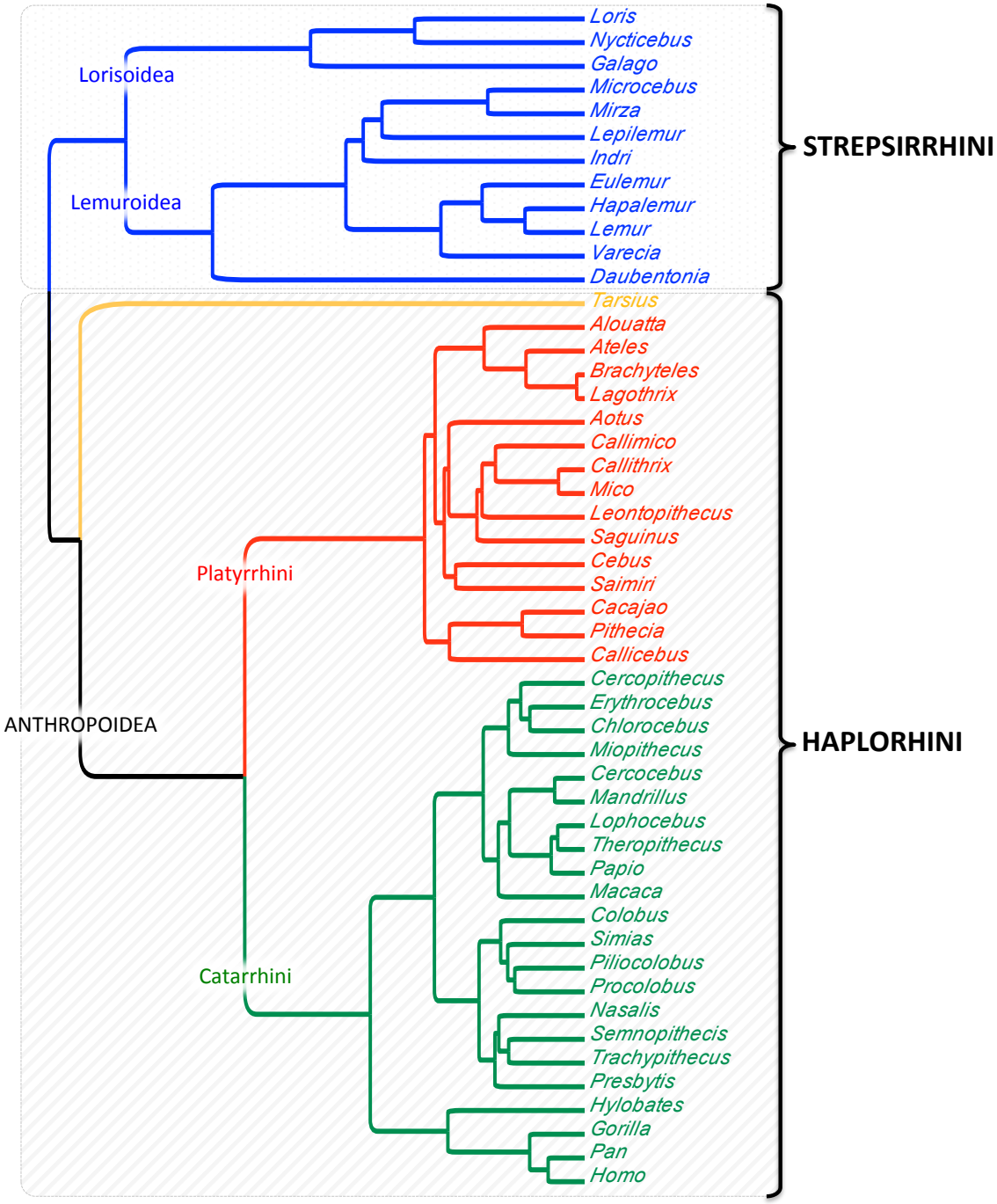

Figure 7: Consensus tree used for phylogenetically-informed endocast shape analyses. Green = Catarrhini, Red = Platyrrhini, Orange = Tarsiidae, Blue = Strepsirrhini. See Appendix B for divergence dates and complete phylogeny in nexus format.

package for *R* (Orme *et al.* 2010). Species mean PC scores were also tested for correlation with residual mass of brain components, generated from the Stephan dataset.

2.3. Results

2.3.1. Analysis of Extant Primate Brain Proportions

PGLS residuals for the relative mass of brain components are available in Appendix C. In most cases, the phylogenetically informed regression analyses (PGLS) of the Stephan (1981) data closely resemble previously published results using traditional regression techniques (Stephan *et al.* 1981; Finlay and Darlington 1995; Finlay *et al.* 2001). Details of the regression results are presented in Figures 8 and 9 and Table 3. With the exception of the olfactory bulb, the mass of the examined brain components are tightly correlated with absolute brain size, with coefficient of determinations (R^2) values ranging from 0.88 to 1.0. In particular, the total mass of each of the three primary developmental components of the mid and forebrains is strongly conserved with respect to brain mass (mesencephalon: $R^2 = 0.96$, diencephalon: $R^2 = 0.98$, telencephalon: $R^2 = 1.00$), as is the cerebellum ($R^2 = 0.99$) and medulla ($R^2 = 0.96$). Despite high λ values detected in some of these analyses, the PGLS regression equations differ little from the OLS results (see Table 3 for details). A complex combination of scaling patterns exist in which some brain mass components scale isometrically (slope = 1.00) with brain mass, while others scale allometrically (slope greater or less than 1.00). The mass of the

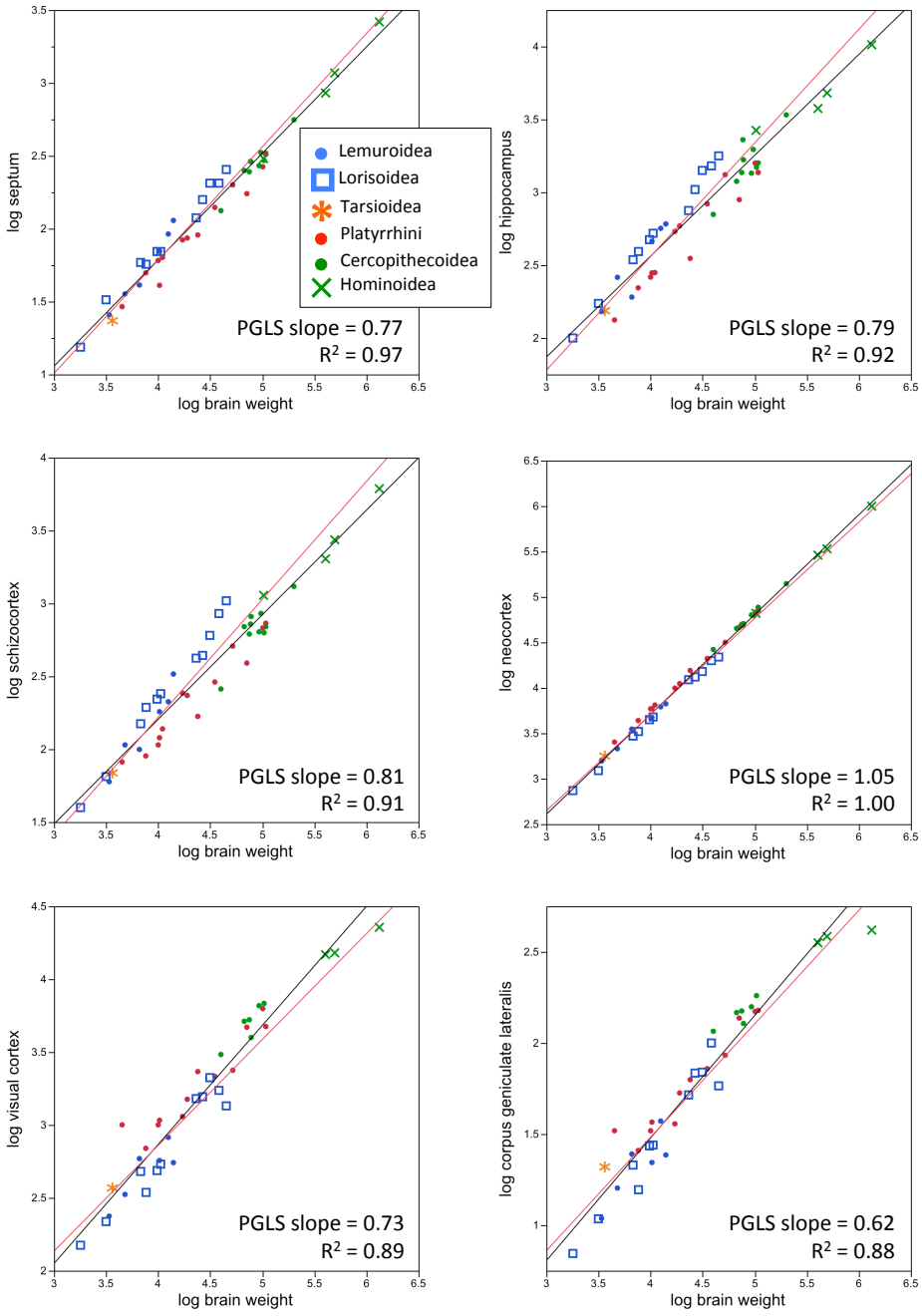

Figure 8: Bivariate plots of the mass of various brain components on brain weight. All measures are log transformed prior to analysis. Data comes from masses reported (in grams) by Stephan *et al.* 1981. Red line = PGLS regression, black line = OLS regression.

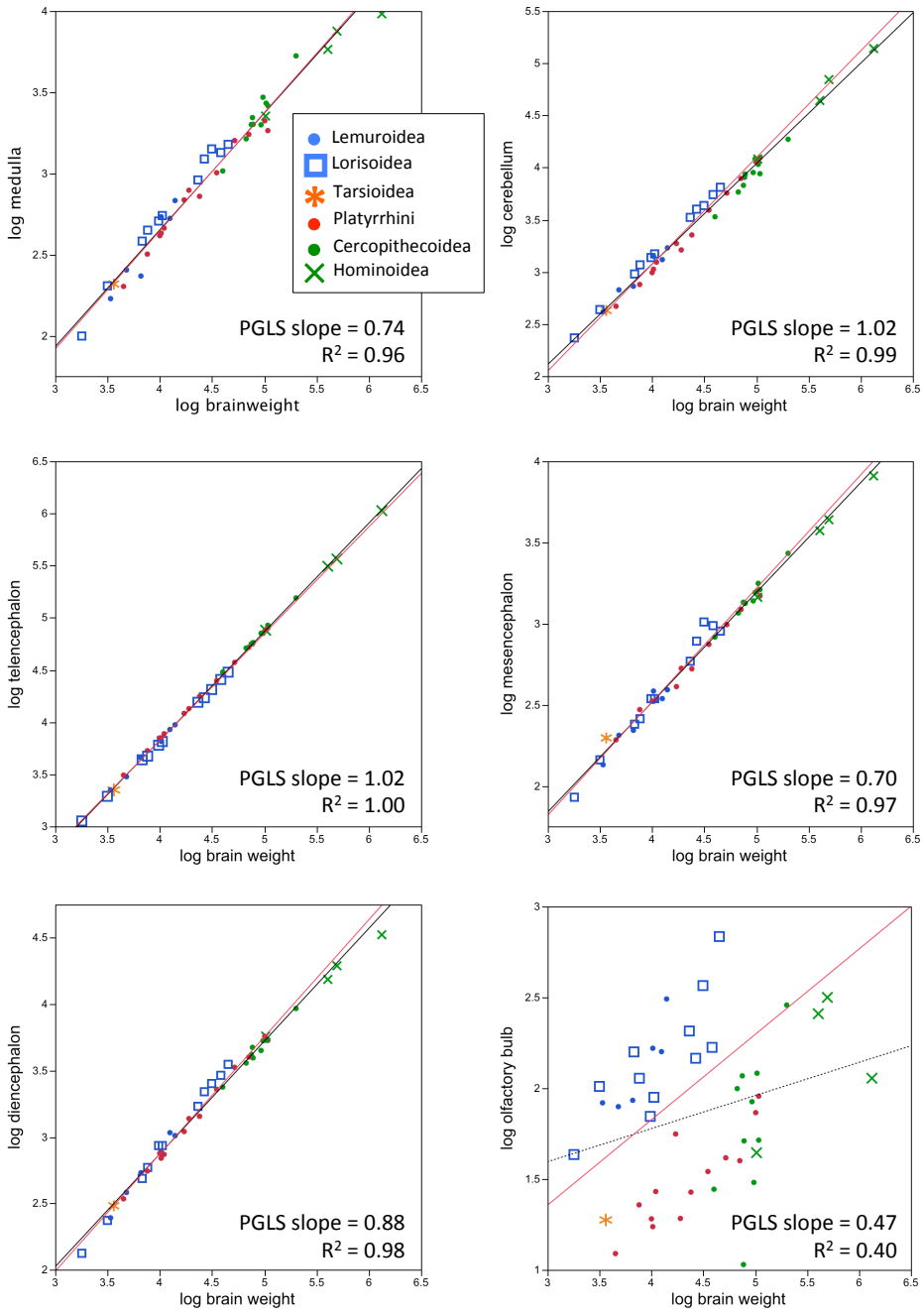

Figure 9: Bivariate plots of the mass of various brain components on brain weight. All measures are log transformed prior to analysis. Data comes from masses reported (in grams) by Stephan *et al.* 1981. Red line = PGLS regression, black line = OLS regression.

Table 3: Summary of regression results for the mass of brain components on brain weight. n = number of species included in analysis, PGLS = phylogenetic analysis, OLS = ordinary least squares regression, lambda refers to values of Pagel's λ estimated from the data and incorporated into the PGLS variation-covariation matrix error term. * = significance at alpha 0.05 level.

			PGLS						OLS				
y	x	n	Slope	Intercept	Lambda	R^2	P-value		Slope	Intercept	R^2	P-value	
brain weight	body weight	45	0.7384	2.0233	0.47	0.91	< 0.0001	*	0.7951	1.8624	0.93	< 0.0001	*
medulla	brain weight	45	0.7287	-0.2685	0.33	0.96	< 0.0001	*	0.7193	-0.2252	0.97	< 0.0001	*
cerebellum	brain weight	45	1.0227	-1.0169	0.90	0.99	< 0.0001	*	0.9627	-0.7752	0.99	< 0.0001	*
mesencephalon	brain weight	45	0.6990	-0.2772	1.00	0.97	< 0.0001	*	0.6764	-0.1898	0.99	< 0.0001	*
diencephalon	brain weight	45	0.8824	-0.6581	0.81	0.98	< 0.0001	*	0.8494	-0.5252	0.99	< 0.0001	*
telencephalon	brain weight	45	1.0236	-0.2700	0.90	1.00	< 0.0001	*	1.0411	-0.3389	1.00	< 0.0001	*
olfactory bulb	brain weight	45	0.4698	-0.0525	0.83	0.40	< 0.0001	*	0.1822	1.0488	0.05	0.07057	
septum	brain weight	45	0.7771	-1.3233	0.55	0.97	< 0.0001	*	0.7299	-1.1321	0.97	< 0.0001	*
schizocortex	brain weight	45	0.8093	-1.0182	0.91	0.91	< 0.0001	*	0.7176	-0.6650	0.92	< 0.0001	*
hippocampus	brain weight	45	0.7792	-0.5575	1.00	0.92	< 0.0001	*	0.6918	-0.2052	0.92	< 0.0001	*
neocortex	brain weight	45	1.0584	-0.5258	0.98	1.00	< 0.0001	*	1.0982	-0.6845	1.00	< 0.0001	*
visual cortex	brain weight	39	0.7260	-0.0434	0.71	0.89	< 0.0001	*	0.8164	-0.3988	0.93	< 0.0001	*
corpus geniculate lateralis	brain weight	39	0.6225	-1.0070	0.60	0.88	< 0.0001	*	0.6728	-1.2124	0.93	< 0.0001	*

cerebellum and the telencephalon scale isometrically with brain mass (slopes: cerbellum = 1.02, telencephalon = 1.02), while one component of the telencephalon, the neocortex, scales with slight positive allometry on brain mass (slope = 1.05). All other structures scale with varying degrees of negative allometry on brain mass (slope < 1.00, see Table 3 for regression slopes). In particular, areas of the brain related to sensory reception and processing are among the lowest slopes when regressed on brain mass (slopes: visual cortex = 0.73, geniculate lateralis corpus = 0.62, olfactory bulb = 0.47).

Variation in residual brain component mass is extremely limited and there are large amounts of range overlap between haplorhines and strepsirrhines; however, there are subtle yet statistically significant differences between the Wilcoxon mean ranks for the diencephalon ($p = 0.045$), telencephalon ($p < 0.0001$), cerebellum ($p < 0.0001$), and medulla ($p = 0.014$) residuals. Neocortex mass is also strongly correlated with brain mass ($R^2 = 1.00$), yet haplorhines tend to lie above the regression line, and possess significantly larger residual neocortices than strepsirrhines (Wilcoxon rank sum $p < 0.0001$). Pairwise comparisons are summarized in Figure 10 and Table 4.

The greatest amount of variation in residual mass is found in structures composing the telencephalon, especially those related to sensory systems. Log brain mass accounts for 89% of the variation in log visual cortex mass and 88% of the logged mass of the corpus geniculate lateralis. Haplorhines have significantly larger residual masses than strepsirrhines for both structures. In accordance with previous studies

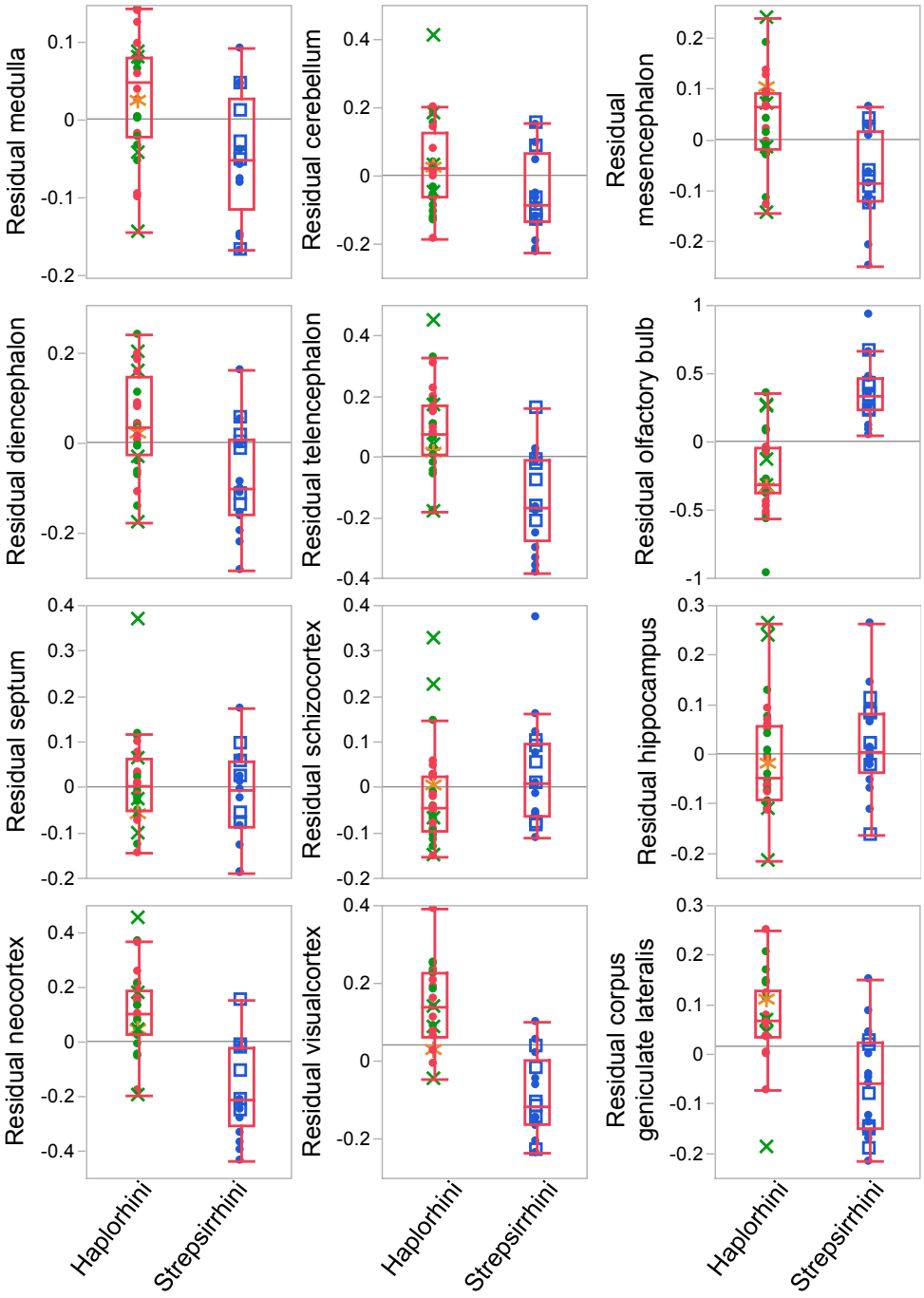

Figure 10: Box and whisker plots for residual mass of brain components between haplorhine and strepsirrhine primates. Pairwise comparisons show significant differences between group mean rank for all analyses ($p < 0.05$), except residual mesencephalon ($p = 0.89$).

Table 4: Results of Wilcoxon pairwise comparisons in residual mass of brain components. * = significant difference at alpha 0.05 level.

Variable	Strepsirrhine Mean	Haplorhine Mean	Z-score	Prob>Z	
medulla	-0.050	0.030	-3.032	0.002	*
cerebellum	-0.056	0.034	-2.165	0.030	*
mesencephalon	-0.072	0.043	-3.500	0.001	*
diencephalon	-0.075	0.046	-3.055	0.045	*
telencephalon	-0.142	0.086	-4.015	0.002	*
olfactory bulb	0.037	-0.223	4.857	<0.001	*
septum	-0.019	0.011	-0.737	0.454	
schizocortex	0.032	-0.020	1.721	0.083	
hippocampus	0.020	-0.012	1.323	0.182	
neocortex	-0.175	0.107	-4.483	<0.001	*
visual cortex	-0.090	0.142	-4.716	<0.001	*
corpus geniculate lateralis	-0.060	0.073	-3.526	<0.001	*

(Stephan and Andy 1964; Stephan and Andy 1969; Stephan *et al.* 1981; Baron *et al.* 1983; Barton *et al.* 1995), there is a great deal of variation in olfactory bulb mass that is unaccounted for by brain mass ($R^2 = 0.40$). This is also the only structure for which the PGLS regression equation drastically differs from results found with non-phylogenetic OLS regression techniques (OLS: slope = 0.1822, $p = 0.07$, PGLS: $\lambda = 0.83$, slope = 0.4698, $p < 0.001$), owing to a strong phylogenetic signal with a major grade shift in residual olfactory bulb mass between the haplorhine and strepsirrhine groups (strepsirrhine mean = 0.037, haplorhine mean = -0.223, Wilcoxon rank sum: $p < 0.001$).

For most (but not all) measures of residual brain component mass, tarsiers lie within one standard deviation of the anthropoid mean, and are closer to the anthropoid than the strepsirrhine mean residual component values (Table 5). In particular, tarsiers are more "anthropoid-like" in the residual mass of the hindbrain components (medulla,

Table 5: Mean and standard deviations for anthropoid and strepsirrhine residual brain component masses with a comparison to tarsier values. SD = standard deviation.

Component	Statistic	Anthropoid	Strepsirrhine	Tarsier	SD from Anthropoid	SD from Strepsirrhine
medulla	mean	0.03	-0.05	-0.02		
	SD	0.07	0.08		-0.09	0.93
cerebellum	mean	0.03	-0.06	-0.02		
	SD	0.13	0.12		-0.07	0.67
mesencephalon	mean	0.04	-0.07	0.08		
	SD	0.09	0.09		0.66	2.05
diencephalon	mean	0.05	-0.08	-0.01		
	SD	0.11	0.12		-0.24	0.82
telencephalon	mean	0.09	-0.14	-0.01		
	SD	0.15	0.15		-0.50	1.00
olfactory bulb	mean	-0.22	0.37	-0.42		
	SD	0.29	0.23		-0.42	-3.10
septum	mean	0.01	-0.02	-0.10		
	SD	0.10	0.10		-0.71	-0.40
schizocortex	mean	-0.02	0.03	-0.05		
	SD	0.11	0.12		0.22	-0.24
hippocampus	mean	-0.01	0.02	-0.07		
	SD	0.11	0.10		-0.07	-0.40
neocortex	mean	0.11	-0.18	0.03		
	SD	0.16	0.17		-0.39	1.34
visual cortex	mean	0.14	-0.09	0.03		
	SD	0.10	0.10		-1.09	1.17
corpus geniculate lateralis	mean	0.07	-0.06	0.11		
	SD	0.09	0.10		0.41	1.64

cerebellum), the diencephalon, both of which are relatively larger in anthropoids and tarsiers than in most strepsirrhines. Tarsiers have a residual mesencephalon that is two standard deviations (SD) above the strepsirrhine mean. The neocortex and visual processing centers are more than one standard deviation about the strepsirrhine mean (neocortex = +1.34 SD, visual cortex = +1.17 SD, corpus geniculate lateralis = +1.64 SD

from strepsirrhine mean), though the visual cortex is also smaller than the anthropoid mean (-1.09 SD from anthropoid mean). The tarsier value for these components overlaps with very few (visual cortex, corpus geniculate lateralis, neocortex) of the strepsirrhines or lies outside the strepsirrhine range completely (mesencephalon). Notably, tarsiers have much smaller olfactory bulbs for their brain size than do strepsirrhines, with a value 3.1 standard deviations below the strepsirrhine mean.

Haplorhines and strepsirrhines display a clear separation in a Principal Components Analysis using all residual brain components as included variables (Figure 11, Table 6). The first Principal Component (PC) accounts for 56.7% of the variance. Loading values (eigenvectors) for included variables are presented in Table 7. Strepsirrhines have significantly lower PC1 scores than haplorhines (Wilcoxon rank sum on PC1 scores: $p = 0.0007$). The residual mass of the telencephalon and neocortex load with positive values on PC1, likely accounting for the high values of anthropoids on this axis, while residual olfactory bulb size loads negatively, further accounting for the strepsirrhine - haplorhine separation. PC1 separates humans from other primates, owing in part to the large telencephalon and very small olfactory bulb of this species. The sole tarsier specimen included in the Stephan dataset is well within the anthropoid distribution for PCs 1 through 3. PC scores fail to separate Platyrrhini from Catarrhini or Lemuroidea from Lorisoidea.

Table 6: Principal Component (PC) scores for analysis of residual brain components. N = number of specimens in Stephan dataset. PC = Principal Component score.

Group	Species from Stephan	Modern taxonomic designation	n	PC1	PC2	PC3
Cercopithecoidea	*Macaca mulatta*	*Macaca mulatta*	1	-0.556	-2.133	0.004
	Cercocebus albigena	*Lophocebus albigena*	1	0.947	-1.829	0.251
	Cercopithecus mitis	*Cercopithecus mitis*	1	-0.162	-1.650	0.809
	Cercopithecus ascanius	*Cercopithecus ascanius*	1	2.877	-0.250	1.290
	Cercopithecus talapoin	*Miopithecus talapoin*	2	4.646	-1.169	0.270
	Colobus badius	*Piliocolobus badius*	2	-0.209	-0.511	0.431
Hominoidea	*Pan troglodytes*	*Pan troglodytes*	1	-0.348	-1.001	-0.349
	Gorilla gorilla	*Gorilla gorilla*	1	-3.339	-1.509	-0.604
	Homo sapiens sapiens	*Homo sapiens sapiens*	1	6.328	3.952	-1.307
Platyrrhini	*Callithrix jacchus*	*Callithrix jacchus*	4	0.959	-0.901	-1.042
	Cebuella pygmaea	*Cebuella pygmaea*	2	1.650	-2.786	0.946
	Saguinus oedipus	*Saguinus oedipus*	3	1.414	-1.344	-0.810
	Saguinus tamarin	*Saguinus tamarin*	2	1.857	-1.415	-0.150
	Aotus trivirgatus	*Aotus trivirgatus*	5	0.640	0.763	-0.254
	Callicebus moloch	*Callicebus moloch*	2	1.556	-0.704	0.595
	Pithecia monacha	*Pithecia monacha*	2	2.675	-0.034	-0.338
	Alouatta sp.	*Alouatta sp.*	2	-3.034	-1.382	-0.294
	Ateles geoffroyi	*Ateles geoffroyi*	1	0.033	-0.893	-0.877
	Lagothrix lagotricha	*Lagothrix lagotricha*	3	3.108	-0.386	0.064
	Cebus sp.	*Cebus sp.*	2	3.087	-1.792	-0.594
	Saimiri sciureus	*Saimiri sciureus*	1	3.894	-1.456	-0.990
Tarsioidea	*Tarsius sp.*	*Tarsius sp.*	2	0.684	-0.938	0.272
Lemuroidea	*Cheirogaleus major*	*Cheirogaleus major*	2	-2.153	1.235	0.237
	Cheirogaleus medius	*Cheirogaleus medius*	2	-3.085	1.021	-1.040
	Microcebus murinus	*Microcebus murinus*	6	-1.228	1.296	-1.465
	Lepilemur ruficaudatus	*Lepilemur ruficaudatus*	3	-5.919	0.976	-0.826
	Lemur fulvus	*Eulemur fulvus*	3	0.835	1.508	0.887
	Lemur variegatus	*Varecia variegatus*	1	0.098	1.640	2.087
	Avahi laniger laniger	*Avahi laniger laniger*	2	-5.075	0.127	0.215
	Avahi laniger occidentalis	*Avahi laniger occidentalis*	2	-2.896	0.764	0.269
	Propithecus verrauxi	*Propithecus verrauxi*	2	-2.788	-0.335	1.218
	Indri Indri	*Indri Indri*	2	-3.708	0.026	2.047
	Daubentonia madagascarensis	*Daubentonia madagascarensis*	1	2.119	5.191	1.317
Lorisoidea	*Loris tardigradus*	*Loris tardigradus*	1	-1.844	-0.952	-0.772
	Nycticebus coucang	*Nycticebus coucang*	2	-0.958	1.023	0.815
	Perodicticus potto	*Perodicticus potto*	2	-2.320	2.915	-0.160
	Galago crassicaudatus	*Otolemur crassicaudatus*	2	-2.853	1.015	-0.513
	Galago demidovii	*Otolemur demidovii*	2	1.499	2.308	-1.263
	Galago senegalensis	*Galago senegalensis*	1	0.349	1.951	-0.041

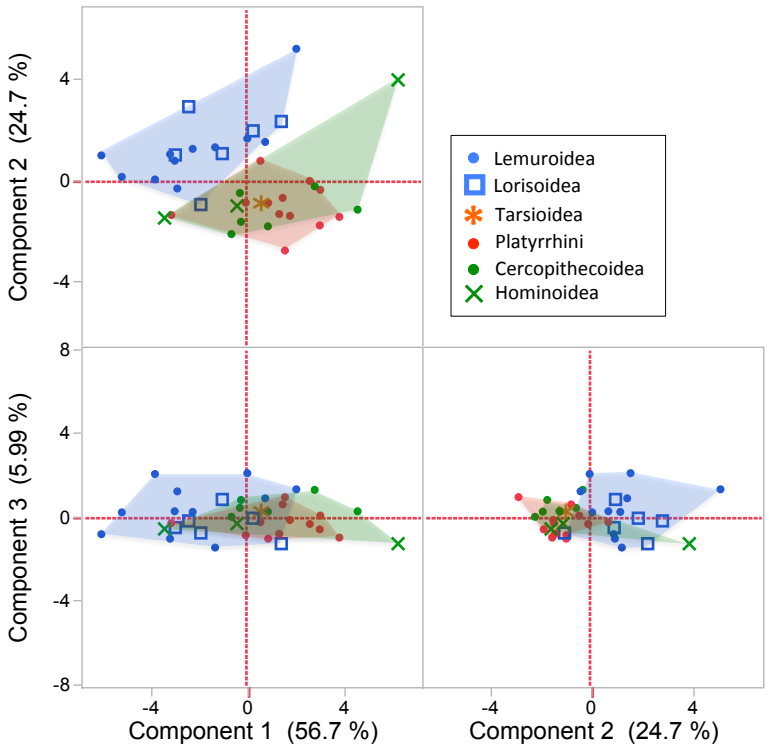

Figure 11: Principal Components Analysis of residual brain components in primates, data from Stephan *et al.* (1981). Red polygon = platyrrhine distribution, blue polygon = strepsirrhine distribution, green polygon = catarrhine distribution.

Table 7. Eigenvectors for Principal Components (PC) analysis of residual mass of brain components.

Variable	PC1	PC2	PC3
residual medulla mass	0.332	0.025	0.111
residual cerebellum mass	0.339	0.119	-0.272
residual mesencephalon mass	0.368	-0.054	0.020
residual diencephalon mass	0.370	-0.008	0.073
residual telencephalon mass	0.367	-0.055	-0.274
residual olfactory bulb mass	-0.143	0.377	0.148
residual septum mass	0.305	0.262	-0.097
residual schizocortex mass	0.175	0.429	0.429
residual hippocampus mass	0.187	0.416	0.368
residual neocortex mass	0.363	-0.106	-0.264
residual visualcortex mass	0.206	-0.444	0.254
residual corpus geniculate lateralis mass	0.121	-0.451	0.591

A discriminant function analysis was performed using all residual brain components under the assumption of equal variances and sample sizes. The analysis achieved a 0% misclassification rate in assigning specimens to the haplorhine and strepsirrhine groups, largely owing to the loading factors for visual cortex, neocortex, olfactory bulb, and cerebellum residuals.

2.3.2 Endocast Shape Analysis

2.3.2.1. Extant-Only Analysis

A broad diversity of endocast shapes was observed in the extant dataset. Figure 12 depicts a sample of primate endocasts and associated wireframes demonstrating varying degrees of rostral-caudal elongation, size and rostral projection of the olfactory fossa, extent of flexion of the brain base around the sellar basin, and position of the occipital pole relative to the posterior point of the cerebellum.

A Principal Components Analysis of Procrustes-aligned landmarks was performed to explore diversity in endocast shape among extant primates. Results of the PCA are presented in Figures 13 and 14 and Table 8. Principal component 1 separates anthropoids (low scores) from strepsirrhines (high scores for PC1) (Wilcoxon pairwise comparison of PC1 scores: $p < 0.001$). Shape changes associated with the first principal component axis include flexion of the brain base (angle formed by landmarks: basion – sella – anterior cribriform plate), size and position of the olfactory fossa, the position of the foramen magnum relative to the rostral-caudal axis, and the placement of the

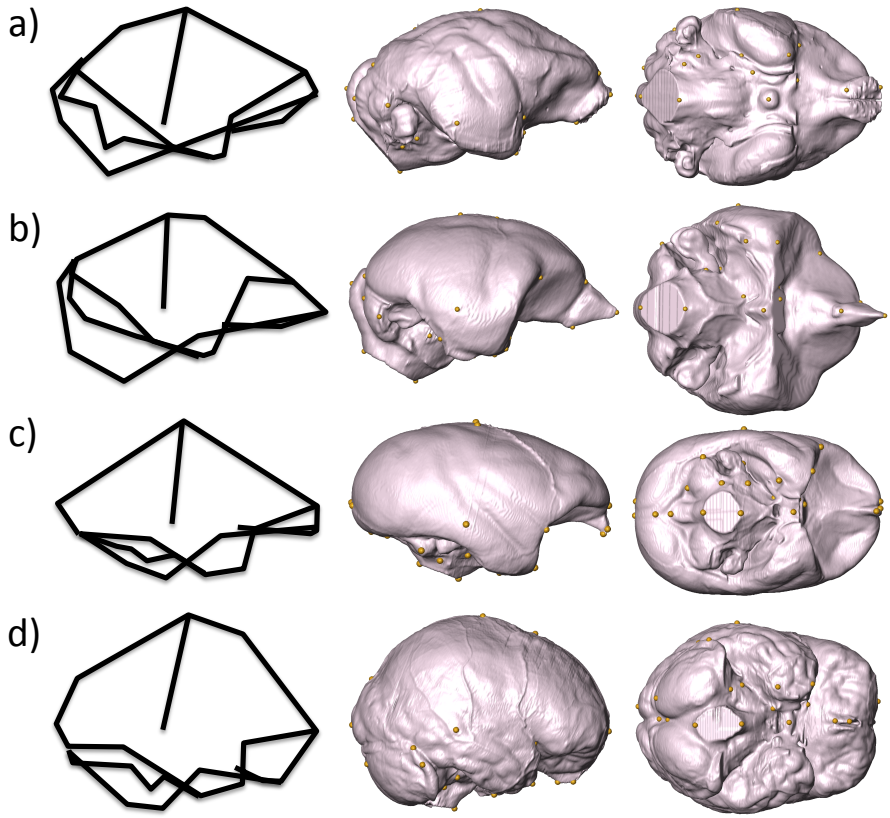

Figure 12: A sample of extant primate endocasts with associated wireframes. Left column: wireframes in lateral view, middle column: endocasts and associated landmarks in lateral view, right column: endocasts in inferior view. a) *Lemur catta*, b) *Alouatta seniculus*, c) *Saimiri sciureus*, d) *Homo sapiens*.

occipital pole relative the posterior extent of the cerebellum. Anthropoids have low scores for PC1, demonstrating more flexion of the brain base, a smaller and more inferiorly directed olfactory fossa, a more anteriorly positioned foramen magnum, and an occipital pole that projects caudally over the posterior cranial fossa. Conversely, lemuroids have higher scores on PC1, with large olfactory fossae that project rostrally, directly anterior to the frontal pole, and unflexed brain bases in which the posterior

Table 8: Genus mean Principal Component (PC) scores for extant-only endocast analysis. Details for species names and samples available in Appendix A.

Haplorhini Group	Genus	PC1	PC2	PC3	Strepsirrhini Group	Species	PC1	PC2	PC3
Cercopithecoidea	*Cercocebus*	-0.077	0.069	0.043	Lemuroidea	*Daubentonia*	0.093	0.039	-0.095
	Cercopithecus	-0.020	-0.001	0.025		*Eulemur*	0.141	-0.016	-0.073
	Chlorocebus	-0.054	-0.040	-0.009		*Hapalemur*	0.133	0.083	-0.007
	Colobus	0.014	-0.018	0.029		*Indri*	0.224	0.049	-0.012
	Erythrocebus	-0.053	0.002	0.003		*Lemur*	0.160	0.071	0.009
	Lophocebus	-0.060	-0.002	0.007		*Lepilemur*	0.204	0.009	0.009
	Macaca	-0.055	0.034	0.043		*Microcebus*	0.149	0.045	-0.042
	Mandrillus	-0.038	0.018	0.031		*Mirza*	0.120	0.019	0.040
	Miopithecus	-0.094	0.008	-0.030		*Varecia*	0.196	-0.034	-0.056
	Nasalis	-0.016	-0.018	-0.033	Lorisoidea	*Galago*	0.078	-0.018	-0.013
	Papio	-0.040	0.055	0.028		*Loris*	0.058	0.056	-0.016
	Piliocolobus	0.016	-0.001	-0.004		*Nycticebus*	0.129	0.043	0.023
	Presbytis	-0.044	-0.001	0.031					
	Procolobus	-0.035	0.003	0.016					
	Semnopithecus	-0.033	0.001	0.035					
	Simias	-0.001	-0.015	0.055					
	Theropithecus	-0.011	-0.002	0.045					
	Trachypithecus	-0.058	0.012	0.025					
Hominoidea	*Gorilla*	-0.027	0.134	-0.041					
	Homo	-0.143	0.153	-0.153					
	Hylobates	-0.029	0.004	0.052					
	Pan	-0.047	0.111	-0.055					
Platyrrhini	*Alouatta*	0.041	-0.043	0.044					
	Aotus	-0.014	-0.047	-0.052					
	Ateles	-0.061	0.006	0.039					
	Brachyteles	-0.035	-0.026	0.011					
	Cacajao	-0.074	0.017	0.002					
	Callicebus	0.000	-0.047	-0.008					
	Callimico	-0.034	-0.082	-0.049					
	Callithrix	-0.006	-0.059	0.011					
	Cebuella	0.009	-0.083	-0.059					
	Cebus	-0.061	-0.022	0.009					
	Lagothrix	-0.058	-0.005	0.051					
	Leontopithecus	0.046	-0.054	-0.020					
	Mico	0.019	-0.082	0.007					
	Pithecia	0.013	-0.041	0.063					
	Saguinus	-0.001	-0.108	-0.031					
	Saimiri	-0.160	-0.093	-0.059					
Tarsioid	*Tarsius*	0.086	-0.015	0.036					

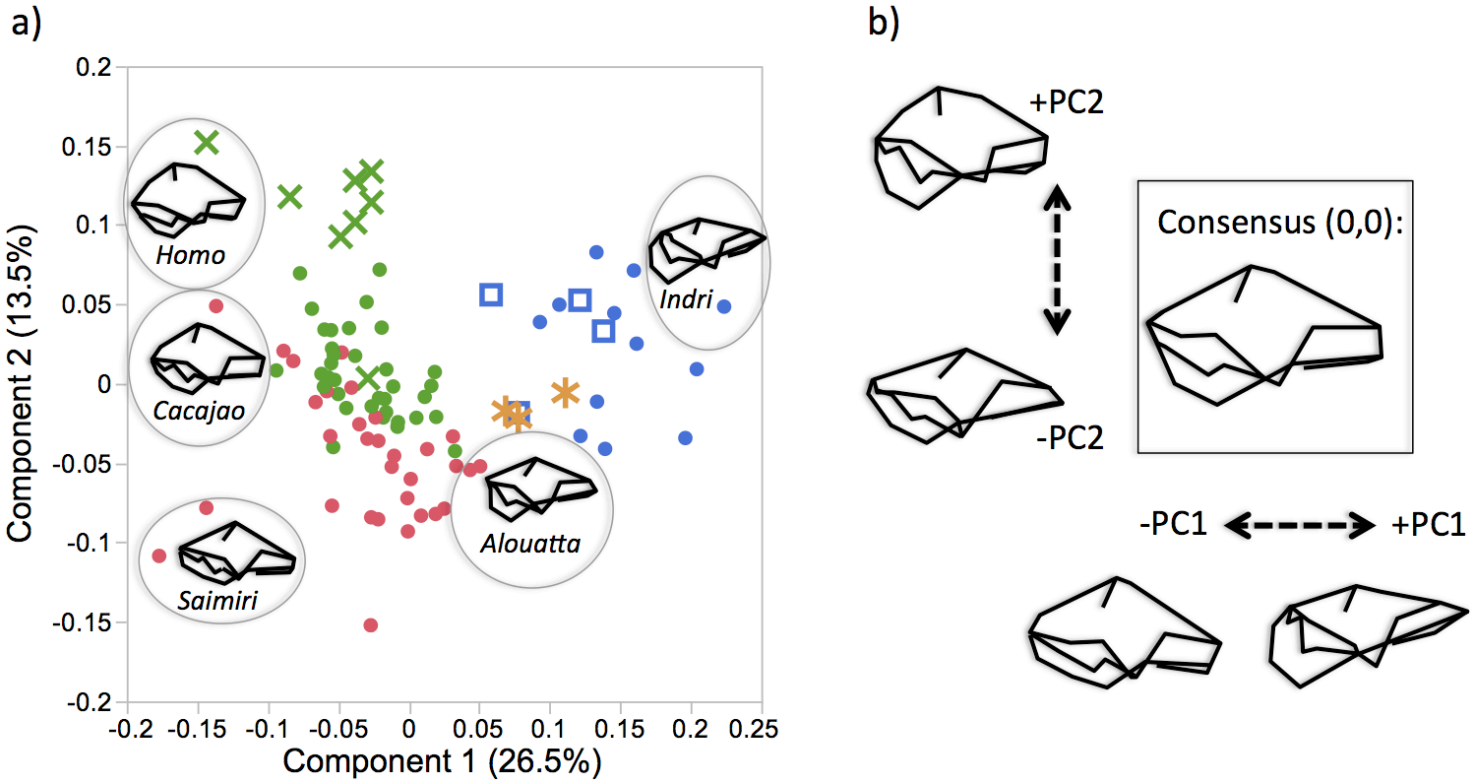

Figure 13: Principal Components analysis of extant primate endocast shape. Left: bivariate score plot of individual specimen values for components 1 and 2. Wireframes depict morphology of the genus contained and labeled within the grey circle. Right: wireframes depicting shape variation along the first two Principal Components (PC). The consensus wireframe represents the morphology at the origin (0,0) of the biplot.

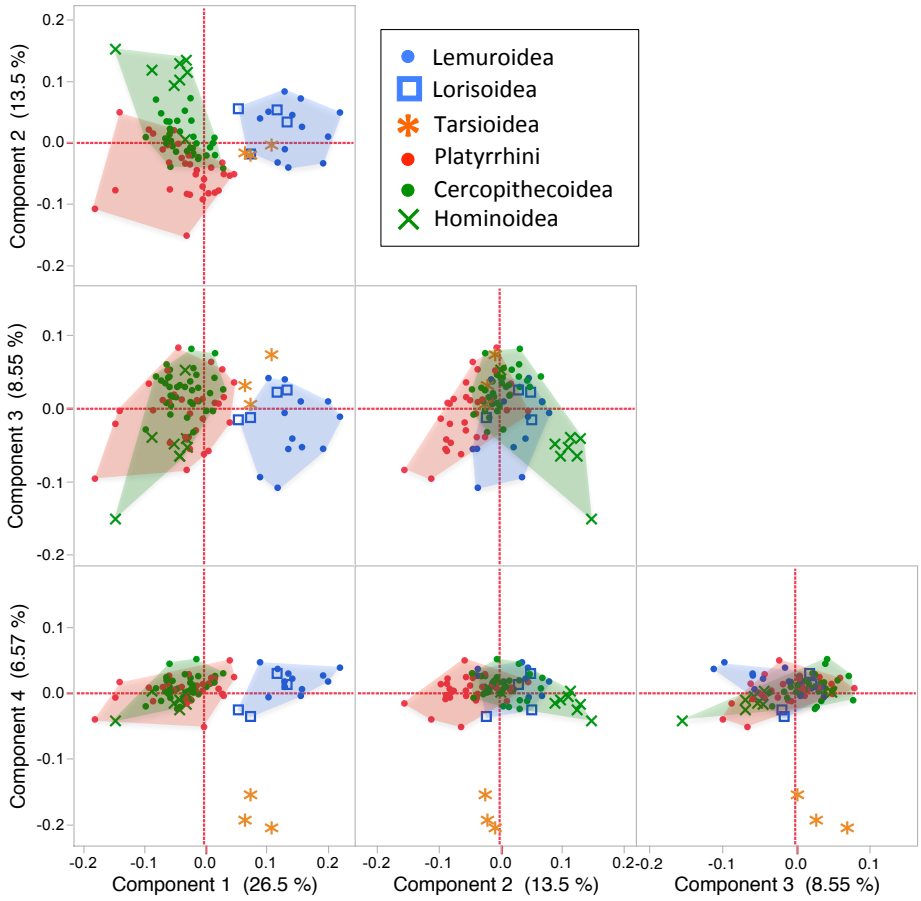

Figure 14: Biplots of Principal Component scores (Components 1, 2, 3) for extant endocast analysis. Points indicate individual specimen values.

cranial fossa is situated posterior to the occipital poles. Lorisoid and tarsioid specimens are intermediately placed on PC1, primarily due to greater brain base flexion and more posterior projection of the occipital pole than is typical of lemuroid. *Alouatta* is the sole anthropoid that overlaps the strepsirrhine range for PC1.

The second Principal Component shows some differentiation in endocast shape between platyrrhines and catarrhines. Positive values for PC2 (i.e. catarrhines) are

associated with greater height of the endocast in the superior-inferior direction, a more anteriorly projecting temporal pole, and a more anteriorly placed maximum breadth of the cerebral region. *Saimiri* and *Saguinus* have the lowest scores for PC2, with a flattened dorsal aspect to the frontal and parietal regions of the endocasts. The third and fourth Principal Components for 8.5 and 6.6 percent of the variation, respectively, and with one notable exception (tarsiers), these components do not separate animals by taxonomic or functional groups. The tarsier specimens are widely separated from all other species on Component 4. Their low numbers for Component 4 relate to their unique proportions in having a particularly rostrocaudally short and mediolaterally broad endocast.

2.3.2.2. Correlated Evolution Between Stephan (1981) Brain Proportion Data and Endocast Shape

Ordinary least squares (OLS) and phylogenetically informed generalized linear regression (PGLS) results are presented in Table 9. Component 1 of the extant endocast shape analysis carries a high degree of phylogenetic signal (Pagel's lambda approaching 1.0). PGLS regressions reveal that, among extant primates, PC1 is not significantly correlated with absolute ECV ($p = 0.45$, Bonferroni criterion = 0.0083), but resECV does explain a moderate amount of variance in Component 1 scores ($R^2 = 0.55$) when phylogeny is taken into account. Although no individual variable from the Stephan dataset (residual mass of brain components) accounts for a large proportion of the

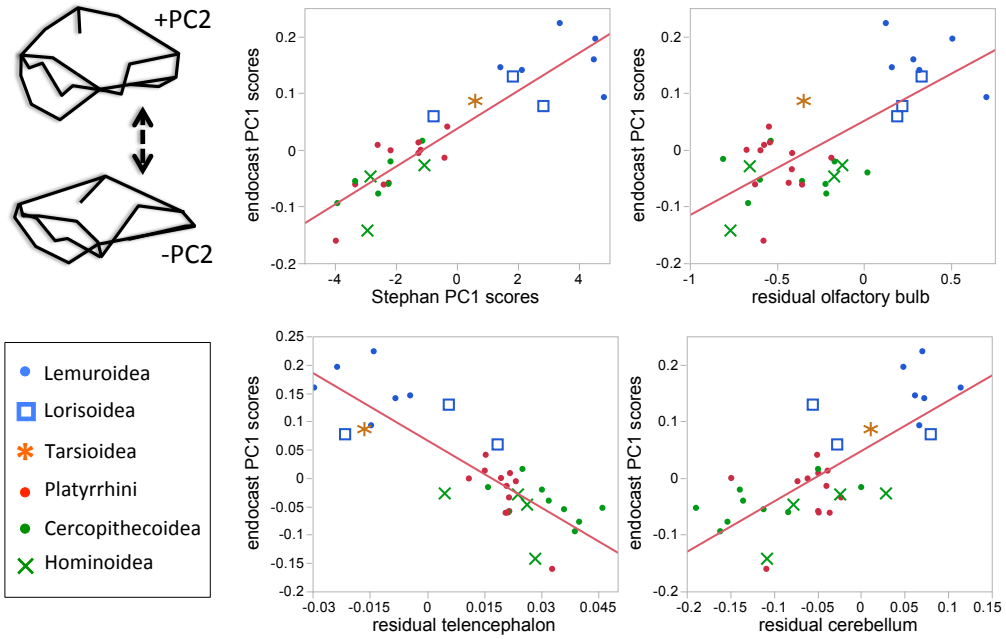

Figure 15: Bivariate plots of endocast shape Principal Component scores and residual brain masses from Stephan dataset. Points represent species means, and PGLS regression is depicted as red line.

variance in PC1 scores (R^2 <0.35), the residual masses of the telencephalon, olfactory bulb, and cerebellum are all significantly correlated with species values for PC1 (Figure 15). Scores for the second and third components of endocast shape (PC2 and 3) are not significantly related to encephalization or brain proportions, but instead show low to moderate correlations with body size, as measured by absolute ECV of the specimen (for both PC2 and PC3) and by species mean body mass (PC2) (see Table 10 for details). Overall, the results of the principal components analysis of endocast landmark configurations resemble those derived from data of residual mass of brain components

Table 9: Phylogenetically informed (PGLS) and ordinary least squares (OLS) regression results for endocast Principal Components (PC endocast), brain Components (PC1 Stephan), and endocranial size, * denotes significance using Bonferroni significance criterion = 0.0083, for multiple comparisons.

			PGLS						OLS				
y	x	n	Slope	Intercept	Lambda	R^2	P-value		Slope	Intercept	R^2	P-value	
log ECV	log BM	51	0.7398	-0.9995	0.59	0.89	2.20E-16	*	0.7829	-1.1139	0.94	2.20E-16	*
PC1	PC1Stephan	30	0.0334	0.0400	0.00	0.80	8.31E-14	*	0.0334	0.0370	0.81	9.11E-12	*
PC1	logECV	51	-0.0355	0.1071	0.87	0.05	0.0447		-0.0897	0.1533	0.33	6.47E-06	*
PC1	resECV	51	-0.2536	0.0631	0.97	0.55	5.45E-14	*	-0.4318	0.0223	0.52	2.59E-09	*
PC1	log cerebellum	35	0.5227	0.0629	0.77	0.16	0.0049	*	0.8890	0.0473	0.55	2.14E-07	*
PC1	log olfactory bulb	35	0.0930	0.0654	0.87	0.11	0.0213		0.1663	0.0510	0.50	1.19E-06	*
PC1	log telencephalon	35	-2.9904	0.0650	0.67	0.34	3.12E-05	*	-3.9643	0.0667	0.70	1.91E-10	*
PC2	log ECV	51	0.0534	-0.0558	0.88	0.20	2.47E-05	*	0.0396	-0.0604	0.17	0.0019	*
PC2	log BM	51	0.0326	-0.0883	0.87	0.12	0.0013	*	-0.0543	0.1982	0.18	0.0013	*
PC2	res ECV	51	0.0816	0.0103	0.97	0.07	0.0140		0.0382	0.0019	0.01	0.4655	
PC2	log cerebellum	35	0.0204	0.0135	0.94	0.01	0.9900		0.0521	0.0063	0.00	0.7061	
PC2	log olfactory bulb	35	-0.0023	0.0135	0.95	0.00	0.9955		0.0471	0.0158	0.07	0.0740	
PC2	log telencephalon	35	0.6488	0.0136	0.96	0.00	0.4543		-0.1427	0.0061	0.00	0.7950	
PC3	log ECV	51	-0.0184	0.0161	0.69	0.01	0.2592		-0.0033	0.0046	0.00	0.7571	
PC3	log BM	51	-0.0038	0.0043	0.68	0.00	0.9099		0.0009	-0.0041	0.00	0.9113	
PC3	res ECV	51	-0.1264	-0.0078	0.91	0.15	0.0003	*	-0.0685	0.0013	0.03	0.1024	
PC3	log cerebellum	35	0.0479	-0.0142	0.68	0.00	0.9312		-0.1269	-0.0167	0.01	0.2392	
PC3	log olfactory bulb	35	0.0343	-0.0132	0.81	0.00	0.4497		-0.0189	-0.0161	0.02	0.3703	
PC3	log telencephalon	35	-0.2985	-0.0139	0.68	0.01	0.8529		0.4224	-0.0174	0.01	0.3245	
PC1 Stephan	log BM	30	0.6944	-1.2458	1.00	0.03	0.1600		-0.7036	1.8587	0.01	0.2480	
PC1 Stephan	res ECV	30	-4.0776	0.8511	0.98	0.23	0.0008	*	-11.1053	-0.0358	0.4193	8.77E-05	*

(presented in section 2.2.1). This is reflected by a significant correlation between PC1 scores from the endocast analysis with PC1 from the Stephan et al. (1981) dataset (Figure 15). PC1 scores for both analyses separate strepsirrhine from anthropoid primates, and are correlated with encephalization.

2.3.2.3. Endocranial Shape of Fossil Specimens

Reconstructed fossil endocasts are presented in Figure 16. When restricting the dataset to those landmarks available in the fossil dataset, the results of the Principal Components Analysis of endocast shape (Figure 17) are broadly similar to those of the full dataset described above (Figure 14). PC1 separates strepsirrhines and tarsiers from the anthropoids, with some overlap between lorisoids and small-brain platyrrhines (i.e. *Alouatta*) while the second component separates hominoids from cercopithecoid and platyrrhine monkeys. The Eocene adapoid specimens *Leptadapis* and *Adapis* have high values for PC1, above the distribution of modern strepsirrhines, owing to a more posteriorly placed foramen magnum, and thus a more extended brain base and posteriorly extended cerebellar poles. When viewing the morphospace in three-dimensions (PCs 1, 2, and 3), the adapiform specimens are well outside the extant primate range, demonstrating an exaggeration of the typical strepsirrhine-like shape. The other Eocene specimen, *Rooneyia* (omomyiform?) lies within the extant strepsirrhine range for Component 1, having a more modern primate-like shape, wherein the posterior cranial fossa lies more directly inferior to the cerebrum, rather than projecting

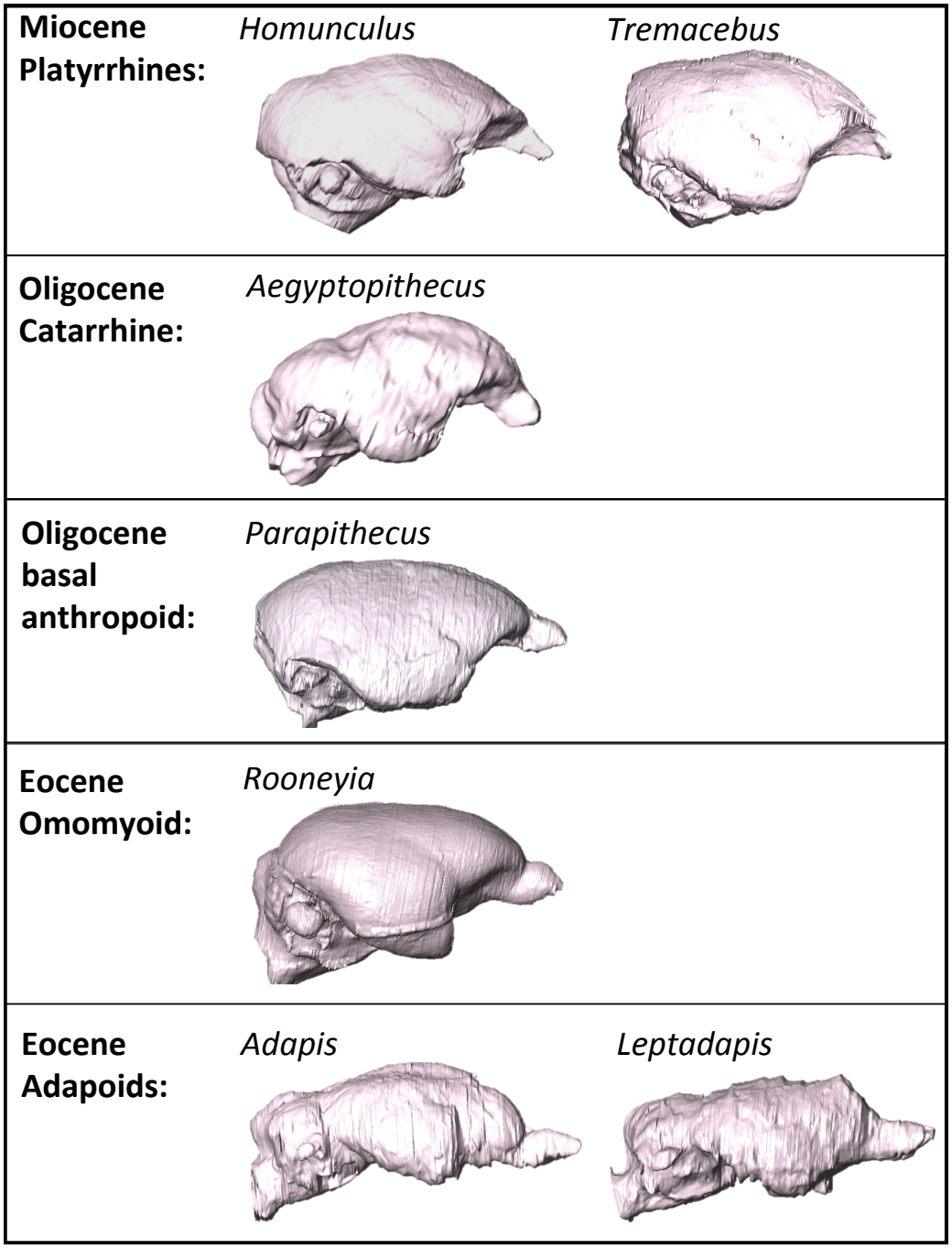

Figure 16: Virtual endocast reconstructions of fossil specimens used in this analysis. All specimens are depicted in lateral view and scaled to equal fronto-occipital pole length (rostal to the right).

Table 10: Principal Component (PC) scores for extant and fossil endocast analysis.

Haplorhini				Strepsirrhini and Fossil Specimens			
Species	PC1	PC2	PC3	Species	PC1	PC2	PC3
Cercocebus	-0.0717	-0.0371	0.0252	*Daubentonia*	0.0760	-0.0841	0.0078
Cercopithecus	-0.0189	0.0225	0.0172	*Eulemur*	0.1168	-0.0093	-0.0015
Chlorocebus	-0.0529	0.0313	-0.0133	*Hapalemur*	0.0907	-0.0262	-0.0084
Colobus	0.0114	-0.0011	0.0308	*Indri*	0.1898	-0.0410	0.0194
Erythrocebus	-0.0449	0.0232	0.0095	*Lemur*	0.1349	-0.0370	-0.0093
Lophocebus	-0.0669	0.0314	0.0302	*Lepilemur*	0.1909	-0.0259	-0.0016
Macaca	-0.0576	-0.0319	0.0564	*Microcebus*	0.1221	-0.0788	0.0186
Mandrillus	-0.0213	0.0198	-0.0016	*Mirza*	0.1119	-0.0356	0.0069
Miopithecus	-0.1078	0.0196	-0.0130	*Varecia*	0.1826	-0.0372	0.0048
Nasalis	-0.0321	0.0081	-0.0054	*Galago*	0.0643	0.0140	-0.0343
Papio	-0.0488	-0.0285	0.0306	*Loris*	0.0324	-0.0221	-0.0263
Piliocolobus	0.0090	-0.0001	0.0214	*Nycticebus*	0.1030	-0.0436	0.0306
Presbytis	-0.0480	-0.0083	0.0080				
Procolobus	-0.0482	-0.0058	0.0162	*Adapis*	0.2730	-0.0213	0.0047
Semnopithecus	-0.0345	-0.0016	0.0091	*Leptadapis*	0.3254	0.0049	0.0197
Simias	-0.0067	0.0009	0.0326	*Rooneya*	0.1684	0.0336	-0.0069
Theropithecus	-0.0203	0.0070	0.0622	*Parapithecus*	0.0752	0.0806	0.0005
Trachypithecus	-0.0638	-0.0207	0.0275	*Aegyptopithecus*	0.0367	0.0737	-0.0739
Gorilla	-0.0490	-0.1052	-0.0304	*Homunculus*	-0.0174	0.0378	-0.0341
Homo	-0.1875	-0.1355	-0.1182	*Tremacebus*	NA	NA	NA
Hylobates	-0.0242	-0.0225	-0.0123				
Pan	-0.0753	-0.0992	-0.0430				
Alouatta	0.0398	0.0197	0.0194				
Aotus	-0.0243	0.0533	-0.0256				
Ateles	-0.0606	-0.0286	0.0093				
Brachyteles	-0.0375	-0.0254	-0.0093				
Cacajao	-0.0789	-0.0254	0.0181				
Callicebus	0.0002	0.0349	0.0047				
Callimico	-0.0466	0.0670	0.0010				
Callithrix	-0.0040	0.0493	0.0040				
Cebuella	-0.0134	0.0677	0.0129				
Cebus	-0.0559	-0.0127	0.0134				
Lagothrix	-0.0619	-0.0263	0.0152				
Leontopithecus	0.0300	0.0585	0.0445				
Mico	0.0250	0.0772	0.0302				
Pithecia	0.0107	0.0116	0.0404				
Saguinus	-0.0082	0.1114	-0.0124				
Saimiri	-0.1678	0.0911	-0.0280				
Tarsius	0.0807	0.0257	-0.1637				

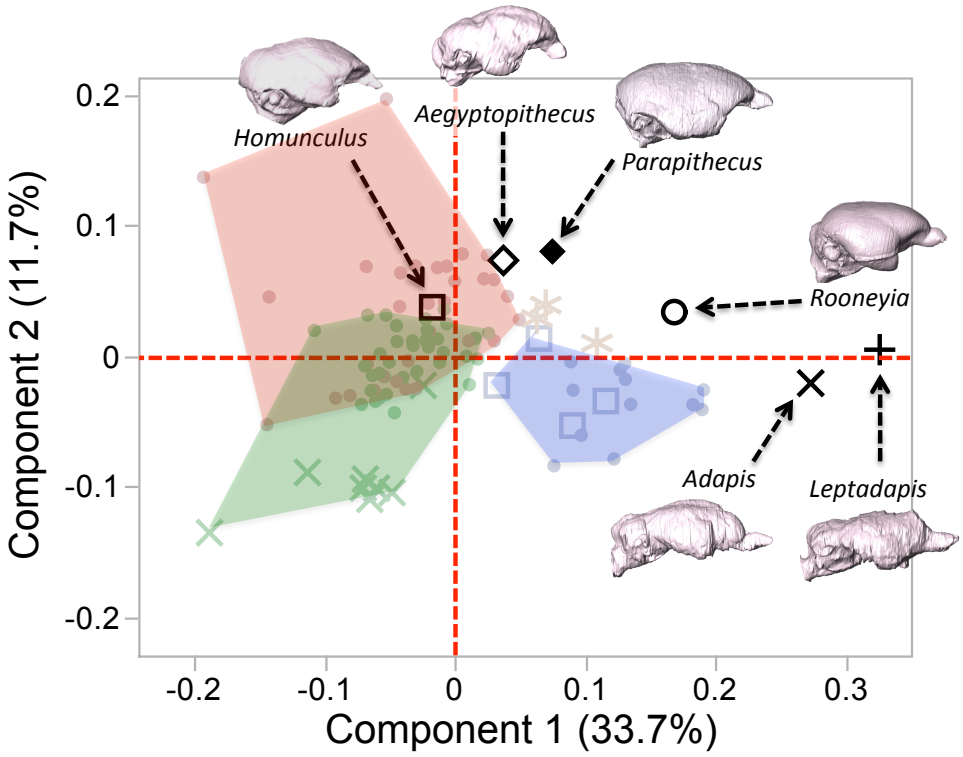

Figure 17: Principal Component Analysis of extant and fossil endocast shape. Blue = strepsirrhines, red = platyrrhines, green = catarrhines, orange stars = tarsiers. Points indicate individual specimen values.

caudally as in the adapiform specimens. While the adapiforms lie outside of the 95% confidence ellipsoid for extant strepsirrhines, the *Rooneyia* endocast is much closer to the extant strepsirrhines in shape, lying right at the edge of the distribution (see Figure 18). *Rooneyia* differs from strepsirrhines on PC2, owing to a wider cerebral breadth, somewhat reminiscent of *Tarsius*; however, *Rooneyia* does not group with tarsiers on PC3, an axis which separates tarsiers from all other extant and extinct primate specimen included in the sample.

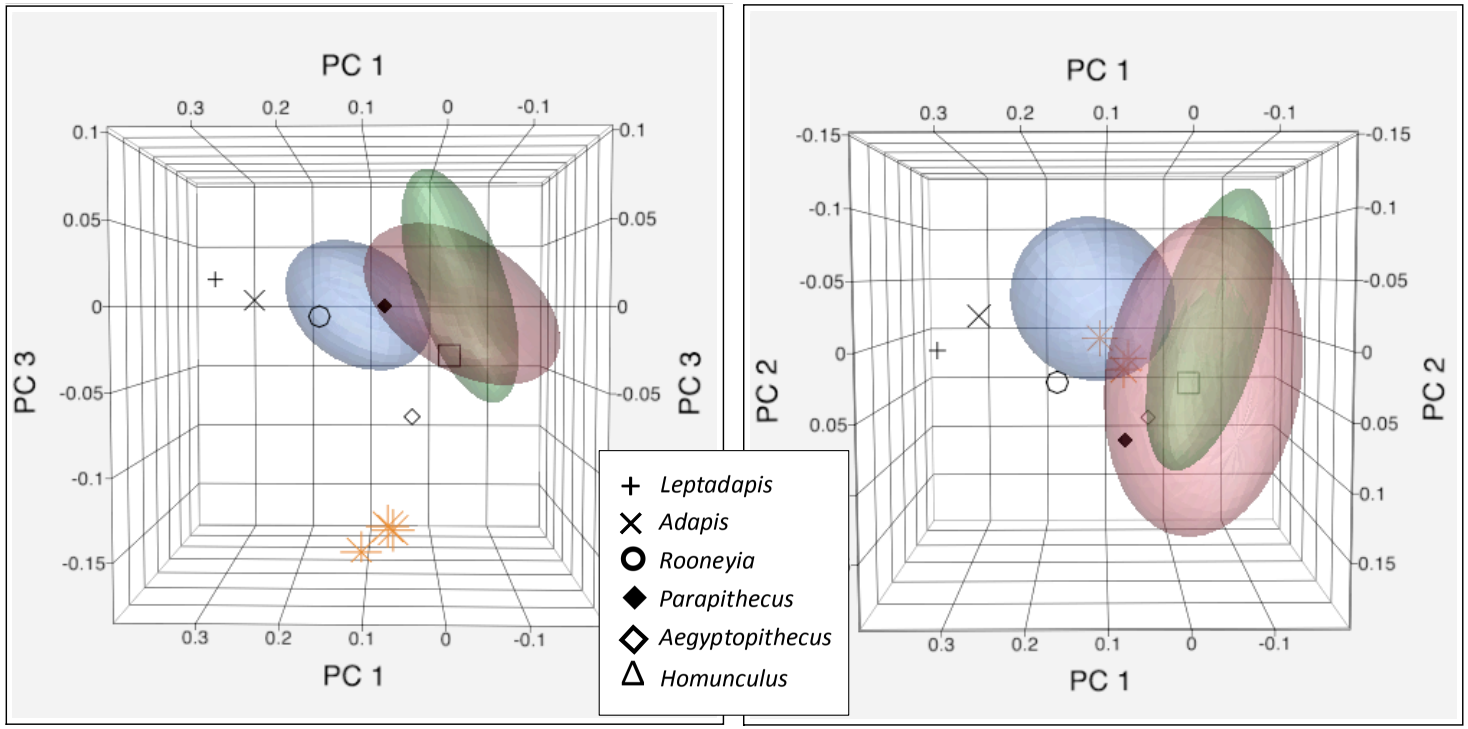

Figure 18: 3D plot of 95% confidence ellipsoids from Principal Components 1, 2, and 3, derived from endocast landmark configurations of extant and fossil primates. Blue = strepsirrhine confidence ellipsoid, red = haplorhine confidence ellipsoid, orange stars = tarsiers. Points indicate individual specimen values.

Early Oligocene anthropoids *Parapithecus* and *Aegyptopithecus* have intermediate morphologies, as evidenced by their placement in the area of overlap between haplorhines (tarsier, *Alouatta*) and strepsirrhines (lorises) on Component 1. Both specimens have relatively large olfactory bulbs as in modern strepsirrhines, but the relative placement of the caudal landmarks is more reminiscent of extant anthropoid primates. Both specimens fall within the haplorhine confidence ellipsoid when PC scores 1 through 3 are considered together (Figure 18). *Aegyptopithecus* falls closer to the group centroid for anthropoids than does *Parapithecus*, owing to a more inferiorly deflected—as opposed to rostrally projecting—olfactory fossa and a higher endovertex in *Aegyptopithecus*.

While the early anthropoids show a mixture of strepsirrhine and anthropoid traits, the Miocene playrrhines *Tremacebus* and *Homunculus* demonstrate a more fully modern anthropoid shape to the endocast. The olfactory fossa of *Homunculus* is further reduced, and somewhat more inferiorly directed than in the extant strepsirrhines, and the occipital poles extend caudally over the posterior cranial fossa. Although the confluence of sinuses is not preserved in the *Tremacebus* specimen, the remaining portions of the endocast resemble modern anthropoids in having a somewhat flexed brain base, a superior-inferiorly "tall" endocast, and a more inferiorly directed olfactory fossa (see Figure 16).

2.4. Discussion

2.4.1. Endocast Shape and Brain Proportions

This geometric morphometric analysis of endocast shape bolsters qualitative observations made by Radinsky (1974) and others (Simons 1993; Simons 1995; Simons 2001; Bush *et al.* 2004; Simons *et al.* 2007), which conclude that strepsirrhine and anthropoid primates fundamentally differ in aspects of endocranial proportions. On the other hand, this analysis demonstrates that modern primates exhibit a broad range of variation in endocranial shape within these clades.

While endocranial shape carries a strong phylogenetic signal, differences in encephalization and body size also account for a proportion of the shape variation among closely related animals. The primary axis of shape variation (captured by PC1) reflects species differences in both residual endocranial volume and brain proportions—specifically, the relative size of the telencephalon, cerebellum, and olfactory bulbs. Thus, it is important to determine whether the effects of encephalization, body size, and brain proportions can be disentangled from one another, so that we may interpret the evolutionary implications of mosaicism: did brain size evolve independent of brain proportions?

One approach to answering this question is to compare pairs of closely related species, which differ widely in encephalization, despite a relatively conserved pattern of

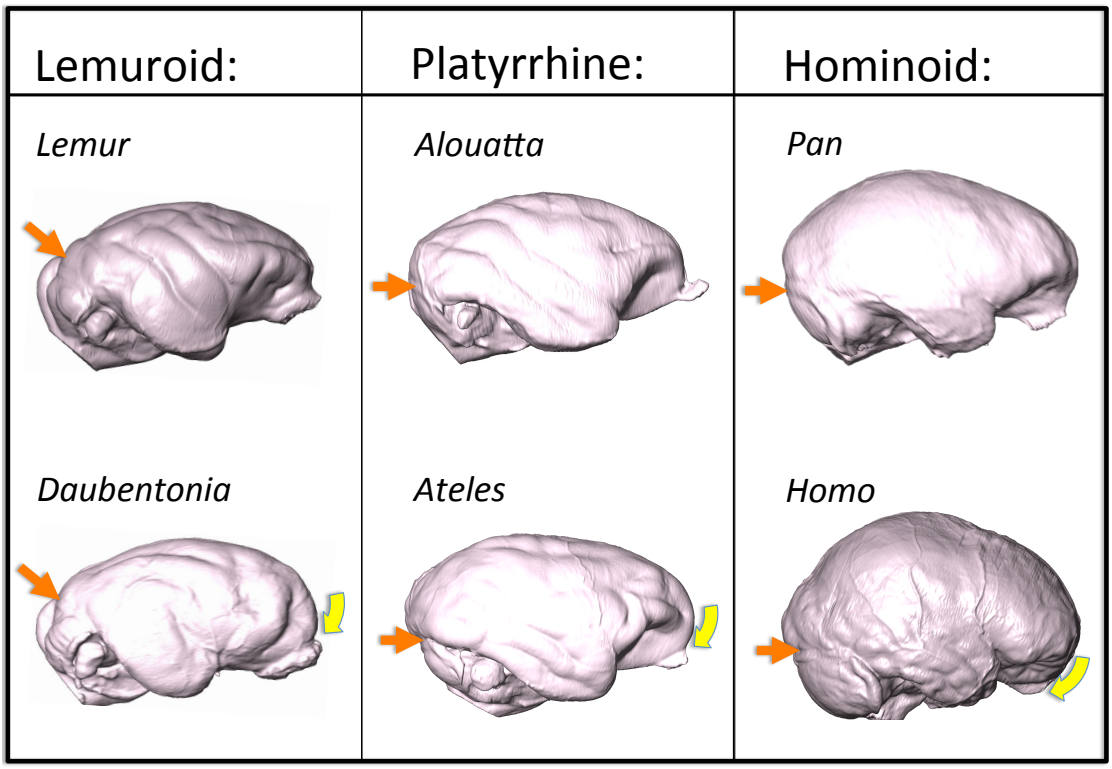

Figure 19: Variation in endocast shape associated with encephalization differences within primate clades. Each column represents a pair of related taxa, scaled to equal fronto-ccipital pole length. Species on the bottom row have greater residual endocranial volume than their relative depicted on the top row. Orange arrows point to the confluence of sinus, yellow arrows highlight the inferior deflection of the olfactory fossa and associated rounding of the frontal region in more encephalized species.

brain proportions (see Figure 19). Within and among extant primate groups, species with greater encephalization tend to have more inferiorly deflected olfactory bulbs, more rounded rostral aspects of the frontal region, and somewhat more flexed brain bases. These trends are particularly evident within extant Anthropoidea, where a broader variation in encephalization occurs as compared to strepsirrhines. Enlow and

McNamara (1973) note the marked inferior displacement of the olfactory fossa in *Homo sapiens*, and theorize that unusually horizontal alignment of the cribriform in humans is associated with frontal lobe expansion and/or enlargement of the cerebrum as a whole. Likewise, Bastir *et al.* (2010) found that within a sample of extant anthropoids, the verticality of the cribriform plate is associated with encephalization. Larger brained anthropoids (hominoids) tend to have shorter and more horizontally aligned cribriform plates. The dataset presented herein demonstrates that this association is a general phenomenon among primates, with more encephalized strepsirrhines (i.e. *Daubentonia*) likewise demonstrating an inferiorly deflected olfactory fossa, resulting in a more horizontally aligned—though in this case not markedly reduced—cribriform than in less encephalized strepsirrhines.

Further accounting for the anthropoid-strepsirrhine dichotomy endocast shape is the size of the olfactory fossa. This analysis supports previous findings that strepsirrhines have large olfactory fossae (Radinsky 1974; Kay *et al.* 2004), reflecting relatively larger olfactory bulbs in strepsirrhines than those found among anthropoids (Stephan *et al.* 1981; Baron *et al.* 1983; Barton *et al.* 1995; Barton and Harvey 2000). However, previous interpretations of brain proportions, including the size of the frontal lobe, based on endocast shape should be re-examined based on data presented herein. For example, several authors (Radinsky 1970; Radinsky 1974; Simons 1993; Simons 1995; Kay and Kirk 2000; Simons 2001; Kay *et al.* 2004; Simons *et al.* 2007; Kay *et al.* 2008; Kay *et*

al. 2012) have interpreted an "inflated" or rounded frontal region of the endocast and the inferior deflection of the olfactory fossa as being anthropoid traits related to the increased size of the frontal lobe and concomitant reduction in olfactory bulb size. In actuality, little data exists concerning the variability in frontal lobe volume among strepsirrhines. Data herein suggest that the position of the olfactory fossa is somewhat independent of olfactory fossa size and is instead related to overall encephalization. Among primates, the frontal lobe has been demonstrated to scale with positive allometry on the rest of the neocortex (Semendeferi *et al.* 2002; Bush *et al.* 2004; Smaers *et al.* 2010), such that more encephalized species have proportionately larger frontal lobes. It is therefore unclear whether the rostral "bulging" of the frontal region in more encephalized extant primates is related to independent selection on frontal lobe volume, or on encephalization in general. Nevertheless, the anatomy of the fossil specimens should more accurately be interpreted as a reflection of their relatively small endocrania, rather than a small frontal lobe. Furthermore, small-bodied and moderately encephalized platyrrhine monkeys (i.e. *Saguinus*) demonstrate similar morphologies, with a rostrally projecting olfactory fossa, and dorsally receding frontal profile. Thus, while the posterior projection of the occipital poles relative to the posterior cranial fossa appears to be a stable anthropoid trait, found in both fossil and extant representatives, and reflective of the enlargement of the telencephalon relative to the cerebellum, the rostral morphology of the endocast is more reflective of encephalization and olfactory

bulb size. This supports previous assessments that multiple secondary reductions in olfactory bulb size and increases in relative brain size occurred within anthropoid primates, following an initial shift in brain proportions at the base of the anthropoid clade.

2.4.2. Tarsier Endocranial Morphology and Its Implication for Haplorhine Brain Evolution

The morphology of *Tarsius* presents a conundrum in the study of primate brain evolution. Although early studies examine tarsiers in the context of the "prosimian" grade, owing to their strepsirrhine-like levels of encephalization (Stephan and Andy 1964; Radinsky 1975; Stephan *et al.* 1988), the results herein support the conclusion of Joffe and Dunbar (1998) in their reanalysis of the Stephan data: tarsiers share many derived features of brain proportions with anthropoids (i.e. enlarged visual and neocortices, reduced olfactory bulb), despite having lower levels of relative brain size than typically observed among extant anthropoid species. This scenario presents strong evidence for the possibility of mosaicism in the relative size of brain components, contrary to a strict adherence to the Developmental Constraints Hypothesis of Finlay and Darlington (1995).

For the present concern—the co-evolution of brain size, brain proportions, and endocranial shape—tarsiers presents a further puzzle. The tarsier endocranium is in many ways unique among the primates sampled herein. The endocast is uniquely rostro-caudally short and medio-laterally broad with temporal poles that do not

protrude rostrally to the extant seen in most other primate species. Large bilateral impressions from the bony orbits are readily observable, suggesting that the endocranium is closely molded around the internal surface of the orbits, while in most other species there is less encroachment of the orbit on the lateral aspects of the parietal and temporal regions of the endocranium. Among most primates, the frontal lobe archs rostrally above the orbits to some degree, with more encephalized species having a greater degree of anterior expansion of the endocranium; the endocranium of tarsiers, in contrast, is primarily restricted to the interorbital and postorbital regions. The placement of *Tarsius* among the strepsirrhines in the first principal component of the endocast shape analysis likely reflects the low level of encephalization in this genus, and the intermediate size of their sensory systems. Although the sensory system of *Tarsius* is derived towards anthropoids in having a reduced olfactory bulb and enlarged visual cortex as compared to extant strepsirrhines, these components deviate moderately from the anthropoid mean. Despite having astonishingly large eyes, tarsiers have smaller visual processing centers of the brain than do most other haplorhines. In absence of a tapetum lucidum, the enlargement of the eye in tarsiers facilitates greater reception of light through the enlarged pupil and an increased surface area of the retina. Nevertheless, it is possible that the increase in light reception does not necessitate an increase in visual integration in the neocortex. Instead, the enlargement of the occipital

region in anthropoids is likely related to an increase in visual acuity within this group (Kirk 2006).

Parsimoniously, it seems most likely that the anthropoid brain *bauplan* was established at the base of Haplorhini (and should more appropriately be called the "haplorhine *bauplan*"), with subsequent encephalization occurring among anthropoid clades. An alternative scenario is possible in which tarsier and anthropoid brain proportions evolved in parallel due to parallel selective pressures, namely increased visual acuity and reduced reliance on olfactory cues (Joffe and Dunbar 1998). Given the strong correspondence between the mosaic enlargement of the visual and auditory sensory systems and what is known about tarsier ecology and behavior, it is possible that their brain proportions are the result of selection for enhanced prey detection and communication with conspecifics. It is difficult to rule out this latter scenario, as the fossil record for basal Haplorhini and basal Tarsioidea is sparse, fragmentary, and controversial in its taxonomic interpretations (Simons 2003).

2.5. Conclusions

This study supports previous efforts in concluding that haplorhine primates differ fundamentally from strepsirrhines in overall brain proportions (relative mass of brain parts). Furthermore, changes in endocast shape associated with changes in brain proportions occurred early in anthropoid evolution, with anthropoids undergoing subsequent parallel encephalization events.

1) Among extant primates, endocast shape is highly correlated with phylogenetic relationships, and significantly separates strepsirrhine from anthropoid primates. Anthropoids display more flexed endocranial bases, smaller and more inferiorly directed olfactory fossa, and more anteriorly shifted posterior cranial fossae.
2) Both allometry and encephalization have some effect on endocranial form. Variation in endocast shape is correlated with residual endocranial volume among extant primates. Endocast shape variables show some correlation with absolute endocranial volume among anthropoids only, with larger species having more flexed endocranial bases and superior-inferiorly taller endocasts.
3) Early anthropoids trend towards modern anthropoid-like endocast shape despite low residual endocranial volume. In particular, early anthropoid fossils under consideration here demonstrate: intermediately sized and somewhat rostrally projecting olfactory fossae, posterior projection of the cerebral hemispheres, moderate flexion of the brain base, and low endovertex height (flattened dorsal profile in lateral view) and less "inflated", or broad, parietal regions than that seen in modern anthropoids.
4) Among extant primates, the genus *Tarsius* has a unique combination of endocranial shape features, with an anteriorly positioned foramen magnum,

moderately large and rostrally projecting olfactory fossa, caudally positioned temporal poles, and rostral-caudally short and mediolaterally broad cerebral regions. This morphology may reflect a combination of anthropoid-like brain proportions at a strepsirrhine-like level of encephalization. Ecological adaptations almost certainly play a further role, with potential spatial constraints imposed by very large orbits and a reorganization of the sensory systems for conspecific communication and insect predation.

In summary, the evidence available from extant brain component mass and fossil primate endocast shape indicate some reduction in relative olfactory bulb volume and an increase in relative telencephalon volume had occurred at least by the base of the anthropoid clade—but perhaps earlier, at the base of Haplorhini—prior to the establishment of modern levels of anthropoid encephalization, with further reduction of the olfactory bulb occurring in the platyrrhine and catarrhine clades, prior to additional parallel encephalization within and between these groups.

3. Co-evolution of Encephalization and Cranial Form in Primates

3.1. Introduction

Variation in encephalization has been explored as an explanatory variable for differences in craniofacial form among primate clades. Although much of this work has focused on the unique combination of characteristics displayed by the human skull—extreme facial reduction, basicranial flexion, and neurocranial globularity—as it relates to encephalization (Enlow and McNamara 1973; Lieberman and McCarthy 1999; Lieberman *et al.* 2000a; Lieberman *et al.* 2000b; Lieberman *et al.* 2000c; Bastir *et al.* 2010), others have explored correlated evolution of these variables to explain overall cranial differences between extant strepsirrhine and anthropoid primates. In particular, strepsirrhines and anthropoids differ in multiple aspects of "cranial organization", including craniofacial hafting—the angle at which the facial skeleton is oriented relative to the cranial base, and/or the flexion of the cranial base (Enlow 1990; Ross and Henneberg 1995; Lieberman and McCarthy 1999; Lieberman *et al.* 2000b; Lieberman *et al.* 2000c; Bastir *et al.* 2010), the relative size of the facial skeleton (Biegert 1963; Bastir *et al.* 2010), the orientation of the bony orbits (Ross and Henneberg 1995; Ross 1995), and the globularity of the neurocranium—i.e. its tendency to approach a spherical shape (Bruner 2004; Martinez-Abadias *et al.* 2009; Neubauer *et al.* 2010; Bienvenu *et al.* 2011). As extant strepsirrhines and anthropoids also differ markedly in brain size, these studies have reasonably suggested that the distinctive phylogenetic trends in cranial shape may be a

result of spatial or developmental constraints imposed on the neurocranium by encephalization, both interspecifically (evolutionary trends) and throughout development within a given individual (ontogenetic trends), and that the unique form of the human cranium—with its extreme facial shortening and highly flexed cranial base—is a result of the exaggeration of these trends in a "hyper-encephalized" species (Weidenreich 1941; Weidenreich 1947; Enlow and McNamara 1973; Lieberman *et al.* 2000a; Lieberman *et al.* 2000b; Lieberman *et al.* 2000c).

3.1.1. The Effects of Encephalization on Cranial Base Angle and Facial Size

The "Spatial Packing Hypothesis" proposed by Biegert (1963) and Gould (1977) suggests that adult interspecific variation in the orientation of the cranial base is the result of spatial constraints on the length and breadth of the neurocranium, relative to body size, and the developmental growth and/or evolution of an enlarged neurocranial volume. Adaptive and allometric processes influence both features. A negatively allometric scaling trend occurs in adult interspecific mammalian brain size, such that small-bodied animals have greater brain volume for their body weight than do large-bodied animals (Count 1947; Gould 1966; Gould 1975). Thus, larger-bodied animals may be expected to have greater flexion of the brain base, as would animals with a larger brain for a given body size, if one assumes that the neurocranium expands rostrally and caudally over the basicranium via the path of least resistance (Lieberman *et al.* 2000b).

Adding to the Spatial Packing Hypothesis, Enlow and Azuma (1975) further proposed that the degree of basicranial flexion may be a compromise between both the size of the neurocranium and the facial skeleton relative to body size. This "Facial Packing Hypothesis" proposes that selection for a large masticatory apparatus may act antagonistically on basicranial flexion, with larger facial size failing to permit the "tucking" of the facial skeleton under the neurocranium, owing to the spatial constraints encountered by the pharyngeal contents (Enlow and Azuma 1975; Bastir *et al.* 2010). This hypothesis proposes that the mechanism for adult interspecific variation in basicranial angle and facial hafting is the interaction between the upper facial skeleton and anterior cranial fossa and the mid-facial skeleton and middle cranial fossa over ontogenetic development. Due to the close proximity of these paired features, an increase in brain size relative to body size is thought to result in a "packing" problem in which the splanchnocranium must rotate upward and/or reduce in size to accommodate the growing brain (Weidenreich 1941; Enlow and Azuma 1975; Enlow 1990; Lieberman *et al.* 2000b; Bastir *et al.* 2008; Lieberman *et al.* 2008). This hypothesis thus predicts the following condition with respect to interspecific variation in adult cranial form: animals with larger brains for their skull size and smaller faces will have greater flexion of the basicranium, while animals with larger faces or smaller brains will exhibit less flexion. Lieberman *et al.* (2008) assert that there is little overt support for aspects of this hypothesis, citing a lack of strong correlation between upper facial morphology (orbit

size and orientation) with the orientation of the anterior cranial base (Ross and Ravosa 1993; Lieberman and McCarthy 1999). Ross and Ravosa (1993) found that a ratio of neocortical volume to palate length is negatively correlated with cranial base angle in platyrrhines only. Nevertheless, Bastir et al. (2010) explore the interplay between facial size, endocranial volumes, and basicranial flexion in anthropoid primates, and find some support for the Facial Packing Hypothesis. Importantly, they suggest that the conflicting forces working on the facial skeleton and neurocranium may account for the relatively unflexed cranial bases in mid-Pleistocene hominins as compared to modern *Homo sapiens* (Bastir *et al.* 2010). Despite having a larger total brain volume than most primate species, these species also demonstrate large facial sizes, perhaps as a result of adaptive selection on the facial skeleton for mastication, or as a consequence of elongated growth periods associated with body size or secondary sexual characteristics.

Fleagle *et al.* (2010) utilized geometric morphometric techniques to demonstrate a quantifiable difference in cranial shape between strepsirrhines and anthropoids. In a Principal Components Analysis of Procrustes-aligned shape variables from extant adult crania, the first component significantly separated extant strepsirrhine from anthropoid primates, with primary shape changes along this axis including orbit orientation, flexion of the skull base, and the size of the facial skeleton and neurocranium (Fleagle *et al.* 2010). These results lend support to the notion that the primary cranial differences among extant primate groups may be a result of differences in residual endocranial

volume. Although the study by Fleagle *et al.* (2010) did not directly test the Spatial or Facial Packing Hypotheses, their results are consistent with the possibility that strepsirrhine-anthropoid adult cranial differences are the result of co-evolution of cranial organization and encephalization as a consequence of spatial and/or developmental constraints on cephalic growth.

3.1.2. Brain Shape and Basicranial Form

Both ontogenetic growth (Lieberman and McCarthy 1999; Lieberman *et al.* 2000c; Lieberman *et al.* 2008) and adult interspecific differences in relative brain size (Ross and Ravosa 1993; Ross and Henneberg 1995; Ross 1995; Lieberman *et al.* 2000b; McCarthy and Lieberman 2001; Bastir *et al.* 2008; Bastir *et al.* 2010) have been explored in terms of their relationship to basicranial angle, facial size, and orbit orientation; however, these hypotheses make several assumptions about the nature of the spatial relationship between the neurocranium, facial skeleton, and basicranium which involve predictable patterns of brain shape differences associated with relative brain size. Jerison (1982) proposed that a relatively larger brain for a given basicranial length would be more spherical, with increased flexion of the cranial base, as a relatively long braincase length would cause an imbalance of the head atop the spine. Lieberman *et al.* (2000c) dispute this logic, pointing to mammals such as llamas, which successfully balance their elongated and extended crania upon an orthograde spine with no apparent locomotor issues. Biegert (1963) also predicts that a larger brain for a given cranial base length

would be more spherical and accompanied by greater flexion of the cranial base. These proposed relationships among encephalization, globularity, and basicranial angle have yet to be systematically tested.

3.1.3. Previous Studies

Despite the apparent association between encephalization and cranial organization in extant primates, the fossil record for hominin evolution has been ambiguous in it's conformity to expectations based on modern associations. For instance, Neanderthal neurocrania, though as large or larger than anatomically modern humans, demonstrate more rostro-caudally elongated endocasts and lower levels of basicranial flexion than the similarly encephalized *Homo sapiens* (Ross and Henneberg 1995; Bastir *et al.* 2010). Furthermore, early anthropoid endocasts possess qualitative similarities with living anthropoids at relatively small endocranial volumes, perhaps indicating a disconnect between endocast shape and encephalization in early anthropoid evolution (Radinsky 1974; Simons 1993; Bush *et al.* 2004; Simons *et al.* 2007). It should be noted that Ross and Ravosa (1993) did not detect a significant relationship between encephalization and cranial base angle among extant adult strepsirrhines. However, it has yet to be tested whether facial size and brain size interact in extant strepsirrhines to account for variation in basicranial flexion.

While expectations about how brain, face, and basicranium interact have focused on two levels—developmental and evolutionary—the same basic rationale applies to

both: the basicranium is preformed in cartilage and its length scales isometrically with respect to bodymass, an enlarged brain relative to length of basicranium would result in rostral and caudal expansion of the brain and flexion of the brain base around the sellar basin (Weidenreich 1941; Lieberman and McCarthy 1999; Lieberman *et al.* 2000a; Lieberman *et al.* 2000b; Lieberman *et al.* 2000c; Bastir *et al.* 2010). According to Biegert's (1963) bi-directional Spatial Constraint Hypothesis, we would expect that increased in brain size relative to body size would be associated with increased neurocranial globularity and basicranial flexion, with some antagonistic association with facial size. Although a relationship between brain size, basicranial flexion, and facial size has been supported by a recent interspecific midline morphology study by Bastir (2010) and may account for some proportion of the unique human cranial morphotype, these methods have yet to be applied to the strepsirrhine-anthropoid cranial shape dichotomy.

Lieberman *et al.* (2000a) define neurocranial globularity as: "the roundedness of the cranial vault in the sagittal, coronal, and transverse planes"; however, it is important to note that "roundness" is a term that carries specific significance in the geological sciences, referring to the continuous smoothness—as opposed to angularity—of a particle's surface (Wadell 1933; Wadell 1935). Globularity, as used in the morphological literature (Lieberman *et al.* 2000a; Gonzalez-Jose *et al.* 2008; Martinez-Abadias *et al.* 2009), more closely approximates the geological principal of "sphericity"—the deviation of the shape from that of a sphere (Wadell 1933). Neurocranial globularity is often qualitatively

assessed, with humans being held as the typification of a globular brain (Holloway 1979; Neubauer *et al.* 2010). Recent efforts to quantify globularity provide a means for examining intra and interspecific variation in this feature (Lieberman *et al.* 2000a; Holloway *et al.* 2004; Gonzalez-Jose *et al.* 2008; Martinez-Abadias *et al.* 2009). Lieberman *et al.* (2000a) explore neurocranial globularity as a defining feature separating anatomically modern humans from archaic *Homo*. This study examines the relationship between neurocranial globularity, cranial base flexion, and facial size and shape to determine whether Biegert's (1963) Spatial Constraints Hypothesis and Enlow's Facial Packing Hypothesis may account for shape differences observed between adult specimens of extant strepsirrhines and anthropoids.

3.2. Materials and Methods

3.2.1. Data Collection

For the endocranial analyses the endocranial volumes, landmarks, and angular measurements were taken on CT scans of adult dry primate crania, using the same sample as Chapter 2). Fossils used in this analysis include: Eocene euprimate *Adapis*, Oligocene anthropoids *Parapithecus* and *Aegyptopithecus*, and the Miocene platyrrhine *Homunculus*. Portions of the basicranium, midline endocranial outline and/or some facial landmarks were unavailable for *Leptadapis* and *Tremacebus* due to breakage of the specimens, therefore, these specimens were excluded from this analysis.

Midsagittal tomographic slices were computed using the "slice" module in *Avizo*. A midsagittal slice was defined by fitting a best-fit plane to the following midline landmarks: prosthion, nasion, bregma, inion, basion, palatine tubercle (for landmark definitions, see table 11). The resulting midsagittal tomograph was extracted and saved as a .jpg image, with associated pixel dimensions preserved in a .txt document. In some cases, it was necessary to extract a slice that was one to three voxels lateral to the midline plane, to avoid the crista galli, the presence of which obscured important anatomical landmarks (i.e. foramen caecum, posterior extent of the cribriform plate). In these cases, I felt justified in doing so, as there was little to no qualitatively identifiable difference in other aspects of endocranial shape among these adjacent slices.

Midsagittal landmark data and angular measurements were collected in the software program tpsDIG (version 2.17, Rohlf, 2013). Data collection included 13 craniofacial landmarks and one landmark curve. The outline of the endocranial cavity was followed using the curve drawing function and selecting a dense number of points along the inner bone table of the neurocranium, anchored anteriorly by the anterior extent of the cribriform plate and posteriorly by opisthion. The curve was then resampled to 30 points (28 along curve, 2 bounding landmarks), which were exported to Microsoft Excel for additional calculations (see Analysis: midline globularity). Table 11 and Figure 20 provide a list of facial landmarks included in this analysis and their definitions.

3.2.2. Variables Used In This Study

Basicranial angle is measured by two methods; basicranial angle 1 (BCA1) is angle formed between two chords: 1) sphenoidale – planum sphenoideum point, 2) opisthion – dorsum sellae; basicranial angle 2 (BCA2) is measured as angle formed between three points: opisthion – sella – anterior cribriform plate. I follow Bastir *et al.* (2010) in using the anterior extent of the cribriform plate to represent the most rostral extent of the anterior cranial base, rather than the foramen caecum, owing to the fact that the foramen caecum is located anterior to the frontal pole in some specimens, but resides superior-anterior to the cribriform in Hominoidea.

"Globularity" is defined here as the sphericity of an object, or its degree of deviation from a perfect sphere. Mathematically, a sphere is defined as having each point on its surface equidistant from the center of the object. Thus, if we sample two three-dimensional landmarks, defined in x, y, z Cartesian coordinates, the following should be true:

distance 1	=	distance 2
$\sqrt{[(x_a-x_c)^2 + (y_a-y_c)^2 + (z_a-z_c)^2]}$	=	$\sqrt{[(x_b-x_c)^2 + (y_b-y_c)^2 + (z_b-z_c)^2]}$

where "a" represents one randomly placed landmark on the sphere's surface, "b" represents a second landmark, "c" represents the center point of the object, and the distance between two points is calculated as the squared root of the sum of squared distances between the three-dimensional points.

If distance 1 ≠ distance 2, then the object cannot be considered spherical. Furthermore, a ratio of any two polar distances from a sphere should be equal (maximum height/maximum breadth = 1). Any deviation from 1 would signify an oblate or otherwise irregular spheroid.

For the purposes of this study, globularity is defined in multiple ways: 1) "midline globularity", a two-dimensional analysis of midline features using a resampled surface outline from the endocranial surface of a midsagittal tomograph, 2) "three-dimensional globularity", a measurement using select three-dimensional landmarks from virtual endocasts analyzed in Chapter 2, and 3) "globularity index", a ratio of two distances representing endocranial height and length.

3.2.2.1. Midline Globularity

As described above, all landmarks placed on the surface of a perfect sphere should be equidistant from the centroid of that sphere. Thus, the deviation of these distances from one another represents the deviation from sphericity. Midline globularity—the degree of sphericity of the endocranial outline in the midsagittal view—is mathematically defined as the variance among each landmark's distance from the centroid of the landmark dataset for the same individual:

$$\text{Globularity} = \text{coefficient of variation} = \sqrt{[\sum(\mu - x)^2]} / \mu$$

where x = distance between a given landmark and the centroid; μ = the mean of all distances for the target specimen.

Table 11: Craniofacial landmarks and angular measurements collected from midsagittal tomographs of primate crania. # refers to the landmark labels in Figure 20.

#	Landmark	Location	Definition
1	prosthion	face	inferior anterior point of alveolus between central incisors
2	acanthion	face	anterior inferior nasal spin
3	rhinion	face	inferior point between nasal sutures
4	glabella	face	the most forward projecting point of the forehead in the midline of the supraorbital ridges
5	palatine tubercle	face	the most posterior extent of the palatine tubercle on the maxillary process
6	basion	endocranial	the most anterior midline point of the foramen magnum
7	opisthion	cranial base	the most posterior midline point of the foramen magnum
8	anterior cribriform point	endocranial	the anterior/rostral most point of the cribriform plate
9	posterior cribriform point	cranial base	the most posterior/caudal point of the cribriform plate
10	sphenoidale	cranial base	the most posterior/superior point on the tuberculum sellae in midsagittal view
11	planum sphenoideum point	cranial base	the most anterior/superior point on the convexity just posterior to the cribriform plate
12	sella	cranial base	the midpoint of the hypophyseal fossa
13	dorsum sellae	cranial base	the posterior point on the bony plate forming the posterior border of the hypophyseal fossa
14	bregma	midline plane	the intersection between the coronal and sagittal sutures
15	inion	midline plane	the posteriormost point of the neurocranial skeleton, often coincident with the nuchal prominence

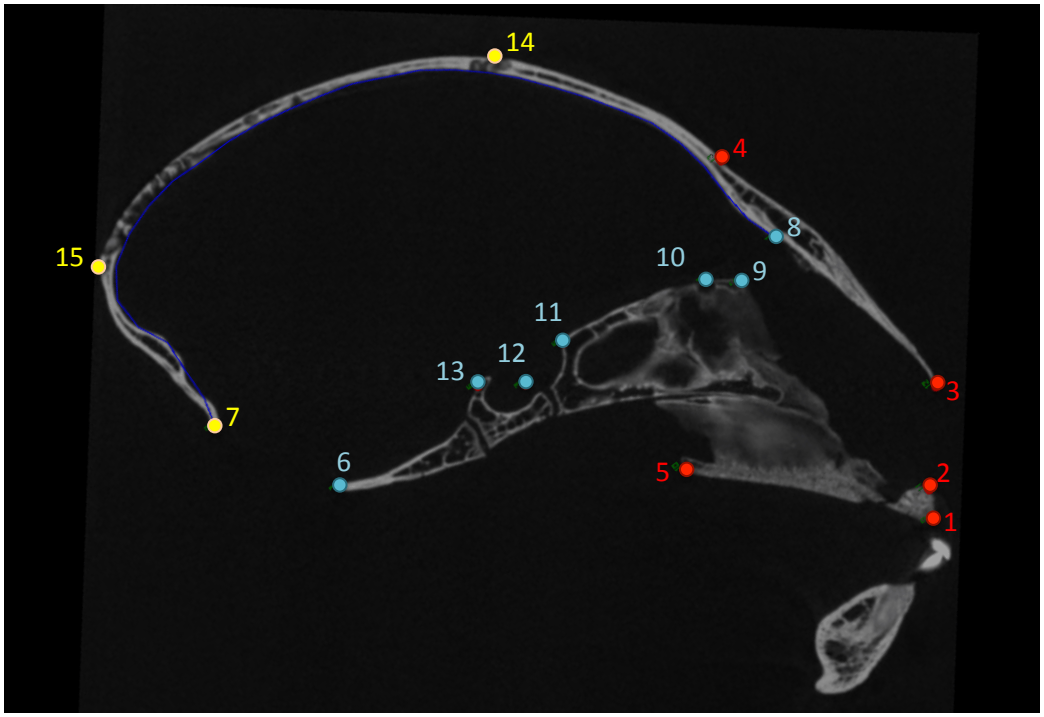

Figure 20: Landmarks taken on midsagittal tomographs of primate crania. Numbering refers to # column of Table 11. Red (1-5) = facial set, blue (6-13) = cranial base, yellow (7, 15, 15) = additional landmarks used to define midsagittal plane.

When all distances to the centroid are equal (a state of sphericity), the coefficient of variation will equal 0 for that individual. Variance ($\sum(\mu-x)^2$) is not a size-independent measure, and as such animals of larger body size may be found to have larger variance if raw landmark points were used. I correct for this possibility by using the coefficient of variation, which is scaled against the mean distance for the individual. Secondly, the landmark data is subject to a Procrustes transformation prior to the calculation of variance. The transformation rotates, translates, and resizes the objects to minimize the

least squared distances among homologous points across specimens within the dataset. The resulting calculations of variance should be size-independent; however, this does not preclude the possibility that midline globularity has allometric properties.

3.2.2.2. Three-Dimensional Globularity

Three-dimensional globularity is defined in the same way as that described above for midline globularity; however, this measure utilizes landmarks placed on the three-dimensional surface of virtual endocasts of the same specimens. This measure utilizes select anatomically homologous points from those identified in Chapter 2 (see Table 2 for endocast landmark definitions). This dataset includes the dorsal and posterior midline landmarks, as well as those on the lateral surface of the endocast (e.g. maximum cerebral breadth, maximum cerebellar breadth), thus incorporating aspect of endocranial breadth. For this analysis, midline and parasagittal landmarks associated with the olfactory (anterior and posterior olfactory points) and optic system (optic canal, clinoid processes) were excluded, owing to group-specific differences in the size and placement of these features. For example, the olfactory fossa of strepsirrhines tends to be larger and more rostrally projecting than it is in anthropoids. Thus inclusion of these points would reduce globularity estimates for strepsirrhines by inflating the degree of sagittal elongation captured by this measurement. As with midline globularity, three-dimensional globularity is quantified as the coefficient of variation among all landmark distances from the object centroid for a given individual (object centroid calculated from

the original endocast volume file), following Procrustes transformation of the entire landmark dataset.

3.2.2.3. Globularity Index

Globularity of the endocast is also measured using a dimensionless ratio, similar to that employed by Lieberman *et al.* (2002) in their examination of "neurocranial globularity" among extant and fossil representations of *Homo sapiens*. Where these authors use distances between pairs of ectocranial landmarks to define their index (euryon-euryon*basion-vertex)/(nasion-opsithocranion), this study utilizes select endocranial landmarks from the dataset provided in Chapter 2. The globularity index is calculated as follows:

$$\text{Globularity Index (GI)} = \frac{\text{endocast breadth} * \text{endocast height}}{\text{endocast length}^2}$$

where *endocast breadth* is defined as the squared distance of the maximum cerebral breadth to the midline plane (midline plane is defined by three landmark points: frontal pole, occipital pole, and endovertex); e*ndocast height* is defined as the distance between endobasion and endovertex; *endocast length* is defined as the distance between the frontal pole and occipital pole.

A perfect sphere would demonstrate a Globularity Index of 1.0, signifying and equal breadth, height, and length of the object. Alternatively, an endocast that is longer than it is high or wide would have a GI < 1.0, while one that is shorter in the sagittal dimension than it is tall or wide would have a GI > 1.0. Other combinations may result

in similar GI values; for example, if the endocast is broad and wide compared to its length it would also have a GI > 1.0.

3.2.2.4. Facial Size and Shape

Thirteen landmarks were placed on the midline plane of the facial skeleton and cranial base for each specimen (Table 11). Landmarks were chosen to represent aspects of facial size and shape—including palate length (prosthion – palatine tubercle), facial height (prosthion – nasion), and craniofacial hafting— cranial base length (basion – palatine tubercle), and cranial base angle. "Facial size" was operationalized as the log10 centroid size of the facial landmark configuration following Procrustes alignment. Residual facial size (resFS) was calculated as the distance from the line in log space from a PGLS regression of species means log facial centroid (y) on log bodymass (x-variable). To calculate these residuals, I used species means body mass taken from (Isler *et al.* 2008).

3.2.3. Analysis

Group level distributions of globularity were examined using a Kruskal-Wallace test, with multiple posthoc pair-wise comparisons (Wilcoxon rank sum, each pair), to determine whether extant strepsirrhines and anthropoids differ in these measures, as would be expected by known differences in encephalization and cranial form. The relationships among facial size, brain size, cranial base angle, and globularity were directly explored using PGLS analyses for correlated evolution using the caper package

for R (Orme *et al.* 2010).

Correlation and partial correlation matrices were constructed for basicranial angle, encephalization, globularity, and facial size, to examine relationships among these variables. Correlation was assessed using Spearman's rank correlation (Spearman's ϱ), a non-parametric measure of statistical dependence (Sokal and Rohlf 2003). Correlation matrices were also constructed to examine relationships among logged (base 10) endocast length, height, and breadth to evaluate the possibility that one of the three dimensions is more or less tightly correlated with absolute (logECV) or residual endocranial (resECV) volume in primates. Significance criterion was determined using Bonferroni correction criterion (α/number of comparisons). Correlation matrices were calculated for catarrhine, platyrrhine, and strepsirrhine primates separately, and associated covariance matrices were compared using the Box's M test in *JMP* (SAS Institute 2013). Box's M test is a component of the MANOVA test that tests the equivalence of two matrices.

Co-variation between the facial landmark configuration and the midline endocranial outline was tested using a two-block partial least squares (2B PLS) analysis in the software MorphoJ (Klingenberg 2011), with a null hypothesis of no association between landmark configurations. The facial landmarks and endocranial outline were Procrustes-aligned as two independent blocks prior to this analysis. Exploratory analyses of shape for the midline endocranial outline and the facial skeleton were

performed via a Principal Components Analysis of Procrustes-Aligned shape configurations to examine group level differences in cranial shape among extant and fossil primates.

3.3. Results

3.3.1. Neurocranial Globularity

Species mean Procrustes-aligned coordinates for midline landmarks are available in Appendix D. Species means for globularity measures are presented in Table 12. Distributions by taxonomic group are listed in Table 13 and Figure 21, with results of multiple sample comparisons among extant primate groups presented in Table 14.

The three globularity measures (3D, midline, and Index) differ in the direction and magnitude of expected values. For both the 3D and midline measures, a higher value indicates a greater degree of variation among distances from endocranial points to the centroid of the landmark set, and thus a greater deviation from a perfect sphere. For both midline and 3D globularity, a perfect sphere would be indicated by a value of 0.0, thus lower values reflect a more globular endocranium. For the globularity index, a value of 1.0 reflects a perfect sphere, as this indicates that the length, breadth, and height of the endocast are equal. If we expect a more encephalized brain (higher resECV) to be more globular (closer to a perfect sphere), then I would predict a negative correlation between resECV and 3D or midline globularity—animals with larger brains for their body size should have lower coefficients of variation among distances from the centroid

to the endocranial surface. Conversely, I predict a positive correlation between resECV and the globularity index.

The three measures of globularity—three-dimensional (3D) globularity, midline globularity, and the globularity index—provide similar results when considering variation among extant primate clades. For all indices, lemuroids have lower globularity (higher 3D and midline globularity and lower globularity indices) than do lorisoids, though significant differences among their distributions occur only with the 3D measure (Wilcoxon rank sum $p = 0.032$). In all three measures, platyrrhines tend to have the least spherical endocasts of all anthropoids (higher midline and 3D coefficients of variation), though they overlap broadly with the cercopithecoid distribution.

Despite capturing similar distributions within the major primate suborders, the three globularity measures differ in some key points. Only midline globularity significantly separates Strepsirrhini from Haplorhini ($p < 0.0001$). Conversely, strepsirrhines and haplorhines demonstrate broad overlap in values for 3D globularity and globularity index values. The relative globularity of the tarsier endocast is dependent on the measure used. *Tarsius* has a midline globularity measure that resembles extant strepsirrhines, while the values for 3D globularity and globularity index indicate that *Tarisus* has a moderately globular endocranium, on par with extant hominoids.

Table 12: Species means for globularity and basicranial variables. See text for abbreviations.

					Globularity Measure					
Group	Group2	Genus	logECV	resECV	3D	Midline	Index	BCA1	BCA2	resFS
Haplorhini	Cercopithecoidea	*Cercocebus*	1.95	0.22	13.23	23.38	0.63	160.3	151.4	-0.0708
		Cercopithecus	1.82	0.11	14.25	29.09	0.59	175.5	173.1	-0.0173
		Chlorbocebus	1.86	0.21	15.20	28.62	0.60	171.7	156.5	-0.0263
		Colobus	1.82	0.01	13.80	32.00	0.52	176.7	155.6	-0.0607
		Erythrocebus	1.90	0.11	16.83	22.81	0.55	157.1	147.5	-0.0454
		Lophocebus	1.98	0.19	15.28	28.44	0.57	159.7	152.8	-0.0054
		Macaca	1.92	0.16	16.64	26.70	0.47	166.4	152.6	-0.0370
		Mandrillus	2.17	0.04	15.25	24.60	0.66	161.8	147.1	0.1020
		Miopithecus	1.61	0.20	16.83	25.70	0.56	165.8	167.1	-0.1072
		Nasalis	1.88	-0.04	16.70	28.89	0.51	162.0	152.5	-0.0926
		Papio	2.19	0.12	13.34	23.89	0.60	160.3	149.4	0.0697
		Piliocolobus	1.81	0.00	15.16	34.30	0.49	171.7	150.6	-0.0398
		Presbytis	1.88	0.04	14.42	26.88	0.51	161.6	151.6	-0.1032
		Procolobus	1.77	0.07	14.28	26.22	0.50	170.6	163.1	-0.0888
		Semnopithecus	1.89	0.03	13.91	25.39	0.59	162.4	147.1	-0.0862
		Simias	1.76	-0.06	15.63	30.78	0.51	166.5	160.3	-0.0602
		Theropithecus	2.12	0.10	16.09	30.96	0.48	162.7	153.0	0.0756
		Trachypithecus	1.87	0.00	13.20	23.63	0.55	164.7	150.5	-0.1151
	Hominoidea	*Gorilla*	2.70	0.05	11.44	29.61	0.66	159.3	149.1	-0.0175
		Homo	3.22	0.66	11.08	18.25	0.75	136.5	114.4	-0.2351
		Hylobates	1.99	0.28	15.63	28.84	0.58	174.4	154.7	-0.0863
		Pan	2.57	0.23	13.43	27.55	0.59	152.2	136.3	-0.0667

	Platyrrhini	*Alouatta*	1.61	0.00	14.01	33.90	0.51	178.3	169.6	-0.0776
		Aotus	1.27	0.02	11.42	27.86	0.57	178.1	168.5	0.0180
		Ateles	2.01	0.21	14.43	24.74	0.48	168.3	155.4	-0.1973
		Cacajao	1.84	0.31	13.66	23.80	0.62	173.2	161.1	-0.1188
		Callicebus	1.25	0.03	12.69	27.79	0.62	172.9	173.8	-0.0826
		Callimico	1.03	0.07	17.70	30.82	0.48	168.8	160.2	-0.1449
		Callithrix	0.82	-0.01	15.59	27.95	0.52	169.2	154.7	-0.0521
		Cebuella	0.62	0.06	17.34	28.84	0.46	164.8	150.6	-0.0793
		Cebus	1.83	0.30	14.33	29.24	0.56	175.1	158.2	-0.0874
		Lagothrix	1.97	0.19	14.84	25.67	0.44	176.2	163.0	-0.1774
		Leontopithecus	1.08	0.05	15.09	31.61	0.50	177.9	170.5	-0.0750
		Mico	0.86	0.01	16.84	28.37	0.47	169.7	160.5	-0.1058
		Pithecia	1.50	0.10	12.00	29.38	0.56	172.3	174.7	-0.0518
		Saguinus	0.88	0.04	17.26	27.78	0.46	174.1	165.7	-0.1194
		Saimiri	1.38	0.24	20.40	18.05	0.51	164.4	165.1	-0.2010
	Tarsioidea	*Tarsius*	0.52	-0.09	13.79	34.99	0.69	169.8	142.7	0.1132
Strepsirrhini	Lemuroidea	*Daubentonia*	1.63	0.17	16.58	42.27	0.46	168.1	158.8	0.0093
		Eulemur	1.39	-0.04	16.04	37.94	0.47	171.1	172.5	0.0424
		Hapalemur	1.16	0.05	17.17	33.62	0.45	178.6	170.3	0.0286
		Indri	1.56	-0.22	18.72	40.99	0.53	173.1	169.0	-0.0028
		Lemur	1.34	-0.08	15.08	36.97	0.55	173.8	173.9	0.0260
		Microcebus	0.33	-0.18	15.63	35.80	0.48	179.0	179.4	-0.0088
		Mirza	0.76	-0.09	14.24	37.91	0.55	177.9	176.4	0.0457
		Varecia	1.50	-0.08	16.14	39.39	0.55	171.9	177.0	0.0920
	Lorisoidea	*Galago*	0.59	-0.12	14.62	32.31	0.54	177.8	175.9	0.0021
		Loris	0.73	0.06	11.86	35.73	0.63	176.7	162.0	0.0682
		Nycticebus	1.06	-0.07	12.99	39.09	0.58	173.5	169.9	0.0790

Table 13: Means and standard deviations (SD) for endocranial globularity measures by taxonomic group. n = number of species per taxonomic group.

		3D Globularity		Midline Globularity		Globularity Index	
Group	n	Mean	SD	Mean	SD	Mean	SD
Lemuroidea	3	13.16	1.39	35.71	3.39	0.58	0.05
Lorisoidea	7	16.20	1.36	38.11	2.78	0.51	0.04
Tarsioidea	1	13.79		34.99		0.69	
Platyrrhini	16	15.17	2.41	27.72	3.70	0.52	0.06
Cercopithecoidea	18	12.90	2.10	26.06	5.28	0.65	0.08
Hominoidea	4	14.89	1.22	27.35	3.26	0.55	0.05
HAPLORHINI	38	14.76	1.94	27.56	3.76	0.55	0.07
STREPSIRRHINI	12	15.37	1.92	37.46	2.99	0.53	0.06

Table 14: Results for multiple sample comparison of endocranial globularity measures by taxonomic group. * denotes significance at the 0.05 level, ** denotes significance using Bonferroni correction criterion of p<0.003.

		3D Globularity			Midline Globularity			Globularity Index		
Group1	Group2	Z-score	P-value		Z-score	P-value		Z-score	P-value	
Lorisoidea	Lemuroidea	-2.143	0.032	*	-1.123	0.262		1.751	0.080	
Lorisoidea	Tarsioidea	0.000	1.000		0.000	1.000		-0.894	0.371	
Lorisoidea	Platyrrhini	-1.303	0.193		2.488	0.013	*	1.782	0.075	
Lorisoidea	Hominoidea	0.177	0.860		1.945	0.052		-1.070	0.285	
Lorisoidea	Cercopithecoidea	-1.799	0.072		2.563	0.010	*	0.907	0.365	
Lemuroidea	Tarsioidea	1.356	0.175		0.968	0.333		-1.379	0.168	
Lemuroidea	Platyrrhini	1.130	0.259		3.776	0.000	**	-0.518	0.604	
Lemuroidea	Hominoidea	2.212	0.027	*	2.633	0.009	*	-2.651	0.008	*
Lemuroidea	Cercopithecoidea	1.865	0.062		3.917	<0.0001	**	-1.926	0.054	
Tarsioidea	Platyrrhini	-0.651	0.515		1.519	0.129		1.524	0.128	
Tarsioidea	Hominoidea	0.354	0.724		1.061	0.289		0.354	0.724	
Tarsioidea	Cercopithecoidea	-0.964	0.335		1.552	0.121		1.557	0.120	
Platyrrhini	Hominoidea	1.550	0.121		0.300	0.764		-2.556	0.011	*
Platyrrhini	Cercopithecoidea	0.302	0.763		0.597	0.551		-1.614	0.107	
Hominoidea	Cercopithecoidea	-1.613	0.107		0.000	1.000		2.049	0.040	*
HAPLORHINI	STREPSIRRHINI	0.957	0.338		4.852	<0.0001	**	-1.032	0.302	

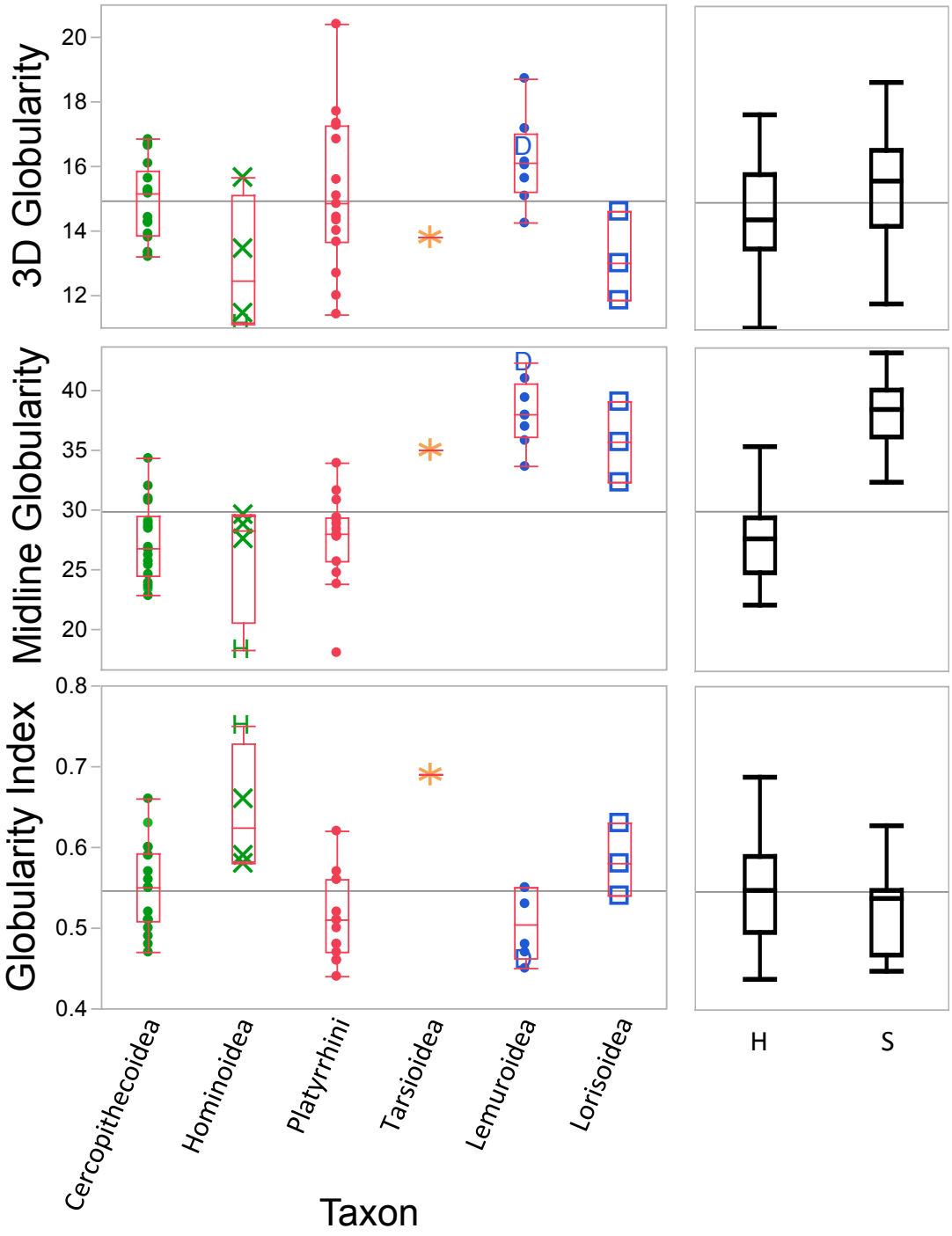

Figure 21: Box-and-whisker plots of endocranial globularity measures by taxonomic group. Among Hominoidea, green 'H' = *Homo sapiens*, among Lemuroidea, blue 'D' = *Daubentonia madagascarensis*. At right: taxon names are H = Haplorhini, S = Strepsirrhini. Points represent species mean values.

3.3.2. Group Differences In Basicranial Angle and Facial Size

The two measures of basicranial angle (BCA1, BCA2) are correlated with one another ($\lambda = 0$, $R^2 = 0.68$, $p < 0.0001$) and show similar patterns of intergroup differences among extant primates (Figure 22). Both measures show significant differences between strepsirrhine and haplorhine distributions (BCA1: $p = 0.003$, BCA2: $p < 0.0001$), with extant strepsirrhines tending to have less basicranial flexion than haplorhines (Tables 15, 16). BCA1 and BCA2 likewise show differences between Cercopithecoidea and both Lemuroidea (BCA1: $p = 0.018$, BCA2: $p = 0.024$) and Lorisoidea (BCA1: $p = 0.002$, BCA2: $p < 0.001$). BCA2 further separates Lemuroidea from Platyrrhini ($p = 0.013$) and Hominoidea ($p = 0.009$) at the $p < 0.05$ level, but fail to distinguish these groups using the Bonferonni correction criterion of $p < 0.003$ for multiple sample comparison (15 comparisons). Platyrrhines also tend to have less flexion of the cranial base than cercopithecoids (BCA1: $p = 0.002$, BCA2: $p = 0.002$) and hominoids (BCA1: $p = 0.051$, BCA2: $p = 0.006$). Among strepsirrhines, *Daubentonia madagascarensis* has the most flexed cranial base (BCA1 = 168.1°, BCA2 = 158.8°). *Homo sapiens* represents an outlier, in having a basicranial angle that is 3.7 standard deviations below the haplorhine mean for both BCA1 and BCA2 (*Homo*: BCA1 = 136.5°, BCA2 = 114.4°, Haplorhini: mean BCA1 = 167.2°, SD = 8.3, mean BCA2 = 156.01°, SD = 11.4). Removal of *Homo* from the sample has little effect on the PGLS regression equation, owing to the phylogenetic correction factor incorporated into the algorithm.

Table 15: Means and standard deviations (SD) for basicranial angles (BCA1 and BC2) and residual facial size (resFS) by taxonomic group. n = number of species per taxonomic group.

		BCA1		BCA2		Residual Facial Size	
Group	n	Mean	SD	Mean	SD	Mean	SD
Lemuroidea	3	176.00	2.21	169.23	6.96	0.05	0.04
Lorisoidea	7	174.19	3.96	172.16	6.44	0.03	0.03
Tarsioidea	1	169.78		142.71		0.11	
Platyrrhini	16	172.21	4.57	163.43	7.14	-0.10	0.06
Cercopithecoidea	18	155.60	15.72	138.61	17.92	-0.10	0.09
Hominoidea	4	165.42	5.67	154.54	7.13	-0.04	0.06
HAPLORHINI	38	167.18	8.32	156.06	11.38	-0.07	0.08
STREPSIRRHINI	12	174.69	3.56	171.36	6.37	0.03	0.03

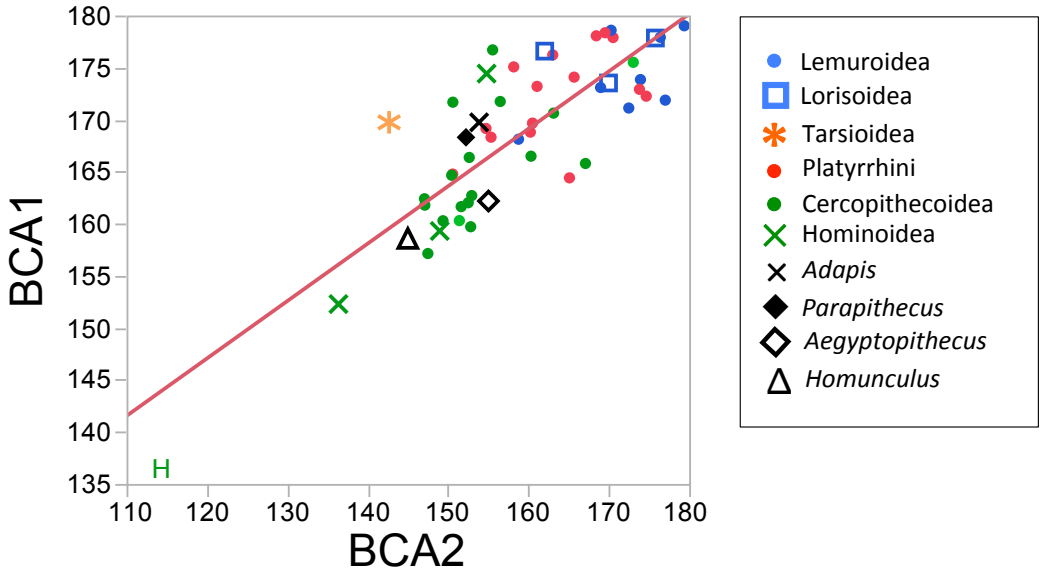

Figure 22: Bivariate plot of basicranial angles 1 (BCA1) and 2 (BCA2). PGLS regression line depicted in red: BCA1 = 0.55*BCA2 + 80.86. $R^2 = 0.68$, $p < 0.0001$. Green 'H' = *Homo sapiens*. Points represent species mean values.

Table 16: Results for multiple sample comparison of basicranial angle (BCA1 and BCA2) and residual facial size (resFS) by taxonomic group. * denotes significance at the 0.05 level, ** denotes significance using Bonferroni correction criterion of p<0.003.

		BCA1			BCA2			resFS		
Group1	Group2	Z-score	P-value		Z-score	P-value		Z-score	P-value	
Lorisoidea	Lemuroidea	0.306	0.760		-0.714	0.475		0.714	0.475	
Lorisoidea	Tarsioidea	0.894	0.371		0.894	0.371		-0.894	0.371	
Lorisoidea	Platyrrhini	1.185	0.236		1.303	0.193		2.488	0.013	*
Lorisoidea	Hominoidea	1.591	0.112		1.945	0.052		1.945	0.052	
Lorisoidea	Cercopithecoidea	2.362	0.018	*	2.261	0.024	*	1.960	0.050	*
Lemuroidea	Tarsioidea	0.968	0.333		1.356	0.175		-1.356	0.175	
Lemuroidea	Platyrrhini	0.871	0.384		2.485	0.013	*	3.647	<0.001	**
Lemuroidea	Hominoidea	1.783	0.075		2.633	0.009	*	2.633	0.009	*
Lemuroidea	Cercopithecoidea	3.139	0.002	**	3.583	<0.001	**	2.694	0.007	*
Tarsioidea	Platyrrhini	-0.217	0.828		-1.519	0.129		1.519	0.129	
Tarsioidea	Hominoidea	0.354	0.724		0.000	1.000		1.061	0.289	
Tarsioidea	Cercopithecoidea	0.639	0.523		-1.552	0.121		1.552	0.121	
Platyrrhini	Hominoidea	1.950	0.051		2.750	0.006	*	-0.350	0.726	
Platyrrhini	Cercopithecoidea	3.127	0.002	**	3.091	0.002	**	-2.549	0.011	*
Hominoidea	Cercopithecoidea	-1.575	0.115		-1.745	0.081		-0.894	0.371	
HAPLORHINI	STREPSIRRHINI	3.007	0.003	**	3.966	<0.0001	**	3.918	<0.0001	**

Haplorhines and strepsirrhines show significant differences in residual facial size ($p < 0.0001$), with haplorhines tending to have smaller faces relative to body size (Figure 23). A notable exception occurs with papionins, which have large facial sizes, overlapping completely with the strepsirrhine distribution. Excluding the papionins, anthropoid primates have minimal overlap with the strepsirrhine range. Among the extant primates sampled here, *Homo sapiens* has the lowest residual facial size (resFS = -0.23), while the cercopithecoid *Mandrillus sphinx* has the largest (resFS = 0.10). Lemuroids have significantly greater resFS than platyrrhines ($p < 0.001$), hominoids ($p = 0.009$), and cercopithecoids ($p = 0.007$).

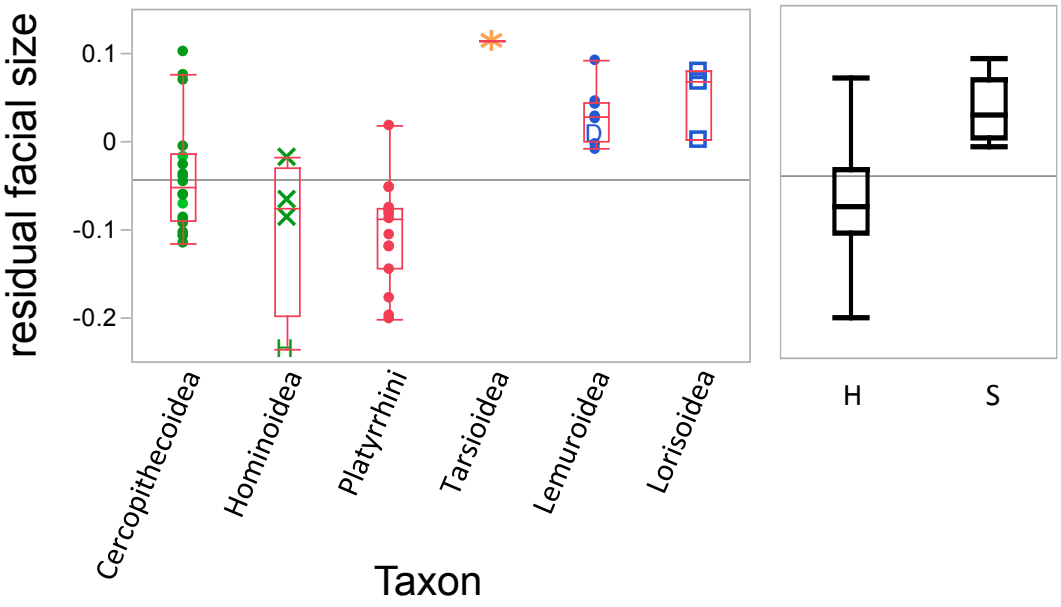

Figure 23: Box-and-whisker plots of residual facial size measures by taxonomic group. Among Hominoidea, green 'H' = *Homo sapiens*, among Lemuroidea, blue 'D' = *Daubentonia madagascarensis*. At right: taxon names are H = Haplorhini, S = Strepsirrhini. Points represent species mean values.

3.3.3. Exploratory Analysis of Midline Landmark Shape

The results of the extant-only Principal Components Analysis of Procrustes-aligned landmark configurations for the midline endocranial outline and facial landmark sets are listed in Table 17 and Figures 24 and 25. Species mean landmark coordinates are available in Appendix D. PC1 accounts for 59.7% of the variance, and separates extant strepsirrhines and tarsiers (high PC1 scores) from extant anthropoids (low PC1 scores), with some overlap between the groups occurring near the origin.

Table 17: Principal Component (scores for analysis of Procrustes-aligned midsagittal landmark configurations.

			Facial Skeleton + Cranial Base			Endocranial Outline		
Group1	Group2	Species	PC1	PC2	PC3	PC1	PC2	PC3
Haplorhini	Cercopithecoidea	*Cercocebus*	-0.0533	-0.0619	-0.0639	-0.0685	0.0152	-0.0081
		Cercopithecus	-0.0429	-0.0250	-0.0588	-0.0054	0.0098	0.0046
		Chlorbocebus	-0.0405	-0.0492	0.0128	-0.0197	-0.0064	-0.0081
		Colobus	-0.0527	-0.0063	0.0681	0.0060	-0.0469	0.0190
		Erythrocebus	-0.0507	-0.0703	-0.0674	-0.0683	0.0220	-0.0133
		Lophocebus	0.0308	-0.0672	-0.0340	-0.0223	0.0057	0.0168
		Macaca	-0.0467	-0.0382	-0.0602	-0.0252	0.0269	0.0115
		Mandrillus	0.1881	-0.1361	-0.0590	-0.0284	0.0854	0.0104
		Miopithecus	-0.1247	0.0124	-0.0642	-0.0490	0.0064	-0.0192
		Nasalis	-0.0199	-0.0499	-0.0233	0.0015	-0.0040	-0.0111
		Papio	0.1104	-0.1672	-0.0796	-0.0491	0.0431	0.0095
		Piliocolobus	-0.0520	-0.0233	0.0414	0.0353	-0.0597	0.0030
		Presbytis	-0.1052	0.0043	0.0138	-0.0256	-0.0026	-0.0067
		Procolobus	-0.0999	0.0016	0.0105	-0.0299	-0.0065	-0.0170
		Semnopithecus	-0.0798	-0.0349	0.0393	-0.0337	0.0025	-0.0059
		Simias	-0.0834	-0.0677	-0.0277	0.0254	0.0112	-0.0042
		Theropithecus	0.0357	-0.1947	-0.0317	0.0108	0.0157	0.0301
		Trachypithecus	-0.0968	-0.0036	0.0249	-0.0562	0.0108	-0.0021
	Hominoidea	*Gorilla*	0.0680	-0.1589	0.0408	-0.0177	0.0166	0.0497
		Homo	-0.0923	-0.0784	-0.0030	-0.1955	-0.0710	0.0295
		Hylobates	-0.0291	0.0082	0.0971	-0.0005	-0.0064	-0.0138
		Pan	-0.0239	-0.1604	0.0810	-0.0613	-0.0098	0.0503
		Mirza	0.1454	0.0861	-0.0003	0.0922	0.0116	0.0096

	Platyrrhini	*Alouatta*	0.0531	0.0549	0.1236	0.0554	-0.0110	-0.0008
		Aotus	-0.0052	-0.0065	-0.1150	-0.0056	0.0661	0.0186
		Ateles	-0.0455	0.0223	0.0772	-0.0678	-0.0095	-0.0046
		Cacajao	-0.0320	0.0217	0.0619	-0.0746	-0.0012	0.0046
		Callicebus	-0.0816	0.0462	0.0222	-0.0189	0.0125	-0.0072
		Callimico	-0.1487	0.0645	-0.0552	0.0219	-0.0185	-0.0427
		Callithrix	-0.1276	0.0642	-0.0750	-0.0021	0.0157	0.0007
		Cebuella	-0.1311	0.0957	-0.0750	0.0247	0.0189	-0.0352
		Cebus	-0.0794	-0.0068	-0.0036	-0.0245	-0.0277	0.0103
		Lagothrix	-0.0360	0.0331	0.1008	-0.0405	-0.0270	-0.0220
		Leontopithecus	-0.1076	0.0750	-0.0166	0.0197	-0.0668	-0.0572
		Mico	-0.1475	0.1134	-0.0422	-0.0024	-0.0219	-0.0309
		Pithecia	-0.0153	0.0427	-0.0059	0.0017	0.0071	-0.0028
		Saguinus	-0.1568	0.1016	-0.0167	-0.0014	-0.0285	-0.0521
		Saimiri	-0.1421	0.0540	-0.0381	-0.1316	0.0345	-0.0714
	Tarsioidea	*Tarsius*	0.0472	-0.0088	-0.0990	0.0636	0.0361	0.0223
Strepsirrhini	Lemuroidea	*Daubentonia*	0.1293	0.0004	0.0386	0.0829	-0.0324	0.0640
		Eulemur	0.1786	0.0405	0.0254	0.0967	-0.0354	-0.0177
		Hapalemur	0.0941	0.0618	-0.0700	0.0630	0.0113	0.0001
		Indri	0.1490	0.0777	0.0542	0.1228	-0.0412	-0.0047
		Lemur	0.1792	0.0379	-0.0056	0.0849	-0.0209	-0.0059
		Microcebus	0.1256	0.1196	0.0288	0.0917	0.0107	-0.0212
		Mirza	0.1691	0.0898	0.0003	0.1412	0.0003	-0.0206
		Varecia	0.2361	0.0441	-0.0115	0.1264	0.0532	0.0127
	Lorisoidea	*Galago*	0.1222	0.0818	-0.0529	0.0552	0.0532	-0.0036
		Loris	0.1830	0.0915	0.0195	0.0683	-0.0034	0.0300
		Nycticebus	0.1930	0.0864	0.0094	0.1105	-0.0293	0.0346

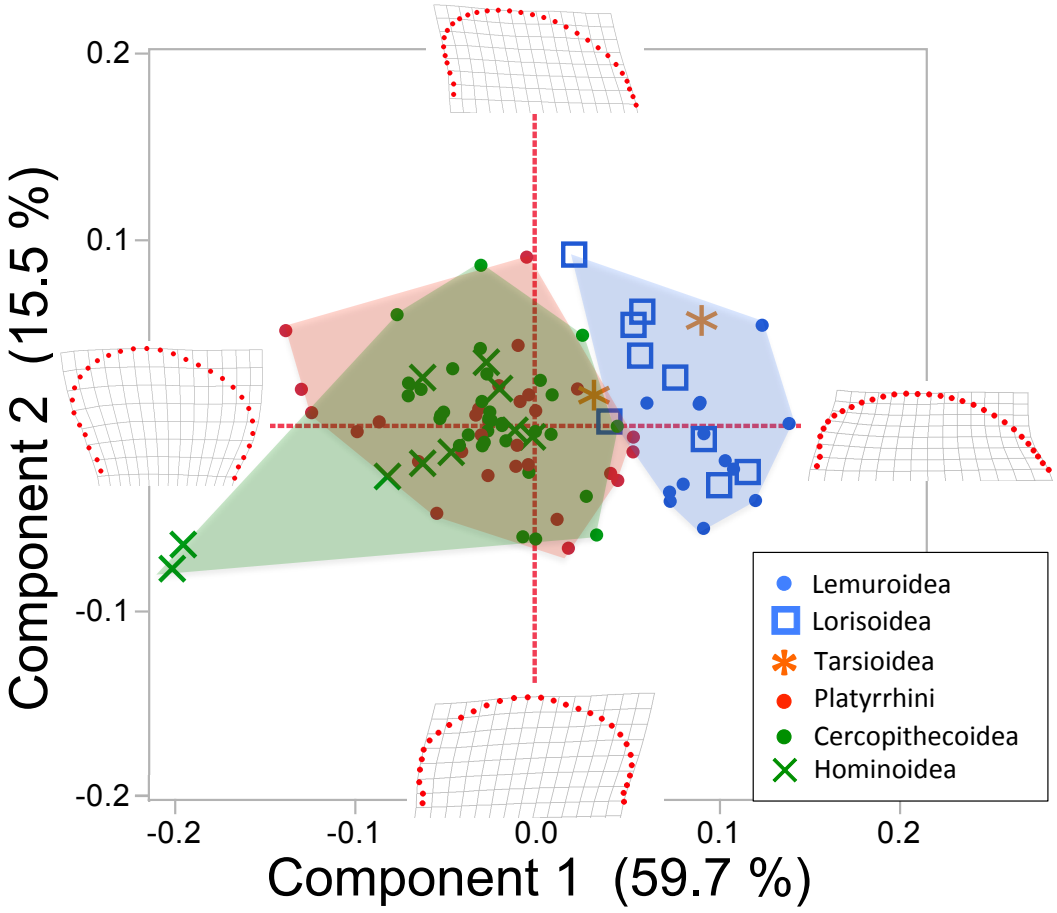

Figure 24: Principal Components Analysis of Procrustes-aligned endocranial outline landmarks for extant-only dataset. Grids represent relative warp deformations of landmark configurations visualizing the maximal and minimal values for each axis. Rostral is to the right. Points represent values for individual specimens.

The distribution of species along PC1 mimics closely the distribution for the midline globularity measure; this allows us to visually explore the variation in shape as it relates to globularity. The less globular primates (strepsirrhines) tend to have lower endovertex height as compared to the length of the braincase (frontal pole – occipital pole). Species with high values for PC1 also have more rostrally projecting olfactory

fossae and a more caudally placed foramen magnum, resulting in a proportionately greater distance between the two landmarks anchoring the landmark curve (the anterior cribriform plate and opisthion). The most encephalized extant anthropoids in the sample—*Homo, Saimiri,* and *Cacajao*—have the lowest values along PC1, with high endovertices, rounded occipital regions, and downwardly flexed anterior endocranial outlines. PC2 (15.5%) reflects the shape of the rostral aspect of the endocast and the placement of the anterior cribriform relative to the frontal pole. Species with high PC2 values (*Galago senegalensis*, *Mico argentata*) have a flattened and dorsally receding frontal region with a more posteriorly placed frontal pole relative to the cribriform plate, while those with low PC2 values (*Procolobus verus*, *Homo sapiens*) have more continuously dorsal profiles and anteriorly "bossed" frontal lobes.

A principal components analysis of the basicranial and facial landmarks is presented in Figure 25. The first component accounts for 41.8% of the variation in the shape space. With respect to the midline basicranial morphology, PC1 reflects differences in the length and verticality of the cribriform plate, and the flexion of the cranial base. Strepsirrhines have longer and somewhat more vertically oriented cribriform plates, while the anthropoids have short and horizontally oriented plates. The primary shape changes along PC1 with respect to the face include the size of the facial skeleton, length of the snout, and verticality of the facial chord (acanthion-glabella). PC1 separates papionins and strepsirrhines from all other anthropoids. Large-

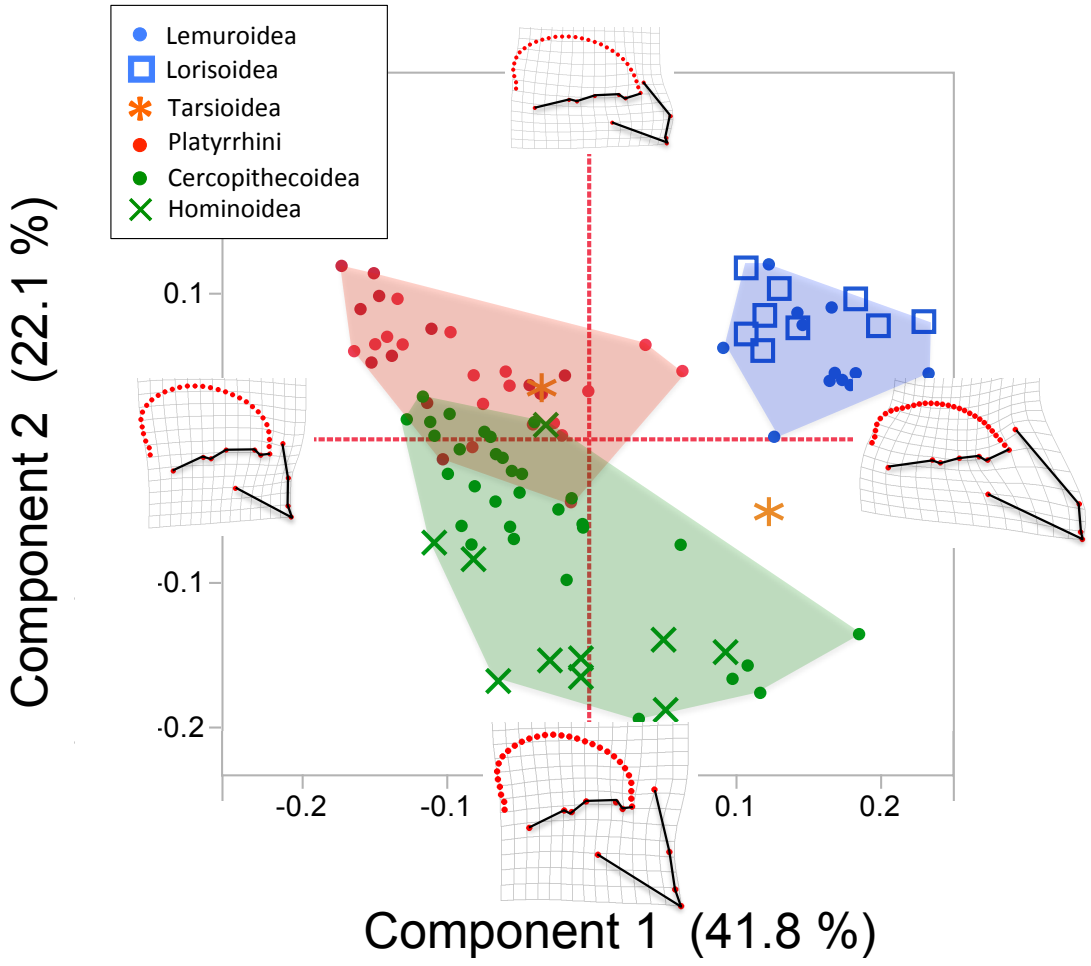

Figure 25: Principal Components Analysis of Procrustes-aligned facial + basicranial landmark set. Grids represent relative warp deformations of landmark configuration visualizing the maximal and minimal values for each axis. The endocranial outline is included in the visualizations for reference, but is not incorporated into the landmark analysis. Rostral is to the right. Points represent values for individual specimens.

Table 18: Principal Component (PC) scores, basicranial angle (BCA) and facial size for fossil specimens.

				Facial + Cranial Base			Endocranial Outline		
Species	BCA1	BCA2	log Facial Centroid	PC1	PC2	PC3	PC1	PC2	PC3
Adapis parisiensis	*169.8	*153.8	-0.559	0.142	0.037	0.131	0.176	0.046	0.002
Parapithecus grangeri	168.4	152.3	-0.636	0.048	0.051	0.043	0.046	-0.050	0.020
Aegyptopithexus zeuxis	*162.3	*155.1	-0.657	0.064	0.038	-0.027	0.069	0.002	-0.067
Homunculus patagonicus	158.5	144.9	-0.672	0.022	-0.010	-0.008	0.019	0.026	-0.017

NOTES: * = estimated, specimen has incurred some damage in this region

bodied papionins *Mandrillus*, *Theropithecus*, and *Papio* are aligned with strepsirrhines in having a long snout for their skull size. Strepsirrhines, platyrrhines, and colobines overlap completely on PC2, while hominoids and most cercopithecines have low values for PC2, reflecting an elongated facial chord and palate in conjunction with a tighter angle between the palate and the basicranium. Variation in PC2 illustrates that long snouted catarrhines have altered angles of facial hafting in absence of changes in basicranial flexion.

Figure 26 depicts the placement of the fossil specimens on the endocranial and facial landmark morphospaces. Midsagittal slices of the fossil specimens are presented in Figure 27, and measured variable are presented in Table 18. The Eocene euprimate *Adapis* shows an exaggerated strepsirrhine-like morphology of the endocranial outline, with a rostro-caudally long endocranium, low endovertex, and large distance between opisthion and the anterior cribriform plate. The stem anthropoid *Parapithecus* differs in

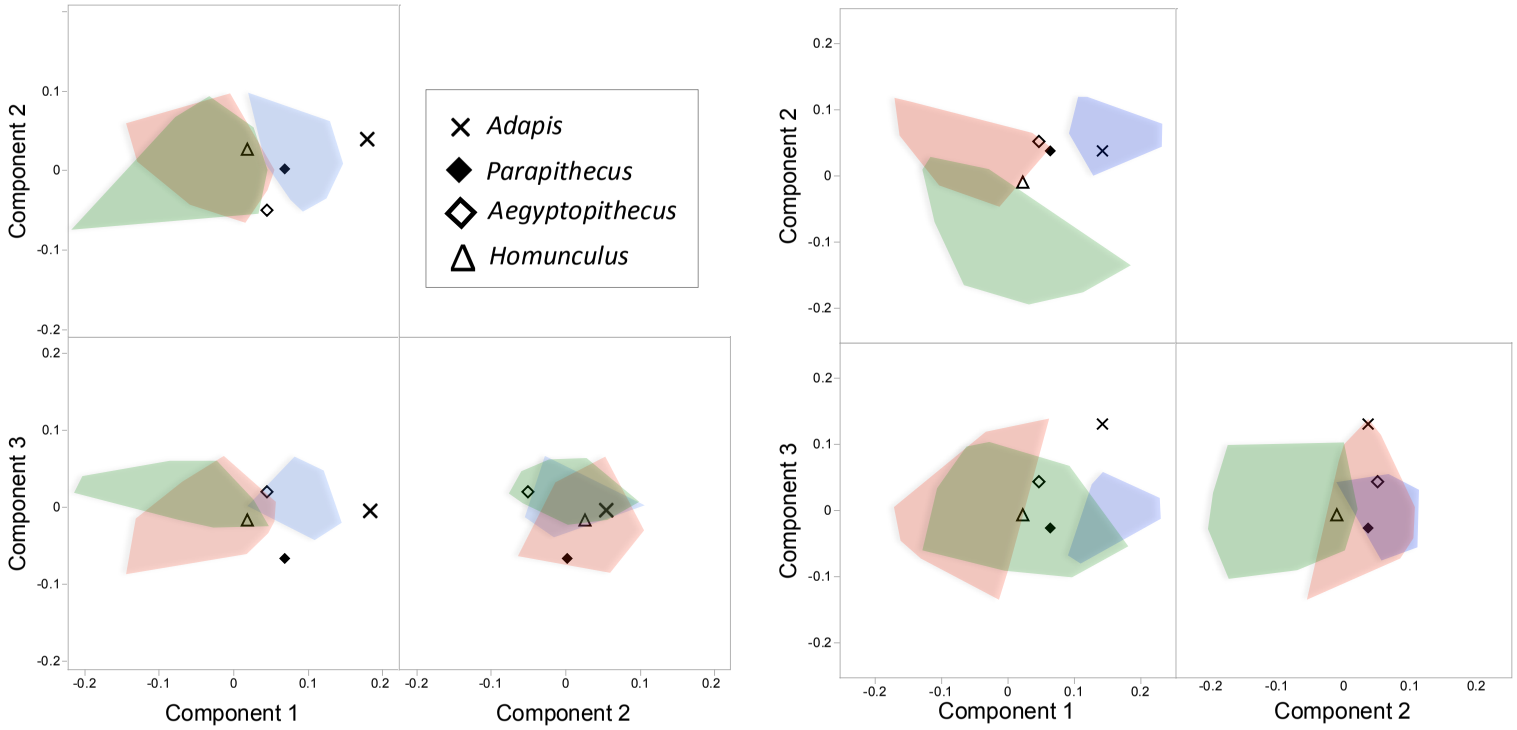

Figure 26: Principal Components Analysis of a) midline endocranial outline and b) midline facial + basicranial landmarks. Green = extant catarrhine distribution, red = extant platyrrhine distribution, blue = extant strepsirrhine distribution.

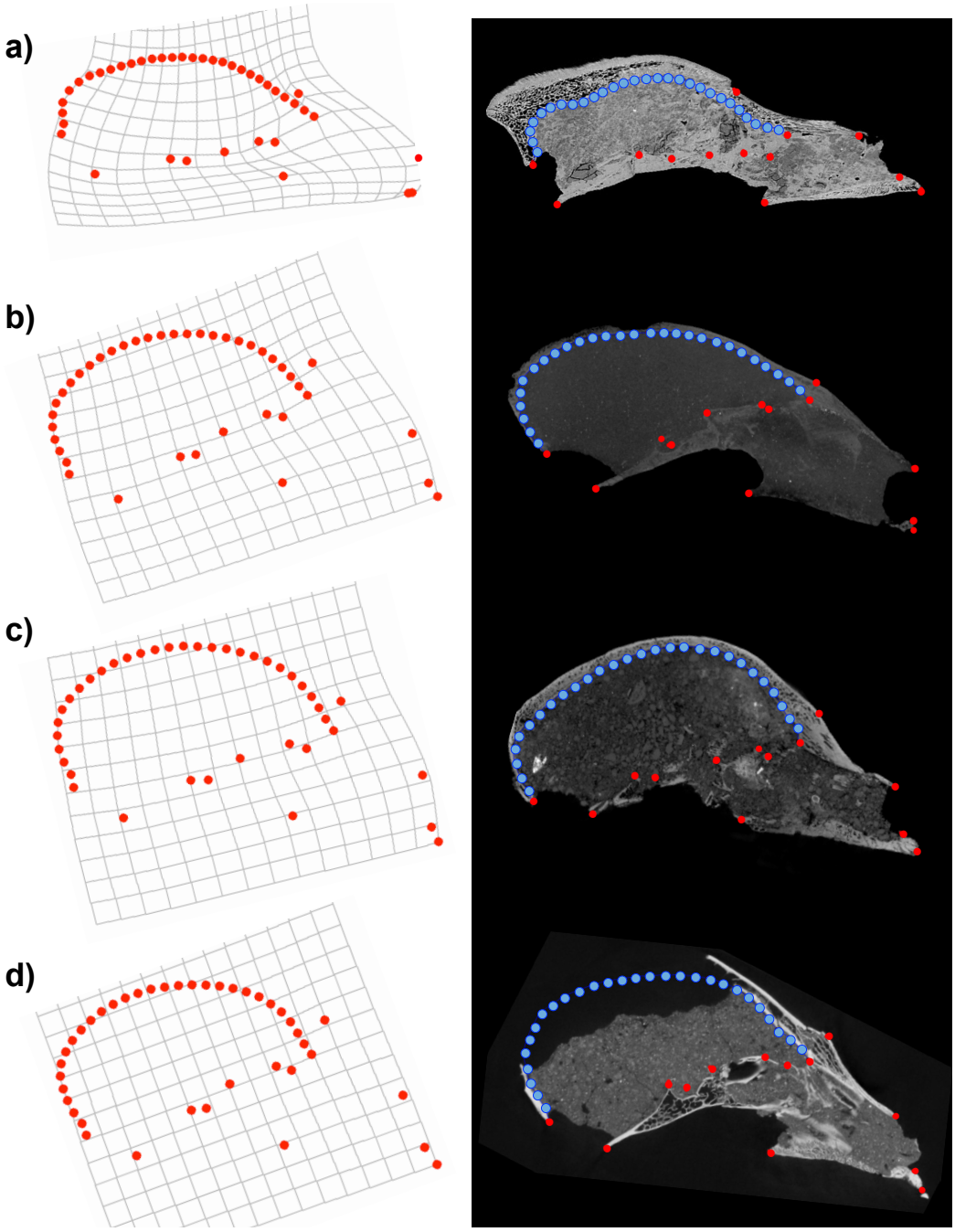

Figure 27: Relative warps visualizations (left) and midsagittal tomographs of fossil specimens illustrating basicranial, facial (in red) and endocranial outline landmarks (in blue). From top to bottom: a) *Adapis*, b) *Parapithecus*, c) *Aegyptopithecus*, d) *Homunculus*—missing points interpolated from surrounding three-dimensional morphology. Specimens are scaled to equal skull length.

endocranial outline from any of the extant anthropoids, with strepsirrhine-like qualities captured by PC1 (low endovertex, anteriorly projecting anterior cribriform plate) and callitrichine platyrrhine-like qualities on PC3, including a posteriorly placed endovertex and dorsally receding frontal lobe. Although *Parapithecus* falls within the strepsirrhine range of PC1, it has very near the value for *Alouatta*, the least encephalized of the extant anthropoids. The stem catarrhine *Aegyptopithecus* lies with the region of overlap between extant anthropoid and strepsirrhine ranges for PC1, owing to the combination of a moderate distance between opisthion and the anterior cribriform plate, and a moderately tall endovertex. On PC2, *Aegyptopithecus* occupies the low range of the extant primate distribution, near the value for *Piliocolobus*, reflecting a shortening of the curve in the rostral region, with the anterior cribriform plate tucked up under the frontal pole. Finally, *Homunculus* demonstrates a fully modern extant anthropoid shape, lying within the platyrrhine distribution on all axes. It is less continuously curved that in humans, but much more so than in strepsirrhines, with the anterior cribriform plate lying inferior to the frontal pole, and some slight embossing of the frontal region. For the facial landmark set, all the fossil anthropoids lies within the extant anthropoid distribution for the first three principal components, reflecting a shortened snout and moderate flexion of the cranial base, as compared to extant strepsirrhines.

Table 19. Correlation (Spearman's ϱ) and partial correlation coefficients for species mean endocranial volume (ECV), residual endocranial volume (resECV), and braincase dimensions. All variables are log transformed prior to analysis. Top right portion of matrix presents correlation coefficients, bottom right represents partial correlation scores. Fill color gradient represents magnitude of the score: red = highest values, green = lowest values.

	endocast length	endocast breadth	endocast height	ECV	resECV
CATARRHINI:					Correlation coefficients
endocast length		0.8769	0.9300	0.9497	0.3148
endocast breadth	0.1374		0.8916	0.9282	0.4284
endocast height	0.0942	-0.0275		0.9763	0.4357
ECV	0.4059	0.5060	0.6767		0.4614
resECV	-0.3457	0.2651	-0.2979	0.3072	
	Partial correlations				
PLATYRRHINI:					Correlation coefficients
endocast length		0.8794	0.9176	0.3588	-0.0059
endocast breadth	0.1121		0.9588	0.4647	0.0441
endocast height	0.3564	0.8695		0.3824	0.0353
ECV	0.1123	-0.1309	0.1626		0.6853
resECV	-0.0013	0.1920	-0.2478	0.8047	
	Partial correlations				
STREPSIRRHINI:					Correlation coefficients
endocast length		0.9640	1.000	-0.1608	0.0409
endocast breadth	0.2326		0.965	-0.1678	0.0595
endocast height	0.8529	0.3025		-0.1608	0.4900
ECV	0.4913	-0.1893	-0.3942		0.4413
resECV	-0.7033	0.2580	0.5548	0.6661	
	Partial correlations				

3.3.4. Correlated Evolution Among Traits

Correlation and partial correlation values for log ECV, resECV, and the endocast dimensions used to calculate the globularity index are presented in Table 19. The

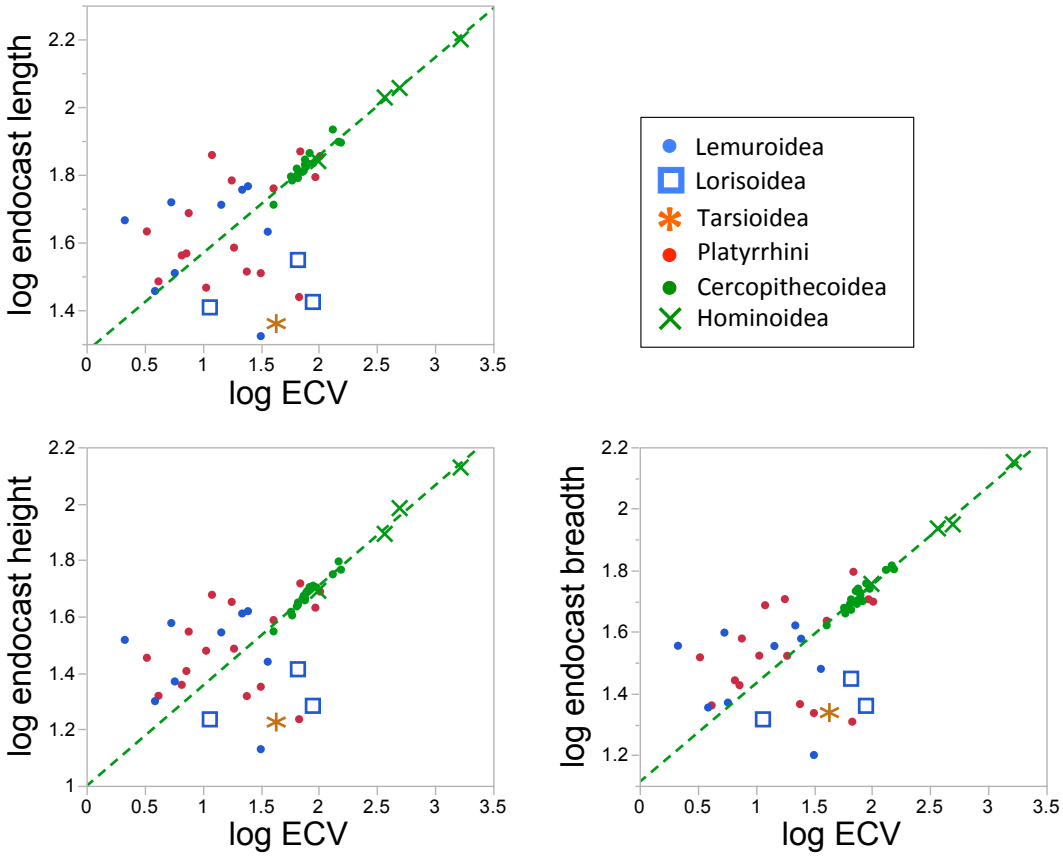

Figure 28. Bivariate plots of endocast maximal dimensions on endocranial volume (ECV). Points represent species means. Dotted green line represents regression fit to catarrhine-only distribution (slope = 0.33, $p < 0.001$ for each).

associated covariance matrix for Catarrhini is significantly different from that of both Platyrrhini and Strepsirrhini (Box's M test, $p < 0.0001$). The strepsirrhine and platyrrhine covariance matrices do not significantly differ from one another ($p = 0.054$).

The maximal dimensions of the endocast—log length, log breadth, and log height of the endocast—are all highly positively and isometrically correlated with one another (95% confidence interval for slope encompasses 1.0). Among catarrhine

primates, all three measures correlate isometrically with log ECV ($p < 0.001$, 95% confidence interval for slope encompasses 0.33), while no significant correlation exists between any of the three maximum endocast dimensions and log ECV in platyrrhines or strepsirrhines ($p > 0.0125$) (Figure 28). When variation in all other dimensions is accounted for, endocast height shows a modest positive correlation with log ECV in catarrhines, while endocast height is strongly positively correlated with endocast breadth in platyrrhines. Finally, while all groups show a negative partial correlation value between endocast length and residual endocranial volume, this correlation only reaches significance among the strepsirrhines. Among strepsirrhines, endocast length and height retain a strong positive correlation when variation in all other dimensions is controlled for. Thus, among catarrhines, the length, breadth, and height of the endocast are all highly conserved relative to one another and independent of absolute or relative brain size. In contrast, platyrrhines have a tendency to conserve the relationship between height and breadth of the endocast. Strepsirrhines retain a strong relationship between the length and height of the endocast when all other variables are controlled for, but more encephalized species tend to have shorter endocasts when effects of all other included variables are controlled for.

Results for the PGLS tests of correlated evolution among endocranial traits are available in Table 20. Of the three globularity measures, only midline globularity is significantly correlated with residual endocranial volume (resECV) when phylogenetic

effects are controlled for (λ = 0.70, R^2 = 0.28, p < 0.001). A significant but very weak correlation exists between the globularity index and basicranial angle (BCA1: λ = 0.58, R^2 = 0.011, p =0.022; BCA1: λ = 0.72, R^2 = 0.11, p =0.022). A much stronger correlation exists between midline globularity and basicranial angle, although the explanatory power of the model is still not high (BCA1: λ = 0.87, R^2 = 0.30, p < 0.0001; BCA2: λ = 0.88, R^2 = 0.19, p =0.002).

Although similar patterns of intergroup differences and correlated evolution are found using BCA1 versus BCA2, differences in model fit do occur between the two angles. Among extant primate species means, BCA2 explains a greater degree of variation in resECV than does BCA1, as illustrated by a lower value for the corrected Akaike Information Criterion (AICc, BCA1 = -62.38, BCA2 = -66.12), a measure of model fit for the PGLS regression of resECV (y) on BCA1 or BCA2 values (x). A lower AICc value indicates a greater likelihood of the fit of a model, given the data, to the alternative model (Akaike 1973; Burnham and Anderson 1998). Conversely, BCA1 is a better model fit for explaining the variation in midline globularity, than is BCA2 (AICc, BCA1 = 255.3, BCA2 = 262.34). These patterns are likewise reflected in differences in R^2 values between PGLS regressions of these variables (Table 20). Nevertheless, BCA1 values more closely correspond to the minimum and maximum resECV values for Haplorhini and Strepsirrhini groups. *Alouatta*, the least encephalized extant haplorhine has the least

Table 20: Results for phylogenetically informed generalized least squares (PGLS) regressions of extant primate endocranial and basicranial varibles. See text for abbreviations.

y-variable	x-variable	Slope	Intercept	Lambda	R^2	P-value	
globularity index	resECV	0.1231	0.5616	0.76	0.07	0.068	
3D globularity	resECV	-2.6868	15.0216	0.00	0.01	0.230	
midline globularity	resECV	-16.3507	33.7931	0.70	0.28	<0.001	**
globularity index	logECV	0.0467	0.5064	0.81	0.08	0.059	
3D globularity	logECV	-0.9287	15.9482	0.54	0.04	0.176	
midline globularity	logECV	-2.5092	36.5310	0.60	0.05	0.097	
facial centroid	logBM	0.0481	-0.7800	0.65	0.11	0.020	*
BCA1	BCA2	0.5516	80.8562	0.00	0.68	<0.0001	**
BCA1	resECV	-23.5034	171.7439	0.57	0.20	0.002	**
BCA2	resECV	-37.8580	161.8041	0.85	0.28	<0.001	**
BCA1	logECV	-10.3060	185.5320	0.00	0.51	<0.0001	**
BCA2	logECV	-12.8800	177.5905	0.75	0.25	<0.001	**
BCA1	globularity index	-37.0000	192.3850	0.58	0.11	0.022	*
BCA2	globularity index	-52.4380	190.9160	0.72	0.11	0.022	*
BCA1	3D globularity	-0.0680	172.2490	0.69	0.00	0.902	
BCA2	3D globularity	0.3926	155.5500	0.75	0.00	0.609	
BCA1	midline globularity	0.9284	140.0366	0.87	0.30	0.000	**
BCA2	midline globularity	1.0143	126.8847	0.88	0.19	0.002	**
BCA1	TOTAL MODEL		219.4013	0.84	0.28	<0.001	**
	facial centroid	40.2761				0.003	**
	+ logBM	-7.4692				<0.001	**
BCA2	TOTAL MODEL		211.2366	0.78	0.18	<0.0001	**
	facial centroid	37.4234				0.061	
	+ logBM	-8.6586				0.005	**
BCA1	TOTAL MODEL		146.8796	0.83	0.32	<0.001	**
	resECV	-10.4621				0.179	
	+ midline globularity	0.7317				0.006	**
BCA2	TOTAL MODEL		145.4376	0.89	0.32	<0.0001	**
	resECV	-30.0492				0.006	**
	+ midline globularity	0.4784				0.175	
facial centroid	TOTAL MODEL		-1.01338	0.89	0.46	<0.0001	**
	logECV	-0.2425				<0.0001	**
	+ logBM	0.226388				<0.0001	**

flexion of the basicranium of all extant haplorhines in the dataset, as measured by BCA1; however, BCA2 indicates that the moderately encephalized haplorhines *Cercopithecus* and *Pithecia* have less basicranial flexion than the far less encephalized *Alouatta*.

A multiple PGLS regression analysis was used to determine the relationships among basicranial angle measures and facial and globularity measures in the extant sample, when body mass and/or encephalization is taken into account. A significant relationship occurs between BCA1 and log facial centroid + log BM (total model: $p < 0.001$, Table 20). Similar results are found using BCA1 (total model: $p < 0.0001$), however, log facial centroid size does not have a significant additive effect to the model. BCA1 is significantly correlated with midline globularity, but resECV does not have a significant additive effect. Conversely, BCA2 is correlated with resECV, while midline globularity has no significant additive effect. Facial centroid size appears to be correlated with encephalization, as evidenced by model significance including both logECV and logBM (total model $p < 0.0001$), with a significant additive effect for both variables.

A correlation matrix and partial correlation matrix was created including variables midline globularity, resECV, resFS, and BCA1, to more closely examine the interactions among these variables (Table 21, Figure 29). Both resFS and BCA1 are positively correlated with midline globularity, while resECV is negatively correlated with midline globularity, resFS, and BCA1. Put in a more general way, the more encephalized species tend to have endocranial that deviate less from a sphere, to have

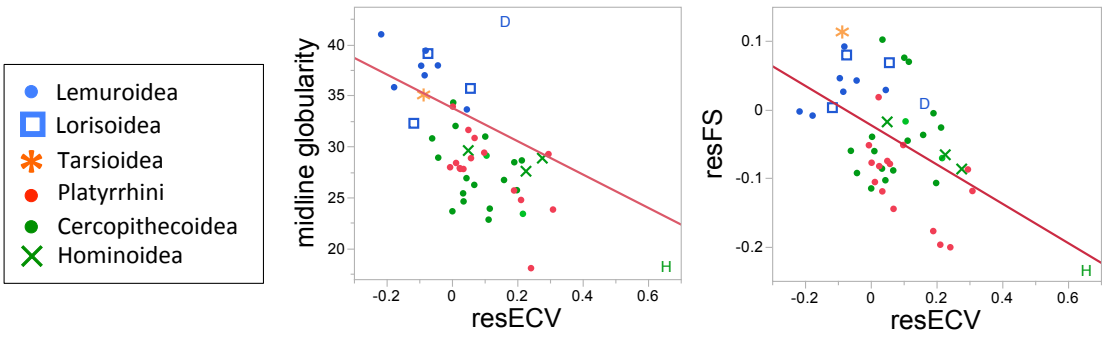

Figure 29: Bivariate plots of PGLS regression results for midline globularity and residual facial size (resFS) with residual endocranial volume (resECV). D = *Daubentonia*, H = *Homo*. Points represent species mean values.

Table 21: Correlation (Spearman's ϱ) and partial correlation matrix for midline globularity, residual endocranial volume (resECV), residual facial size (resFS), and basicranial angle (BCA1). Top right portion of matrix presents correlation coefficients, bottom right represents partial correlation scores. Fill color gradient represents magnitude of the score: red = highest values, green = lowest values.

	midline globularity	resECV	resFS	BCA1
				Correlation coefficients
midline globularity		-0.647	0.630	0.550
resECV	-0.291		-0.548	-0.536
resFS	0.467	-0.285		0.267
BCA1	0.367	-0.323	-0.202	
	Partial correlation			

smaller faces, and to have more flexed basicrania. The partial correlation analysis indicates that when all other variables are controlled for, there remains a positive relationship between midline globularity and residual facial size, and between midline globularity and basicranial angle.

For the midline landmark dataset, a two-block partial least squares analysis demonstrates covariation between the endocranial outline landmark configuration, and a block combining the basicranial and facial landmarks (RV coefficient = 0.5464, $p < 0.0001$ for 1000 permutations, see Figure 30). When considered as two landmark sets within the same configuration, an even higher degree of covariation is found to exist between the endocranial outline and facial landmark configurations (RV coefficient for w/in configuration: 0.85, 250 permutations $p<0.001$). When the landmark dataset is constrained to include the basicranial and facial landmarks only the two blocks show moderate degrees of covariation (w/in configuration analysis: basicranium + face, RV coefficient = 0.488, 250 permutations, $p < 0.001$). These results indicate that the shape of the midline facial landmark configuration covaries with that of the endocranial outline shape and the shape of the midline basicranium and that these results are robust to methodological differences—i.e. whether I evaluate shape within the configuration or between blocks segregates as two separately Procrustes-aligned datasets.

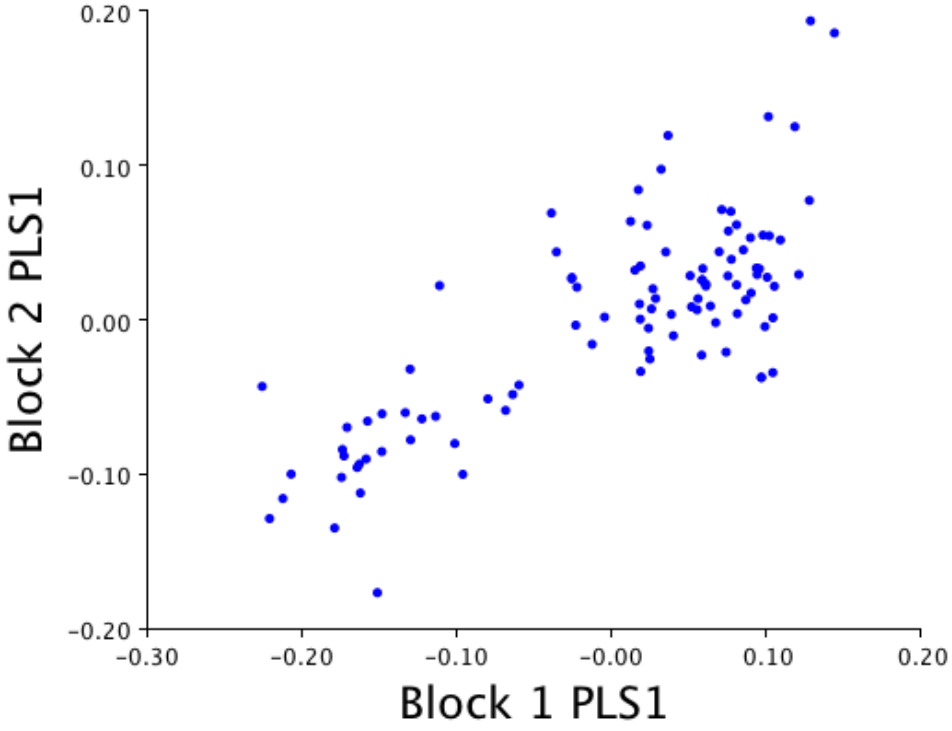

Figure 30: Bivariate plot representing two-block partial least-squares (2B PLS) analysis of covariation among the midline endocranial and facial landmark configurations.

3.4. Discussion

Supporting the conclusions of previous work (Ross and Ravosa 1993; Lieberman *et al.* 2000b; Lieberman *et al.* 2000c), this study finds that strepsirrhines have less flexed cranial bases than do anthropoids, with *Homo sapiens* having even greater flexion of the cranial base than expected for its encephalization. Furthermore, I find that although facial size is positively correlated with body size, the relative size of the facial skeleton (resFS) is negatively correlated with encephalization in extant primate species. Bastir

(2010) reports a similar pattern for an anthropoid-only dataset. It is difficult to explicitly test the association between basicranial angle, facial size, and encephalization in the strepsirrhines alone, as the low number of available species does not provide robust statistical power for detecting correlations (MacLean *et al.* 2009), nevertheless, there does appear to be a weak negative trend among the strepsirrhines between facial size and encephalization.

It should be noted that the explanatory power in the primate-wide model is quite low and many additional factors likely influence facial size among primates. Facial size is undoubtedly influenced by sexual dimorphism—via selection for large canines and/or extended growth periods associated with body size dimorphism (Schaefer *et al.* 2004; Cobb and O'Higgens 2007; Wang *et al.* 2007)—and is constrained by the demands of the masticatory system. For example, among Old World monkeys, increases in both body size and canine size associated with intrasexual male competition have been linked to the extreme prognathism of large-bodied papionins, a feature which increases the jaw gape necessary to utilize and display such grossly enlarged canine teeth (Smith 1984; Ravosa 1990). Thus, the relationship between facial size and encephalization is not clear cut: encephalized, highly prognathic *Mandrillus*, *Theropithecus*, and *Papio* do not have unusually unflexed basicrania, as would be expected if there were a strict trade-off between encephalization and facial size. Instead, the Principal Components Analysis of facial shape indicates that these species achieve their unique craniofacial form via

changes in craniofacial hafting, independent of endocranial outline shape or flexion of the cranial base.

3.4.1. Interaction Between Endocranial Shape and Craniofacial Form

The analyses presented herein indicate that with some exceptions (especially among larger papionins, as previously described) a general relationship exists between facial form and endocranial shape, including globularity. Extant species with greater degrees of encephalization tend to have more globular endocrania (when considering midline globularity measures) more flexed basicrania, and smaller facial skeletons. This lends support to Biegert's (1963) hypothesis that increased encephalization is achieved through anterior and posterior expansion of the brain in such a way that the base of the endocranium is downwardly flexed, which in turn constrains the achievable size of the facial skeleton. Furthermore, the significant separation among strepsirrhine and anthropoid distributions in facial size, basicranial flexion, and globularity, as well as the existence of moderate partial correlation scores among these three variables together support the possibility that interactions among these variables may account for some of the differences in cranial form evidence between extant strepsirrhine and anthropoid primates.

Despite a general correlation among basicranial, facial, and endocranial outline shape, it should be emphasized that the correlation coefficients for these analyses are quite low, and many exceptions do occur. The interactions among endocranial and

cranial variables for the most encephalized haplorhine (*Homo sapiens*) and strepsirrhine (*Daubentonia madagascarensis*) species are particularly illuminating. Although both tend to have greater basicranial flexion and encephalization than other representatives of their respective suborders, *Homo sapiens* is more globular, and *Daubentonia magascarensis* less globular than would be expected by a linear relationship between midline globularity and residual endocranial volume (Figure 28). This deviation may in some part be explained by differences in relative facial size. Although *Daubentonia* does not have a large face by strepsirrhine standards, its facial skeleton is somewhat larger than would be expected based on encephalization alone, while the human facial skeleton is considerably smaller than expected from its encephalization value. Thus, the interplay between facial size and encephalization may to some degree account for variation in globularity among extant primates, but many other factors must come into play.

Despite weak support for these apparent trade-offs in facial packing, the results further indicate that the relative size of the facial and endocranial skeletons in themselves are not the only factors affecting globularity and basicranial flexion. As evidenced by the results of the 2BPLS analysis of the midline landmark data, the shape of the facial skeleton covaries with that of the endocranial outline, and facial shape covaries with basicranial midline shape. As the shape variables themselves also correlate with encephalization (resECV), it is difficult to tease apart whether encephalization itself or endocranial shape is driving the correlation with basicranial and facial form. R^2 values

range from 0.14 to 0.43 for multiple regression analyses of basicranial angle measurements on facial size, encephalization, and/or globularity, leaving the majority of variation in basicranial angle unexplained by these features. It is possible that differences in body size, brain proportion, or other as yet unknown features also have an effect on both basicranial flexion and globularity.

3.4.2. Implications of the Fossil Record

The morphology of the early anthropoid fossils provides mixed support for the role of spatial constraints in the early differentiation of anthropoid cranial form. When compared to one another, the distribution of basicranial flexion, encephalization, and facial shape among the early anthropoid specimens is consistent with expectations based on the craniofacial relationships observed among extant primates. For example, the stem anthropoid *Parapithecus*, the least encephalized fossil anthropoid in the sample (Bush *et al.* 2004), also has the least flexed basicranium, the most strepsirrhine-like midline endocranial outline, and most prognathic facial skeleton. Conversely, the most encephalized of the fossil specimens included here is the stem platyrrhine *Homunculus* (Kay *et al.* 2012), which displays features consistent with its relative higher level of encephalization, including a more flexed basicranium, a fully anthropoid-like shape to the midline endocranial outline, and a facial skeleton on the cusp of the extant platyrrhine range of shape variation. The contrast in each component among the four fossil species is consistent with their extant primate patterns of covariation among

encephalization and cranial form; however, when compared to the values for extant anthropoid groups, it should be noted that the degree of basicranial flexion and PC scores for endocranial outline and basicranial/facial shape are more consistent with the phylogenetic placement of these fossils than with their degree of encephalization. For instance, all fossil specimens included here have much lower levels of encephalization than extant anthropoid species, but demonstrate higher degrees of basicranial flexion than seen in the least encephalized anthropoid primates (*Alouatta* BCA1 = 178, *Colobus* BCA1 = 177). Despite the correlation between residual endocranial volume, facial size, and basicranial angle observed among extant primates, a direct comparison of fossil values to the extant distribution suggests that phylogenetic differences in cranial form emerged prior to encephalization.

3.4.3. Additional Factors Affecting Globularity

3.4.3.1. Variability in Measurements of Endocranial Globularity

Of the three measures used herein to approximate endocranial globularity, only the midline globularity measure significantly separates extant clades and co-varies with both encephalization and basicranial flexion. This may be the result of multiple factors: first, the original observations of basicranial flexion and its relationship to encephalization were made considering the midline morphology (Weidenreich 1941; Biegert 1963; Enlow and McNamara 1973), and thus, measurements of this view most capture the variation in basicranial and neruocranial morphology around which the

Spatial Constraints/Facial Packing Hypotheses were derived; secondly, it is possible that three-dimensional measures of globularity fail as they include information on lateral structures, which may themselves act on a separate set of constraints related to allometric patterns or sensory function; finally, it is also a possibility that there is no consistent relationship between the sphericity of the brain and encephalization, facial size, and/or basicranial angle, and that the midline globularity measure used here may produce an inaccurate representation of brain shape, as it may inadvertently capture information about the location of the foramen magnum and cribriform plate relative to the rest of the endocast—both of which were found in Chapter 2 to be related to encephalization and relative brain proportions. It is likely that a combination of the above factors are at play.

The inability of three-dimensional globularity measures to capture any meaningful differences in globularity among taxonomic groups is almost certainly in part the result of clade specific scaling patterns between the length, breadth, and height of the endocast. Lieberman *et al.* (2000b) propose that variation in primate cranial morphology suggests that neurocranial length is less constrained than neurocranial breadth in adults. The correlation analysis among maximum endocranial length, breadth, and height (Table 19) reveals this to be somewhat true only in anthropoids, while among strepsirrhines, longer endocasts tend also to be taller, and species with higher levels of encephalization tend to have relatively shorter endocasts, when the

effects of all other included variables are controlled for. Although the length, breadth, and height of the endocast scale with isometry on endocranial volume, they show varied patterns of partial correlation with one another and with encephalization. This reflects the large amount of variation in overall endocast shape in primates and indicate that the endocranium does not adhere to primate-wide scaling patterns in overall dimensions. In other words, not all big brain are big in the same way.

3.4.3.2. Adaptive Implications of Brain Sphericity

It should be noted that in addition to the Spatial Constraints and Facial Packing Hypotheses examined here, multiple other factors have been proposed that may affect globularity, though these are not testable with the data presented herein. For example, it has been proposed that on a global (Holloway 1966; Holloway 1979; Holloway *et al.* 2004) and local level (Van Essen 1997), globularity of the brain is related to the degree of neural connectivity among adjacent brain regions. Hofer (1969) proposed that:

> "the brain as a whole attempts to become the form of a ball or of a sphere, because the sphere has a maximum of capacity connected with a minimum of surface." (p. 18).

Hofner's (1969) proposal implies both that a spherical shape to the brain is optimal in maximizing the potential for connectivity among adjacent structures, and for minimizing the space needed to pack in a given surface area. Holloway (1966, 1979, 2004) proposes that a more spherical brain would be adaptive, as it reflects shortened

pathways among interconnected brain components, which may increase cognitive speed. On a more local level, Van Essen (1997) has proposed that the complex folding of the brain may be the result of tension among closely connected regions during growth and development. It is possible that a similar mechanism may be partly responsible for the overall globularity of the brain, as the cerebral and cerebellar cortices are strongly connected (Snider and Eldred 1952; Miall 2013), and it is plausible to extend Van Essen's (1997) idea to the possibility that tension among these connections coincident with further expansion of the telencephalon in development may be responsible for increases in sphericity of the whole organ. With the availability of advance neuroimaging methods, such as diffusion tractography, it is becoming possible to map *in vivo* neural pathways in a relatively non-invasive manner (Parker *et al.* 2002; Sporns *et al.* 2005; Toga *et al.* 2012). These methods, if applied both interspecifically and ontogenetically, may allow researchers to test the hypothesis that the sphericity of the brain in humans coincides with reduced neural pathways among interconnected brain regions.

3.5. Conclusions

In conclusion, the data presented herein provide very weak support for some aspects of both the Spatial Packing Hypothesis proposed by Biegert (1963) and the Facial Packing Hypothesis of Enlow and Azuma (1975). It is likely that additional factors are at play to ultimately explain adult interspecific variation in extant primate endocranial globularity and basicranial flexion. Specifically, it was found that:

1) For all three measures of endocast globularity, haplorhines are found to have more globular endocasts than strepsirrhines; however, the three-dimensional measures of endocranial globularity (3D globularity and the globularity index) produce conflicting patterns of differing endocast sphericity among extant primate clades, highlighting the broad variation in primate endocast shapes.
2) Haplorhines tend to have greater midline globularity—a measure of the deviation in distance from midline endocranial surface points to the centroid—than strepsirrhines, and a small proportion of the variation in this feature is explained by variation in encephalization.
3) Mixed levels of support were found for the Spatial Packing Hypothesis (Biegert 1963), which predicts that a relatively larger brain will assume a more spherical shape, as the brain grows around the basicranium, causing flexion of the anterior and posterior cranial planes. This study reinforces the results of previous studies in that variation in encephalization explains a moderate amount of the variation in cranial base flexion among primates; however, the analysis herein calls into question the magnitude of the previously proposed relationship between neurocranial globularity and basicranial angle. While more encephalized species tend to have greater cranial flexion and greater midline globularity, basicranial angle has very weak explanatory power concerning the variation in the

sphericity once the effects of phylogeny and encephalization are taken into account.

4) This study provides support for key predictions made by Enlow and Azuma (1975)'s Facial Packing Hypothesis, namely that: i) the orientation of the anterior cranial base (planum sphenoideum-sphenoidale and the cribriform plane) is more horizontally oriented in more encephalized species, and ii) variation in facial size is constrained by encephalization and the orientation of the facial skeleton relative to the cranial base. More encephalized primates tend to have shorter faces and more flexed basicrania. Moderately encephalized and long snouted anthropoids (large papionins) appear to bypass the constraints on facial size by downwardly flexing the palate relative to the anterior cranial base, thus effectively shortening the anterior protrusion of the facial skeleton.
5) If we were to rank the fossil specimens relative to one another, the distribution of cranial and endocranial features within the fossil specimens is consistent with patterns found in extant primates, namely that the more encephalized the species (in order from least to most encephalized: *Adapis Parapithecus, Aegyptopithecus, Homunculus*) have greater flexion of the basicranium, a rounder and taller endocranial surface outline, and a less prognathic facial skeleton. Nevertheless, the absolute values for these specimens are more consistent with a shift in cranial

features at the base of the haplorhine, anthropoid, catarrhine, and platyrrhine clades, prior to the achievement of modern levels of encephalization.

4. Conclusions and Future Directions

4.1. Order of Acquisition of Traits in Primate Brain Evolution

This study demonstrates that strepsirrhine and anthropoid primates show clear differences in endocast shape and that these differences reflect differences in both brain proportions and encephalization (Figure 31). Furthermore, the analyses detailed herein bolster the results of previous studies which find a relationship between encephalization and those variables characterizing the anthropoid-strepsirrhine cranial shape dichotomy (Ross 1995; Lieberman *et al.* 2000c; Fleagle *et al.* 2010); however, if the cranial differences between strepsirrhines and anthropoids are the direct result of correlated effects of encephalization due to spatial constraints on the neurocranium imposed by basicranial and facial size, we would expect that the divergence in anthropoid-strepsirrhine cranial morphotype would occur in concert with increases in encephalization within as well as between these groups. Instead, we find that the earliest anthropoid in the sample, *Parapithecus*, shows an intermediate morphology between that of extant strepsirrhines and haplorhine in both endocranial and facial morphology, despite having a relatively small brain for its body size (Figure 32). The contemporaneous stem catarrhine *Aegyptopithecus* is more anthropoid-like in both endocranial and facial form—with a higher endovertex, smaller and more inferiorly directed olfactory bulb, a smaller face, and greater flexion of the cranial base—despite having a strepsirrhine-like relative brain size that is only slightly larger than that of *Parapithecus* (Simons *et al.* 2007). Finally, the

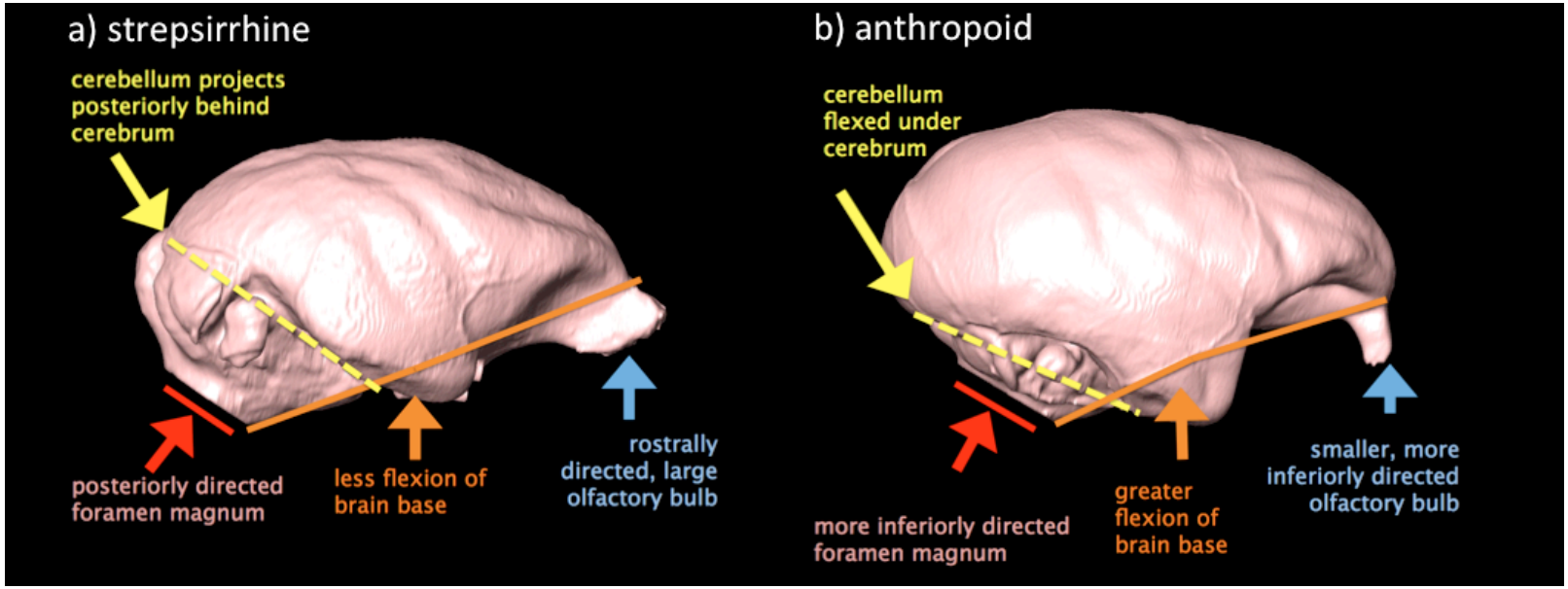

Figure 31: Endocast shape differences between extant strepsirrhines and anthropoids. a) ***Lemur catta*****, b)** ***Saimiri sciurus*****.**

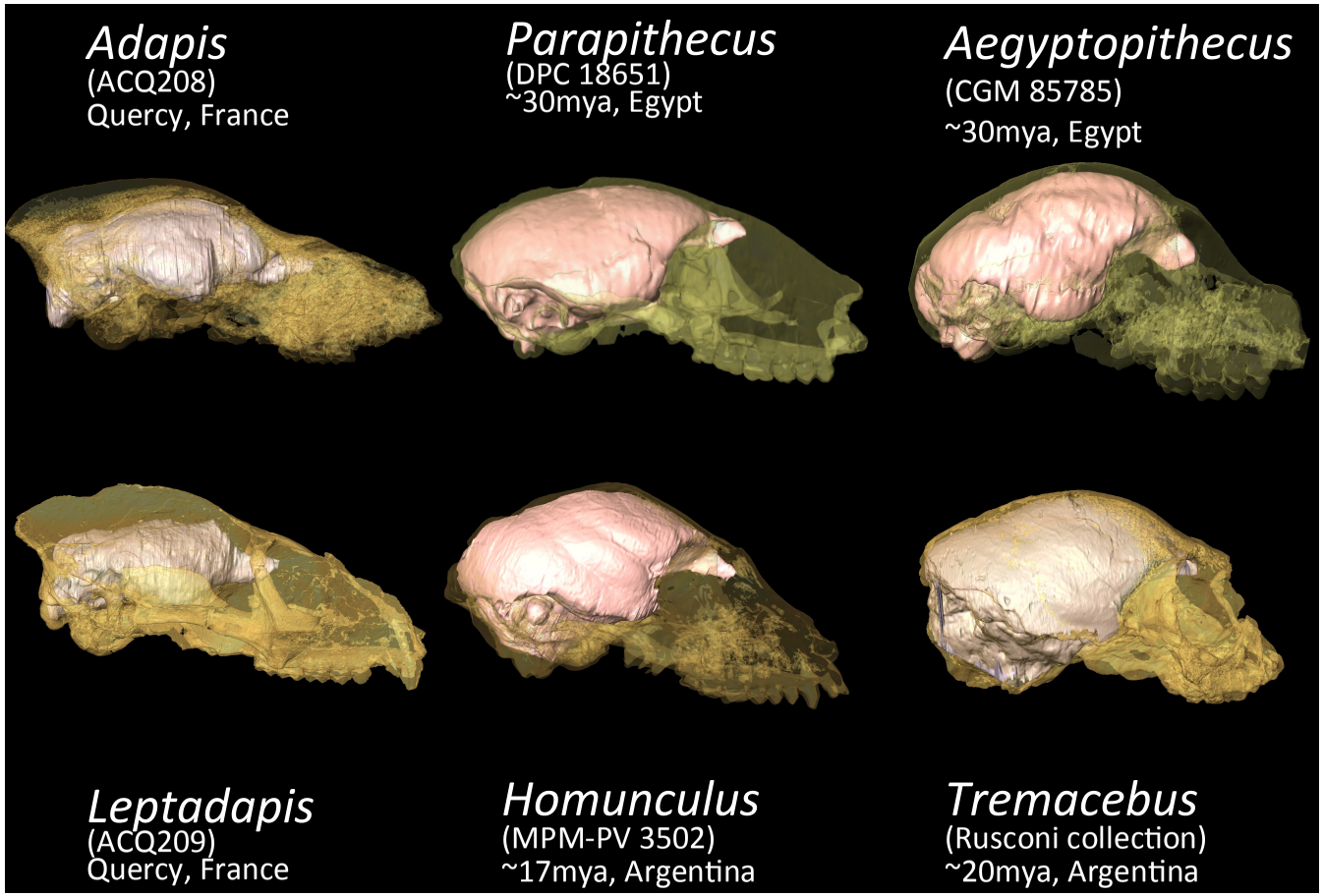

Figure 32. Fossil primate endocasts and associated skulls in lateral view. All specimens are scaled to equal length.

Miocene platyrrhines *Tremacebus* and *Homunculus* likewise differ from strepsirrhines in sharing a higher endovertex, small olfactory fossa, reduced snout, and greater basicranial flexion with extant anthropoids, and *Homunculus* demonstrates and even higher endovertex, smaller olfactory bulb, and greater basicranial flexion than the Oligocene primates, despite a brain size below that of the extant platyrrhine distribution.

In summary, the extant data suggest a moderately conserved pattern of craniofacial organization, which may explain differences in endocranial and facial shape between extant strepsirrhines and anthropoids; however, the fossil record of early anthropoid evolution demonstrates that key anthropoid-like traits of the endocranium (reduced size of the olfactory fossa, posterior extension of the occipital poles relative to the cerebellar pole), basicranium (increased basicranial flexion), and facial skeleton (reduced snout length and facial size) were initiated early in anthropoid evolution, with encephalization occurring within and among more recent members of this clade (Figure 33).

4.2. Implications of Tarsier Morphology for Brain Shape and Cranial Evolution in Haplorhini

In any morphological or ecological comparison of anthropoid and strepsirrhine clades, one would be remiss to ignore the tarsioids. Given their phylogenetic placement as the living sister taxon to Anthropoidea, tarsioids should present a useful outgroup comparison for determining the order of acquisition of traits in haplorhine evolution. Unfortunately, most studies ignore tarsier morphology completely in these discussions,

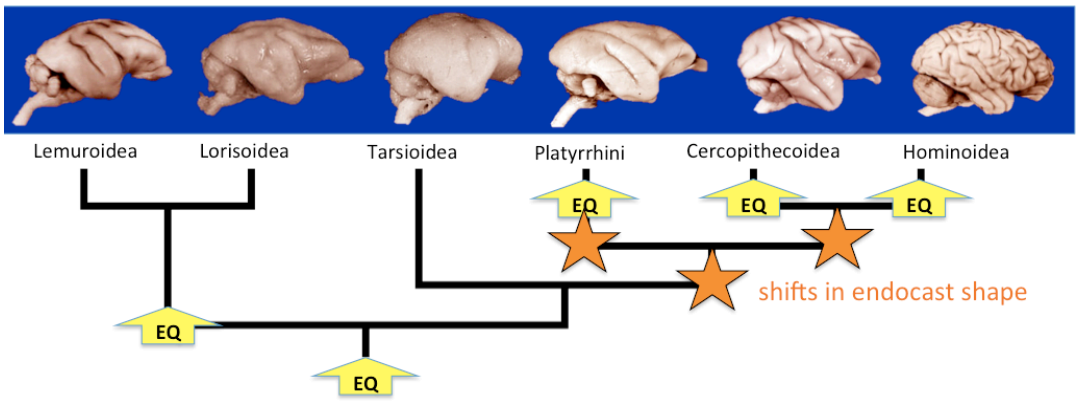

Figure 33. A phylogeny of extant primate clades illustrating the proposed timing of shifts in encephalization (EQ) and endocast shape (indicated by orange stars) as evidenced by a combination of modern distributions and fossil evidence.

owing to their confusing mixture of symplesiomorphic and/or convergent conditions shared with strepsirrhines (i.e. small body size and nocturnality), haplorhine synapomorphies (i.e. dry rhinarium, loss of tapetum lucidum—the reflective layer of the eye), and exaggerated apomorphies (i.e. extremely large eyes, ultrasonic vocalizations). The re-analysis of Stephan's data on brain component masses (Chapter 2) reinforces the crucial yet rarely cited results of Joffe and Dunbar (1998) that tarsiers share many aspects of brain proportions—including an enlarged neocortex, visual cortex and lateral geniculate body, and reduced olfactory bulb—with other haplorhines, despite having small brains within the strepsirrhine range. Furthermore, the analysis herein adds unusual endocast shape to the list of tarsier apomorphies. Tarsiers differ from all other sampled primates (extant or fossil) in having a relatively short and extremely broad

endocast at the level of the cerebral hemispheres with particular attenuation of the anterior and middle cranial fossae.

Although it is tempting to dismiss tarsiers as "extremely derived" and therefore irrelevant to the interpretation of early anthropoid cranial evolution, a comparison of anthropoid, tarsier, and strepsirrhine brain proportions bring up some interesting—though admittedly difficult to test—thoughts on the nature of encephalization and cranial form in primates. The combination of a reorganization of brain proportions, particularly of the sensory systems, with a relatively small brain size suggest that one or more of the following scenarios may be true: i) a fundamental shift in the sensory system of the brain occurred at the base of the crown Haplorhine clade, prior to the divergence of tarsiers and anthropoids, with anthropoids experiencing subsequent parallel encephalization events and strepsirrhine undergoing less encephalization or retaining a small brain size; or ii) tarsiers and anthropoids experienced parallel selective pressures on their sensory systems as a result of a shift towards diurnality at the base of Haplorhini, with tarsiers increasing the size of their visual system as a result of a reversion to nocturnality in absence of a tapetum lucidum.

Differences in encephalization between tarsiers and anthropoids may be the result of: i) the absence of selective pressures for encephalization in tarsiiforms, owing to more strepsirrhine-like lower levels of social complexity and social group size than in anthropoids (MacKinnon and MacKinnon 1980; Dunbar 1992), or ii) spatial constraints

on the tarsier endocranium as a result of massive eyeball size. This latter scenario is supported by the tarsier endocast shape, which is unique in being broad with very room afforded the anterior and middle cranial fossae, as the endocast wraps itself around the posterior aspect of the orbit.

4.3. Implications for Cognitive Interpretations from the Fossil Record

The data provided herein make no specific predictions concerning the evolution of cognitive abilities among primates; however, they do speak to some opportunities and limitations for future interpretations of cognitive evolution from endocast form. The overall shape of the endocast is the result of the complex interplay of body size, encephalization, mosaic evolution in the mass of brain components, and spatial constraints imposed by skull form. As such, any attempt to compare endocasts of differing sizes or skull forms should consider the possibility that selection for body size and facial architecture, rather than for cognition, may be the root cause of differences in endocast shape. Furthermore, some variation in endocast shape, such as the midline globularity and "bossing" or continuous curvature of the frontal lobe, reflect variation in overall encephalization rather than the independent enlargement of the frontal lobe, per se.

This study identifies some features of endocast shape related to differences in brain proportions among extant primates. The most obvious of these is olfactory fossa size, which loads heavily on the first principal component axes of endocast shape

(Chapter 2), which itself is correlated with the residual mass of the olfactory bulb. This is not surprising given previous work concerning the predictive capabilities of olfactory fossa morphology for estimating olfactory bulb size. In particular, Kay *et al.* (2004) found success in using the breadth of the olfactory fossa, relative to maximum endocranial breadth, as an osteological proxy for olfactory bulb size. Furthermore, Pihlstrom *et al.* (2005) demonstrate that the area of the cribriform plate is predictive of both olfactory bulb mass and olfactory sensitivity thresholds across Mammalia.

Endocast shape variables used herein likewise correlate with the relative size of the telencephalon and the cerebellum. Species with enlarged telencephalons relative to brain mass tend to have occipital poles of the cerebrum that extend posteriorly over the cerebellar poles, such that the cerebellar tentorium is oriented horizontally rather than obliquely relative to the fronto-occipital plane. The result is a posterior cranial fossa that is tucked under the occipital region of the endocast. This morphology is ubiquitous among anthropoids and *Tarsius*, though it covaries slightly in magnitude with residual telencephalon and residual brain mass. The presence of haplorhine-like brain proportions in the stem anthropoid *Parapithecus grangeri* can be inferred from the presence of this diagnostic shape of the posterior aspect of the endocast. Although studies by Reader and Laland (2002), Deaner *et al.* (2007), MacLean *et al.* (2014) find interspecific variation in key aspects of cognitive performance is correlated with absolute and/or relative brain size, very little is known about the cognitive implications

for brain proportions. As no studies have directly tested cognitive performance and the relative size of the telencephalon versus the cerebellum, the implications for increased relative telencephalon size remains for now only a theoretical, albeit plausible, link on the basis of Jerison's Principal of Proper Mass (1963).

4.4. Avenues for Future Research

Any analysis of endocranial form is limited in its interpretation by the fact that the endocast captures only the most superficial aspects of brain form. Although some endocranial surface details convey information on the anatomical subdivisions of the brain (i.e. sulci, gyri, ossification of the cerebellar tentorium), the size and shape of subcortical structures and the microarchitecture of the brain cannot be captured in the fossil record. Furthermore, attempts to link endocranial surface anatomy to brain proportions—residual mass of brain components—is limited by the available data from postmortem dissections of the brain. The Stephan dataset (Stephan and Andy 1964; Stephan and Andy 1969; Stephan *et al.* 1981; Stephan *et al.* 1982; Baron *et al.* 1983; Jolicoeur *et al.* 1984; Matano *et al.* 1985a; Matano *et al.* 1985b; Stephan *et al.* 1988) has proven to be an indispensible resource for researchers examining patterns of mosaicism versus constraints in the scaling of mammalian brain components (Barton *et al.* 1995; Finlay and Darlington 1995; Barton and Dunbar 1997; Barton 1998; Finlay *et al.* 1998; Barton and Harvey 2000; Finlay *et al.* 2001; Whiting and Barton 2003), and due to the limited availability of primate specimens for research, and the difficulties inherent in

preserving these specimens for accurate volumetric measurements (Baker 1958), a dataset of this magnitude and detail would be exceedingly difficult replicate in the future.

As fertile as this resource has been, however, there are some methodological problems inherent in the use of postmortem brain mass data. The limited availability of specimens constrains analyses to only those species for which cadaveric material is readily available, and sample sizes are generally quite small. Furthermore, the use of species mean data from different source material can undermine the ability to statistically detect fine levels of correlated variation among closely related individuals (intraspecific variation) or groups (interspecific variation within a clade). Body mass within a single species can vary widely among subspecies (Isler *et al.* 2008), between sexes (Plavcan 2003), and across the life of the individual (Glander 2006). Thus, individual, sex, and subspecies differences between datasets introduce varying levels of error, thus reducing statistical power.

One potentially fruitful avenue for future research involves the use of *in vivo* high resolution MRI to directly observe variation in the size and shape of gross anatomical components in a relatively non-invasive fashion. Although once again limited by access to research subjects, high resolution imaging technique would allow us to directly compare the gross anatomy and some microanatomical components of the brain tissue of an individual subject with impressions made on the endocranial surface

without sacrificing the individual. Analysis such as these would be the ideal test case to determine the fidelity with which endocranial surface morphology captures intraspecific and interspecific variation in residual mass and shape of brain components.

Finally, the incorporation of additional fossil specimens would help to flesh out the picture of primate encephalization and endocranial variation from a temporal perspective. Recent analyses of hominin fossils—e.g. the earliest complete hominid specimen, *Sehalanthropus tchadensis* (Zollikofer *et al.* 2005; Bienvenu *et al.* 2013), and a geologically young species of australopithecine, proposed to be sister species to the *Homo* lineage, *Australopithecus sediba* (Carlson *et al.* 2011)—have shown that the evolution of phylogenetically diagnostic endocast shape, thought to reflect differences in brain proportions, preceded encephalization within the hominid clade. A primate-wide fossil analysis, including available stem representatives of Primates (pleasiadapiforms), Strepsirrhini (adapiforms), Haplorhini (omomyiforms), Cercopithecoidae (Victoriapithecidae), and Hominidae would reveal whether changes in endocranial proportions consistently precede encephalization in primate evolution.

Appendix A: CT Scan Information

Species	n	Specimen #	Provenience	Scan facility	Voxel size	Pixels	Resampled voxel size	# slices through endocast	ECV
Alouatta fusca	1	NMNH 518255	Brazil	UTCT	0.1016 x 0.1016 x 0.111	1024 x 1024 x 871	0.2031 x 0.2031 x 0.1628	400	48.8
Alouatta seniculus	1	USNM 281756	Colombia	UTCT	0.1586 x 0.1586 x 0.1896	512 x 512 x 490	--	316	33.5
Aotus trivirgatus	2	Kay 1492	Panama	UTCT	0.0508 x 0.0508 x 0.0571	1024 x 1024 x 815	0.1142 x 0.1142 x 0.1035	400	18.3
		USNM 503920	Unknown	UTCT	0.1035 x 0.1035 x 0.1189	512 x 512 x 522	--	388	18.8
Ateles geoffroyi	1	Kay	Unknown	UTCT	0.0908 x 0.0908 x 0.1017	1024 x 1024 x 1090	0.1816 x 0.1816 x 0.1796	400	0.0
		BAA na	Unknown	Duke SMiF	0.0588 x 0.0588 x 0.0588	1539 x 1592 x 1869	0.1767 x 0.1827 x 0.0952	400	106.5
Brachyteles arachnoides	1	AMNH 80405	Brazil	AMNH	0.0886 x 0.0886 x 0.0886	869 x 770 x 976	0.1500 x 0.1330 x 0.1820	400	110.9
Cacajao calvus	3	USNM 302626	Unknown	UTCT	0.2003 x 0.2003 x 0.1699	512 x 512 x 489	--	338	68.8
		USNM 319516	Unknown	UTCT	0.2003 x 0.2003 x 0.1758	512 x 512 x 476	--	337	71.9
		USNM 395027	Unknown	UTCT	0.2003 x 0.2003 x 0.1699	512 x 512 x 481	--	329	71.5
Cacajao melanocephalus	1	USNM 406427	Venezuela	UTCT	0.1465 x 0.1465 x 0.1754	512 x 512 x 472	--	331	66.2
Callicebus torquatus	3	USNM 406416	Venezuela	UTCT	0.0714 x 0.0714 x 0.0664	1024 x 1024 x 863	0.1328 x 0.1328 x 0.1135	400	20.5
		USNM 269827	Unknown	UTCT	0.1230 x 0.1230 x 0.1528	512 x 512 x 438	--	306	18.1
		USNM 397933	Colombia	UTCT	0.1211 x 0.1211 x 0.1629	512 x 512 x 372	--	260	14.7
Callimico goeldi	2	USNM 303323	Unknown	UTCT	0.0410 x 0.0410 x 0.0464	1024 x 1024 x 1175	0.0820 x 0.0820 x 0.1020	400	11.1
		USNM 395455	Unknown	UTCT	0.0820 x 0.0820 x 0.1449	512 x 512 x 344	--	270	10.4
Callithrix jacchus	2	USNM 503885	Unknown	UTCT	0.0342 x 0.0342 x 0.0334	1024 x 1024 x 1150	0.0684 x 0.0684 x 0.0768	400	6.3
		USNM 503895	Unknown	UTCT	0.0352 x 0.0352 x 0.041	1024 x 1024 x 1140	0.0703 x 0.0703 x 0.0934	400	6.9
Cebuella pygmaea	1	USNM 337324	Brazil	UTCT	0.0273 x 0.0273 x 0.0319	1024 x 1024 x 1100	0.0547 x 0.0547 x 0.0733	400	4.2
Cebus apella	1	USNM 518266	Brazil	UTCT	0.1563 x 0.1563 x 0.1879	512 x 512 x 481	--	323	63.2
Cebus olivaceous	1	USNM 338960	Guyana	UTCT	0.0771 x 0.0771 x 0.0772	1024 x 1024 x	0.1543 x 0.1543 x 0.1598	400	71.2
Lagothrix lagotricha		Kay	Unknown	Duke SMiF	0.1758 x 0.1758 x 0.2232	512 x 512 x 654	0.1398 x 0.1225 x 0.1803	400	93.2
Leontopithecus rosalia	2	USNM 337333	Brazil	UTCT	0.0830 x 0.0830 x 0.1449	512 x 512 x 361	--	281	11.9
Mico argentata	1	USNM 239463	Brazil	UTCT	0.0352 x 0.0352 x 0.038	1024 x 1024 x 1185	0.0703 x 0.0703 x 0.0884	400	7.3

Pithecia sp.	1	Fleagle NP5	Unknown	UTCT	0.0635 x 0.0635 x 0.1450	1024 x 1024 x 532	0.1269 x 0.1269 x 0.145	367	31.7
Saginus fuscicollis	3	Kay 1492	Unknown	UTCT	0.0366 x 0.0366 x 0.041	1024 x 1024 x 1080	0.0732 x 0.0732 x 0.0842	400	6.7
		USNM 306845	Panama	UTCT	0.0801 x 0.0801 x 0.0967	512 x 512 x 520	--	400	9.8
		USNM 518577	Brazil	UTCT	0.0378 x 0.0378 x 0.0352	1024 x 1024 x 1125	0.0703 x 0.0703 x 0.0873	400	6.9
Saimiri sciureus	1	USNM 518538	Brazil	UTCT	0.0479 x 0.0479 x 0.0551	1024 x 1024 x 1134	0.1066 x 0.1066 x 0.1102	400	23.5
		USNM 398699	Unknown	UTCT	0.1045 x 0.1045 x 0.1145	512 x 512 x 557	--	425	24.7
Cercocebus torquatus	1	KUPRI 1030	Unknown	KUPRI	0.2130 x 0.2140 x 0.2000	512 x 512 x 385	--	335	90.1
Cercopithecus mona	1	AMNH 52483	Congo	AMNH	0.0653 x 0.0653 x 0.0653	1185 x 1007 x 1564	0.1511 x 0.1284 x 0.1574	400	61.5
Cercopithecus albogularis kolbi	2	USNM 452574	Kenya	USNM	0.1758 x 0.1758 x 0.2000	512 x 512 x 1036	--	332	69.5
		USNM 452581	Kenya	USNM	0.1445 x 0.1445 x 0.2000	512 x 512 x 886	--	331	74.0
Cercopithecus nictitans martini	2	USNM 481007	Cameroon	USNM	0.1367 x 0.1367 x 0.2000	512 x 512 x 828	--	313	62.3
		USNM 481770	Liberia	USNM	0.1367 x 0.1367 x 0.2000	512 x 512 x 828	--	313	60.8
Chlorocebus sabaeus	1	USNM 381445	Gambia	USNM	0.1758 x 0.1758 x 0.2000	512 x 512 x 1071	--	323	71.7
Colobus polykomos	2	KUPRI 1043	Unknown	KUPRI	0.2000 x 0.2000 x 0.2000	512 x 512 x 512	--	316	63.8
		KUPRI 1100	Unknown	KUPRI	0.2000 x 0.2000 x 0.2000	512 x 512 x512	--	326	67.0
		KUPRI 1103	Unknown	KUPRI	0.2000 x 0.2000 x 0.2000	512 x 512 x 512	--	331	69.8
		KUPRI 1105	Unknown	KUPRI	0.2000 x 0.2000 x 0.2000	512 x 512 x 512	--	328	61.6
Erythrocebus patas	1	USNM 270440	Mauritana	USNM	0.1445 x 0.1445 x 0.2000	512 x 512 x 1011	--	349	79.7
Lophocebus albigena	3	KUPRI 1725	Unknown	KUPRI	0.2920 x 0.2920 x 0.2000	512 x 512 x 398	--	270	95.8
Macaca mulatta	1	KUPRI 1701	Unknown	KUPRI	0.2250 x 0.2250 x 0.2000	512 x 512 x 631	--	358	83.2
Mandillus leucopus	1	KUPRI 1487	Unknown	KUPRI	0.3990 x 0.3990 x 0.3000	512 x 512 x 325	--	399	146.8
Miopithecus talapoin	1	Kay	Unknown	UTCT	0.0615 x 0.0615 x 0.1450	512 x 512 x 510	--	399	40.9
Nasalis larvatus		USNM 198277	Indonesia	USNM	0.1641 x 0.1641 x 0.2000	512 x 512 x 988	--	355	76.4
Papio hamadryas	4	KUPRI 1677	Unknown	KUPRI	0.1990 x 0.1990 x 0.2000	512 x 512 x 801	--	390	132.6
		KUPRI 3390	Unknown	KUPRI	0.2500 x 0.2500 x 0.2000	512 x 512 x 861	--	380	129.1

Papio hamadryas		KUPRI 4450	Unknown	KUPRI	0.2500 x 0.2500 x 0.2000	512 x 512 x 1011	--	402	174.3
		KUPRI 7147	Unknown	KUPRI	0.2500 x 0.2500 x 0.2000	512 x 512 x 1056	0.2500 x 0.2500 x 0.2209	400	162.2
Piliocolobus badius	1	USNM 481795	Liberia	USNM	0.1719 x 0.1719 x 0.2000	512 x 512 x 976	--	326	64.8
Presbytis melalophos	1	AMNH 113723	Burma	AMNH	0.0731 x 0.0731 x 0.0731	1256 x 1226 x 1532	0.1793 x 0.1750 x 0.1983	400	114.9
Presbytis potenziana	2	USNM 121668	Indonesia	USNM	0.1602 x 0.1602 x 0.2000	512 x 512 x 896	--	320	63.8
		USNM 121692	Indonesia	USNM	0.1484 x 0.1484 x 0.2000	512 x 512 x 868	--	325	60.8
Procolobus badius	1	AMNH 52283	Unknown	AMNH	0.0706 x 0.0706 x 0.0706	1256 x 1226 x 1532	0.1732 x 0.1691 x 0.17610	400	79.7
Procolobus verus	3	USNM 477327	Cote d'Ivoire	USNM	0.1465 x 0.1465 x 0.2000	512 x 512 x 796	--	302	52.1
		USNM 477331	Cote d'Ivoire	USNM	0.1641 x 0.1641 x 0.2000	512 x 512 x 828	-	307	56.9
		USNM 481799	Liberia	USNM	0.1484 x 0.1484 x 0.2000	512 x 512 x 883	--	322	66.8
Semnopithecus priam	2	USNM 122634	India	USNM	0.1719 x 0.1719 x 0.2000	512 x 512 x 946	--	355	84.1
		USNM 196986	Sri Lanka	USNM	0.1836 x 0.1836 x 0.2000	512 x 512 x 1006	--	337	72.5
Simias concolor	2	USNM 121654	Indonesia	USNM	0.1484 x 0.1484 x 0.2000	512 x 512 x 878	--	312	54.6
		USNM 121663	Indonesia	USNM	0.1484 x 0.1484 x 0.2000	512 x 512 x 878	--	314	60.0
Theropithecus gelada	1	KUPRI 9030	Unknown	KUPRI	0.3000 x 0.3000 x 0.3000	512 x 512 x 567	--	277	131.0
Trachypithecus cristatus	2	USNM 257685	Thailand	USNM	0.1406 x 0.1406 x 0.2000	512 x 512 x 803	--	303	57.4
		USNM 277618	Myanmar	USNM	0.1719 x 0.1719 x 0.2000	512 x 512 x 928	--	375	95.5
Gorilla gorilla	4	KUPRI 7219	Unknown	KUPRI	0.3820 x 0.3820 x 0.5000	512 x 512 x 533	--	249	502.7
		USNM 176211	Cameroon	USNM	0.3555 x 0.3555 x 0.5000	512 x 512 x 581	--	260	597.4
		USNM 297857	Unknown	USNM	0.3513 x 0.3513 x 0.5000	512 x 512 x 567	--	241	440.4
		USNM 176209	Cameroon	USNM	0.3711 x 0.3711 x 0.5000	512 x 512 x 613	--	265	608.4
Homo sapiens	2	ULAC 012	Germany	EVAN Archives German repository	**	512 x 512 x 544	0.3890 x 0.3890 x 0.4275	400	1675.4
		ULAC 013	Germany	EVAN Archives German repository	0.3321 x 0.3321 x 0.3321	512 x 512 x 574	0.3321 x 0.3321 x 0.3979	400	1247.9
Hylobates lar	1	USNM 111989	Myanmar	UTCT	0.1758 x 0.1758 x 0.2232	512 x 512 x 494	--	337	97.4
Pan troglodytes	5	UCL CA14A	Unknown	EVAN archives UK repository	0.4883 x 0.4883 x 0.6250	351 x 290 x 345	--	149	372.3
		UCL CA14E	Unknown	EVAN archives UK repository	0.4530 x 0.4530 x 0.6250	331 x 333 x 355	--	147	359.4
		USNM 236971	Uganda	USNM	**	512 x 512 x 391	--	204	305.8
		USNM 297856	Unknown	USNM	**	512 x 512 x 383	--	215	321.9
		USNM 395820	Unknown	USNM	**	512 x 512 x 429	--	225	447.6

Tarsius syrichta	2	DPC 0127	Duke Lemur Center	Duke SMiF	0.0222 x 0.0222 x 0.0222	1548 x 1262 x 2225	0.0672 x 0.05477 x 0.1236	400	3.2
		DPC 045	Duke Lemur Center	Duke SMiF	0.0444 x 0.0444 x 0.0444	794 x 527 x 914	0.0689 x 0.0457 x 0.0720	400	3.0
Tarsius bancanus	1	USNM 488084	Malaysia	UTCT	0.0371 x 0.0371 x 0.0840	1024 x 1024 x 465	0.0742 x 0.0742 x 0.0840	339	3.3
Daubentonia madagascarensis	1	AMNH 185643	Unknown	Duke SMIF	0.0855 x 0.0855 x 0.0855	902 x 1023 x 999	0.1506 x 0.1708 x 0.1419	400	43.1
Eulemur fulvus	4	DPC 057	Duke Lemur Center	Duke SMIF	0.0501 x 0.0501 x 0.0501	1164 x 1252 x 1923	0.1063 x 0.1102 x 0.1377	400	21.7
		DPC 058	Duke Lemur Center	Duke SMIF	0.0481 x 0.0481 x 0.0481	1249 x 1101 x 1929	0.1207 x 0.1036 x 0.1250	400	24.2
		DPC 061	Duke Lemur Center	Duke SMIF	0.0536 x 0.0536 x 0.0536	1174 x 1274 x 1964	0.1178 x 0.1184 x 0.1272	400	28.1
		DPC 101	Duke Lemur Center	Duke SMIF	0.0488 x 0.0488 x 0.0488	1293 x 1215 x 1963	0.1110 x 0.0982 x 0.1259	400	21.8
Galago senegalensis	5	AMNH 187355	AMNH	AMNH	0.0321 x 0.0321 x 0.0321	942 x 684 x 1277	0.0591 x 0.0429 x 0.0707	400	3.9
		DPC 005	Duke Lemur Center	Duke SMIF	0.0224 x 0.0224 x 0.0224	751 x 538 x 938	0.0657 x 0.0471 x 0.0753	400	3.8
		DPC 007	Duke Lemur Center	Duke SMIF	0.0536 x 0.0536 x 0.0536	697 x 619 x 950	0.0716 x 0.0636 x 0.0731	400	5.2
		DPC 083	Duke Lemur Center	Duke SMIF	0.0233 x 0.0233 x 0.0233	1278 x 1326 x 1876	0.0626 x 0.0574 x 0.0730	400	4.1
		DPC 088	Duke Lemur Center	Duke SMIF	0.0233 x 0.0233 x 0.0233	1306 x 1249 x 1886	0.0614 x 0.0523 x 0.0727	400	3.9
Hapalemur griseus	1	DPC 1311	Duke Lemur Center	UTCT	0.1055 x 0.1055 x 0.1157	512 x 512 x 610	--	403	14.5
Indri indri	1	AMNH 100506	AMNH	AMNH	0.0638 x 0.0638 x 0.0638	***	0.1350 x 0.0972 x 0.1398	400	35.9
Lemur catta	2	BAA 0089	Duke Lemur Center	Duke SMIF	0.0462 x 0.0462 x 0.0462	1159 x 1314 x 1974	0.2091 x 0.2371 x 0.2577	400	27.2
		DPC 092	Duke Lemur Center	Duke SMIF	0.0501 x 0.0501 x 0.0501	1161 x 1158 x 1923	0.1136 x 0.1133 x 0.0603	400	27.2
Lepilemur mustelinus	1	AMNH 170563	AMNH	AMNH	0.0428 x 0.0428 x 0.0428	710 x 711 x 960	0.0598 x 0.0595 x 0.0868	400	6.2
Loris tardigratus	2	BAA 0006	Duke Lemur Center	Duke SMIF	0.0287 x 0.0287 x 0.0287	650 x 551 x 957	0.0364 x 0.0309 x 0.860	400	6.2
		DPC 0175	Duke Lemur Center	Duke SMIF	0.0324 x 0.0324 x 0.0324	1347 x 1440 x 1932	0.0852 x 0.0911 x 0.0505	400	12.4
Mircocebus murinus	1	DPC 098	Duke Lemur Center	Duke SMIF	0.0189 x 0.0189 x 0.0189	1249 x 1288 x 1881	0.0461 x 0.0475 x 0.0298	400	2.2
Mirza coquereli	2	DPC 0137	Duke Lemur Center	Duke SMIF	0.0294 x 0.0294 x 0.0294	1239 x 1247 x 1833	0.0711 x 0.0716 x 0.0405	400	6.4
		DPC 1139	Duke Lemur Center	Duke SMIF	0.0294 x 0.0294 x 0.0294	1214 x 1176 x 1857	0.0697 x 0.0675 x 0.0406	400	5.1
Nycticebus coucang	2	BAA 0002	Duke Lemur Center	Duke SMIF	0.0346 x 0.0346 x 0.0346	1397 x 1404 x 1919	0.0944 x 0.0949 x 0.0475	400	11.4
		DPC 0161	Duke Lemur Center	Duke SMIF	0.0349 x 0.0349 x 0.0349		0.0982 x 0.0655 x 0.0977	400	11.6
Propithecus verreauxi	1	DPC 6756	Duke Lemur Center	UTCT	0.0767 x 0.0767 x 0.0693	1024 x 1024 x 1075	0.1534 x 0.1534 x 0.1296	400	31.3
Varecia variegata	1	DPC 050	Duke Lemur Center	Duke SMIF	0.0582 x 0.0582 x 0.0582	1152 x 973 x 1926	0.1310 x 0.1106 x 0.0664	400	31.3
Adapis parisiensis	1	ACQ 208	Quercy, France	E.S.R.F.	0.064 x 0.064 x 0.064	545 x 410 x 821	--	505	2.6
Leptadapis magnus	1	ACQ 209	Quercy, France	E.S.R.F.	0.094 x 0.094 x 0.094	750 x 529 x 1172	0.1377 x 0.0971 x 0.1277	400	1.7
Parapithecus grangeri	1	DPC 18651	Fayum, Egypt	U Penn	0.0480 x 0.0480 x 0.0444	1024 x 1024 x 1334	0.0888 x 0.0888 x 0.0198	400	11.7
Aegyptopithecus zeuxis	1	CGM 40237	Fayum, Egypt	U Penn	0.0675 x 0.0675 x 0.07599	1024 x 1024 x 1476	0.1120 x 0.1120 x 0.1093	400	14.7
Tremacebus harringtoni	1	Rusconi	Argentina	UTCT	0.0466 x 0.0466 x 0.0420	1024 x 1024 x 1177	0.0839 x 0.0839 x 0.1035	400	*14.7
Homunculus patagonicus	1	Perry	Argentina	UTCT	0.0449 x 0.0449 x 0.0484	1024 x 1024 x 1535	0.0898 x 0.0898 x 0.1161	400	*12.4

Appendix B: Primate Phylogeny

```
#NEXUS
BEGIN TREES;
        TRANSLATE
                1 Cercopithecus,
                2 Chlorocebus,
                3 Erythrocebus,
                4 Miopithecus,
                5 Daubentonia,
                6 Eulemur,
                7 Hapalemur,
                8 Indri,
                9 Lemur,
                10 Lepilemur,
                11 Microcebus,
                12 Mirza,
                13 Varecia,
                14 Alouatta,
                15 Ateles,
                16 Brachyteles,
                17 Lagothrix,
                18 Aotus,
                19 Callimico,
                20 Callithrix,
                21 Mico,
                22 Cebus,
                23 Leontopithecus,
                24 Saguinus,
                25 Saimiri,
                26 Loris,
                27 Nycticebus,
                28 Gorilla,
                29 Homo,
                30 Hylobates,
                31 Pan,
                32 Cacajao,
                33 Callicebus,
                34 Pithecia,
                35 Cercocebus,
```

36 Lophocebus,
37 Macaca,
38 Mandrillus,
39 Papio,
40 Theropithecus,
41 Colobus,
42 Nasalis,
43 Piliocolobus,
44 Presbytis,
45 Procolobus,
46 Semnopithecis,
47 Trachypithecus,
48 Galago,
49 Tarsius,
50 Simias;

TREE 'consensus_endocasts+' =
(((((((1:9.848126,(3:8.627245,2:8.627244):1.220881):1.644988,4:11.493113):3.382065,(((35:5.304298,38:5.304297):6.046166,((36:4.896861,40:4.896862):0.872302,39:5.769163):5.5813):1.502062,37:12.852525):2.022653):6.535196,((41:12.537452,(50:11.592451[%selected = on],(43:10.64745,45:10.64745):0.945001):0.945001):2.897705,((42:12.784647,(46:11.461377,47:11.461378):1.32327):0.523455,44:13.308102):2.127056):5.975217):8.589626,(30:19.605945,(28:8.652233,(29:6.17588,31:6.175879):2.476353):10.953713):10.394055):16.811821,(((14:14.76024,(15:9.147391,(16:2.35377,17:2.35377):6.793621):5.612849):6.56106,((18:19.487521,(((19:13.232628,(20:4.789812,21:4.789812):8.442815):1.797437,23:15.030065):0.682187,24:15.712253):3.775269):0.605006,(22:18.569905,25:18.569905):1.522623):1.228773):1.411478,((32:9.642879,34:9.642879):9.753209,33:19.396088):3.336691):24.079043):22.028211,49:68.840033):4.162986,((((((11:14.271122,12:14.271123):14.157972000000001,10:28.429095):2.51681,8:30.945905):2.318811,((6:15.019597,(7:9.280518,9:9.280517):5.739079):5.523206,13:20.542802):12.721914):17.859349,5:51.124065):11.612487,((26:24.057527,27:24.057528):13.942473,48:38.000001):24.736553):10.266465);

END;

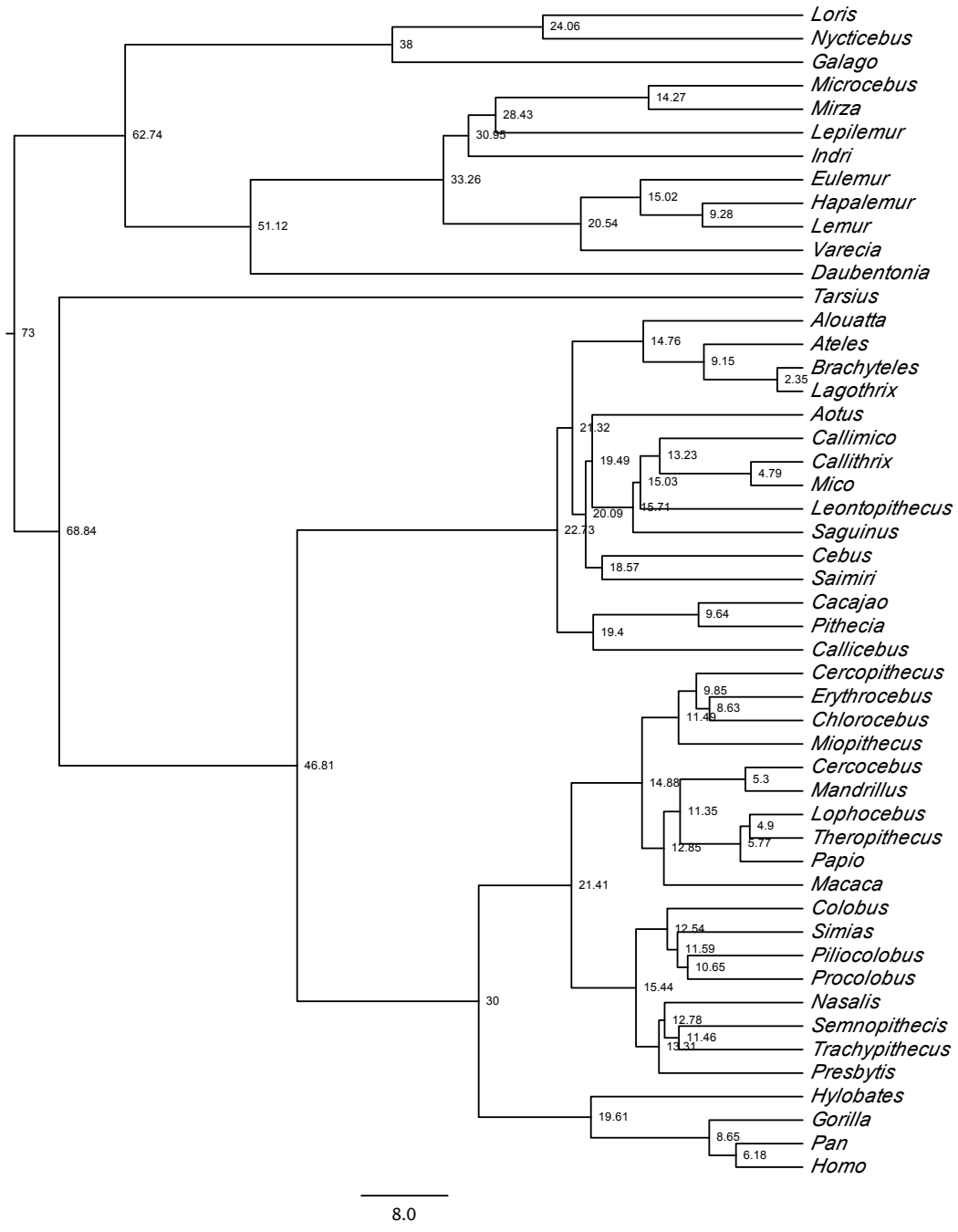

NOTES: Numbers at nodes denote divergence dates in millions of years (myr) before present. Scale bar represents 8 myr.

Appendix C: Residual mass of brain parts

Species	medulla	cerebellum	mesen-cephalon	dien-cephalon	telen-cephalon	olfactory bulb	septum	schizo-cortex	hippo-campus	neo-cortex	visual cortex	corpus geniculate lateralis
Cercocebus albigena	0.0773	0.0200	0.0779	0.0334	0.0629	0.0889	-0.0311	-0.1141	-0.0732	0.0783	0.2355	0.1441
Cercopithecus ascanius	0.0736	0.0406	0.0941	0.1125	0.1876	0.0803	0.1186	0.1472	0.0417	0.2125	0.2517	0.1702
Cercopithecus mitis	0.0035	-0.1039	0.0149	-0.0070	0.0074	0.0948	-0.0499	-0.0642	-0.0527	0.0245	0.2262	0.1485
Cercopithecus talapoin	0.1429	0.1560	0.1918	0.2410	0.3297	-0.3792	0.1126	-0.0099	0.0760	0.3707	0.1860	0.2069
Colobus badius	-0.0217	-0.0325	-0.0167	-0.0630	-0.0180	-0.2728	-0.0087	0.0287	0.0084	-0.0067	0.0920	0.0690
Erythrocebus patas	0.0656	-0.0647	0.0427	0.0430	0.1089	-0.2784	0.0223	-0.0693	-0.0401	0.1332		
Macaca mulatta	-0.0528	-0.0536	-0.0272	-0.0400	0.0325	-0.0669	-0.0632	-0.1046	-0.1104	0.0486	0.2549	0.1130
Nasalis larvatus	-0.0330	-0.1210	-0.1132	-0.1401	-0.1780	-0.5643	-0.1253	-0.1302	-0.0949	-0.1765		
Papio anubis	0.0733	-0.1291	-0.0090	-0.0700	-0.0456	0.3597	-0.0505	-0.0961	-0.0027	-0.0448		
Pygathrix nemaeus	0.0016	-0.0863	-0.0291	-0.0050	-0.0556	-0.9598	-0.0236	-0.0407	0.1289	-0.0512		
Gorilla gorilla	-0.1432	-0.0462	-0.1422	-0.1772	-0.1811	0.2715	-0.1004	-0.1503	-0.2144	-0.1968	0.0873	0.0439
Homo sapiens sapiens	0.0875	0.4139	0.2401	0.2010	0.4491	-0.1278	0.3712	0.3268	0.2387	0.4527	-0.0433	-0.1858
Hylobates lar	0.0808	0.1821	0.0710	0.1591	0.1737	-0.3219	0.0651	0.2269	0.2639	0.1819		
Pan troglodytes	-0.0424	0.0330	-0.0133	-0.0316	0.0423	0.2565	-0.0260	-0.0667	-0.1095	0.0445	0.1395	0.0679
Alouatta sp.	-0.0991	-0.1833	-0.1265	-0.1082	-0.1758	-0.3578	-0.1439	-0.1511	-0.0715	-0.1793	-0.0049	0.0044
Aotus trivirgatus	0.0589	0.0252	-0.0265	0.0155	0.0658	-0.0416	0.0075	0.0583	0.0519	0.0849	0.0286	-0.0716
Ateles geoffroyi	-0.0951	0.0801	-0.0022	0.0283	0.0744	-0.0389	0.0078	-0.0522	-0.1126	0.0868	0.0647	0.0528
Callicebus moloch	0.0977	-0.0647	0.0670	0.0892	0.0823	-0.5139	-0.0002	0.0208	0.0693	0.1045	0.1137	0.0695
Callimico goeldii	0.0257	0.0316	0.0226	0.0064	0.0662	-0.3089	0.0289	-0.0450	-0.0937	0.1040		
Callithrix jacchus	0.0036	-0.0002	0.0882	0.0415	0.0964	-0.3335	0.0630	-0.0905	-0.0628	0.1356	0.0660	0.0012
Cebuella pygmaea	-0.0178	0.0257	0.0653	0.0382	0.1098	-0.5387	0.0107	0.0483	-0.1094	0.1593	0.3925	0.2515
Cebus sp.	0.1246	0.2024	0.1374	0.1847	0.2277	-0.3082	-0.0166	-0.0790	-0.0609	0.2591	0.1926	0.1239
Lagothrix lagotricha	0.0762	0.1831	0.1278	0.1868	0.1998	-0.0903	0.0338	0.0279	0.0603	0.2169	0.2088	0.0652

Pithecia monacha	0.0747	0.1442	0.0943	0.1578	0.1669	-0.3018	0.0771	-0.0204	0.0930	0.1877	0.0776	0.0376
Saguinus oedipus	0.0388	0.0103	0.0687	0.0846	0.1098	-0.4380	0.0684	-0.0948	-0.0655	0.1508	0.1407	0.0356
Saguinus tamarin	0.0829	0.0807	0.0937	0.0804	0.1497	-0.4710	-0.0728	-0.0160	-0.0087	0.1918	0.1623	0.0749
Saimiri sciureus	0.1398	0.1844	0.1369	0.1984	0.3104	-0.3409	0.1008	-0.0424	-0.0757	0.3646	0.2300	0.0791
Tarsius sp.	0.0240	0.0253	0.1032	0.0193	0.0128	-0.3442	-0.0579	0.0039	-0.0202	0.0453	0.0297	0.1114
Avahi laniger laniger	-0.1468	-0.2224	-0.2061	-0.2195	-0.3581	0.1210	-0.1857	-0.0590	-0.0684	-0.3946	-0.1457	-0.0580
Avahi laniger occidentalis	-0.0807	-0.1185	-0.1087	-0.1006	-0.2506	0.0527	-0.0842	0.0098	-0.0110	-0.2786	-0.1643	-0.0392
Cheirogaleus major	-0.0384	-0.0636	-0.1116	-0.1537	-0.1641	0.4643	0.0130	0.0051	0.0142	-0.2150	-0.0596	-0.0462
Cheirogaleus medius	-0.0758	-0.0835	-0.1120	-0.1945	-0.1773	0.3587	-0.0035	-0.1105	-0.0516	-0.2460	-0.1589	-0.1363
Daubentonia madagascarensis	0.0917	0.1512	0.0275	0.1623	0.0271	0.9357	0.1741	0.3751	0.2647	-0.0245	-0.2040	-0.1232
Indri Indri	-0.1675	-0.1904	-0.1245	-0.1613	-0.3326	0.2526	-0.1270	0.0759	-0.0043	-0.3674	-0.0440	0.1524
Lemur fulvus	0.0470	0.0978	0.0092	0.0532	-0.0128	0.4788	0.0244	0.1620	0.0653	-0.0226	0.0565	0.0010
Lemur variegatus	0.0453	-0.0504	0.0662	-0.0042	-0.1666	0.6608	0.0652	0.1223	0.1453	-0.2108	0.1023	0.0451
Lepilemur ruficaudatus	-0.1502	-0.2140	-0.2462	-0.2810	-0.3800	0.2544	-0.1874	-0.0649	-0.1109	-0.4334	-0.2338	-0.2156
Microcebus murinus	-0.0806	0.0473	-0.0627	-0.0855	0.0120	0.0911	-0.0231	-0.0135	0.0057	-0.0178	-0.1432	-0.1693
Propithecus verrauxi	-0.0576	-0.1354	-0.0845	-0.1098	-0.2992	0.2477	-0.0857	-0.0538	-0.0210	-0.3315	0.0225	0.0879
Galago crassicaudatus	-0.0512	-0.1049	-0.0595	-0.1373	-0.2106	0.4281	-0.0768	-0.0759	-0.0220	-0.2476	-0.1133	-0.1465
Galago demidovii	0.0472	0.1567	0.0415	0.0578	0.1645	0.3405	0.0971	0.0553	0.0858	0.1561	-0.1439	-0.1522
Galago senigalensis	0.0109	0.0866	0.0267	0.0017	-0.0063	0.2443	0.0244	0.0910	0.1121	-0.0212	-0.1055	-0.0804
Loris tardigradus	-0.1673	-0.0645	-0.0722	-0.0127	-0.0212	0.2294	-0.0566	-0.0824	-0.1612	-0.0104	0.0398	0.0203
Nycticebus coucang	-0.0454	-0.1176	-0.0917	0.0181	-0.0756	0.4149	0.0576	0.0086	0.0823	-0.1073	-0.0156	0.0285
Perodicticus potto	-0.0286	-0.1276	-0.1230	-0.1117	-0.1606	0.6720	0.0567	0.1037	0.0217	-0.2104	-0.2248	-0.1882

Appendix D: Species Mean Coordinates for Procrustes-Aligned Landmarks

Appendix D.1: Procrustes aligned landmark data for extant primate endocasts analyzed in chapter 2

	frontal pole			occipital pole			endovertex			endobregma			endolambda			confluence of sinuses		
Species	X 1	Y 1	Z 1	X 2	Y 2	Z 2	X 3	Y 3	Z 3	X 4	Y 4	Z 4	X 5	Y 5	Z 5	X 6	Y 6	Z 6
Alouatta	0.037	-0.005	-0.314	0.014	-0.129	0.204	0.025	-0.207	-0.047	0.066	-0.202	-0.060	0.066	-0.156	0.180	0.068	-0.119	0.204
Aotus	0.030	-0.017	-0.302	0.025	-0.127	0.237	0.027	-0.234	-0.090	0.058	-0.211	-0.147	0.074	-0.160	0.218	0.068	-0.084	0.220
Ateles	0.029	0.027	-0.334	0.018	-0.128	0.228	0.010	-0.247	-0.014	0.065	-0.236	-0.064	0.069	-0.185	0.198	0.067	-0.102	0.215
Brachyteles	0.018	0.016	-0.329	0.003	-0.123	0.217	0.051	-0.245	-0.092	0.054	-0.250	-0.056	0.066	-0.134	0.209	0.066	-0.111	0.218
Cacajao	0.025	-0.007	-0.318	0.024	-0.139	0.237	0.056	-0.257	-0.051	0.056	-0.241	-0.100	0.063	-0.193	0.199	0.062	-0.081	0.215
Callicebus	0.039	0.003	-0.302	0.018	-0.125	0.229	0.040	-0.219	-0.080	0.051	-0.209	-0.112	0.059	-0.162	0.211	0.058	-0.109	0.217
Callimico	0.021	0.008	-0.319	0.016	-0.124	0.244	0.042	-0.214	-0.053	0.050	-0.199	-0.124	0.062	-0.135	0.238	0.060	-0.099	0.238
Callithrix	0.015	0.007	-0.319	0.014	-0.137	0.223	0.057	-0.210	-0.072	0.058	-0.212	-0.071	0.061	-0.168	0.203	0.059	-0.118	0.221
Cebuella	0.016	0.018	-0.316	0.013	-0.134	0.233	0.049	-0.204	-0.057	0.052	-0.171	-0.133	0.055	-0.121	0.227	0.053	-0.107	0.231
Cebus	0.022	0.014	-0.324	0.027	-0.126	0.234	0.054	-0.242	-0.069	0.054	-0.241	-0.067	0.072	-0.162	0.216	0.070	-0.089	0.225
Cercocebus	0.028	-0.012	-0.324	0.017	-0.143	0.222	0.064	-0.267	-0.031	0.062	-0.234	-0.107	0.074	-0.238	0.146	0.062	-0.104	0.216
Cercopithecus	0.038	-0.011	-0.329	0.013	-0.121	0.230	0.041	-0.235	-0.054	0.070	-0.218	-0.111	0.073	-0.194	0.165	0.067	-0.101	0.208
Chlorocebus	0.040	0.004	-0.341	0.021	-0.116	0.242	0.023	-0.224	-0.097	0.064	-0.228	-0.100	0.058	-0.167	0.214	0.061	-0.088	0.210
Colobus	0.034	0.001	-0.337	0.014	-0.123	0.212	0.028	-0.230	-0.048	0.062	-0.218	-0.091	0.073	-0.154	0.183	0.073	-0.109	0.202
Daubentonia	0.031	-0.038	-0.347	-0.012	-0.112	0.190	0.028	-0.230	-0.058	0.081	-0.210	-0.189	0.066	-0.106	0.209	0.069	-0.135	0.173
Erythrocebus	0.035	0.014	-0.339	0.013	-0.137	0.229	0.039	-0.237	-0.060	0.066	-0.219	-0.127	0.067	-0.205	0.182	0.053	-0.088	0.213
Eulemur	0.044	-0.024	-0.327	-0.007	-0.118	0.193	0.034	-0.198	-0.082	0.071	-0.160	-0.173	0.065	-0.121	0.203	0.062	-0.133	0.179
Galago	0.017	-0.045	-0.311	0.006	-0.134	0.196	0.039	-0.210	-0.042	0.057	-0.192	-0.125	0.061	-0.154	0.178	0.062	-0.145	0.196
Gorilla	0.037	-0.012	-0.282	0.007	-0.135	0.237	0.033	-0.256	-0.025	0.055	-0.209	-0.153	0.064	-0.223	0.149	0.080	-0.064	0.220
Hapalemur	0.037	-0.030	-0.319	0.004	-0.107	0.215	0.040	-0.198	-0.038	0.073	-0.178	-0.138	0.059	-0.191	0.076	0.062	-0.122	0.199
Homo	0.016	0.018	-0.316	0.039	-0.115	0.262	0.029	-0.300	-0.085	0.063	-0.237	-0.196	0.069	-0.207	0.196	0.067	-0.055	0.224
Hylobates	0.034	0.010	-0.325	0.012	-0.127	0.226	0.044	-0.220	-0.082	0.075	-0.232	-0.030	0.080	-0.192	0.172	0.074	-0.119	0.208
Indri	0.055	-0.035	-0.307	-0.038	-0.112	0.164	0.043	-0.183	-0.060	0.074	-0.155	-0.141	0.068	-0.139	0.112	0.066	-0.132	0.140

Lagothrix	0.034	0.014	-0.341	0.033	-0.145	0.221	0.017	-0.244	-0.036	0.076	-0.239	-0.028	0.058	-0.186	0.196	0.055	-0.091	0.217
Lemur	0.047	-0.048	-0.316	-0.014	-0.112	0.197	0.059	-0.212	-0.055	0.079	-0.187	-0.138	0.076	-0.180	0.097	0.069	-0.134	0.165
Leontopithecus	0.031	-0.014	-0.318	0.023	-0.147	0.221	0.046	-0.188	-0.092	0.061	-0.182	-0.117	0.061	-0.173	0.206	0.060	-0.109	0.219
Lepilemur	0.036	-0.040	-0.308	-0.020	-0.123	0.156	0.046	-0.188	-0.072	0.072	-0.175	-0.102	0.065	-0.146	0.149	0.069	-0.152	0.120
Lophocebus	0.037	-0.004	-0.326	0.015	-0.152	0.230	0.038	-0.244	-0.063	0.067	-0.216	-0.109	0.068	-0.207	0.178	0.064	-0.066	0.236
Loris	0.025	-0.049	-0.281	0.006	-0.126	0.220	0.040	-0.222	-0.037	0.067	-0.196	-0.126	0.077	-0.191	0.137	0.077	-0.112	0.218
Macaca	0.044	0.006	-0.361	0.013	-0.122	0.206	0.020	-0.255	-0.027	0.064	-0.225	-0.105	0.060	-0.203	0.170	0.062	-0.095	0.215
Mandrillus	0.049	-0.002	-0.300	0.024	-0.176	0.243	0.040	-0.231	-0.083	0.073	-0.221	-0.101	0.102	-0.227	0.168	0.065	-0.067	0.208
Mico	0.024	0.005	-0.329	0.019	-0.146	0.216	0.030	-0.208	-0.061	0.056	-0.202	-0.088	0.057	-0.151	0.207	0.060	-0.108	0.218
Microcebus	0.016	-0.055	-0.298	-0.022	-0.133	0.179	0.044	-0.202	0.010	0.071	-0.160	-0.157	0.067	-0.150	0.190	0.076	-0.158	0.151
Miopithecus	0.029	0.003	-0.328	0.026	-0.130	0.263	0.032	-0.252	-0.040	0.057	-0.210	-0.144	0.073	-0.212	0.201	0.074	-0.070	0.219
Mirza	0.027	-0.050	-0.315	-0.012	-0.119	0.186	0.051	-0.209	-0.033	0.076	-0.201	-0.075	0.080	-0.166	0.148	0.080	-0.148	0.169
Nasalis	0.037	0.003	-0.327	-0.005	-0.124	0.237	0.038	-0.217	-0.066	0.068	-0.193	-0.130	0.072	-0.158	0.207	0.068	-0.114	0.229
Nycticebus	0.036	-0.047	-0.305	-0.006	-0.108	0.205	0.035	-0.220	-0.021	0.068	-0.192	-0.110	0.074	-0.159	0.131	0.074	-0.133	0.176
Pan	0.039	0.010	-0.317	0.022	-0.115	0.235	0.034	-0.256	-0.039	0.067	-0.227	-0.143	0.076	-0.192	0.162	0.075	-0.089	0.220
Papio	0.036	0.010	-0.313	0.024	-0.130	0.226	0.027	-0.244	-0.025	0.068	-0.222	-0.107	0.067	-0.215	0.153	0.067	-0.086	0.220
Piliocolobus	0.035	-0.002	-0.334	0.012	-0.131	0.223	0.034	-0.217	-0.050	0.068	-0.198	-0.126	0.076	-0.172	0.187	0.070	-0.098	0.217
Pithecia	0.031	0.001	-0.319	0.014	-0.135	0.208	0.036	-0.230	-0.041	0.062	-0.229	-0.049	0.058	-0.158	0.184	0.059	-0.117	0.201
Presbytis	0.036	0.021	-0.331	0.008	-0.140	0.217	0.029	-0.240	-0.048	0.061	-0.228	-0.080	0.067	-0.178	0.181	0.064	-0.103	0.220
Procolobus	0.040	0.022	-0.334	0.021	-0.143	0.224	0.032	-0.247	0.000	0.063	-0.216	-0.113	0.071	-0.177	0.188	0.070	-0.112	0.204
Saguinus	0.022	0.007	-0.319	0.021	-0.141	0.225	0.038	-0.193	-0.099	0.062	-0.195	-0.085	0.061	-0.147	0.217	0.062	-0.116	0.219
Saimiri	0.023	0.029	-0.321	0.026	-0.145	0.274	0.032	-0.249	-0.075	0.066	-0.247	-0.096	0.069	-0.166	0.269	0.063	-0.077	0.247
Semnopithecus	0.040	0.006	-0.332	0.010	-0.141	0.214	0.040	-0.234	-0.071	0.065	-0.232	-0.079	0.064	-0.179	0.166	0.062	-0.102	0.209
Simias	0.036	0.005	-0.336	0.001	-0.127	0.215	0.030	-0.221	-0.030	0.067	-0.211	-0.062	0.065	-0.169	0.171	0.064	-0.109	0.203
Tarsius	0.026	-0.014	-0.280	-0.011	-0.124	0.206	0.025	-0.208	-0.048	0.055	-0.194	-0.093	0.073	-0.161	0.153	0.078	-0.146	0.166
Theropithecus	0.030	0.016	-0.343	0.015	-0.122	0.210	0.033	-0.232	-0.014	0.063	-0.208	-0.081	0.068	-0.179	0.173	0.069	-0.106	0.216
Trachypithecus	0.037	0.019	-0.330	0.012	-0.135	0.222	0.031	-0.260	-0.017	0.061	-0.235	-0.101	0.066	-0.178	0.186	0.063	-0.102	0.211
Varecia	0.022	-0.036	-0.311	-0.029	-0.116	0.167	0.038	-0.196	-0.064	0.076	-0.159	-0.162	0.067	-0.095	0.233	0.077	-0.158	0.125

D.1: continued…

	endopisthion			endobasion			sella			posterior cribriform			anterior cribriform			optic canal		
Species	X 7	Y 7	Z 7	X 8	Y 8	Z 8	X 9	Y 9	Z 9	X 10	Y 10	Z 10	X 11	Y 11	Z 11	X 12	Y 12	Z 12
Alouatta	0.065	0.003	0.215	0.057	0.099	0.147	0.057	0.099	-0.032	0.046	0.073	-0.301	0.041	0.055	-0.348	0.029	0.088	-0.126
Aotus	0.068	0.018	0.200	0.071	0.110	0.133	0.064	0.108	-0.044	0.055	0.062	-0.277	0.041	0.059	-0.329	0.041	0.078	-0.102
Ateles	0.066	0.029	0.192	0.064	0.105	0.113	0.057	0.098	-0.063	0.041	0.093	-0.263	0.032	0.096	-0.307	0.032	0.077	-0.118
Brachyteles	0.082	0.006	0.202	0.073	0.100	0.107	0.067	0.105	-0.036	0.043	0.083	-0.259	0.031	0.067	-0.301	0.027	0.085	-0.130
Cacajao	0.062	0.019	0.193	0.057	0.103	0.111	0.054	0.102	-0.067	0.043	0.094	-0.269	0.039	0.082	-0.295	0.030	0.079	-0.109
Callicebus	0.062	0.025	0.202	0.062	0.107	0.146	0.060	0.105	-0.061	0.050	0.066	-0.298	0.047	0.063	-0.319	0.032	0.066	-0.118
Callimico	0.059	0.008	0.193	0.062	0.097	0.112	0.060	0.085	-0.045	0.043	0.088	-0.309	0.034	0.096	-0.330	0.034	0.062	-0.114
Callithrix	0.060	0.027	0.205	0.058	0.117	0.128	0.054	0.096	-0.041	0.044	0.075	-0.299	0.034	0.077	-0.333	0.033	0.060	-0.126
Cebuella	0.050	0.009	0.211	0.051	0.102	0.124	0.052	0.075	-0.033	0.042	0.075	-0.304	0.031	0.079	-0.338	0.040	0.047	-0.132
Cebus	0.069	0.015	0.196	0.063	0.092	0.111	0.058	0.088	-0.058	0.044	0.083	-0.278	0.036	0.085	-0.309	0.032	0.065	-0.115
Cercocebus	0.061	0.077	0.197	0.056	0.119	0.099	0.053	0.083	-0.059	0.042	0.081	-0.278	0.038	0.081	-0.298	0.036	0.056	-0.100
Cercopithecus	0.062	0.024	0.199	0.057	0.107	0.127	0.056	0.098	-0.043	0.045	0.068	-0.295	0.041	0.071	-0.324	0.034	0.055	-0.105
Chlorocebus	0.059	0.023	0.201	0.065	0.104	0.123	0.062	0.090	-0.054	0.054	0.090	-0.293	0.051	0.099	-0.312	0.042	0.043	-0.103
Colobus	0.066	0.009	0.207	0.066	0.111	0.136	0.057	0.100	-0.042	0.044	0.067	-0.294	0.042	0.052	-0.325	0.031	0.068	-0.126
Daubentonia	0.066	0.026	0.226	0.070	0.140	0.141	0.066	0.086	-0.049	0.033	0.084	-0.221	-0.001	0.036	-0.341	0.016	0.073	-0.138
Erythrocebus	0.057	0.051	0.197	0.050	0.121	0.123	0.046	0.084	-0.042	0.044	0.074	-0.296	0.041	0.078	-0.323	0.036	0.036	-0.099
Eulemur	0.060	0.030	0.245	0.055	0.119	0.162	0.055	0.101	-0.066	0.037	0.059	-0.258	0.040	0.013	-0.353	0.019	0.062	-0.135
Galago	0.060	0.041	0.234	0.063	0.127	0.116	0.060	0.114	-0.038	0.047	0.069	-0.265	0.041	0.051	-0.372	0.033	0.084	-0.119
Gorilla	0.083	0.017	0.219	0.081	0.139	0.133	0.057	0.086	-0.071	0.043	0.115	-0.247	0.045	0.101	-0.298	0.014	0.046	-0.126
Hapalemur	0.055	0.066	0.225	0.056	0.131	0.135	0.061	0.108	-0.054	0.046	0.062	-0.257	0.026	0.024	-0.357	0.033	0.081	-0.143
Homo	0.069	0.080	0.175	0.063	0.121	0.066	0.065	0.068	-0.072	0.057	0.108	-0.178	0.059	0.114	-0.213	0.020	0.056	-0.122
Hylobates	0.078	0.014	0.208	0.071	0.108	0.116	0.062	0.092	-0.053	0.037	0.079	-0.270	0.036	0.064	-0.326	0.018	0.065	-0.120
Indri	0.060	0.030	0.261	0.051	0.129	0.201	0.065	0.095	-0.062	0.052	0.057	-0.277	0.034	0.000	-0.350	0.017	0.065	-0.167
Lagothrix	0.060	0.021	0.208	0.061	0.093	0.121	0.052	0.096	-0.062	0.045	0.098	-0.259	0.033	0.092	-0.306	0.027	0.088	-0.128
Lemur	0.063	0.012	0.254	0.059	0.140	0.159	0.063	0.113	-0.063	0.046	0.060	-0.256	0.045	0.003	-0.338	0.018	0.071	-0.133
Leontopithecus	0.056	0.016	0.203	0.047	0.099	0.149	0.051	0.092	-0.026	0.045	0.049	-0.282	0.039	0.037	-0.331	0.027	0.060	-0.150

Lepilemur	0.059	0.024	0.258	0.049	0.147	0.178	0.061	0.116	-0.050	0.044	0.046	-0.276	0.029	0.007	-0.346	0.024	0.073	-0.156
Lophocebus	0.059	0.047	0.192	0.053	0.106	0.091	0.049	0.097	-0.045	0.048	0.068	-0.299	0.043	0.077	-0.314	0.037	0.049	-0.115
Loris	0.074	0.032	0.229	0.060	0.110	0.152	0.050	0.104	-0.034	0.041	0.104	-0.239	0.043	0.066	-0.353	0.028	0.082	-0.132
Macaca	0.057	0.030	0.179	0.058	0.125	0.130	0.057	0.104	-0.056	0.057	0.063	-0.250	0.047	0.092	-0.326	0.035	0.037	-0.082
Mandrillus	0.060	0.015	0.198	0.055	0.116	0.149	0.047	0.077	-0.064	0.048	0.077	-0.277	0.037	0.078	-0.309	0.029	0.037	-0.116
Mico	0.055	0.027	0.208	0.043	0.120	0.149	0.047	0.093	-0.024	0.043	0.062	-0.310	0.028	0.083	-0.349	0.030	0.064	-0.123
Microcebus	0.056	0.041	0.250	0.056	0.126	0.145	0.053	0.106	-0.058	0.031	0.068	-0.252	0.027	0.043	-0.354	0.019	0.083	-0.149
Miopithecus	0.068	0.013	0.195	0.061	0.100	0.093	0.062	0.096	-0.042	0.042	0.087	-0.281	0.039	0.094	-0.298	0.042	0.058	-0.104
Mirza	0.072	-0.006	0.239	0.057	0.127	0.157	0.059	0.106	-0.051	0.035	0.073	-0.259	0.026	0.049	-0.373	0.027	0.086	-0.132
Nasalis	0.071	0.022	0.208	0.065	0.105	0.109	0.060	0.073	-0.053	0.041	0.084	-0.287	0.037	0.080	-0.323	0.035	0.047	-0.112
Nycticebus	0.066	0.004	0.232	0.048	0.120	0.173	0.054	0.107	-0.054	0.041	0.083	-0.254	0.028	0.033	-0.363	0.018	0.087	-0.160
Pan	0.074	0.032	0.205	0.068	0.111	0.109	0.059	0.071	-0.069	0.046	0.100	-0.226	0.044	0.095	-0.284	0.022	0.053	-0.139
Papio	0.066	0.041	0.204	0.056	0.126	0.120	0.052	0.097	-0.065	0.045	0.082	-0.284	0.041	0.076	-0.291	0.032	0.039	-0.126
Piliocolobus	0.064	0.014	0.222	0.056	0.109	0.130	0.053	0.078	-0.069	0.044	0.066	-0.280	0.040	0.056	-0.327	0.034	0.054	-0.124
Pithecia	0.064	0.019	0.194	0.064	0.109	0.145	0.058	0.115	-0.054	0.046	0.059	-0.295	0.038	0.062	-0.335	0.035	0.085	-0.126
Presbytis	0.063	0.034	0.203	0.061	0.115	0.104	0.059	0.089	-0.050	0.053	0.081	-0.292	0.048	0.077	-0.318	0.033	0.059	-0.113
Procolobus	0.064	0.024	0.195	0.056	0.102	0.105	0.055	0.098	-0.051	0.047	0.079	-0.283	0.045	0.073	-0.325	0.038	0.064	-0.117
Saguinus	0.057	0.023	0.211	0.053	0.104	0.084	0.052	0.100	0.020	0.048	0.059	-0.297	0.038	0.070	-0.340	0.031	0.059	-0.136
Saimiri	0.055	0.024	0.161	0.055	0.091	0.022	0.051	0.090	0.016	0.049	0.097	-0.281	0.041	0.100	-0.297	0.032	0.068	-0.102
Semnopithecus	0.066	0.034	0.201	0.061	0.126	0.103	0.060	0.093	-0.047	0.049	0.071	-0.288	0.047	0.069	-0.329	0.038	0.048	-0.107
Simias	0.070	0.012	0.203	0.060	0.118	0.114	0.058	0.100	-0.070	0.048	0.073	-0.306	0.046	0.081	-0.330	0.037	0.055	-0.128
Tarsius	0.095	0.045	0.240	0.092	0.140	0.130	0.080	0.106	-0.059	0.059	0.070	-0.248	0.062	0.066	-0.343	0.042	0.080	-0.115
Theropithecus	0.065	0.010	0.204	0.050	0.128	0.116	0.053	0.092	-0.063	0.040	0.093	-0.298	0.040	0.073	-0.310	0.028	0.038	-0.172
Trachypithecus	0.062	0.021	0.194	0.060	0.120	0.110	0.055	0.095	-0.048	0.047	0.083	-0.289	0.043	0.084	-0.316	0.034	0.063	-0.111
Varecia	0.065	0.014	0.244	0.060	0.126	0.183	0.055	0.107	-0.059	0.045	0.053	-0.263	0.050	-0.006	-0.352	0.018	0.074	-0.141

D.1: continued…

Species	anterior clinoid process			petrous apex			max. curve of tranverse and petrous lines			foramen ovale			internal acoustic meatus			jugular foramen		
	X 13	Y 13	Z 13	X 14	Y 14	Z 14	X 15	Y 15	Z 15	X 16	Y 16	Z 16	X 17	Y 17	Z 17	X 18	Y 18	Z 18
Alouatta	0.018	0.082	-0.086	0.014	0.072	-0.012	-0.078	-0.013	0.089	-0.036	0.107	-0.025	-0.031	0.049	0.084	-0.036	0.053	0.141
Aotus	0.020	0.080	-0.087	0.022	0.083	-0.010	-0.055	-0.036	0.078	-0.051	0.111	-0.014	-0.043	0.053	0.068	-0.039	0.044	0.132
Ateles	0.016	0.074	-0.087	0.005	0.059	-0.028	-0.040	-0.020	0.070	-0.027	0.098	-0.034	-0.037	0.062	0.070	-0.036	0.073	0.118
Brachyteles	0.018	0.077	-0.086	0.025	0.086	-0.008	-0.068	-0.014	0.078	-0.036	0.099	-0.019	-0.041	0.056	0.076	-0.027	0.085	0.119
Cacajao	0.019	0.078	-0.090	0.011	0.067	-0.019	-0.075	-0.012	0.069	-0.027	0.111	-0.028	-0.032	0.055	0.076	-0.021	0.067	0.113
Callicebus	0.027	0.075	-0.086	0.005	0.070	-0.031	-0.053	-0.025	0.088	-0.045	0.110	-0.027	-0.046	0.049	0.090	-0.020	0.062	0.122
Callimico	0.022	0.061	-0.098	0.020	0.062	-0.010	-0.056	-0.034	0.064	-0.036	0.103	-0.020	-0.038	0.041	0.084	-0.018	0.057	0.117
Callithrix	0.015	0.060	-0.111	0.022	0.067	-0.016	-0.061	-0.018	0.075	-0.035	0.113	-0.009	-0.030	0.061	0.088	-0.020	0.063	0.129
Cebuella	0.016	0.050	-0.117	0.026	0.061	-0.006	-0.041	-0.036	0.081	-0.033	0.110	-0.026	-0.027	0.057	0.086	-0.022	0.061	0.122
Cebus	0.016	0.068	-0.095	0.015	0.054	-0.014	-0.085	-0.013	0.086	-0.034	0.107	-0.005	-0.041	0.045	0.077	-0.018	0.056	0.105
Cercocebus	0.012	0.055	-0.077	-0.002	0.065	0.020	-0.077	0.009	0.062	-0.032	0.152	0.015	-0.038	0.047	0.058	-0.031	0.114	0.105
Cercopithecus	0.027	0.066	-0.074	0.009	0.083	0.015	-0.068	-0.002	0.071	-0.042	0.110	-0.004	-0.039	0.052	0.087	-0.021	0.062	0.126
Chlorocebus	0.016	0.051	-0.096	0.018	0.086	0.003	-0.059	-0.014	0.072	-0.051	0.097	0.001	-0.039	0.046	0.084	-0.017	0.056	0.108
Colobus	0.018	0.069	-0.091	0.007	0.081	0.014	-0.076	-0.009	0.083	-0.038	0.107	0.005	-0.036	0.057	0.081	-0.032	0.066	0.143
Daubentonia	0.037	0.059	-0.079	0.008	0.074	-0.005	-0.099	-0.036	0.119	-0.022	0.085	0.005	-0.022	0.063	0.089	-0.026	0.091	0.159
Erythrocebus	0.022	0.045	-0.072	0.026	0.070	-0.015	-0.063	0.005	0.065	-0.032	0.110	0.001	-0.037	0.060	0.091	-0.018	0.073	0.113
Eulemur	0.002	0.063	-0.106	0.002	0.079	-0.001	-0.079	-0.002	0.098	-0.030	0.073	0.007	-0.031	0.053	0.103	-0.026	0.052	0.151
Galago	0.025	0.096	-0.088	0.017	0.096	-0.020	-0.074	-0.023	0.094	-0.036	0.109	-0.015	-0.031	0.063	0.073	-0.030	0.067	0.137
Gorilla	-0.007	0.051	-0.123	0.022	0.073	-0.026	-0.109	-0.026	0.122	-0.056	0.107	-0.058	-0.035	0.062	0.067	-0.022	0.086	0.120
Hapalemur	0.008	0.076	-0.120	0.008	0.087	-0.026	-0.104	-0.056	0.131	-0.022	0.060	0.008	-0.037	0.059	0.115	-0.040	0.057	0.165
Homo	0.018	0.040	-0.081	0.031	0.059	-0.032	-0.131	-0.032	0.135	-0.030	0.109	-0.027	-0.029	0.053	0.048	-0.020	0.069	0.082
Hylobates	0.020	0.064	-0.088	0.024	0.079	-0.007	-0.081	-0.003	0.076	-0.038	0.118	-0.015	-0.028	0.078	0.065	-0.016	0.092	0.107
Indri	-0.004	0.063	-0.141	0.000	0.077	0.005	-0.088	-0.041	0.153	-0.041	0.086	0.000	-0.036	0.050	0.103	-0.016	0.072	0.173
Lagothrix	0.004	0.083	-0.104	0.008	0.056	-0.025	-0.054	-0.029	0.092	-0.031	0.101	-0.031	-0.023	0.059	0.075	-0.016	0.063	0.105
Lemur	-0.006	0.073	-0.113	-0.005	0.092	-0.024	-0.081	-0.017	0.123	-0.048	0.076	0.005	-0.046	0.062	0.111	-0.028	0.079	0.146

Leontopithecus	0.008	0.063	-0.127	0.022	0.088	0.001	-0.062	-0.013	0.084	-0.052	0.111	0.010	-0.043	0.073	0.105	-0.028	0.063	0.135
Lepilemur	0.008	0.074	-0.135	0.014	0.090	-0.016	-0.081	-0.049	0.141	-0.037	0.088	0.002	-0.045	0.060	0.098	-0.043	0.085	0.161
Lophocebus	0.009	0.040	-0.102	0.004	0.083	-0.025	-0.062	0.010	0.096	-0.043	0.138	0.028	-0.038	0.031	0.062	-0.045	0.073	0.141
Loris	-0.014	0.081	-0.137	0.027	0.059	-0.027	-0.086	-0.025	0.097	-0.031	0.102	-0.051	-0.030	0.054	0.076	-0.019	0.072	0.113
Macaca	0.009	0.045	-0.078	0.001	0.116	-0.048	-0.059	-0.006	0.081	-0.046	0.097	0.035	-0.031	0.052	0.104	-0.019	0.080	0.115
Mandrillus	0.014	0.042	-0.083	-0.002	0.062	-0.036	-0.041	0.011	0.059	-0.064	0.115	0.006	-0.053	0.072	0.088	-0.031	0.058	0.115
Mico	0.009	0.053	-0.117	0.009	0.073	0.006	-0.046	-0.012	0.063	-0.028	0.104	-0.008	-0.037	0.053	0.085	-0.026	0.040	0.161
Microcebus	0.023	0.093	-0.101	0.013	0.074	-0.022	-0.092	-0.038	0.139	-0.033	0.096	-0.046	-0.024	0.060	0.107	-0.005	0.082	0.129
Miopithecus	0.039	0.069	-0.082	0.014	0.076	0.007	-0.065	-0.006	0.065	-0.025	0.107	-0.014	-0.029	0.058	0.061	-0.041	0.065	0.112
Mirza	0.006	0.086	-0.108	0.015	0.083	-0.028	-0.080	-0.024	0.117	-0.054	0.090	-0.017	-0.029	0.062	0.096	-0.026	0.076	0.137
Nasalis	0.023	0.055	-0.094	0.014	0.059	-0.002	-0.069	-0.009	0.073	-0.055	0.095	-0.003	-0.042	0.037	0.075	-0.025	0.071	0.109
Nycticebus	0.019	0.093	-0.117	0.012	0.081	-0.004	-0.089	-0.027	0.108	-0.054	0.091	-0.019	-0.039	0.060	0.094	-0.027	0.061	0.145
Pan	0.012	0.047	-0.103	0.021	0.078	-0.027	-0.123	-0.021	0.120	-0.038	0.114	-0.040	-0.031	0.059	0.063	-0.023	0.078	0.117
Papio	0.019	0.044	-0.094	0.006	0.076	-0.004	-0.065	-0.012	0.086	-0.050	0.101	0.003	-0.042	0.055	0.079	-0.018	0.069	0.118
Piliocolobus	0.015	0.053	-0.091	0.017	0.091	-0.025	-0.069	-0.004	0.088	-0.041	0.106	0.002	-0.041	0.042	0.095	-0.028	0.068	0.133
Pithecia	0.017	0.091	-0.100	0.009	0.096	-0.021	-0.059	-0.042	0.084	-0.044	0.106	-0.004	-0.045	0.056	0.102	-0.018	0.067	0.120
Presbytis	0.018	0.066	-0.088	0.004	0.088	-0.013	-0.072	-0.006	0.078	-0.037	0.099	0.001	-0.034	0.060	0.075	-0.017	0.074	0.114
Procolobus	0.019	0.066	-0.090	0.014	0.078	-0.006	-0.079	0.004	0.068	-0.041	0.107	0.002	-0.037	0.056	0.072	-0.036	0.062	0.119
Saguinus	0.020	0.062	-0.114	0.017	0.060	-0.007	-0.061	-0.010	0.075	-0.035	0.107	-0.007	-0.036	0.050	0.084	-0.022	0.057	0.138
Saimiri	0.017	0.070	-0.082	0.015	0.051	-0.028	-0.070	-0.010	0.045	-0.033	0.106	-0.017	-0.025	0.043	0.046	-0.024	0.038	0.109
Semnopithecus	0.024	0.063	-0.076	0.014	0.095	0.002	-0.083	-0.009	0.082	-0.041	0.110	0.001	-0.039	0.057	0.071	-0.031	0.072	0.124
Simias	0.024	0.066	-0.099	0.004	0.080	-0.005	-0.071	-0.009	0.081	-0.037	0.106	-0.002	-0.044	0.046	0.085	-0.028	0.064	0.135
Tarsius	0.015	0.067	-0.104	0.050	0.064	-0.019	-0.042	-0.027	0.069	-0.083	0.117	-0.006	-0.013	0.050	0.085	-0.116	0.051	0.105
Theropithecus	0.018	0.024	-0.100	0.002	0.095	0.021	-0.073	0.011	0.055	-0.036	0.097	0.025	-0.032	0.059	0.081	-0.025	0.053	0.156
Trachypithecus	0.017	0.071	-0.083	0.007	0.078	-0.003	-0.071	0.003	0.073	-0.038	0.109	-0.015	-0.035	0.059	0.070	-0.026	0.077	0.116
Varecia	0.009	0.079	-0.114	0.010	0.080	-0.032	-0.078	-0.003	0.103	-0.036	0.062	0.041	-0.033	0.059	0.109	-0.029	0.062	0.176

D.1: continued…

Species	maximum cerebral breadth			maximum cerebellar breadth			posterior cerebellum			temporal pole			sylvian fissure		
	X 19	Y 19	Z 19	X 20	Y 20	Z 20	X 21	Y 21	Z 21	X 22	Y 22	Z 22	X 23	Y 23	Z 23
Alouatta	-0.153	-0.022	0.033	-0.095	-0.019	0.166	-0.002	-0.059	0.217	-0.075	0.099	-0.159	-0.097	0.051	-0.169
Aotus	-0.170	-0.026	0.023	-0.105	-0.017	0.151	-0.035	-0.029	0.184	-0.033	0.123	-0.087	-0.133	0.011	-0.156
Ateles	-0.155	-0.056	0.004	-0.108	-0.019	0.168	-0.017	-0.060	0.220	-0.052	0.115	-0.126	-0.099	0.046	-0.158
Brachyteles	-0.178	-0.064	-0.004	-0.112	-0.005	0.157	-0.009	-0.070	0.225	-0.063	0.094	-0.138	-0.090	0.058	-0.150
Cacajao	-0.168	-0.063	0.041	-0.110	0.001	0.155	-0.019	-0.042	0.206	-0.050	0.118	-0.113	-0.098	0.058	-0.156
Callicebus	-0.167	-0.031	0.026	-0.084	-0.027	0.177	-0.020	-0.043	0.199	-0.057	0.121	-0.109	-0.120	0.029	-0.164
Callimico	-0.159	-0.023	0.029	-0.096	-0.027	0.170	-0.039	-0.045	0.200	-0.031	0.119	-0.094	-0.112	0.012	-0.173
Callithrix	-0.155	-0.029	0.042	-0.102	-0.021	0.162	-0.040	-0.054	0.199	-0.036	0.117	-0.114	-0.105	0.027	-0.165
Cebuella	-0.158	-0.028	0.043	-0.098	-0.029	0.185	-0.036	-0.053	0.211	-0.023	0.113	-0.120	-0.107	0.026	-0.174
Cebus	-0.168	-0.035	-0.018	-0.111	-0.024	0.164	-0.020	-0.039	0.204	-0.058	0.134	-0.128	-0.099	0.063	-0.137
Cercocebus	-0.169	-0.061	0.016	-0.110	-0.012	0.150	-0.010	-0.041	0.205	-0.035	0.118	-0.108	-0.099	0.056	-0.129
Cercopithecus	-0.172	-0.036	0.005	-0.102	0.001	0.166	-0.015	-0.033	0.204	-0.063	0.127	-0.116	-0.111	0.025	-0.147
Chlorocebus	-0.183	-0.046	0.023	-0.090	-0.007	0.165	-0.014	-0.026	0.197	-0.059	0.125	-0.120	-0.120	0.002	-0.126
Colobus	-0.160	-0.047	-0.017	-0.101	-0.013	0.170	-0.011	-0.050	0.208	-0.062	0.120	-0.116	-0.097	0.045	-0.155
Daubentonia	-0.143	-0.064	-0.020	-0.117	-0.016	0.157	-0.034	-0.031	0.218	-0.029	0.109	-0.099	-0.065	0.052	-0.142
Erythrocebus	-0.170	-0.054	0.019	-0.102	-0.009	0.163	-0.014	-0.023	0.204	-0.054	0.145	-0.096	-0.106	0.006	-0.129
Eulemur	-0.150	0.003	0.021	-0.107	-0.023	0.169	-0.001	-0.058	0.239	-0.040	0.108	-0.120	-0.077	0.023	-0.148
Galago	-0.174	-0.036	0.002	-0.083	-0.030	0.170	-0.030	-0.066	0.221	-0.031	0.129	-0.085	-0.097	-0.012	-0.139
Gorilla	-0.149	-0.061	-0.006	-0.118	0.011	0.151	-0.011	-0.024	0.232	-0.046	0.087	-0.111	-0.067	0.030	-0.125
Hapalemur	-0.146	-0.002	0.031	-0.117	-0.020	0.176	-0.018	-0.046	0.240	-0.028	0.097	-0.126	-0.057	0.043	-0.138
Homo	-0.181	-0.053	0.030	-0.143	0.010	0.122	0.009	-0.019	0.244	-0.038	0.101	-0.119	-0.101	0.012	-0.141
Hylobates	-0.164	-0.046	0.022	-0.147	-0.021	0.138	-0.024	-0.060	0.228	-0.064	0.114	-0.115	-0.105	0.043	-0.135
Indri	-0.143	0.004	0.034	-0.094	-0.027	0.188	-0.012	-0.036	0.248	-0.046	0.093	-0.136	-0.067	0.039	-0.142
Lagothrix	-0.149	-0.045	0.037	-0.094	-0.011	0.145	-0.028	-0.052	0.211	-0.063	0.126	-0.142	-0.105	0.051	-0.163
Lemur	-0.160	0.027	0.014	-0.106	-0.023	0.170	-0.007	-0.039	0.247	-0.052	0.113	-0.113	-0.069	0.031	-0.138

Leontopithecus	-0.143	-0.034	0.068	-0.095	-0.026	0.169	-0.030	-0.038	0.195	-0.039	0.114	-0.151	-0.084	0.059	-0.171
Lepilemur	-0.145	-0.004	0.040	-0.087	-0.027	0.196	-0.029	-0.052	0.236	-0.023	0.109	-0.117	-0.067	0.037	-0.158
Lophocebus	-0.158	-0.045	0.033	-0.093	-0.029	0.162	-0.023	-0.039	0.185	-0.029	0.126	-0.102	-0.099	0.056	-0.137
Loris	-0.176	-0.030	0.024	-0.096	-0.024	0.190	-0.054	-0.031	0.226	-0.033	0.110	-0.129	-0.075	0.031	-0.136
Macaca	-0.162	-0.097	0.048	-0.100	-0.016	0.168	-0.008	-0.013	0.164	-0.048	0.131	-0.128	-0.109	0.054	-0.157
Mandrillus	-0.171	-0.002	-0.018	-0.093	0.021	0.182	-0.030	0.001	0.223	-0.051	0.104	-0.116	-0.108	0.038	-0.136
Mico	-0.144	-0.020	0.010	-0.079	-0.014	0.165	-0.025	-0.044	0.204	-0.025	0.109	-0.116	-0.102	0.018	-0.168
Microcebus	-0.159	-0.041	0.003	-0.103	-0.022	0.173	-0.030	-0.081	0.229	-0.018	0.122	-0.128	-0.066	0.042	-0.141
Miopithecus	-0.170	-0.061	0.033	-0.110	0.004	0.147	-0.042	-0.019	0.195	-0.062	0.117	-0.105	-0.111	0.011	-0.154
Mirza	-0.158	-0.023	0.008	-0.099	-0.007	0.168	-0.052	-0.050	0.216	-0.032	0.130	-0.113	-0.069	0.033	-0.137
Nasalis	-0.166	-0.034	0.020	-0.112	-0.004	0.180	-0.004	-0.038	0.229	-0.057	0.113	-0.124	-0.092	0.046	-0.152
Nycticebus	-0.162	-0.027	0.013	-0.085	-0.021	0.185	-0.020	-0.048	0.222	-0.032	0.109	-0.131	-0.058	0.052	-0.148
Pan	-0.161	-0.048	0.026	-0.136	0.005	0.157	-0.009	-0.040	0.235	-0.056	0.099	-0.115	-0.083	0.035	-0.145
Papio	-0.175	-0.055	0.000	-0.094	-0.012	0.167	-0.017	-0.031	0.213	-0.047	0.132	-0.116	-0.098	0.059	-0.164
Piliocolobus	-0.161	-0.031	-0.004	-0.100	-0.025	0.182	-0.029	-0.036	0.209	-0.054	0.132	-0.111	-0.095	0.043	-0.147
Pithecia	-0.157	-0.042	0.034	-0.092	-0.035	0.162	-0.024	-0.059	0.194	-0.046	0.128	-0.116	-0.109	0.051	-0.168
Presbytis	-0.163	-0.054	0.013	-0.108	-0.011	0.165	0.002	-0.053	0.217	-0.070	0.115	-0.111	-0.106	0.035	-0.143
Procolobus	-0.158	-0.037	0.042	-0.108	-0.009	0.164	-0.012	-0.046	0.209	-0.065	0.118	-0.115	-0.096	0.034	-0.156
Saguinus	-0.149	-0.020	0.043	-0.095	-0.023	0.175	-0.036	-0.046	0.201	-0.039	0.111	-0.116	-0.107	0.023	-0.169
Saimiri	-0.162	-0.025	0.026	-0.092	-0.006	0.150	-0.013	-0.046	0.176	-0.058	0.120	-0.096	-0.116	0.043	-0.149
Semnopithecus	-0.169	-0.057	0.049	-0.113	-0.010	0.162	0.001	-0.048	0.203	-0.068	0.117	-0.119	-0.096	0.052	-0.141
Simias	-0.162	-0.042	0.026	-0.106	-0.040	0.182	-0.007	-0.048	0.210	-0.061	0.120	-0.112	-0.092	0.049	-0.147
Tarsius	-0.186	0.021	0.008	-0.079	-0.015	0.198	-0.021	-0.059	0.226	-0.107	0.108	-0.090	-0.094	-0.036	-0.180
Theropithecus	-0.166	-0.048	0.027	-0.101	-0.037	0.187	-0.027	-0.031	0.186	-0.044	0.121	-0.119	-0.070	0.052	-0.158
Trachypithecus	-0.161	-0.063	0.033	-0.109	-0.008	0.151	0.004	-0.055	0.205	-0.063	0.116	-0.109	-0.096	0.041	-0.150
Varecia	-0.159	-0.004	-0.015	-0.099	-0.029	0.172	0.002	-0.058	0.230	-0.055	0.103	-0.124	-0.076	0.041	-0.147

Appendix D.2: Procrustes aligned landmark data for extant primate midsagittal endocranial outline analyzed in Chapter 3

	opisthion		endocranial outline semi-landmark curve											
Genus	X 1	Y 1	X 2	Y 2	X 3	Y 3	X 4	Y 4	X 5	Y 5	X 6	Y 6	X 7	Y 7
Cercocebus	-0.170	-0.143	-0.177	-0.120	-0.191	-0.088	-0.195	-0.055	-0.193	-0.033	-0.196	-0.011	-0.196	0.015
Cercopithecus	-0.196	-0.127	-0.195	-0.105	-0.202	-0.075	-0.203	-0.045	-0.201	-0.026	-0.203	-0.007	-0.199	0.015
Chlorbocebus	-0.194	-0.128	-0.190	-0.105	-0.198	-0.077	-0.198	-0.047	-0.201	-0.027	-0.205	-0.007	-0.202	0.016
Colobus	-0.216	-0.127	-0.207	-0.105	-0.213	-0.078	-0.214	-0.051	-0.210	-0.033	-0.206	-0.014	-0.200	0.009
Erythrocebus	-0.174	-0.136	-0.178	-0.113	-0.188	-0.085	-0.186	-0.054	-0.189	-0.033	-0.195	-0.011	-0.194	0.013
Lophocebus	-0.189	-0.123	-0.193	-0.103	-0.201	-0.077	-0.200	-0.049	-0.204	-0.031	-0.206	-0.012	-0.200	0.010
Macaca	-0.189	-0.131	-0.194	-0.107	-0.201	-0.078	-0.198	-0.048	-0.195	-0.029	-0.201	-0.011	-0.195	0.009
Mandrillus	-0.191	-0.126	-0.180	-0.102	-0.183	-0.073	-0.182	-0.046	-0.191	-0.029	-0.195	-0.010	-0.189	0.013
Miopithecus	-0.164	-0.120	-0.173	-0.100	-0.186	-0.071	-0.196	-0.043	-0.204	-0.027	-0.208	-0.009	-0.204	0.012
Nasalis	-0.191	-0.114	-0.195	-0.093	-0.206	-0.068	-0.206	-0.041	-0.206	-0.024	-0.208	-0.008	-0.201	0.010
Papio	-0.186	-0.137	-0.182	-0.111	-0.188	-0.082	-0.188	-0.052	-0.193	-0.035	-0.195	-0.015	-0.194	0.009
Piliocolobus	-0.213	-0.119	-0.217	-0.096	-0.221	-0.069	-0.218	-0.042	-0.212	-0.026	-0.211	-0.008	-0.203	0.012
Presbytis	-0.188	-0.125	-0.191	-0.103	-0.202	-0.076	-0.207	-0.050	-0.203	-0.032	-0.199	-0.013	-0.195	0.010
Procolobus	-0.186	-0.124	-0.187	-0.103	-0.199	-0.076	-0.201	-0.048	-0.198	-0.029	-0.202	-0.010	-0.199	0.012
Semnopithecus	-0.192	-0.130	-0.192	-0.108	-0.201	-0.081	-0.202	-0.052	-0.197	-0.033	-0.197	-0.013	-0.193	0.009
Simias	-0.201	-0.117	-0.202	-0.095	-0.209	-0.067	-0.207	-0.039	-0.205	-0.022	-0.205	-0.004	-0.198	0.014
Theropithecus	-0.207	-0.127	-0.201	-0.104	-0.211	-0.077	-0.208	-0.049	-0.205	-0.030	-0.203	-0.010	-0.195	0.012
Trachypithecus	-0.183	-0.130	-0.184	-0.107	-0.196	-0.080	-0.196	-0.052	-0.192	-0.034	-0.196	-0.015	-0.194	0.006
Gorilla	-0.202	-0.136	-0.201	-0.109	-0.201	-0.079	-0.201	-0.050	-0.203	-0.032	-0.203	-0.013	-0.196	0.009
Homo	-0.137	-0.143	-0.149	-0.124	-0.172	-0.102	-0.181	-0.071	-0.195	-0.055	-0.208	-0.037	-0.211	-0.014
Hylobates	-0.198	-0.123	-0.198	-0.101	-0.207	-0.074	-0.203	-0.046	-0.199	-0.028	-0.202	-0.008	-0.199	0.013
Pan	-0.187	-0.135	-0.188	-0.111	-0.198	-0.083	-0.203	-0.055	-0.205	-0.037	-0.206	-0.019	-0.201	0.003
Alouatta	-0.215	-0.111	-0.213	-0.089	-0.219	-0.064	-0.216	-0.039	-0.211	-0.023	-0.207	-0.007	-0.198	0.012
Aotus	-0.189	-0.121	-0.185	-0.097	-0.189	-0.067	-0.191	-0.040	-0.199	-0.024	-0.203	-0.008	-0.198	0.012
Ateles	-0.174	-0.131	-0.178	-0.109	-0.189	-0.081	-0.193	-0.051	-0.198	-0.032	-0.202	-0.012	-0.200	0.010
Cacajao	-0.174	-0.133	-0.174	-0.111	-0.186	-0.084	-0.191	-0.054	-0.197	-0.036	-0.204	-0.017	-0.204	0.006
Callicebus	-0.194	-0.128	-0.184	-0.105	-0.191	-0.075	-0.199	-0.045	-0.198	-0.025	-0.202	-0.007	-0.202	0.013

Callimico	-0.187	-0.103	-0.194	-0.083	-0.204	-0.058	-0.213	-0.036	-0.213	-0.023	-0.210	-0.010	-0.204	0.008
Callithrix	-0.198	-0.122	-0.187	-0.100	-0.197	-0.074	-0.207	-0.049	-0.208	-0.032	-0.203	-0.014	-0.197	0.009
Cebuella	-0.184	-0.104	-0.189	-0.084	-0.204	-0.061	-0.212	-0.041	-0.207	-0.027	-0.205	-0.010	-0.200	0.011
Cebus	-0.188	-0.125	-0.191	-0.103	-0.203	-0.077	-0.208	-0.050	-0.211	-0.033	-0.211	-0.015	-0.204	0.006
Lagothrix	-0.176	-0.116	-0.186	-0.099	-0.197	-0.075	-0.199	-0.047	-0.204	-0.030	-0.208	-0.013	-0.203	0.006
Leontopithecus	-0.192	-0.114	-0.195	-0.093	-0.206	-0.066	-0.209	-0.038	-0.209	-0.019	-0.212	-0.001	-0.209	0.019
Mico	-0.198	-0.124	-0.191	-0.102	-0.199	-0.075	-0.206	-0.047	-0.205	-0.028	-0.203	-0.009	-0.200	0.014
Pithecia	-0.198	-0.129	-0.197	-0.106	-0.206	-0.078	-0.209	-0.050	-0.204	-0.031	-0.203	-0.012	-0.196	0.011
Saguinus	-0.190	-0.116	-0.188	-0.094	-0.199	-0.069	-0.207	-0.043	-0.205	-0.026	-0.204	-0.007	-0.201	0.014
Saimiri	-0.126	-0.111	-0.129	-0.088	-0.149	-0.063	-0.173	-0.043	-0.190	-0.035	-0.200	-0.020	-0.206	0.000
Tarsius	-0.217	-0.123	-0.214	-0.096	-0.214	-0.062	-0.216	-0.032	-0.213	-0.014	-0.205	0.004	-0.194	0.022
Daubentonia	-0.232	-0.108	-0.227	-0.085	-0.236	-0.059	-0.233	-0.035	-0.227	-0.021	-0.218	-0.011	-0.199	0.002
Eulemur	-0.224	-0.099	-0.220	-0.077	-0.225	-0.050	-0.226	-0.026	-0.221	-0.012	-0.215	0.002	-0.203	0.014
Hapalemur	-0.203	-0.110	-0.205	-0.089	-0.211	-0.060	-0.217	-0.033	-0.219	-0.017	-0.216	-0.001	-0.207	0.014
Indri	-0.245	-0.096	-0.232	-0.077	-0.234	-0.052	-0.229	-0.028	-0.222	-0.014	-0.210	-0.003	-0.200	0.015
Lemur	-0.223	-0.098	-0.217	-0.079	-0.220	-0.053	-0.222	-0.029	-0.218	-0.015	-0.216	-0.001	-0.205	0.011
Microcebus	-0.217	-0.106	-0.217	-0.084	-0.219	-0.056	-0.217	-0.029	-0.215	-0.013	-0.208	0.002	-0.198	0.021
Mirza	-0.230	-0.098	-0.227	-0.075	-0.227	-0.047	-0.223	-0.024	-0.218	-0.012	-0.209	-0.003	-0.191	0.004
Varecia	-0.232	-0.095	-0.220	-0.076	-0.222	-0.049	-0.223	-0.026	-0.215	-0.013	-0.208	0.001	-0.196	0.018
Galago	-0.202	-0.105	-0.200	-0.084	-0.204	-0.056	-0.205	-0.030	-0.206	-0.014	-0.206	0.002	-0.199	0.016
Loris	-0.221	-0.115	-0.218	-0.093	-0.223	-0.064	-0.222	-0.038	-0.216	-0.022	-0.208	-0.008	-0.197	0.009
Nycticebus	-0.237	-0.100	-0.231	-0.080	-0.231	-0.055	-0.227	-0.033	-0.223	-0.019	-0.216	-0.007	-0.203	0.006
Adapis	-0.233	-0.085	-0.224	-0.061	-0.231	-0.034	-0.228	-0.010	-0.222	0.002	-0.211	0.010	-0.196	0.025
Aegypto	-0.212	-0.104	-0.213	-0.084	-0.219	-0.059	-0.222	-0.036	-0.221	-0.021	-0.220	-0.008	-0.209	0.003
Homunculus	-0.191	-0.120	-0.193	-0.094	-0.203	-0.066	-0.206	-0.040	-0.205	-0.022	-0.206	-0.005	-0.197	0.013
Parapithecus	-0.187	-0.096	-0.197	-0.079	-0.207	-0.054	-0.214	-0.030	-0.212	-0.014	-0.211	0.002	-0.207	0.021

Appendix D.2: continued…

Genus	X 8	Y 8	X 9	Y 9	X 10	Y 10	X 11	Y 11	X 12	Y 12	X 13	Y 13	X 14	Y 14	X 15	Y 15
Cercocebus	-0.187	0.036	-0.174	0.055	-0.158	0.070	-0.135	0.079	-0.110	0.088	-0.083	0.096	-0.055	0.102	-0.027	0.104
Cercopithecus	-0.187	0.033	-0.172	0.049	-0.153	0.061	-0.131	0.070	-0.105	0.075	-0.079	0.081	-0.050	0.084	-0.022	0.084
Chlorbocebus	-0.192	0.035	-0.175	0.048	-0.154	0.059	-0.132	0.069	-0.108	0.080	-0.081	0.082	-0.052	0.084	-0.023	0.085
Colobus	-0.188	0.029	-0.171	0.046	-0.150	0.058	-0.126	0.068	-0.099	0.077	-0.071	0.083	-0.042	0.085	-0.013	0.083
Erythrocebus	-0.187	0.035	-0.177	0.054	-0.158	0.066	-0.138	0.079	-0.115	0.089	-0.089	0.094	-0.060	0.097	-0.031	0.098
Lophocebus	-0.190	0.030	-0.174	0.045	-0.154	0.057	-0.131	0.068	-0.106	0.078	-0.077	0.083	-0.048	0.088	-0.019	0.090
Macaca	-0.182	0.029	-0.169	0.047	-0.151	0.063	-0.129	0.075	-0.105	0.084	-0.079	0.089	-0.052	0.094	-0.025	0.093
Mandrillus	-0.181	0.036	-0.169	0.054	-0.152	0.063	-0.130	0.071	-0.107	0.082	-0.084	0.088	-0.059	0.092	-0.033	0.091
Miopithecus	-0.197	0.031	-0.183	0.046	-0.164	0.058	-0.142	0.069	-0.115	0.075	-0.086	0.082	-0.057	0.088	-0.027	0.089
Nasalis	-0.188	0.025	-0.172	0.041	-0.154	0.055	-0.130	0.066	-0.106	0.076	-0.080	0.083	-0.052	0.086	-0.025	0.083
Papio	-0.185	0.032	-0.171	0.051	-0.153	0.067	-0.133	0.081	-0.108	0.090	-0.082	0.096	-0.054	0.099	-0.027	0.100
Piliocolobus	-0.188	0.026	-0.169	0.040	-0.149	0.055	-0.126	0.067	-0.101	0.074	-0.073	0.077	-0.043	0.075	-0.014	0.072
Presbytis	-0.185	0.031	-0.172	0.048	-0.153	0.061	-0.131	0.070	-0.106	0.079	-0.081	0.089	-0.054	0.094	-0.026	0.093
Procolobus	-0.190	0.032	-0.176	0.048	-0.156	0.061	-0.134	0.071	-0.110	0.081	-0.084	0.089	-0.056	0.092	-0.028	0.089
Semnopithecus	-0.181	0.028	-0.166	0.046	-0.150	0.064	-0.131	0.078	-0.107	0.088	-0.082	0.095	-0.055	0.099	-0.028	0.097
Simias	-0.185	0.030	-0.169	0.045	-0.149	0.056	-0.127	0.066	-0.103	0.074	-0.077	0.079	-0.050	0.082	-0.023	0.079
Theropithecus	-0.183	0.032	-0.167	0.049	-0.146	0.060	-0.124	0.072	-0.098	0.079	-0.072	0.084	-0.045	0.084	-0.018	0.084
Trachypithecus	-0.184	0.026	-0.170	0.045	-0.154	0.061	-0.133	0.075	-0.110	0.087	-0.085	0.096	-0.058	0.100	-0.030	0.101
Gorilla	-0.185	0.029	-0.168	0.046	-0.148	0.060	-0.125	0.071	-0.100	0.081	-0.073	0.087	-0.044	0.089	-0.016	0.089
Homo	-0.201	0.009	-0.184	0.032	-0.166	0.057	-0.141	0.079	-0.113	0.099	-0.082	0.117	-0.050	0.127	-0.016	0.130
Hylobates	-0.187	0.032	-0.173	0.048	-0.156	0.062	-0.132	0.069	-0.107	0.077	-0.080	0.082	-0.052	0.085	-0.023	0.085
Pan	-0.188	0.021	-0.171	0.038	-0.150	0.054	-0.127	0.069	-0.101	0.082	-0.073	0.090	-0.045	0.098	-0.016	0.100
Alouatta	-0.185	0.029	-0.168	0.043	-0.147	0.052	-0.123	0.059	-0.098	0.069	-0.071	0.074	-0.044	0.077	-0.017	0.077
Aotus	-0.187	0.030	-0.171	0.045	-0.153	0.060	-0.131	0.068	-0.107	0.076	-0.081	0.082	-0.053	0.083	-0.026	0.082
Ateles	-0.193	0.030	-0.179	0.046	-0.160	0.060	-0.139	0.072	-0.114	0.082	-0.086	0.090	-0.057	0.093	-0.027	0.094
Cacajao	-0.194	0.026	-0.179	0.045	-0.160	0.063	-0.138	0.078	-0.112	0.089	-0.083	0.094	-0.053	0.099	-0.023	0.101
Callicebus	-0.194	0.032	-0.179	0.047	-0.159	0.060	-0.136	0.071	-0.109	0.078	-0.080	0.083	-0.051	0.085	-0.021	0.087

Callimico	-0.192	0.025	-0.177	0.041	-0.158	0.055	-0.135	0.065	-0.110	0.070	-0.081	0.074	-0.052	0.075	-0.022	0.075
Callithrix	-0.187	0.031	-0.174	0.051	-0.154	0.066	-0.133	0.077	-0.107	0.084	-0.079	0.087	-0.050	0.086	-0.020	0.085
Cebuella	-0.189	0.030	-0.176	0.047	-0.157	0.061	-0.134	0.069	-0.108	0.075	-0.081	0.078	-0.052	0.080	-0.024	0.082
Cebus	-0.193	0.026	-0.176	0.044	-0.157	0.060	-0.132	0.070	-0.104	0.076	-0.075	0.084	-0.045	0.087	-0.015	0.089
Lagothrix	-0.193	0.024	-0.179	0.042	-0.161	0.058	-0.139	0.073	-0.114	0.083	-0.086	0.089	-0.056	0.091	-0.026	0.090
Leontopithecus	-0.200	0.036	-0.185	0.049	-0.165	0.059	-0.142	0.064	-0.113	0.068	-0.084	0.070	-0.052	0.071	-0.020	0.068
Mico	-0.190	0.035	-0.177	0.052	-0.158	0.065	-0.136	0.075	-0.111	0.080	-0.082	0.083	-0.053	0.083	-0.023	0.082
Pithecia	-0.185	0.031	-0.168	0.048	-0.149	0.063	-0.127	0.075	-0.100	0.078	-0.073	0.083	-0.045	0.088	-0.018	0.092
Saguinus	-0.194	0.033	-0.179	0.048	-0.161	0.061	-0.139	0.070	-0.114	0.077	-0.086	0.082	-0.056	0.083	-0.026	0.080
Saimiri	-0.203	0.020	-0.192	0.040	-0.177	0.060	-0.159	0.079	-0.135	0.092	-0.107	0.099	-0.077	0.102	-0.044	0.102
Tarsius	-0.175	0.030	-0.153	0.029	-0.133	0.037	-0.116	0.051	-0.093	0.064	-0.070	0.075	-0.046	0.081	-0.021	0.082
Daubentonia	-0.177	0.015	-0.158	0.034	-0.135	0.048	-0.110	0.050	-0.083	0.055	-0.055	0.060	-0.028	0.064	-0.002	0.067
Eulemur	-0.185	0.021	-0.165	0.028	-0.144	0.039	-0.121	0.050	-0.095	0.058	-0.068	0.063	-0.041	0.067	-0.013	0.068
Hapalemur	-0.187	0.021	-0.166	0.033	-0.147	0.049	-0.122	0.060	-0.097	0.071	-0.071	0.076	-0.042	0.078	-0.015	0.076
Indri	-0.181	0.024	-0.158	0.029	-0.136	0.038	-0.112	0.042	-0.089	0.054	-0.064	0.062	-0.037	0.065	-0.010	0.066
Lemur	-0.186	0.018	-0.164	0.026	-0.143	0.039	-0.120	0.051	-0.094	0.060	-0.067	0.066	-0.040	0.071	-0.013	0.072
Microcebus	-0.183	0.033	-0.162	0.037	-0.140	0.044	-0.119	0.054	-0.096	0.063	-0.071	0.071	-0.046	0.071	-0.020	0.070
Mirza	-0.176	0.018	-0.160	0.033	-0.140	0.045	-0.117	0.054	-0.093	0.061	-0.067	0.066	-0.041	0.070	-0.015	0.068
Varecia	-0.176	0.027	-0.153	0.032	-0.129	0.037	-0.105	0.046	-0.084	0.060	-0.062	0.068	-0.039	0.070	-0.018	0.066
Galago	-0.185	0.027	-0.168	0.038	-0.148	0.047	-0.126	0.055	-0.101	0.062	-0.076	0.069	-0.049	0.074	-0.023	0.076
Loris	-0.180	0.023	-0.161	0.036	-0.141	0.048	-0.118	0.061	-0.093	0.069	-0.067	0.074	-0.039	0.077	-0.011	0.077
Nycticebus	-0.182	0.015	-0.162	0.028	-0.140	0.041	-0.114	0.053	-0.088	0.064	-0.060	0.070	-0.032	0.072	-0.004	0.071
Adapis	-0.176	0.033	-0.156	0.031	-0.133	0.025	-0.109	0.026	-0.086	0.034	-0.063	0.043	-0.039	0.050	-0.014	0.053
Aegypto	-0.190	0.013	-0.173	0.027	-0.150	0.039	-0.123	0.047	-0.096	0.058	-0.067	0.067	-0.037	0.073	-0.006	0.076
Homunculus	-0.184	0.031	-0.171	0.050	-0.152	0.061	-0.131	0.070	-0.107	0.076	-0.081	0.079	-0.053	0.081	-0.026	0.079
Parapithecus	-0.194	0.034	-0.178	0.044	-0.157	0.055	-0.133	0.062	-0.107	0.067	-0.080	0.073	-0.052	0.071	-0.025	0.066

Appendix D.2: continued…

Genus	X 16	Y 16	X 17	Y 17	X 18	Y 18	X 19	Y 19	X 20	Y 20	X 21	Y 21	X 22	Y 22	X 23	Y 23
Cercocebus	0.000	0.098	0.027	0.089	0.053	0.078	0.078	0.063	0.105	0.050	0.132	0.033	0.156	0.013	0.179	-0.007
Cercopithecus	0.005	0.082	0.032	0.076	0.058	0.068	0.084	0.059	0.109	0.049	0.134	0.035	0.158	0.020	0.179	0.003
Chlorbocebus	0.005	0.084	0.032	0.078	0.057	0.067	0.084	0.059	0.111	0.047	0.138	0.034	0.163	0.019	0.185	0.000
Colobus	0.016	0.080	0.043	0.072	0.069	0.065	0.096	0.057	0.121	0.048	0.145	0.036	0.167	0.021	0.185	0.003
Erythrocebus	-0.002	0.094	0.026	0.089	0.053	0.080	0.079	0.065	0.106	0.051	0.133	0.035	0.160	0.017	0.183	-0.003
Lophocebus	0.009	0.088	0.036	0.081	0.061	0.073	0.087	0.063	0.112	0.053	0.136	0.038	0.159	0.022	0.180	0.005
Macaca	0.002	0.090	0.028	0.083	0.053	0.075	0.078	0.064	0.103	0.050	0.128	0.034	0.153	0.017	0.177	0.000
Mandrillus	-0.008	0.089	0.018	0.084	0.042	0.074	0.067	0.065	0.092	0.055	0.118	0.041	0.144	0.026	0.170	0.009
Miopithecus	0.003	0.087	0.032	0.081	0.059	0.071	0.087	0.061	0.115	0.050	0.142	0.037	0.167	0.022	0.188	0.003
Nasalis	0.003	0.077	0.031	0.072	0.058	0.065	0.085	0.056	0.112	0.047	0.138	0.035	0.162	0.019	0.184	0.002
Papio	0.000	0.096	0.026	0.087	0.051	0.077	0.076	0.065	0.100	0.050	0.126	0.035	0.150	0.019	0.174	0.001
Piliocolobus	0.015	0.068	0.044	0.062	0.071	0.057	0.098	0.052	0.123	0.043	0.147	0.030	0.169	0.017	0.189	0.002
Presbytis	0.002	0.090	0.029	0.082	0.055	0.071	0.083	0.061	0.110	0.048	0.136	0.032	0.162	0.017	0.184	-0.003
Procolobus	0.001	0.084	0.029	0.077	0.057	0.068	0.085	0.059	0.113	0.047	0.141	0.034	0.165	0.017	0.188	-0.001
Semnopithecus	-0.001	0.092	0.026	0.084	0.052	0.071	0.079	0.060	0.107	0.047	0.134	0.032	0.160	0.016	0.184	-0.004
Simias	0.003	0.074	0.029	0.066	0.054	0.058	0.080	0.053	0.106	0.045	0.132	0.034	0.157	0.021	0.179	0.005
Theropithecus	0.008	0.078	0.034	0.072	0.059	0.066	0.083	0.057	0.107	0.048	0.131	0.039	0.153	0.024	0.174	0.008
Trachypithecus	-0.003	0.096	0.025	0.087	0.052	0.076	0.081	0.066	0.109	0.053	0.137	0.038	0.163	0.021	0.186	-0.001
Gorilla	0.011	0.087	0.038	0.082	0.062	0.074	0.084	0.062	0.107	0.050	0.131	0.039	0.155	0.027	0.177	0.014
Homo	0.017	0.128	0.049	0.119	0.078	0.104	0.108	0.089	0.134	0.068	0.160	0.046	0.182	0.021	0.198	-0.006
Hylobates	0.006	0.082	0.034	0.077	0.060	0.071	0.086	0.059	0.111	0.045	0.136	0.030	0.159	0.013	0.181	-0.004
Pan	0.012	0.098	0.040	0.093	0.065	0.083	0.091	0.073	0.117	0.062	0.142	0.049	0.165	0.032	0.184	0.011
Alouatta	0.010	0.072	0.036	0.069	0.061	0.062	0.085	0.052	0.110	0.041	0.134	0.029	0.155	0.014	0.177	0.000
Aotus	0.002	0.082	0.028	0.076	0.054	0.071	0.079	0.064	0.103	0.055	0.127	0.044	0.148	0.030	0.167	0.012
Ateles	0.003	0.091	0.033	0.084	0.062	0.077	0.091	0.068	0.120	0.059	0.146	0.042	0.171	0.024	0.191	0.003
Cacajao	0.007	0.098	0.036	0.091	0.063	0.081	0.089	0.069	0.114	0.053	0.139	0.037	0.163	0.019	0.184	-0.001
Callicebus	0.008	0.086	0.035	0.083	0.060	0.075	0.085	0.063	0.109	0.051	0.134	0.036	0.157	0.019	0.178	0.000

Callimico	0.007	0.074	0.036	0.071	0.063	0.068	0.089	0.059	0.114	0.046	0.138	0.030	0.161	0.012	0.183	-0.006
Callithrix	0.008	0.080	0.036	0.074	0.062	0.067	0.087	0.059	0.111	0.048	0.133	0.035	0.153	0.018	0.172	0.000
Cebuella	0.004	0.079	0.031	0.072	0.056	0.062	0.081	0.051	0.105	0.039	0.130	0.026	0.153	0.012	0.175	-0.004
Cebus	0.014	0.086	0.042	0.081	0.069	0.075	0.095	0.066	0.119	0.052	0.143	0.036	0.165	0.020	0.185	0.002
Lagothrix	0.005	0.085	0.035	0.077	0.063	0.068	0.092	0.058	0.120	0.047	0.146	0.032	0.170	0.016	0.191	-0.003
Leontopithecus	0.012	0.066	0.043	0.061	0.072	0.055	0.100	0.046	0.127	0.035	0.152	0.023	0.175	0.007	0.193	-0.011
Mico	0.007	0.079	0.036	0.073	0.064	0.066	0.090	0.055	0.116	0.042	0.140	0.027	0.163	0.011	0.183	-0.007
Pithecia	0.009	0.093	0.034	0.085	0.059	0.076	0.083	0.065	0.107	0.052	0.129	0.034	0.149	0.014	0.169	-0.007
Saguinus	0.004	0.076	0.034	0.071	0.062	0.063	0.090	0.054	0.117	0.042	0.142	0.025	0.166	0.008	0.187	-0.011
Saimiri	-0.011	0.100	0.022	0.094	0.053	0.084	0.084	0.072	0.113	0.056	0.142	0.037	0.168	0.015	0.192	-0.007
Tarsius	0.004	0.079	0.030	0.076	0.053	0.071	0.076	0.062	0.099	0.051	0.123	0.039	0.146	0.026	0.168	0.008
Daubentonia	0.024	0.067	0.047	0.066	0.069	0.062	0.091	0.057	0.112	0.050	0.134	0.042	0.156	0.034	0.176	0.022
Eulemur	0.013	0.066	0.039	0.062	0.063	0.056	0.087	0.048	0.111	0.038	0.133	0.024	0.156	0.010	0.179	-0.004
Hapalemur	0.013	0.073	0.038	0.067	0.063	0.061	0.087	0.055	0.108	0.043	0.128	0.029	0.147	0.015	0.166	-0.001
Indri	0.016	0.068	0.041	0.063	0.064	0.056	0.088	0.049	0.110	0.038	0.131	0.021	0.154	0.010	0.175	-0.005
Lemur	0.013	0.071	0.039	0.066	0.063	0.061	0.086	0.053	0.109	0.042	0.131	0.028	0.154	0.016	0.175	0.000
Microcebus	0.005	0.067	0.030	0.064	0.054	0.058	0.078	0.050	0.101	0.040	0.125	0.027	0.148	0.014	0.170	-0.003
Mirza	0.011	0.066	0.035	0.062	0.059	0.057	0.081	0.049	0.103	0.039	0.125	0.028	0.146	0.016	0.166	0.000
Varecia	0.005	0.066	0.026	0.064	0.047	0.057	0.068	0.052	0.089	0.043	0.112	0.034	0.135	0.022	0.158	0.008
Galago	0.003	0.075	0.028	0.071	0.052	0.065	0.075	0.058	0.099	0.049	0.123	0.038	0.145	0.024	0.167	0.007
Loris	0.016	0.077	0.042	0.072	0.066	0.064	0.089	0.055	0.113	0.045	0.134	0.033	0.153	0.019	0.172	0.005
Nycticebus	0.023	0.068	0.049	0.061	0.071	0.051	0.094	0.043	0.116	0.035	0.137	0.027	0.155	0.017	0.172	0.007
Adapis	0.010	0.055	0.033	0.054	0.056	0.053	0.078	0.051	0.099	0.045	0.118	0.035	0.135	0.022	0.154	0.009
Aegypto	0.023	0.077	0.051	0.075	0.077	0.072	0.102	0.064	0.126	0.055	0.147	0.042	0.165	0.026	0.179	0.005
Homunculus	0.002	0.075	0.029	0.070	0.055	0.064	0.081	0.057	0.107	0.050	0.132	0.037	0.155	0.022	0.176	0.004
Parapithecus	0.003	0.061	0.031	0.056	0.058	0.051	0.083	0.042	0.108	0.032	0.132	0.020	0.154	0.006	0.175	-0.010

Appendix B.2: continued…

Genus	X 24	Y 24	X 25	Y 25	X 26	Y 26	X 27	Y 27	X 28	Y 28	X 29	Y 29	anterior cribriform plate X 30	Y 30
Cercocebus	0.200	-0.029	0.216	-0.051	0.227	-0.071	0.228	-0.090	0.222	-0.106	0.210	-0.120	0.216	-0.146
Cercopithecus	0.198	-0.016	0.213	-0.037	0.223	-0.058	0.226	-0.080	0.225	-0.099	0.225	-0.119	0.227	-0.152
Chlorbocebus	0.205	-0.021	0.220	-0.041	0.228	-0.061	0.226	-0.082	0.222	-0.098	0.219	-0.114	0.212	-0.140
Colobus	0.199	-0.017	0.210	-0.039	0.217	-0.058	0.217	-0.077	0.214	-0.092	0.211	-0.106	0.215	-0.125
Erythrocebus	0.203	-0.025	0.218	-0.049	0.224	-0.072	0.224	-0.093	0.221	-0.108	0.218	-0.124	0.215	-0.149
Lophocebus	0.198	-0.014	0.212	-0.036	0.221	-0.058	0.224	-0.081	0.220	-0.102	0.218	-0.125	0.218	-0.161
Macaca	0.198	-0.018	0.215	-0.040	0.227	-0.060	0.229	-0.082	0.225	-0.103	0.225	-0.125	0.225	-0.163
Mandrillus	0.192	-0.013	0.211	-0.038	0.230	-0.062	0.238	-0.087	0.236	-0.113	0.235	-0.141	0.241	-0.191
Miopithecus	0.204	-0.019	0.217	-0.042	0.225	-0.064	0.222	-0.086	0.217	-0.104	0.219	-0.125	0.209	-0.155
Nasalis	0.204	-0.017	0.219	-0.039	0.227	-0.060	0.229	-0.080	0.225	-0.097	0.220	-0.114	0.225	-0.142
Papio	0.195	-0.020	0.211	-0.044	0.221	-0.067	0.227	-0.089	0.226	-0.108	0.227	-0.129	0.228	-0.168
Piliocolobus	0.204	-0.015	0.215	-0.034	0.221	-0.052	0.222	-0.068	0.216	-0.083	0.212	-0.097	0.215	-0.118
Presbytis	0.202	-0.024	0.217	-0.045	0.226	-0.064	0.225	-0.084	0.221	-0.100	0.220	-0.116	0.219	-0.139
Procolobus	0.206	-0.022	0.217	-0.045	0.225	-0.066	0.224	-0.085	0.220	-0.101	0.217	-0.115	0.218	-0.136
Semnopithecus	0.203	-0.025	0.217	-0.048	0.225	-0.069	0.225	-0.088	0.221	-0.103	0.219	-0.116	0.222	-0.135
Simias	0.200	-0.014	0.216	-0.035	0.226	-0.055	0.232	-0.076	0.232	-0.095	0.233	-0.114	0.231	-0.147
Theropithecus	0.193	-0.010	0.210	-0.030	0.221	-0.052	0.229	-0.075	0.228	-0.098	0.229	-0.122	0.227	-0.165
Trachypithecus	0.202	-0.025	0.216	-0.049	0.224	-0.071	0.224	-0.092	0.219	-0.109	0.215	-0.125	0.214	-0.147
Gorilla	0.195	-0.005	0.210	-0.027	0.223	-0.051	0.225	-0.078	0.217	-0.105	0.213	-0.132	0.220	-0.178
Homo	0.206	-0.034	0.208	-0.062	0.199	-0.086	0.187	-0.106	0.173	-0.118	0.158	-0.124	0.148	-0.143
Hylobates	0.201	-0.021	0.213	-0.042	0.219	-0.063	0.225	-0.083	0.226	-0.098	0.227	-0.111	0.231	-0.127
Pan	0.200	-0.012	0.210	-0.037	0.213	-0.064	0.212	-0.091	0.206	-0.114	0.200	-0.134	0.200	-0.165
Alouatta	0.197	-0.015	0.210	-0.034	0.222	-0.051	0.224	-0.073	0.226	-0.091	0.233	-0.107	0.250	-0.128
Aotus	0.186	-0.008	0.204	-0.029	0.220	-0.053	0.227	-0.083	0.230	-0.113	0.238	-0.142	0.249	-0.186
Ateles	0.207	-0.021	0.214	-0.048	0.217	-0.072	0.216	-0.093	0.209	-0.109	0.204	-0.123	0.208	-0.144
Cacajao	0.202	-0.021	0.212	-0.045	0.217	-0.068	0.217	-0.091	0.211	-0.110	0.206	-0.126	0.210	-0.151

Callicebus	0.197	-0.021	0.211	-0.043	0.217	-0.066	0.219	-0.088	0.220	-0.104	0.227	-0.119	0.239	-0.143
Callimico	0.200	-0.026	0.213	-0.048	0.222	-0.067	0.227	-0.081	0.230	-0.090	0.232	-0.100	0.236	-0.118
Callithrix	0.189	-0.018	0.203	-0.039	0.215	-0.060	0.223	-0.081	0.230	-0.100	0.234	-0.119	0.243	-0.148
Cebuella	0.194	-0.022	0.208	-0.041	0.220	-0.061	0.229	-0.079	0.238	-0.094	0.246	-0.109	0.253	-0.136
Cebus	0.201	-0.016	0.208	-0.040	0.213	-0.063	0.216	-0.084	0.215	-0.100	0.214	-0.115	0.214	-0.138
Lagothrix	0.208	-0.023	0.220	-0.044	0.225	-0.063	0.223	-0.082	0.215	-0.098	0.209	-0.113	0.203	-0.134
Leontopithecus	0.209	-0.025	0.219	-0.042	0.222	-0.059	0.219	-0.073	0.216	-0.080	0.217	-0.085	0.219	-0.092
Mico	0.198	-0.028	0.211	-0.049	0.220	-0.066	0.221	-0.081	0.222	-0.091	0.227	-0.099	0.233	-0.115
Pithecia	0.184	-0.032	0.198	-0.055	0.215	-0.072	0.227	-0.086	0.233	-0.097	0.238	-0.108	0.245	-0.128
Saguinus	0.205	-0.031	0.216	-0.052	0.223	-0.069	0.225	-0.081	0.224	-0.089	0.225	-0.095	0.228	-0.106
Saimiri	0.210	-0.032	0.223	-0.057	0.225	-0.082	0.219	-0.104	0.212	-0.119	0.209	-0.134	0.205	-0.155
Tarsius	0.186	-0.013	0.202	-0.037	0.213	-0.061	0.224	-0.083	0.233	-0.100	0.248	-0.117	0.271	-0.149
Daubentonia	0.192	0.004	0.206	-0.017	0.222	-0.038	0.228	-0.065	0.229	-0.091	0.222	-0.116	0.212	-0.154
Eulemur	0.199	-0.019	0.217	-0.033	0.228	-0.048	0.232	-0.063	0.232	-0.078	0.233	-0.091	0.244	-0.113
Hapalemur	0.185	-0.015	0.202	-0.033	0.218	-0.050	0.228	-0.070	0.233	-0.091	0.241	-0.111	0.266	-0.141
Indri	0.194	-0.021	0.212	-0.033	0.225	-0.045	0.230	-0.060	0.229	-0.074	0.239	-0.084	0.254	-0.108
Lemur	0.194	-0.017	0.211	-0.034	0.225	-0.051	0.233	-0.068	0.237	-0.083	0.237	-0.098	0.241	-0.125
Microcebus	0.189	-0.021	0.206	-0.041	0.220	-0.059	0.237	-0.070	0.246	-0.081	0.253	-0.096	0.265	-0.125
Mirza	0.185	-0.016	0.201	-0.035	0.215	-0.054	0.230	-0.068	0.243	-0.079	0.255	-0.095	0.277	-0.129
Varecia	0.180	-0.010	0.200	-0.030	0.221	-0.049	0.235	-0.070	0.250	-0.090	0.265	-0.111	0.291	-0.153
Galago	0.188	-0.012	0.208	-0.033	0.222	-0.055	0.230	-0.080	0.240	-0.100	0.253	-0.121	0.267	-0.163
Loris	0.188	-0.010	0.199	-0.028	0.205	-0.048	0.211	-0.072	0.221	-0.093	0.237	-0.112	0.272	-0.142
Nycticebus	0.188	-0.003	0.201	-0.016	0.206	-0.034	0.208	-0.059	0.220	-0.081	0.234	-0.105	0.272	-0.135
Adapis	0.176	-0.002	0.199	-0.015	0.212	-0.039	0.222	-0.071	0.241	-0.095	0.273	-0.106	0.319	-0.139
Aegypto	0.191	-0.016	0.206	-0.034	0.212	-0.055	0.214	-0.075	0.218	-0.091	0.225	-0.105	0.222	-0.130
Homunculus	0.192	-0.020	0.204	-0.044	0.215	-0.068	0.224	-0.086	0.235	-0.098	0.245	-0.113	0.255	-0.142
Parapithecus	0.192	-0.027	0.210	-0.043	0.223	-0.058	0.234	-0.070	0.243	-0.080	0.252	-0.090	0.264	-0.113

Appendix D.3: Procrustes aligned landmark data for extant primate midsagittal face + basicranium analyzed in Chapter 3

	posterior cribriform plate		sella		planum sphenoideum		sphenoidale		dorsum sella		basion	
Species	X 1	Y 1	X 2	Y 2	X 3	Y 3	X 4	Y 4	X 5	Y 5	X 6	Y 6
Cercocebus	0.100	0.111	-0.231	0.086	0.029	0.163	-0.150	0.152	-0.275	0.082	-0.451	-0.028
Cercopithecus	0.079	0.118	-0.238	0.062	0.045	0.159	-0.142	0.133	-0.285	0.054	-0.458	0.009
Chlorbocebus	0.060	0.103	-0.245	0.074	0.024	0.143	-0.141	0.151	-0.281	0.086	-0.458	0.018
Colobus	0.064	0.083	-0.250	0.072	0.038	0.099	-0.116	0.124	-0.275	0.100	-0.507	0.036
Erythrocebus	0.070	0.131	-0.243	0.080	0.031	0.172	-0.175	0.167	-0.274	0.073	-0.424	-0.028
Lophocebus	0.024	0.098	-0.227	0.087	0.016	0.139	-0.144	0.150	-0.263	0.083	-0.438	0.007
Macaca	0.076	0.118	-0.234	0.069	0.050	0.157	-0.158	0.158	-0.256	0.091	-0.475	-0.021
Mandrillus	-0.029	0.109	-0.202	0.102	-0.051	0.146	-0.161	0.151	-0.228	0.116	-0.361	0.040
Miopithecus	0.114	0.108	-0.259	0.055	0.079	0.179	-0.154	0.140	-0.308	0.047	-0.462	-0.015
Nasalis	0.075	0.109	-0.224	0.099	0.013	0.146	-0.153	0.144	-0.284	0.094	-0.466	-0.004
Papio	-0.003	0.136	-0.211	0.097	-0.042	0.169	-0.147	0.151	-0.236	0.111	-0.370	-0.003
Piliocolobus	0.047	0.089	-0.247	0.073	0.030	0.108	-0.114	0.126	-0.275	0.100	-0.490	0.011
Presbytis	0.094	0.098	-0.241	0.088	0.058	0.122	-0.147	0.136	-0.320	0.071	-0.481	-0.003
Procolobus	0.090	0.103	-0.231	0.079	0.056	0.128	-0.143	0.131	-0.312	0.060	-0.486	0.010
Semnopithecus	0.077	0.094	-0.230	0.093	0.022	0.118	-0.149	0.150	-0.303	0.075	-0.466	0.008
Simias	0.084	0.123	-0.224	0.083	0.051	0.164	-0.143	0.149	-0.288	0.075	-0.472	-0.007
Theropithecus	0.003	0.140	-0.209	0.087	-0.009	0.160	-0.134	0.165	-0.238	0.081	-0.395	0.009
Trachypithecus	0.089	0.089	-0.223	0.089	0.063	0.114	-0.148	0.138	-0.314	0.078	-0.497	0.000
Gorilla	-0.031	0.098	-0.206	0.106	-0.050	0.126	-0.138	0.134	-0.237	0.117	-0.417	0.028
Homo	0.027	0.101	-0.221	0.124	0.023	0.112	-0.149	0.152	-0.266	0.149	-0.436	-0.096
Hylobates	0.046	0.068	-0.244	0.083	0.038	0.077	-0.140	0.121	-0.286	0.099	-0.499	0.054
Pan	0.012	0.085	-0.207	0.114	-0.011	0.106	-0.155	0.140	-0.260	0.111	-0.433	0.012
Mirza	0.024	0.081	-0.232	0.087	-0.062	0.116	-0.137	0.101	-0.288	0.095	-0.467	0.068
Alouatta	0.051	0.053	-0.278	0.093	0.018	0.066	-0.136	0.085	-0.297	0.123	-0.494	0.111
Aotus	0.101	0.116	-0.217	0.056	0.070	0.133	-0.134	0.108	-0.260	0.081	-0.482	0.005
Ateles	0.057	0.087	-0.236	0.094	0.053	0.107	-0.159	0.131	-0.298	0.107	-0.519	0.035

Cacajao	0.081	0.068	-0.228	0.080	0.046	0.098	-0.149	0.104	-0.267	0.119	-0.525	0.040
Callicebus	0.090	0.093	-0.239	0.059	0.039	0.148	-0.146	0.124	-0.272	0.081	-0.531	0.017
Callimico	0.134	0.130	-0.272	0.057	0.082	0.186	-0.135	0.143	-0.301	0.083	-0.512	-0.042
Callithrix	0.154	0.102	-0.259	0.051	0.085	0.138	-0.099	0.139	-0.284	0.075	-0.529	-0.040
Cebuella	0.158	0.102	-0.268	0.056	0.102	0.150	-0.116	0.140	-0.303	0.093	-0.529	-0.049
Cebus	0.089	0.111	-0.255	0.062	0.060	0.135	-0.134	0.125	-0.279	0.100	-0.488	0.004
Lagothrix	0.053	0.073	-0.229	0.077	0.034	0.091	-0.139	0.105	-0.279	0.108	-0.542	0.050
Leontopithecus	0.092	0.132	-0.255	0.059	0.068	0.142	-0.097	0.125	-0.312	0.056	-0.523	-0.001
Mico	0.129	0.125	-0.264	0.056	0.084	0.152	-0.115	0.141	-0.314	0.057	-0.535	-0.036
Pithecia	0.074	0.122	-0.247	0.063	0.038	0.132	-0.140	0.112	-0.275	0.088	-0.509	0.039
Saguinus	0.126	0.124	-0.261	0.055	0.074	0.155	-0.112	0.142	-0.316	0.051	-0.535	-0.022
Saimiri	0.134	0.115	-0.237	0.079	0.063	0.185	-0.154	0.159	-0.324	0.049	-0.494	-0.020
Tarsius	0.102	0.094	-0.214	0.091	-0.013	0.135	-0.145	0.142	-0.282	0.095	-0.433	-0.011
Daubentonia	-0.010	0.057	-0.227	0.102	-0.055	0.096	-0.179	0.112	-0.232	0.122	-0.461	0.065
Eulemur	-0.027	0.084	-0.228	0.085	-0.052	0.093	-0.159	0.101	-0.252	0.099	-0.458	0.090
Hapalemur	0.059	0.092	-0.238	0.073	-0.002	0.113	-0.109	0.106	-0.273	0.083	-0.490	0.031
Indri	-0.013	0.075	-0.231	0.090	-0.024	0.080	-0.120	0.097	-0.266	0.100	-0.509	0.096
Lemur	-0.012	0.086	-0.216	0.089	-0.049	0.106	-0.150	0.104	-0.255	0.100	-0.467	0.075
Microcebus	0.026	0.079	-0.239	0.087	-0.038	0.106	-0.189	0.081	-0.277	0.110	-0.489	0.074
Mirza	0.002	0.085	-0.220	0.089	-0.060	0.113	-0.144	0.090	-0.270	0.102	-0.479	0.070
Varecia	-0.014	0.086	-0.212	0.094	-0.055	0.101	-0.176	0.094	-0.255	0.103	-0.432	0.104
Galago	0.038	0.095	-0.234	0.077	-0.049	0.135	-0.176	0.096	-0.284	0.085	-0.452	0.050
Loris	-0.021	0.056	-0.231	0.086	-0.027	0.066	-0.107	0.097	-0.292	0.091	-0.471	0.100
Nycticebus	-0.004	0.052	-0.233	0.085	-0.019	0.063	-0.083	0.082	-0.275	0.085	-0.493	0.110
Adapis	0.055	-0.005	-0.196	0.106	-0.008	0.038	-0.099	0.072	-0.270	0.155	-0.529	0.129
Parapithecus	0.024	0.115	-0.253	0.083	0.009	0.125	-0.135	0.141	-0.266	0.103	-0.470	0.022
Aegyptopithecus	0.033	0.075	-0.274	0.099	0.013	0.097	-0.107	0.095	-0.320	0.116	-0.462	0.047
Homunculus	0.055	0.106	-0.229	0.099	-0.003	0.139	-0.153	0.144	-0.271	0.131	-0.478	-0.005

Appendix D.3: continued…

Species	prosthion X 7	prosthion Y 7	palatine tubercle X 8	palatine tubercle Y 8	acanthion X 9	acanthion Y 9	rhinion X 10	rhinion Y 10	glabella X 11	glabella Y 11
Cercocebus	0.329	-0.329	-0.108	-0.096	0.301	-0.268	0.256	-0.083	0.200	0.212
Cercopithecus	0.302	-0.336	-0.092	-0.083	0.302	-0.272	0.288	-0.059	0.199	0.214
Chlorbocebus	0.335	-0.333	-0.077	-0.114	0.316	-0.265	0.260	-0.033	0.208	0.169
Colobus	0.332	-0.308	-0.086	-0.117	0.308	-0.251	0.270	-0.012	0.221	0.173
Erythrocebus	0.308	-0.362	-0.077	-0.093	0.303	-0.275	0.279	-0.048	0.202	0.182
Lophocebus	0.340	-0.333	-0.106	-0.078	0.334	-0.281	0.286	-0.082	0.178	0.209
Macaca	0.311	-0.293	-0.081	-0.132	0.287	-0.273	0.272	-0.106	0.208	0.230
Mandrillus	0.382	-0.357	-0.095	-0.095	0.364	-0.285	0.308	-0.135	0.071	0.208
Miopithecus	0.275	-0.318	-0.097	-0.095	0.273	-0.241	0.290	-0.052	0.248	0.192
Nasalis	0.329	-0.317	-0.050	-0.125	0.307	-0.269	0.257	-0.088	0.196	0.210
Papio	0.375	-0.364	-0.082	-0.098	0.344	-0.303	0.247	-0.128	0.124	0.233
Piliocolobus	0.325	-0.313	-0.098	-0.112	0.293	-0.249	0.283	-0.031	0.247	0.199
Presbytis	0.308	-0.301	-0.087	-0.112	0.281	-0.236	0.272	-0.043	0.263	0.180
Procolobus	0.298	-0.315	-0.087	-0.117	0.281	-0.244	0.285	-0.021	0.248	0.185
Semnopithecus	0.331	-0.313	-0.104	-0.114	0.305	-0.257	0.262	-0.014	0.255	0.161
Simias	0.312	-0.338	-0.037	-0.158	0.272	-0.268	0.240	-0.049	0.206	0.226
Theropithecus	0.381	-0.390	-0.104	-0.123	0.350	-0.259	0.188	-0.100	0.167	0.229
Trachypithecus	0.310	-0.317	-0.061	-0.106	0.281	-0.251	0.266	-0.018	0.235	0.185
Gorilla	0.375	-0.363	-0.061	-0.171	0.294	-0.242	0.259	-0.083	0.211	0.251
Homo	0.265	-0.339	-0.112	-0.170	0.247	-0.215	0.335	-0.026	0.287	0.209
Hylobates	0.341	-0.309	-0.087	-0.110	0.313	-0.224	0.291	-0.017	0.229	0.158
Pan	0.380	-0.391	-0.072	-0.162	0.280	-0.209	0.221	-0.030	0.247	0.224
Mirza	0.345	-0.258	-0.058	-0.027	0.338	-0.249	0.377	-0.144	0.158	0.130
Alouatta	0.356	-0.263	-0.019	-0.123	0.341	-0.229	0.285	-0.064	0.173	0.148
Aotus	0.251	-0.314	-0.041	-0.135	0.258	-0.264	0.318	-0.119	0.136	0.334
Ateles	0.324	-0.295	0.001	-0.141	0.298	-0.228	0.265	-0.048	0.216	0.152

Cacajao	0.323	-0.285	-0.079	-0.129	0.309	-0.239	0.288	-0.042	0.202	0.185
Callicebus	0.300	-0.291	-0.067	-0.118	0.280	-0.212	0.295	-0.062	0.252	0.162
Callimico	0.263	-0.289	-0.035	-0.117	0.254	-0.223	0.285	-0.072	0.238	0.143
Callithrix	0.252	-0.306	-0.082	-0.076	0.259	-0.237	0.305	-0.056	0.199	0.210
Cebuella	0.263	-0.271	-0.069	-0.078	0.257	-0.224	0.303	-0.092	0.203	0.173
Cebus	0.307	-0.300	-0.105	-0.132	0.297	-0.238	0.277	-0.063	0.230	0.197
Lagothrix	0.341	-0.286	-0.040	-0.121	0.287	-0.217	0.275	-0.048	0.241	0.168
Leontopithecus	0.282	-0.280	-0.080	-0.098	0.265	-0.228	0.312	-0.061	0.248	0.154
Mico	0.261	-0.270	-0.065	-0.067	0.256	-0.213	0.307	-0.072	0.257	0.126
Pithecia	0.308	-0.286	-0.054	-0.132	0.285	-0.231	0.321	-0.098	0.199	0.192
Saguinus	0.271	-0.274	-0.067	-0.079	0.259	-0.213	0.293	-0.051	0.268	0.112
Saimiri	0.279	-0.288	-0.070	-0.123	0.262	-0.229	0.300	-0.048	0.241	0.121
Tarsius	0.304	-0.322	-0.112	-0.063	0.320	-0.257	0.342	-0.118	0.131	0.213
Daubentonia	0.308	-0.281	-0.016	-0.156	0.304	-0.233	0.371	-0.122	0.196	0.237
Eulemur	0.345	-0.279	-0.036	-0.061	0.337	-0.255	0.378	-0.132	0.154	0.174
Hapalemur	0.313	-0.293	-0.052	-0.037	0.293	-0.253	0.365	-0.151	0.134	0.236
Indri	0.333	-0.264	-0.002	-0.077	0.330	-0.256	0.364	-0.111	0.137	0.168
Lemur	0.341	-0.291	-0.020	-0.053	0.329	-0.263	0.374	-0.140	0.124	0.187
Microcebus	0.313	-0.248	-0.007	-0.047	0.335	-0.230	0.381	-0.137	0.186	0.123
Mirza	0.339	-0.260	-0.038	-0.029	0.332	-0.249	0.390	-0.152	0.149	0.141
Varecia	0.362	-0.287	-0.032	-0.049	0.340	-0.247	0.397	-0.166	0.078	0.167
Galago	0.289	-0.269	-0.020	-0.054	0.309	-0.252	0.396	-0.154	0.182	0.192
Loris	0.294	-0.266	-0.024	-0.060	0.355	-0.236	0.398	-0.137	0.128	0.201
Nycticebus	0.304	-0.273	-0.016	-0.054	0.349	-0.244	0.378	-0.144	0.091	0.237
Adapis	0.380	-0.283	-0.023	-0.115	0.343	-0.223	0.294	-0.069	0.054	0.195
Parapithecus	0.323	-0.279	-0.080	-0.086	0.323	-0.255	0.360	-0.120	0.163	0.150
Aegyptopithecus	0.349	-0.282	-0.082	-0.076	0.319	-0.219	0.337	-0.099	0.194	0.146
Homunculus	0.330	-0.306	-0.048	-0.114	0.321	-0.252	0.304	-0.097	0.173	0.156

References

Ackermann RR, and Cheverud JM. 2004. Morphological integration in primate evolution. In: Pigliucci M, and Preston K, editors. Phenotypic Integration: Studying the Ecology and Evolution of Complex Phenotypes. Oxford: Oxford University Press. p 302-319.

Adams DC, Rohlf FJ, and Slice DE. 2004. Geometric morphometrics: ten years of progress following the 'revolution'. Italian Journal of Zoology 71:5-16.

Akaike H. 1973. Maximum likelihood identification of Gaussian autoregressive moving average models. Biometrika 60(2):255-265.

Aldridge K. 2011. Patterns of differences in brain morphology in humans as compared to extant apes. Journal of Human Evolution 60:94-105.

Allman J. 1982. Reconstructing the evolution of the brain in primates through the use of comparative neurophysiological and neuroanatomical data. In: Armstrong E, and Falk D, editors. Primate Brain Evolution: Methods and Concepts. p 13-28.

Allman JM, McLaughlin T, and Hakeen A. 1993. Brain-weight and life-span in primate species. Proceedings of the National Academy of Sciences 90:118-122.

Arnold C, Matthews LJ, and Nunn CL. 2010. The 10k trees website: a new online resource for primate phylogeny. Evolutionary Anthropology 19:114-118.

Baker JR. 1958. Principles of Biological Microtechnique: A Study of Fixation and Dyeing. London: Metheun and Co. Ltd.

Baron G, Frahm HD, Bhatnagar KP, and Stephan H. 1983. Comparison of brain structure volumes in Insectivora and Primates. III. Main olfactory bulb (MOB). Journal Hirnforsch 24(5):551-568.

Barton R, and Dunbar R. 1997. Evolution of the social brain. In: Whiten A, and Byrne R, editors. Machiavellian Intelligence II: Extensions and Evaluations. Cambridge: Cambridge University Press.

Barton RA. 1998. Visual specialization and brain evolution in primates. Proceedings of the Royal Biological Society 265:1933-1937.

Barton RA, and Harvey PH. 2000. Mosaic evolution of brain structure in mammals. Nature 405:1055-1058.

Barton RA, Purvis A, and Harvey PH. 1995. Evolutionary radiation of visual and olfactory brain systems in primates, bats and insectivores. Philosophical Transactions: Biological Sciences 348(1326):381-392.

Bastir M, Rosas A, Lieberman DE, and O'Higgens P. 2008. Middle cranial fossa anatomy and the origin of modern humans. The Anatomical Record 291:130-140.

Bastir M, Rosas A, Stringer C, Cuétara JM, Kruszynski R, Weber GW, Ross CF, and Ravosa MJ. 2010. Effects of brain and facial size on basicranial form in human and primate evolution. Journal of Human Evolution 58:424-431.

Benefit BR, and McCrossin ML. 1997. Earliest known Old World monkey skull. Nature 388:368-371.

Biegert J. 1963. The evaluation of characteristics of the skull, hands and feet for primate taxonomy. In: Washburn SL, editor. Classification and Human Evolution. Chicago: Aldine. p 116-145.

Bienvenu T, Falk D, Semendeferi K, Guy F, Zollikofer C, Ponce de Leon M, Tafforeau P, Mackaye HT, Likius A, Vignaud P et al. . 2013. The endocast of *Sahelanthropus tchadensis*, the earliest known hominid (7Ma, Chad). Americal Journal of Physical Anthropology 150(S56):80-81.

Bienvenu T, Guy F, Coudyzer W, Gilissen E, Roualde G, Vignaud P, and Brunet M. 2011. Assessing endocranial variations in great apes and humans using 3D data from virtual endocasts. American Journal of Physical Anthropology 145:231-246.

Bishop A. 1964. Use of the hand in lower primates. In: Buettner-Janusch J, editor. Evolutionary and Genetic Biology of Primates. New York: Academy Press. p 133-225.

Bookstein FL. 1997. Morphometric Tools for Landmark Data: Geometry and Biology. Cambridge, UK: Cambridge University Press.

Bruner E. 2004. Geometric morphometrics and paleoneurobiology: brain shape evolution in the genus *Homo*. Journal of Human Evolution 47:279-303.

Bruner E, Mantini S, and Manzi G. 2004. A geometric morphometric approach to airorhynchy and functional cranial morphology in *Alouatta* (Atelidae, Primates). Journal of Anthropological Sciences 82:47-66.

Burnham KP, and Anderson DR. 1998. Model Selection and Multimodel Inference: A Practical Information-Theoretic Approach. New York: Springer.

Bush EC, Simons EL, and Allman JM. 2004. High-resolution computer tomography study of the cranium of a fossil anthropoid primate, *Parapithecus grangeri*: new insights into the evolutionary history of a primate sensory system. The Anatomical Record Part A(281A):1083-1087.

Carlson KJ, Stout D, Jashashvili T, Carlson K, and Berger LR. 2011. The endocast of MH1, *Australopithecus sediba*. Science 333(6048):1402-1407.

Cobb SN, and O'Higgens P. 2007. The ontogeny of sexual dimorphism in the facial skeleton of the African apes. Journal of Human Evolution 53(2):176-190.

Conroy GC, Vannier MW, and Tobias PV. 1990. Endocranial features of *Australopithecus africanus* revealed by 2-D and 3-D computed tomography. Science 247(4944):838-841.

Count EW. 1947. Brain and body weight in man: their antecedents in growth and evolution: a study in dynamic somatometry. Annals of the New York Academy of Sciences 46(10):993-1122.

de Winter W, and Oxnard CE. 2001. Evolutionary radiations and convergences in the structural organization of mammalian brains. Nature 409:710-714.

Deaner RO, Isler K, Burkhart J, and van Schaik CP. 2007. Overall brain size, and not encephalization quotient, best predicts cognitive ability across non-human primates. Brain, Behavior and Evolution 70:115-124.

Dunbar R. 1998. The social brain hypothesis. Evolutionary Anthropology:178-190.

Dunbar RIM. 1992. Neocortex size as a constraint on group size in primates. Journal of Human Evolution 22(6):469-493.

Edinger T. 1948. Paleoneurology versus comparative brain anatomy. Confinia neurologica 9:5-24.

Enlow DH. 1990. Facial Growth. Philadelphia: W.B. Saunders Company.

Enlow DH, and Azuma M. 1975. Functional growth boundaries in the human and mammalian face. Birth defects original article series 11(7):217.

Enlow DH, and McNamara JA. 1973. The neurocranial basis for facial form and pattern. The Angle Orthodontist 43(3):256-270.

Falk D. 1982. Mapping fossil endocasts. Primate Brain Evolution: Methods and Concepts. 1982: Plenum Press. p 217-226.

Falk D. 2007. Evolution of the Primate Brain. In: Henke W, and Tattersall I, editors. Handbook of Paleoanthropology Vol2: Primate Evolution and Human Origins: Springer-Verlag. p 1133-1162.

FEI Visualization Sciences Group. 2013. Avizo.

Finarelli JA. 2006. Estimation of endocranial volume through the use of external skull measures in the carnivora (Mammalia). Journal of Mammalogy 87(5):1027-1036.

Finarelli JA, and Flynn JJ. 2007. The evolution of encephalization in caniform carnivorans. Evolution 61(7):1758-1772.

Finlay BL, and Darlington RB. 1995. Linked regularities in the development and evolution of mammalian brains. Science 268(5217):1578-1584.

Finlay BL, Darlington RB, and Nicastro N. 2001. Devlopmental structure in brain evolution. Behavioral and Brain Sciences 24:263-308.

Finlay BL, Hersman MN, and Darlington RB. 1998. Patterns of vertebrate neurogenesis and the paths of vertebrate evolution. Brain Behavior and Evolution 52:232-242.

Fleagle JG, Gilbert CC, and Baden AL. 2010. Primate cranial diversity. American Journal of Physical Anthropology 142(2):565.

Frahm HD, Stephan H, and Stephan M. 1982. Comparison of brain structure volumes in Insectivora and Primates. I. Neocortex. Journal Hirnforsch 23(4):375-389.

Gabi M, Herculano-Houzel S, Collins CE, Wong PY, Torres LB, and Kaas JH. 2010. Cellular scaling rules for the brains of an extended number of primate species. Brain, Behavior and Evolution 76(1):32-44.

Gibson KR, Rumbaugh D, and Beran M. 2001. Bigger is better: primate brain size in relationship to cognition. In: Falk D, and Gibson K, editors. Evolutionary Anatomy of the Primate Cerebral Cortex: Cambridge University Press.

Gilad Y, Przeworski M, and Lancet D. 2004. Loss of olfactory receptor genes coincides with acquisition of full trichomatic vision in primates. PLoS Biology 2:E5.

Gingerich PD. 1978. The Stuttgart collection of Oligocene primates from the Fayum Province of Egypt. Paläontologische Zeitschrift 52(1/2):82-92.

Glander KE. 2006. Average body weight for mantled howling monkeys (*Alouatta palliata*): an assessment of average values and variability. In: Estrada A, Garber PA, Pavelka MSM, and Luecke L, editors. New Perspectives in the Study of Mesoamerican Primates: Distribution, Ecology, Behavior, and Conservation: Springer. p 247-263.

Gonzales L, Benefit B, Spoor F, Morrison P, and McCrossin M. 2010. The combination of a small brain, large olfactory bulb, and high visual acuity in the stem middle Miocene cercopithecoid *Victoriapithecus macinnesi* (abstract). American Journal of Physical Anthropology 141(S50):112-113.

Gonzalez-Jose R, Escapa I, Neves WA, Cuneo R, and Pucciarelli HM. 2008. Cladistic analysis of continuous modularized traits provides phylogenetic signals in Homo evolution. Nature 453:775-778.

Goswami A. 2006. Cranial modularity shifts during mammalian evolution. The American Naturalist 168:270-280.

Gould SJ. 1966. Allometry and size in ontogeny and phylogeny. Biological Reviews 4(587):587-640.

Gould SJ. 1975. Allometry in primates, with special emphasis on scaling and the evolution of the brain. Contributions to Primatology 5:244-292.

Gould SJ. 1977. Ontogeny and Phylogeny. Cambridge: Belknap Press.

Gould SJ. 2001. Size matters and function counts. In: Falk D, and Gibson KR, editors. Evolutionary anatomy of the primate cerebral cortex. Cambridge: Cambridge University Press. p xiii-xvii.

Gregory WK. 1915. On the classification and phylogeny of the Lemuroidea. Bulletin of Geolofical Society of America 26:426-446.

Groves C, and Shekelle M. 2010. The genera and species of Tarsiidae. International Journal of Primatology 31:1071-1082.

Gunz P, Mitteroecker P, and Bookstein FL. 2004. Semilandmarks in three dimensions. In: Slice DE, editor. Modern Morphometrics in Physical Anthropology. New York: Plenum Publishers. p 73-98.

Gurche JA. 1982. Early Primate Brain Evolution. In: Armstrong E, and Falk D, editors. Primate Brain Evolution: Methods and Concepts. New York: Plenum Press. p 227-246.

Gursky-Doran S. 2012. Acoustic characterization of ultrasonic vocalizations in a nocturnal primate *Tarsius syrichta*. Primates 54(3):293-299.

Harmon LJ, Weir JT, Brock CD, Glor RE, and Challenger W. 2008. GEIGER: investigating evolutionary radiations. Bioinformatics 24:129-131.

Harris HA. 1926. Endocranial form of gorilla skulls with special reference to the existance of dolichocephaly as a normal feature of certain primates. American Journal of Physical Anthropology 4(2):157-172.

Haug H. 1987. Brain sizes, surfaces, and neuronal sizes of the cortex cerebri - a stereological investigation of man and his variability and a comparison with some mammals. American Journal of Anatomy 180(2):126-142.

Healy SD, and Rowe C. 2007. A critique of comparative studies of brain size. Proceedings of the Royal Society B: Biological Sciences 274:453-464.

Heesy CP, and Ross C. 2004. Mosaic evolution of acuity patterns, diet, and color vision in haplorhine primates. In: Ross C, and Kay RF, editors. Anthropoid Origins: New Visions. New York: Kluwer Academic/Plenum Publishers. p 649-682.

Herculano-Houzel S. 2007. Encephalization, neuronal excess, and neuronal index in rodents. The Anatomical Record 290:1280-1287.

Herculano-Houzel S. 2009. The human brain in numbers: a linearly scaled-up primate brain. Frontiers in Human Neuroscience 3.

Herculano-Houzel S, Kaas JH, Collins CE, and Wong PY. 2007. Cellular scaling rules for primate brains. Proceedings of the National Academy of Sciences of the United States of America 104(9):3562-3567.

Hill WCO. 1955. Primates: Comparative Anatomy and Taxonomy. II. Haplorhini: Tarsioidea. Edinburgh: Edinburgh University Press.

Hofer H. 1969. On the evolution of the craniocerebral topography in primates. Annals of the New York Academy of Sciences 162(341-356).

Hofer HO, and Wilson JA. 1967. An endocranial cast of an early Oligocene primate. Folia Primatologica 5:148-152.

Holloway RL. 1966. Cranial capacity, neural reorganization, and hominid evolution: a search for more suitable parameters. American Anthropologist 68:103-121.

Holloway RL. 1974. The casts of fossil hominid brains. Scientific American 231(1):106-115.

Holloway RL. 1978. The relevance of endocasts for studying primate brain evolution. In: Norback CR, editor. Advances in Primatology: The Sensory Systems of Primates: Springer-Verlag. p 181-200.

Holloway RL. 1979. Brain size, allometry, and reorganization. In: Hahn M, editor. Development and Evolution of Brain Size: Behavioral Implications: Elsevier. p 59-88.

Holloway RL, Broadfield DC, and Yuan MS. 2004. The Human Fossil Record, Brain Endocasts: The Paleoneurological Evidence. Hoboken, New Jersey: John Wiley and Sons, Inc.

Hrdlicka A. 1925. The Taung ape. American Journal of Physical Anthropology Oct-Dec.:379-392.

Isler K, Kirk EC, Miller JMA, Albrecht GA, Gelvin BR, and Martin RD. 2008. Endocranial volumes of primate species: scaling analyses using a comprehensive and reliable data set. Journal of Human Evolution In Press.

Jacobs GH. 2008. Primate color vision: a comparative perspective. Visual Neuroscience 25:619-633.

Jeffrey N, and Spoor F. 2002. Brain size and the human cranial base: a prenatal perspective. American Journal of Physical Anthropology 118:324-340.

Jerison HJ. 1955. Brain to body ratios and the evolution of intelligence. Science 121:447-449.

Jerison HJ. 1970. Gross brain indices and the analysis of fossil endocasts. In: Noback CR, and montagna W, editors. Advances in Primatology Volume II: The Primate Brain. New York: Meredith Corporation. p 225-244.

Jerison HJ. 1973. Evolution of the Brain and Intelligence. New York: Academic Press.

Jerison HJ. 1979. Brain, body and encephalization in early primates. Journal of Human Evolution 8:615-635.

Jerison HJ. 1982. Allometry, brain size, and convolutedness. In: Armstrong E, and Falk D, editors. Primate Brain Evolution: Methods and Concepts. New York: Plenum Press. p 77-84.

Jerison HJ. 2001. The study of primate brain evolution: where do we go from here? In: Falk D, and Gibson KR, editors. Evolutionary Anatomy of the Primate Cerebral Cortex. Cambridge: Cambridge University Press. p 305-334.

Jerison HJ. 2007. What fossils tell us about the evolution of the neocortex. Evolution of the Nervous System. New York: Elsevier.

Joffe TH, and Dunbar RIM. 1998. Tarsier brain component composition and Its implications for systematics. Primates 39(2):211-216.

Jolicoeur P, Pirlot P, Baron G, and Stephan H. 1984. Brain structure and correlation patterns in Insectivora, Chiroptera, and Primates. Systematic Zoology 33(1):14-29.

Kay RF. 1994. "Giant" tamarin from the Miocene of Colombia. American Journal of Physical Anthropology 95(3):333-353.

Kay RF, Campbell VM, Rossie JB, Colbert MW, and Rowe TB. 2004. Olfactory fossa of *Tremacebus harringtoni* (Platyrrhini, early Miocene, Sacanana, Argentina): implications for activity pattern. The Anatomical Record Part A 281A:1157-1172.

Kay RF, Fleagle JG, Mitchell TRT, Colbert M, Bown T, and Powers DW. 2008. The anatomy of *Dolichocebus gaimanensis*, a stem platyrrhine monkey from Argentina. Journal of Human Evolution 54:323-382.

Kay RF, and Kirk EC. 2000. Osteological evidence for the evolution of activity pattern and visual acuity in primates. American Journal of Physical Anthropology 113(2):235-262.

Kay RF, and Kirk EC. 2008. New data on encephalization in Miocene New World monkeys: implications for anthropoid brain evolution. Journal of Vertebrate Paleontology 28:151A.

Kay RF, Kirk EC, Malinzak M, and Colbert MW. 2006. Brain size, activity pattern, and visual acuity in *Homunculus patagonicus*, an early Miocene stem platyrrhine: the

mosaic evolution of brain size and visual acuity in Anthropoidea. Journal of Vertebrate Paleontology 26:83A-84A.

Kay RF, Perry JMG, Malinzak M, Allen KL, Kirk C, Plavcan JM, and Fleagle JG. 2012. Paleobiology of Santacrucian primates. In: Vizcaino S, Kay RF, and Bargo MS, editors. Early Miocene Paleobiology in Patagonia. Cambridge: Cambridge University Press.

Kirk C. 2006. Visual influences on primate encephalization. Journal of Human Evolution 51:76-90.

Klingenberg CP. 2011. MorphoJ: an integrated software package for geometric morphometrics. Molecular Ecology Resources 11:353-357.

Le Gros Clark WE. 1959. The Antecedents of Man: An Introduction to the Evolution of the Primates. New York: Quadrangle/The New York Times Book Co.

Le Gros Clark WE, Cooper DM, and Zuckerman S. 1936. The endocranial cast of the chimpanzee. The Journal of the Royal Anthropological Institute of Great Britain and Ireland:249-268.

Lebrun R. 2008. Evolution and development of the strepsirrhine primate skull: Universitat Zurich.

Lieberman DE, Hallgrímsson B, Liu W, Parsons TE, and Jamniczky HA. 2008. Spatial packing, cranial base angulation, and craniofacial shape variation in the mammalian skull: testing a new model using mice. Journal of Anatomy 212(6):720-735.

Lieberman DE, McBratney BM, and Krovitz G. 2000a. The evolution and development of cranial form in *Homo sapiens*. Proceedings of the National Academy of Sciences 99(3):1134-1139.

Lieberman DE, and McCarthy RC. 1999. The ontogeny of cranial base angulation in humans and chimpanzees and its implications for reconstructing pharyngeal dimensions. Journal of Human Evolution 36(5):487-517.

Lieberman DE, Pearson OM, and Mowbray KM. 2000b. Basicranial influence on overall cranial shape. Journal of Human Evolution 38:291-315.

Lieberman DE, Ross CF, and Ravosa MJ. 2000c. The primate cranial base: ontogeny, function, and integration. Yearbook of Physical Anthropology 43:117-169.

MacKinnon J, and MacKinnon K. 1980. The behavior of wild spectral tarsiers. International Journal of Primatology 1(4):361-379.

MacLean EL, Barrickman NL, Johnson EM, and Wall CE. 2009. Sociality, ecology, and relative brain size in lemurs. Journal of Human Evolution:471-478.

MacLean EL, Hare B, Nunn CL, Addessi E, Amici F, Anderson RC, Aureli F, Baker JM, Bania AE, Barnard AM et al. . 2014. The evolution of self-control. Proceedings of the National Academy of Sciences(Early edition).

Marino L. 1998. A comparison of encephalization between odontocete cetaceans and anthropoid primates. Brain, Behavior and Evolution 51:230-238.

Marino L. 2002. Convergence of complex cognitive abilities in cetaceans and primates. Brain, Behavior and Evolution 59:21-32.

Martinez-Abadias N, Paschetta C, de Azevedo S, Esparza M, and Gonzales-Jose R. 2009. Developmental and genetic constraints on neurocranial globularity: insights from analyses of deformed skulls and quantitative genetics. Evolutionary Biology 36:37-56.

Matano S, Baron G, Stephan H, and Frahm HD. 1985a. Volume comparisons in the cerebellar complex of primates. II. cerebellar nuclei. Folia Primatologica 44(3-4):182-203.

Matano S, Stephan H, and Baron G. 1985b. Volume comparisons in the cerebellar complex of primates. I. ventral pons. Folia Primatologica 44(3-4):171-181.

McCarthy RC, and Lieberman DE. 2001. The posterior maxillary (PM) plane and anterior cranial architecture in primates. The Anatomical Record 264:247-260.

Merritt D, MacLean EL, Jaffe S, and Brannon EM. 2007. A comparative analysis of serial ordering in ring-tailed lemurs (*Lemur catta*). Journal of Comparative Psychology 121(4):363-371.

Miall RC. 2013. Cerebellum: anatomy and function. In: Pfaff DW, editor. Neuroscience in the 21st Century: From Basic to Clincial. New York: Springer. p 1149-1167.

Montgomery SH, Capellini I, Barton RA, and Mundy NI. 2010. Reconstructing the ups and downs of primate brain evolution: implications for adaptive hypotheses and *Homo floresiensis*. BMC Biology 8:9.

Murphy WJ, Eizirik E, O'Brien SJ, Madsen O, Scally M, Douady CJ, Teeling E, Ryder OA, Stanhope MJ, Jong WWd et al. . 2001. Resolution of the early placental mammal radiation using Bayesian phylogenetics. Science 294:2348-2351.

Musser GG, and Dagosto M. 1987. The identity of *Tarsius pumilus*, a pygmy species endemic to the montane mossy forests of Central Sulawesi. American Museum Novitates 2867:1-53.

Neubauer S, Gunz P, and Hublin J-J. 2010. Endocranial shape changes during growth in chimpanzees and humans: A morphometric analysis of unique and shared aspects. Journal of Human Evolution 59:555-566.

Neubauer S, Gunz P, and Hubline J-J. 2009. The pattern of endocranial ontogenetic shape changes in humans. Journal of Anatomy 215:240-255.

Niimura Y, and Nei M. 2007. Extensive gains and losses of olfactory receptor genes in mammalian evolution. PLoS One 2:e708.

O'Higgins P, and Jones N. 2006. Morphologika.

Olson EC, and Miller RL. 1958. Morphological Integration. Chicago: University of Chicago Press.

Orme D, Freckleton R, Thomas G, Petzoldt T, Fritz S, and Isaac N. 2010. caper: Comparative analyses of phylogenetics and evolution in R. R package version 0.4.

Parker GJM, Stephan KE, Barker GJ, Rowe JB, MacManus DG, Wheeler-Kingshott CAM, Ciccarelli O, Passingham RE, Spinks RL, Lemon RN et al. . 2002. Initial demonstration of in vivo tracing of axonal projections in the macaque brain and comparison with the human brain using diffusion tensor imaging and fast marching tractography. NeuroImage 15(4):797-809.

Perelman P, Johnson WE, Roos C, Seuanez HN, Horvath JE, Moreira MAM, Kessing B, Pontius J, Roelke M, Rumpler Y et al. . 2011. A molecular phylogeny of living primates. PLOS Genetics 7(3):e1001342.

Pihlstrom H, Fortelius M, Hemila S, Forsman R, and Reuter T. 2005. Scaling of mammalian ethmoid bones can predict olfactory organ size and performance. Proceedings of Biological Society 272(1566):957-962.

Plavcan JM. 2003. Scaling relationships between craniofacial sexual dimorphism and body mass dimorphism in primates: implications for the fossil record. American Journal of Physical Anthropology 120:38-60.

Pocock RI. 1918. On the external characters of the lemurs and of *Tarsius*. Proceedings of the Zoological Society of London:19-53.

Porto A, de Oliveira FB, Shirai LT, De Conto V, and Marriog B. 2009. The evolution of modularity in the mammalian skull I: morphological integration patterns and magnitudes. Evolutionary Biology 36:118-135.

Preuss T. 2001. The discovery of cerebral diversity: an unwelcome scientific revolution. In: Falk D, and Gibson KR, editors. Evolutionary Anatomy of the Primate Cerebral Cortex. Cambridge: Cambridge University Press. p 138-164.

Radinsky L. 1970. The fossil evidence of primate brain evolution. In: Noback CR, and Montagna W, editors. Advances in Primatology, Volume I: The Primate Brain. New York: Meredith Corporation. p 209-224.

Radinsky L. 1974. The fossil evidence of anthropoid brain evolution. American Journal of Physical Anthropology 41(1):15-28.

Radinsky L. 1975. A new approach to mammalian cranial analysis, illustrated by examples of prosimian primates. Journal of Morphology 124:167-180.

Radinsky LB. 1967. Brief communication: The oldest primate endocast. American Journal of Physical Anthropology 27:385-388.

Radinsky LB. 1968. A new approach to mammalian cranial analysis, illustrated by examples of prosimian primates. Journal of Morphology 124:167-180.

Radinsky LB. 1977. Early primate brains: facts and fiction. Journal of Human Evolution 6:79-86.

Ramsier MA, Cunningham AJ, Moritz GL, Finneran JJ, Williams CV, Ong PS, Gursky-Doyen SL, and Dominy NJ. 2012. Primate communication in the pure ultrasound. Biology Letters 8:508-511.

Ravosa MJ. 1990. Functional assessment of subfamily varation in maxillomandibular morphology among Old World monkeys. Americal Journal of Physical Anthropology 82(2):199-212.

Reader SM, and Laland KN. 2002. Social intelligence, innovation, and enhanced brain size in primates. Proceedings of the National Academy of Sciences 99(7):4436-4441.

Ross C, and Henneberg M. 1995. Basicranial flexion, relative brain size, and facial kyphosis in *Homo sapiens* and some fossil hominids. American Journal of Physical Anthropology 98:575-593.

Ross CF. 1995. Allometric and functional influences on primate orbit orientation and the origins of the Anthropoidea. Journal of Human Evolution 29(3):201-227.

Ross CF, and Ravosa MJ. 1993. Basicranial flexion, relative brain size, and facial kyphosis in nonhuman primates. American Journal of Physical Anthropology 91(3):305-324.

Sandel AA, MacLean EL, and Hare B. 2011. Evidence from four lemur species that ringtailed lemur social cognition converges with that of haplorhine primates. Animal Behaviour 81(5):925-931.

SAS Institute. 2013. JMP Pro. 11.0 ed.

Schaefer K, Mitteroecker P, Gunz P, Bernhard M, and Bookstein aFL. 2004. Craniofacial sexual dimorphism patterns and allomery among extant hominids. Annals of Anatomy 186:471-478.

Scheumann M, Rabesandratana A, and Zimmerman E. 2007. Predation, communication, and cognition in lemurs. In: Gursky S, and Nekaris KAI, editors. Primate Anti-Predator Strategies. New York: Springer. p 100-126.

Schmitz J, Ohme M, and Zischler H. 2001. Phylogenetic affiliations of *Tarsius bancanus* to other primates. Genetics 157(2):777-794.

Sears KE, Finarelli JA, Flynn JJ, and Wyss AR. 2008. Estimating body mass in New World "monkeys" (Platyrrhini, Primates), with a consideration of the Miocene platyrrhine, *Chilecebus carrascoensis*. American Museum Novitates 3617:1-29.

Semendeferi K, Lu A, Schenker N, and Damasio H. 2002. Humans and great apes share a large prefrontal cortex. Nature 5(3):272-276.

Shakelle M. 2008. Distribution of tarsier acoustic forms, north and central Sulawesi: with notes on the primary taxonomy of Sulawesi's tarsiers. In: Shekelle M, Maryanto I, Groves C, Schulze H, and Fitch-Snyder H, editors. Primates of the Oriental

Night. Jakarta: Indonesian Institute of Sciences (LIPI) Research Center for Biology. p 35-50.

Shellshear JL, and Smith GE. 1934. A comparative study of the endocranial cast of *Sinanthropus*. Philosophical Transactions of the Royal Society, London 223:469-487.

Simons E. 1959. An anthropoid frontal bone from the Fayum Oligocene of Egypt: The oldest skull fragment of a higher primate. American Museum Novitates:1-16.

Simons EL. 1993. New endocasts of *Aegyptopithecus*: oldest well-preserved record of the brain in Anthropoidea. American Journal of Science 293-A:383-390.

Simons EL. 1995. Crania of *Apidium*: primitive anthropoidean (Primates, Parapithecidae) from the Egyptian Oligocene. American Museum Novitates 3124:1-10.

Simons EL. 1997. Preliminary description of the cranium of *Proteopithecus sylviae*, an Egyptian late Eocene anthropoidean primate. Proceedings of the National Academy of Sciences 94(26):14970-14975.

Simons EL. 2001. Cranium and adaptations of *Parapithecus grangeri*. In: Ross CF, and Kay RF, editors. Anthropoid Origins: New Visions. New York: Plenum Publishers. p 183-203.

Simons EL. 2003. The fossil record of tarsier evolution. In: Simons EL, editor. Tarsiers: Past, Present, and Future. New Brunswick, New Jersey: Rutgers University Press. p 9-34.

Simons EL, and Rasmussen DT. 1994. A remarkable cranium of *Plesiopithecus teras* (Primates, Prosimii) from the Eocene of Egypt. Proceedings of the National Academy of Sciences 91:9946-9950.

Simons EL, and Rasmussen DT. 1996. Skull of *Catopithecus browni*, an early Tertiary catarrhine. American Journal of Physical Anthropology 100:261-292.

Simons EL, Seiffert ER, Ryan TM, and Attia Y. 2007. A remarkable female cranium of the early Oligocene anthropoid *Aegyptopithecus zeuxius* (Catarrhini, Propliopithecidae). Proceedings of the National Academy of Sciences 104(21):8731–8736.

Smaers JB, Schleicher A, Zilles K, and Vinicius L. 2010. Frontal white matter volume is associated with brain enlargement and higher structural connectivity in anthropoid primates. PLoS One 5(2):e9123.

Smaers JB, and Soligo C. 2013. Brain reorganization, not relative brain size, primarily characterizes anthropoid brain evolution. Proceedings of the Royal Society B: Biological Sciences 280(1759):20130269.

Smith GE. 1928. Endocranial cast obtained from the Rhodesian skull. Rhodesian Man and Associated Remains. London: British Museum of Natural History. p 52-58.

Smith RJ. 1984. Comparative functional morphology of maximum mandibular opening (gape) in primates. In: Chivers DJ, Wood BA, and Bilsborough A, editors. Food Acquisition and Processing in Primates: Springer. p 231-255.

Snider RS, and Eldred E. 1952. Cerebrocerebellar relationships in the monkey. Journal of Neurophysiology 15(1):27-40.

Sokal RR, and Rohlf FJ. 2003. Biometry: The Principles and Practice of Statistics in Biological Research. New York: W.H. Freeman and Co. 887 p.

Sporns O, Tononi G, and Kotter R. 2005. The Human Connectome: a structural description of the human brain. PLOS Computational Biology 1(4):0245-0251.

Stanhope MJ, Waddell VG, Madsen O, de Jong W, Hedges SB, Cleven GC, Kao D, and Springer MS. 1998. Molecular evidence for multiple origins of Insectivora and for a new order of endemic African insectivore mammals. Proceedings of the National Academy of Sciences of the United States of America 95(17):9967-9972.

Stephan H, and Andy OJ. 1964. Quantitative Comparisons of Brain Structures from Insectivores to Primates. American Zoologist 4:59-74.

Stephan H, and Andy OJ. 1969. Quantitative comparative neuroanatomy of primates: an attempt at a phylogenetic interpretation. Annals of the New York Academy of Sciences 167(1):370-387.

Stephan H, Baron G, and Frahm H. 1988. Comparative size of brains and brain components. In: Steklis HD, and Erwin K, editors. Comparative Primate Biology. New York: Alan Liss. p 1-38.

Stephan H, Baron G, and Frahm HD. 1982. Comparison of brain structure volumes in Insectivora and Primates. II. accessory olfactory bulb (AOB). J Hirnforsch 23(5):575-591.

Stephan H, Frahm H, and Baron G. 1981. New and revised data on volumes of brain structures in insectivores and primates. Folia Primatologica 35(1):1-29.

Tobias PV. 2001. Re-creating ancient hominid virtual endocasts by CT-scanning. Clinical Anatomy 14(2):134-141.

Toga AW, Clark KA, Thompson PM, Shattuck DW, and Van Horn JD. 2012. Mapping the Human Connectome. Neurosurgery 71(1):1-5.

Van Essen DC. 1997. A tension-based theory of morphogenesis and compact wiring in the central nervous system. Nature 385:313-318.

vanWoerden JT, vanSchaik CP, and Isler K. 2010. Effects of seasonality on brain size evolution: evidence from strepsirrhine primates. The American Naturalist 176(6):758-767.

Waddell PJ, Kishino H, and Ota R. 2001. A phylogenetic foundation for comparative mammalian genomics. Genome Informatics 12:141-154.

Wadell H. 1933. Sphericity and roundness of rock particles. The Journal of Geology 41(3):310-331.

Wadell H. 1935. Volume, shape, and roundness of quartz particles. Journal of Geology 43(3):250-280.

Wang Q, Dechow PC, and Hens SM. 2007. Ontogeny and diachronic changes in sexual dimorphism in the craniofacial skeleton of rhesus macaques from Cayo Santiago, Puerto Rico. Journal of Human Evolution:350-361.

Weidenreich F. 1936. Observations on the form and proportions of the endocranial casts of *Sinanthropus pekinensis* and the great apes: a comparative study of brain size. Paleontologica Sinica, Series D 7(4):1-50.

Weidenreich F. 1941. The brain and its role in the phylogenetic transformation of the human skull. Transactions of the American Philosophical Society 31(5):320-442.

Weidenreich F. 1947. Some particulars of skull and brain of early hominids and their bearing on the problem of the relationship between man and anthropoids. Americal Journal of Physical Anthropology 5(4):387-427.

Whiting BA, and Barton RA. 2003. Evolution of the cortico-cerebellar complex in primates: anatomical connections predict patterns of correlated evolution. Journal of Human Evolution 44(1):3-10.

Williams BA, Kay RF, and Kirk EC. 2010. New perspectives on anthropoid origins. Proceedings of the National Academy of Sciences 107(11):4797-4804.

Wong P, Collins CE, and Kaas JH. 2010. Overview of sensory systems of *Tarsius*. International Journal of Primatology 31:1002-1031.

Yoder AD. 2003. The phylogenetic position of the genus *Tarsius*: whose side are you on? In: Wright PC, Simons EL, and Gursky S, editors. Tarsiers: Past, Present, and Future. New Brunswick, New Jersey: Rutgers University Press. p 161-175.

Zelditch ML, Swiderski DL, and Sheets HD. 2012. Geometric Morphometrics For Biologists: A Primer: Academic Press.

Zietkiewicz E, Richer C, and Labuda D. 1999. Phylogenetic affinities of tarsiers in the context of primate Alu repeats. Molecular Phylogenetics and Evolution 11(1):77-83.

Zollikofer C, Ponce de Leon M, and Martin RD. 1998. Computer-assisted paleoanthropology. Evolutionary Anthropology 6(2):41-54.

Zollikofer C, Ponce de Leon MS, Lieberman DE, Guy F, Pilbeam D, Likius A, Mackaye HT, Vignaud P, and Brunet M. 2005. Virtual cranial reconstruction of *Sahelanthropus tchadensis*. Nature 434:755-759.

Biography

Kari Leigh Allen was born in Rome, NY on August 28, 1983, to Debra Barber Allen and grew up in Oneida, NY, with older siblings, Chris and Melissa. Kari graduated from the State University of New York at Potsdam in 2005, with a B.A. in Anthropology and minors in Biological Anthropology and Studio Art. She pursued a Master's degree in Biological Anthropology at New Mexico State University and completed her thesis titled "The Hand of *Kenyapithecus* from Maboko Island (Kenya)" under the tutelage of Drs. Monte L. McCrossin and Brenda Benefit (M.A., 2008). In 2008, Kari entered the Ph.D. program at Duke University, Department of Evolutionary Anthropology.

Publications

Kay, R. F., Perry, J. M. G., Malinzak, M., **Allen, K.L.**, Kirk, E. C., Plavcan, J. M., (2012). The Paleobiology of Santacrucian Primates. In: Vizcaino, S., Bargo, S., Kay, R.F., (Eds.), Early Miocene Paleobiology in Patagonia. Cambridge: Cambridge University Press.

Allen, K. L., & Kay, R. F., (2011). Dietary Quality and Encephalization in Platyrrhine Primates. Proceedings of the Royal Society B: Biological Sciences. 279(1729): 715-21.

Gongora, J., Cuddahee, R. E., do Nascimento, F. F., Palgrave, C. J., Lowden, S., Ho, S. Y. W., Simond, D., Damayanti, C. S., White, D. J., Tay, W. T., Randi, E., Klingel, H., Rodrigues-Zarate, C. J., **Allen, K.**, Moran, C. & Larson, G. (2011). Rethinking the evolution of extant sub-Saharan African suids (Suidae, Artiodactyla). Zoologica Scripta, 40(4), 327-335.

Awards and Research Grants

2013 Bass Instructorship, Duke University competitive fellowship, teaching award.

2013 Mentoring Award, Duke University, Evolutionary Anthropology ($800)

2013 American Association of Physical Anthropologists Pollitzer Travel Award ($400)

2012 NSF Doctoral Dissertation Improvement Grant, "Brain Size and Shape in Early Anthropoid Primates." ($19,152)

2012 Duke University Graduate School Dissertation Research Travel Award ($1,750)

2011 Leakey Foundation Research Grant, "Brain Size and Shape in Early Anthropoid Primates." ($11,000)

2011 Mentoring Award, Duke University, Evolutionary Anthropology ($500)

2007 Merit-Based Graduate Assistant Enhancement Fellowship, New Mexico State University

2007 Mike Watts Outstanding Leadership Fellowship, New Mexico State University

2007 Graduate Student Conference Travel Awards, New Mexico State University

2001 Mountain Scholar, State University of New York at Potsdam (2001-2005)